

COUPLED DYNAMICS OF CABLE-HARNESSED STRUCTURES: ANALYTICAL MODELING AND EXPERIMENTAL VALIDATION

by

Karthik Yerrapragada

A thesis

presented to the University of Waterloo

in fulfillment of the

thesis requirement for the degree of

Doctor of Philosophy

in

Mechanical and Mechatronics Engineering

Waterloo, Ontario, Canada, 2019

© Karthik Yerrapragada, 2019

Examining Committee Membership

The following served on the Examining Committee for this thesis. The decision of the Examining Committee is by majority vote.

External Examiner:

Luc Mongeau
Professor
Department of Mechanical Engineering
McGill University

Supervisor(s):

Armaghan Salehian
Associate Professor
Department of Mechanical and Mechatronics Engineering
University of Waterloo

Internal Member:

Kirsten Morris
Professor
Department of Mechanical and Mechatronics Engineering
University of Waterloo

Internal Member:

Giovanni Montesano
Assistant Professor
Department of Mechanical and Mechatronics Engineering
University of Waterloo

Internal-external Member:

Nima Maftoon
Assistant Professor
Department of System Design Engineering
University of Waterloo

AUTHOR'S DECLARATION

I hereby declare that I am the sole author of this thesis. This is a true copy of the thesis, including any required final revisions, as accepted by my examiners.

I understand that my thesis may be made electronically available to the public.

Abstract

This thesis presents analytical models to study the vibration characteristics of cable-harnessed beam structures motivated by space structure applications. The distributed parameter models proposed in this work considers into account the effect of coupling between various coordinates of vibration such as the bending in the out of plane, in-plane direction, axial and the torsion coordinates. The mathematical models are presented for structures with straight cable wrapping pattern at an offset distance, periodic and non-periodic wrapping pattern. Numerous theoretical simulations are performed to highlight the importance of having a coupled vibration model and the analytical models are validated with experiments.

Chapter 2.1 presents a distributed parameter model to study the vibrations of beam with straight cable pattern at an offset distance. The structure is modelled using Euler-Bernoulli and Timoshenko beam theories. The presented model studies the effects of coupling between various coordinates of vibrations. Strain and kinetic energy expressions are developed using linear displacement field assumptions and Green-Lagrange strain tensor. The governing coupled partial differential equations for the cable-harnessed beam that includes the effects of the cable pre-tension are found using Hamilton's principle. The effects of the offset position of the cable, pre-tension and radius are studied on the natural frequencies of the system. The natural frequencies from the coupled Euler Bernoulli, Timoshenko and decoupled analytical models are found and compared to the results of the Finite Element Analysis.

In Chapter 2.2, a mathematical model to study the coupled vibrations in cable-harnessed beam with periodic wrapping pattern is presented. The structure is modeled using Euler-Bernoulli and Timoshenko beam theories. The fundamental element of the wrapping pattern consists of diagonal cable section along with lumped mass section at the end of each element. An equivalent fully coupled continuum model is presented with goal of obtaining constant coefficient partial differential equations. Sensitivity analysis by the varying the cable radius, number of fundamental elements on the natural frequencies is also performed. The concept of transition frequency in Timoshenko beam theory is also studied for cable-harnessed structures. The effect of cable radius on the transition frequency is presented. Natural frequencies and mode shapes for both the spectra are presented for simply supported boundary condition and the results are compared to the bare

beam to show the effect of cabling on the behavior of the structure for both the spectra of Timoshenko beam theory.

Chapter 2.3, presents an analytical model to study the coupled vibrations of cable-harnessed structures with non-periodic wrapping pattern. The exact coupled partial differential equations of the structure are developed using Euler-Bernoulli (EB) theory. The analytical model assumes each fundamental element of the structure has different displacement, which means the structure is discretized at the interface of two different fundamental elements by applying the continuity conditions along with the cantilever boundary condition and the model is solved for natural frequencies, mode shapes and frequency response functions. In non-periodic wrapping, the wrapping angle changes for each fundamental element. The coupled exact model developed in Chapter 2.3 is an improvement of the model presented for the periodic wrapping patterns and is compared to the decoupled model for non-periodic wrapping patterns.

In Chapter 3.1, the experimental study and model validations for the coupled dynamics of a cable-harnessed beam structure are presented. The system under consideration for the experiment consists of multiple pre-tensioned cables attached along the length of the host beam structure positioned at an offset distance from the beam centerline. Analytical model presented by the coupled partial differential equations (PDEs) for various coordinates of vibrations are found and the frequency response functions (FRFs) obtained for both Euler-Bernoulli and Timoshenko-based models are compared to those from the experiments for validation.

In Chapters 3.2 and 3.3, experiments are performed on the cabled beam structures with periodic and non-periodic wrapping patterns and the frequency response functions obtained from coupled and decoupled models are compared to the experimental frequency response functions. The experimental mode shape animation plots of the torsion dominant and in-plane dominant modes are also presented to identify the type of modes associated with the sharp peaks observed in the out-of-plane bending frequency response functions.

Acknowledgements

I would like to thank my doctoral advisor Dr. A Salehian for encouraging me to pursue PhD in the field of Structural Vibrations. I would like to thank her for providing technical guidance during my PhD and the financial support. She constantly provided very good feedback on a timely basis on the results I have obtained and also on the writing part of my journal papers. I wish to utilize the technical experience that I have gained during my PhD to contribute more to the field of vibrations in the future. I would like to thank Dr. Mongeau, Dr. Morris, Dr. Montesano and Dr. Maftoon for agreeing to be in my PhD committee and going through my thesis. I would like to thank Dr. Morris for also providing feedback on the part of non-periodic structures. I would like to thank my lab mates: Blake Martin, Pranav Agrawal, Egon Fernandes, Nabil Al Aid, Dilpreet Bath, Hamza Edher, Gary Chan. The technical discussions with Blake Martin were also helpful. I would like to thank NSERC funding agency for providing financial support for the research and the University of Waterloo for the International Doctoral Student Award. I would like to thank my parents, family members and friends for all the support they have given me over the past few years.

Table of Contents

Abstract	iv
Acknowledgements	vi
List of Figures	ix
List of Tables	xvii
Nomenclature	xix
Chapter 1: Introduction	1
1.1 Literature Review.....	1
1.1.1 Motivation.....	1
1.1.2 Research by U.S Air force Group in Cable-Harnessed Structures	3
1.1.3 Other Structural Application of Vibration Analysis of Cables.....	6
1.1.4 Research by Other Research Groups in Cable-Harnessed Structures.....	9
1.1.5 Effect of Coupling between Vibrations Coordinates in Other Structures.....	13
1.1.6 Transition Frequency in Timoshenko Beams	18
1.1.7 Key Gaps in the Literature	19
1.2 Objectives and Scope	20
Chapter 2: Mathematical Modeling and Theoretical Analysis of Coupled Vibrations of Cable-Harnessed Structures	24
2.1 Coupled Vibrations of Straight Cable Harness at Offset Distance	25
2.1.1 Mathematical Model.....	25
2.1.2 Results and Discussion of numerical simulations	38
2.2 Coupled Vibrations in Structure with Periodic Wrapping Pattern.....	62
2.2.1 Mathematical Model.....	62
2.2.2 Numerical Simulations and Analysis	66
2.3 Coupled Vibrations in Structure with Non-Periodic Wrapping Pattern.....	83
2.3.1 Mathematical Model.....	83
2.3.2 Numerical Results.....	91
2.4 Conclusions of the Chapter	96
Chapter 3: Experimental Validation of Coupled Vibrations of Cable-Harnessed Structures	98
3.1 Experimental Validation of Straight Cable Pattern with Offset Distance.....	98
3.2 Experimental Validation of Periodic Wrapping Pattern	112

3.3 Experimental Validation of Non-Periodic Wrapping Pattern	125
3.4 Conclusions of the Chapter	141
Chapter 4	142
Conclusion and Future Work	142
4.1 Conclusions	142
4.2 Future Work	144
References	146
Appendix A	158
Strain and Kinetic Energy Coefficients for Straight Cable at Offset Pattern.....	158
Appendix B	159
Strain and Kinetic Energy Coefficients for Periodic Cable Wrapping Pattern.....	159
Appendix C	161
Additional mode shapes for bare beam and cabled beam using Timoshenko beam theory for both Spectra.....	161
Appendix D	164
Strain and Kinetic Energy Coefficients for Non-Periodic Cable Wrapping Pattern.....	164

List of Figures

Fig. 1. 1 Cable Harness in NASA satellite structure, Image Courtesy: NASA ICESat Website [13].
 2

Fig. 1. 2 Cable Harness in NASA satellite structure. Image Courtesy: NASA ICESat Website [13].
 3

Fig. 1. 3 Setup of NASA Satellite structure on shaker for vibration testing, Image Courtesy: NASA LADEE Website [14]. 3

Fig. 1. 4 Cable Harnesses in beam and plate structures by the U.S Air force research laboratory group. Image Courtesy: (a) NASA ICESat; (b) Babuska et al, JSR, 2010 [2]; (c) Coombs et al, JSR, 2011 [1]. 4

Fig. 1. 5 Applications of cables in power lines. Courtesy: McClure et al, Computers and Structures, 2003 [25] 6

Fig. 1. 6 Marine applications of cables. Courtesy: Huang et al, Appl Sci, 1999 [26] 7

Fig. 1. 7 Applications of cables in bridge structures. Courtesy: Fujino et al, Appl Sci, 2017 [27] 7

Fig. 1. 8 Cable harnessed structure experimental setup by Inman research group. Courtesy: Spak, PhD thesis, 2014, Virginia Tech [12] 9

Fig. 1. 9 Cable harnessed structure to validate the spectral element method by Inman research group. Courtesy: Choi et al, JSV 2014 [44]. 9

Fig. 1. 10 Periodic wrapped cable-harnessed structure. Courtesy: Martin et al, AIAA 2016 [51] 11

Fig. 1. 11 Experimental setup of periodically wrapped cable-harnessed structure. Courtesy: Martin et al, AIAA 2016 [52]. 11

Fig. 1. 12 Non-periodic wrapped cable-harnessed structure. Martin et al, AIAA 2018 [53] 11

Fig. 1. 13 Coupling due to geometry of C cross-section beam. Courtesy: Bishop et al [73] 13

Fig. 1. 14 Material coupling in composite structures. Courtesy: Mei et al, Composite and Structures, 2005 [76].....	14
Fig. 1. 15 Coupled Bending-torsion vibrations in piezoelectric composite structure. Courtesy: Xie et al, MSSP, 2018 [83].....	14
Fig. 1. 16 Coupled bending-torsion vibrations in beams with eccentric tip mass boundary conditions. Courtesy: Al-Solihat et al, 2018 [84]	15
Fig. 1. 17 Coupled bending torsion motion in piezoelectric beam. Courtesy: Shan et al, Appl Sci, 2017 [95].....	19
Fig. 2. 1 Representation of the cable harness beam along with the coordinate axes for (a) Timoshenko theory (b) Euler-Bernoulli theory.	26
Fig. 2. 2 Schematic of the cable-harnessed beam subjected to harmonic base excitation and the coordinate axes.....	35
Fig. 2. 3 Finite Element Analysis discretization along with the nodal displacements.	39
Fig. 2. 4 Vibrations mode shapes for fixed-fixed boundary conditions using coupled EB theory for fixed-fixed boundary conditions using coupled EB theory for Out of plane bending dominant (Modes 1, 2 and 4), In plane bending dominant (Mode 3), Torsion dominant (Mode 5) and Axial dominant (Mode 22).	42
Fig. 2. 5 Vibrations mode shapes for cantilever boundary conditions using coupled EB theory for	43
Fig. 2. 6 Vibrations mode shapes for simply supported boundary conditions using coupled EB theory for Out of plane bending dominant (Modes 1, 2 and 5), In plane bending dominant (Mode 3), Torsion dominant (Mode 6) and Axial dominant (Mode 23).....	44
Fig. 2. 7 Percentage for the strain energy contribution of each modal coordinate with respect to mode number ● denotes axial; ■ denotes in plane bending; ◆ denotes out of plane bending; ★ denotes torsion.	45

Fig. 2. 8 Effects of cable radius on the coupled natural frequencies. Solid lines denote Out of plane dominant modes; Dash dot lines denote In plane bending dominant; Dashed line denote Torsion dominant. 50



Fig. 2. 9 Error comparisons for natural frequencies between the coupled and decoupled models and the FEA.  denotes error between decoupled analytical and FEA and  error between coupled analytical and FEA..... 51

Fig. 2. 10 Effect of cable offset position on the coupled natural frequencies. Solid lines denote Out of plane dominant modes; Dash dot lines denote In plane bending dominant; Dashed line denote Torsion dominant. 52

Fig. 2. 11 Mode shapes corresponding to n=1 for the system with coupled bending at 0.0043 m cable offset position 53



Fig. 2. 12 Strain energy and natural frequency with respect to cable offset position.  denotes out of plane bending dominant mode.  denotes in plane bending dominant mode. 54




Fig. 2. 13 Effect of cable pre-tension on the natural frequencies for first in-plane bending, out-of-plane bending and torsional mode using the system parameters of Table (2.1).  denotes out of plane bending dominant mode.  denotes torsion dominant mode.  denotes in plane bending dominant mode..... 55




Fig. 2. 14 Effect of cable pre-tension on the natural frequencies for first in-plane bending, out-of-plane bending and torsional mode using the system parameters of Table. (2.5).  denotes out of plane bending dominant mode.  denotes torsion dominant mode.  denotes in plane bending dominant mode..... 57

Fig. 2. 15 Bar graph of strain energy contributions for mode 1 for beam with parameters from a) Table (2.1); b) Table (2.5) for fixed-fixed boundary condition. 58

Fig. 2. 16 I-beam cross section and dimensions 59


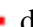
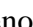
Fig. 2. 17 Effect of cable pre-tension on the natural frequencies of first in plane bending, out-of-plane bending and torsional mode using the system parameters of Table (2.6) for an I-cross section beam.  denotes out of plane bending dominant mode.  denotes torsion dominant mode.  denotes in plane bending dominant mode. 59

Fig. 2. 18 Frequency response functions for a) Fixed-fixed b) Cantilever c) Simply Supported boundary conditions. denotes cabled beam analytical (Euler Bernoulli coupled) denotes cabled beam analytical (Timoshenko coupled) denotes FEA (coupled) Cabled beam analytical (decoupled). 61

Fig. 2. 19 (a) Representation of the cable harnessed structure with periodic wrapping pattern along with the coordinates of motion. (b) Fundamental element of wrapping pattern..... 62

Fig. 2. 20 Representation of the top view cable harnessed structure with periodic wrapping pattern along with the dimensions. (a) Sample 1 (b) Sample 2 (c) Sample 3..... 66

Fig. 2. 21 Comparison of theoretical frequency response functions for coupled (EB and TBT) and decoupled models for (a) Sample 1 (b) Sample 2 (c) Sample 3. Cabled Analytical (Decoupled) Cabled Analytical (coupled EB) Cabled Analytical (coupled Timoshenko). 67

Fig. 2. 22 Effect of variation in number of fundamental elements vs the fundamental natural frequency of a) Out of plane dominant mode b) In-plane bending dominant mode c) Torsion dominant mode. Present work (Coupled) Martin et al [52]. 71

Fig. 2. 23 Effect of variation in cable radius vs the fundamental natural frequency of a) Out of plane dominant mode b) In-plane bending dominant mode c) Torsion dominant mode. Present work (Coupled); Martin et al [52]. 72

Fig. 2. 24 Variation of normalized transition frequency of cabled beam with respect to the radius of the cable. Bare beam Cabled beam. 76

Fig. 2. 25 Mode shapes for (a)-(c) frequencies in first spectrum; (d) transition frequency; (e)-(g) frequencies in the second spectrum. 77

Fig. 2. 26 Mode shapes for (a)-(c) frequencies in first spectrum; (d) transition frequency; (e)-(g) frequencies in the second spectrum. 80

Fig. 2. 27 The nature of mode shape parameters of out of plane dominant modes in spectra 1 and shear dominant modes in spectra 2. $\text{Im} [\alpha 1], \text{Im} [\alpha 3], \text{Im} [\alpha 5], \text{Re} [\alpha 7]$ $\text{Im} [\alpha 2], \text{Im} [\alpha 4], \text{Im} [\alpha 6], \text{Im} [\alpha 7]$ $\text{Re} [\alpha 8]$ $\text{Im} [\alpha 8]$ 81

Fig. 2. 28 Representation of non-periodically wrapped cable harnessed structure pattern along with the coordinates of motion..... 84

Fig. 2. 29 Top view representation of (a) Sample 1; (b) Sample 2; (c) Sample 3 92

Fig. 2. 30 Frequency response functions of coupled and decoupled models for (a) Sample 1; (b) Sample 2; (c) Sample 3. Cabled Analytical (Decoupled) Cabled Analytical (Coupled)..... 93

Fig. 3. 1 Base excitation experimental setup for the cantilevered cable harnessed beam, (a) beam structure, accelerometer and shaker, (b) laser vibrometer controller, sensor head, power amplifier, and LMS data acquisition system. 100

Fig. 3. 2 Experimental frequency response functions from shaker tests for substrate beam + tape and no cables and substrate beam without tape at $x_s=95$ mm sensing location. Bare beam experimental (Uncabled). Bare beam + Tape experimental (Uncabled). 102

Fig. 3. 3 Comparison between the frequency response functions at $x_s=95$ mm sensing location; Martin et al ; Cabled Experimental; Cabled Analytical (Coupled EB); Bare beam Experimental; Bare beam analytical;..... 103

Fig. 3. 4 Schematic of beam width view and cable offset position. 103

Fig. 3. 5 Comparison of the cable harnessed frequency response functions from shaker experiment, decoupled and coupled analytical models for $x_s=95$ mm. Cabled Analytical (Decoupled EB) Cabled Experimental Cabled Analytical (Coupled EB) Cabled Analytical (Coupled Timoshenko)..... 104

Fig. 3. 6 Comparison of the cable harnessed frequency response functions from shaker experiment, decoupled and coupled analytical models for $x_s=248$ mm. Cabled Analytical (Decoupled EB) Cabled Experimental Cabled Analytical (Coupled EB) Cabled Analytical (Coupled Timoshenko)..... 104

Fig. 3. 7 Zoom in plots for frequency response functions for shaker experiment, coupled and decoupled models of $x_s=95$ mm for a) Mode 1 b) Modes 2 and 3 and c) Mode 4. Cabled Analytical (Decoupled EB) Cabled Experimental Cabled Analytical (Coupled EB) Cabled Analytical (Coupled Timoshenko). 106

Fig. 3. 8 Zoom in plots for frequency response functions for shaker experiment, coupled and decoupled models of $x_s=248$ mm for a) Mode 1 b) Modes 2 and 3 and c) Mode 4. . ----- Cabled Analytical (Decoupled EB) ——— Cabled Experimental ——— Cabled Analytical (Coupled EB) Cabled Analytical (Coupled Timoshenko). 107

Fig. 3. 9 Sensing and actuation locations for the two in-plane impact hammer tests..... 108

Fig. 3. 10 Frequency response functions for in-plane impact tests. a) impact test for $(x_{a1}, x_{s1}) = (55, 95)$ mm, b) impact test for $(x_{a2}, x_{s2}) = (31, 248)$ mm. 108

Fig. 3. 11 Coherence plots for the in-plane impact hammer tests. (a) $(x_{a1}, x_{s1}) = (55, 95)$ mm, (b) $(x_{a2}, x_{s2}) = (31, 248)$ mm. 109

Fig. 3. 12 First in plane bending dominant mode shape from the coupled analytical model. U, V, W, θ denote the axial, in-plane bending, out-of-plane bending and torsional mode shapes at the first in-plane dominant mode respectively..... 109

Fig. 3. 13 Experimental setup of the cable harnessed structure (a) Sample 2 (b) Sample 3. 112

Fig. 3. 14 Comparison of experimental frequency response function with theoretical frequency response function for Sample 2. ----- Cabled Analytical (Decoupled EB) ——— Cabled Experimental ——— Cabled Analytical (Coupled EB) Cabled Analytical (Coupled Timoshenko) 113

Fig. 3. 15 Experimental snapshot mode shapes for (a) first in-plane dominant (b) second in-plane dominant (c) first torsion dominant modes for sample 2..... 115

Fig. 3. 16 Theoretical mode shapes for (a) First in-plane bending dominant; (b) Second in-plane bending dominant; (c) First torsion dominant for sample 2 116

Fig. 3. 17 Comparison of experimental frequency response function with theoretical frequency response function for Sample 3. ----- Cabled Analytical (Decoupled EB) ——— Cabled Experimental ——— Cabled Analytical (Coupled EB) Cabled Analytical (Coupled Timoshenko) 117

Fig. 3. 18 Experimental snapshot mode shapes for (a) first in-plane dominant (b) second in-plane dominant (c) first torsion dominant modes for sample 3..... 118

Fig. 3. 19 Theoretical mode shapes for (a) First in-plane bending dominant; (b) Second in-plane bending dominant; (c) First torsion dominant for sample 3.	119
Fig. 3. 20 Frequency response function obtained from in-plane impact test (a) Sample 2 (b) Sample 3.....	121
Fig. 3. 21 Frequency response function of in-plane bending vibration of bare beam of sample 3	124
Fig. 3. 22 Top isometric view of the cable-harnessed structure undergoing in plane bending vibration	124
Fig. 3. 23 Experimental setup of a) Sample 1 b) Sample 2 for non-periodic wrapping pattern.	125
Fig. 3. 24 FRF comparison between the coupled, decoupled analytical models and the experiment for sample 1. Cabled Analytical (Decoupled) Cabled Experimental Cabled Analytical (Coupled).	126
Fig. 3. 25 Comparison of experimental and theoretical out of plane bending mode shapes for (a) Mode 4 (b) Mode 5. Experimental Centerline Analytical....	126
Fig. 3. 26 Theoretical plots for curvature for (a) Mode 4 (b) Mode 5 for sample 1	127
Fig. 3. 27 Coupled theoretical mode shapes (a) First in plane bending dominant (b) First torsion dominant (c) Second in-plane bending dominant for sample 1	128
Fig. 3. 28 Experimental snapshot mode shapes for (a) First torsion dominant mode (b) First in-plane bending dominant mode (c) Second in-plane bending dominant mode (d) FRF obtained from impact testing for sample 1	129
Fig. 3. 29 FRF comparison between the coupled, decoupled analytical models and the experiment for sample 2. Cabled Analytical (Decoupled) Cabled Experimental Cabled Analytical (Coupled).	131
Fig. 3. 30 Experimental testing of preliminary sample	132
Fig. 3. 31 Top view of the preliminary sample.....	133



Fig. 3. 32 Comparison of in plane impact FRFs for experiment of cabled beam of preliminary sample with and without glue.  cabled beam without glue  cabled beam with glue 133




Fig. 3. 33 Comparison of experimental and theoretical out of plane bending mode shapes for (a) Mode 4 (b) Mode 5 (c) Mode 6 for sample 2.  Experimental  Centerline  Analytical. 135

Fig. 3. 34 Theoretical plots for curvature for (a) Mode 4 (b) Mode 5 (c) Mode 6 for sample 2 136

Fig. 3. 35 Coupled theoretical mode shapes (a) First in plane bending dominant (b) First torsion dominant (c) Second torsion dominant (d) Second in-plane bending dominant for sample 2 ... 137

Fig. 3. 36 Experimental snapshot mode shapes for (a) First torsion dominant mode; (b) Second torsion dominant mode; (c) First in-plane bending dominant mode; (d) Second in-plane bending dominant mode; (e) FRF obtained from impact testing for sample 2..... 138

List of Tables

Table 2. 1 Material and geometrical properties of the cable harnessed beam structure. 41

Table 2. 2 Natural Frequencies for coupled and decoupled models for fixed-fixed boundary conditions (Hz)..... 46

Table 2. 3 Natural Frequencies for coupled and decoupled models for cantilever boundary conditions (Hz)..... 46

Table 2. 4 Natural Frequencies for coupled and decoupled models for simply supported boundary conditions (Hz)..... 47

Table 2. 5 Material and geometrical properties for the tension case study, rectangular cross-section beam..... 56

Table 2. 6 Material and geometrical properties for the tension case study, I-cross section beam58

Table 2. 7 System parameters for the samples 1, 2 and 3. 66

Table 2. 8 Coupled and Decoupled Natural Frequencies for sample 1..... 69

Table 2. 9 Coupled and Decoupled Natural Frequencies for sample 2..... 69

Table 2. 10 Coupled and Decoupled Natural Frequencies for sample 3..... 69

Table 2. 11 System parameters for the sensitivity analysis..... 70

Table 2. 12 System parameters for the sensitivity analysis in Table. 2.13 73

Table 2. 13 Sensitivity analysis for multiple frequencies with respect to the straight and periodic pattern cases 73

Table 2. 14 System parameters for transition frequency case study 75

Table 2. 15 Natural Frequencies for bare and cabled beam for both first and second spectra using TBT 78

Table 2. 16 System parameters for the samples 1, 2 and 3.	92
Table 2. 17 Coupled and Decoupled Natural Frequencies for Sample 1	94
Table 2. 18 Coupled and Decoupled Natural Frequencies for Sample 2	94
Table 2. 19 Coupled and Decoupled Natural Frequencies for Sample 3	94
Table 3. 1 Material and geometrical properties of the cable harnessed beam structure.	101
Table 3. 2 Natural frequencies for analytical and experimental models for cabled harnessed beam.	110
Table 3. 3 Natural frequencies for two different experiment sets for cabled harnessed beam. .	110
Table 3. 4 Effect of product of inertia terms on the natural frequencies.....	111
Table 3. 5 Comparison of Theoretical Natural Frequencies with Experiment for Sample 2.	120
Table 3. 6 Comparison of Theoretical Natural Frequencies with Experiment for Sample 3.	120
Table 3. 7 Natural Frequencies after updating the width parameter	122
Table 3. 8 Comparison of theoretical and experimental in plane bending dominant natural frequencies for bare beam of Sample 3.....	123
Table 3. 9 Coupled and Decoupled Natural Frequencies for Sample 1	127
Table 3. 10 System parameters for the sample for preliminary testing.....	132
Table 3. 11 Coupled and Decoupled Natural Frequencies for Sample 2	139
Table 3. 12 Ratio of the natural frequencies for different models	140

Nomenclature

$u(x, t)$	Axial displacement
$v(x, t)$	In plane bending displacement
$w(x, t)$	Out of plane bending displacement
$\theta(x, t)$	Torsional displacement
$\varphi(x, t)$	Rotation of cross-section about z axis
$\psi(x, t)$	Rotation of cross-section about y axis
ν	Poisson's Ratio
κ	Shear Correction Factor
E_b	Young's Modulus of the beam
G_b	Shear Modulus of the beam
A_b	Area of cross section of the beam
A_c	Area of cross section of the cable
E_c	Young's modulus of the cable
$b_1 - b_9$	Strain energy coefficients of Euler Bernoulli model
$c_1 - c_{15}$	Strain energy coefficients of Timoshenko model
$k_1 - k_6$	Kinetic energy coefficients
ω	Natural Frequency
ω_f	Driving frequency
x_s	Sensing location
x_a	Actuation location
$(\varepsilon_{xx})_b$	Direct strain in the beam in the x direction
$(\varepsilon_{xx})_c$	Direct strain in the cable in the x-direction
$(\gamma_{xy})_b$	Shear strain in the beam in the xy plane
$(\gamma_{xz})_b$	Shear strain in the beam in the xz plane
ρ_b	Density of the beam
ρ_c	Density of the cable
l	Length of the beam
b	Width of the beam

h	Depth of the beam
T	Pre-tension of the cable
r_c	Radius of the cable
y_c	y coordinate of the cable where the strains are evaluated
z_c	z coordinate of the cable where the strains are evaluated
A_c	Area of cross-section of the cable ($A_c = \pi r_c^2$), circular cross-section
A_b	Area of cross-section of the beam
μ	Cable wrapping angle for structure with periodic wrapping pattern
c_{ki}	Strain energy coefficients for Euler Bernoulli-based model of i^{th} fundamental element in non-periodic wrapping pattern. k and i are the indices.
$k_{1i} - k_{4i}$	Kinetic energy coefficients of i^{th} fundamental element in non-periodic wrapping pattern. i is the index
$u_i(x, t)$	Axial displacement of i^{th} fundamental element in non-periodic wrapping pattern
$v_i(x, t)$	In plane bending displacement of i^{th} fundamental element in non-periodic wrapping pattern
$w_i(x, t)$	Out of plane bending displacement of i^{th} fundamental element in non-periodic wrapping pattern
$\theta_i(x, t)$	Torsional displacement of i^{th} fundamental element in non-periodic wrapping pattern
ψ_i	Cable wrapping angle i^{th} fundamental element in non-periodic wrapping pattern

Chapter 1: Introduction

1.1 Literature Review

1.1.1 Motivation

Large space structures are often too large for dynamic ground testing as a whole. Therefore, a common approach to model validations for these structures entails ground testing the individual components prior to their launch. One major component for these structures include electronic cords and power cables that have been commonly ignored the effect of cabling in modeling these structures. These cables have shown to weigh up to 20% of the mass of the host structure [1]. This number will increase significantly with the use of composite materials in aerospace applications. Therefore, obtaining a dynamic model that accurately accounts for the mass, stiffness and damping effects of these cables is of paramount importance and has received a lot of attention in the past few years [2–11]. As an example, the satellite structures of National Aerospace and Space Administration (NASA) are shown in Figs. (1.1) and (1.2). The structures are harnessed with significant amount of cabling which will affect the dynamic characteristics of the host structure. The arrangement of cables can be in a straight or in a periodic or non-periodic manner and the cables come in various sizes. The U. S Air force Research Laboratory (AFRL), Space Vehicles Directorate group were the first to perform significant study in this area. Fig. (1.3) shows the setup of the space structure on the vibration shaker to perform vibration testing. Spak [12] points out that the space structures are usually tested prior to harnessing them with cables. Therefore, in the experimental testing, the effects of cabling are not usually seen. Depending on the amount of cabling on the structure, there will be significant shift in the peaks of the frequency response function of the structure. The structures usually exhibit large amplitude motions near the resonant regions. Hence, there is a need to develop good theoretical models that can predict the effect of cabling on the dynamics of host structure to accurately have an information regarding the natural frequencies of the structure. In the initial stage of research in this area, the effect of cabling is investigated using finite element models. Finite element analysis is a numerical technique, which often involves discretizing the structures into large number of elements to obtain good results. As the structure gets complicated, it becomes difficult to obtain physical insight into the problem

using FEA models. In case of cable-harnessed structures, there is an important need to obtain physical insight as to how the cabling affects the natural frequencies of a structure and what parameters or effects play an important role. This is better possible by developing analytical or distributed parameter models. In the research performed by the U.S Air force research group, experimental and theoretical studies are performed on scaled down structures where the host structure is modelled using beam theories (Fig. (1.4)). Deeper analysis on scaled down structures will help us physically understand how the dynamic characteristics are affected by cabling and the models on small-scale structures can later be extended to understand the behavior of larger scale structures. In their studies, cables are attached to the beam and plate host structures. In addition, in space structures, the beam and plate structures are the major load carrying members. The theoretical models developed are for beam structures due to their theoretical simplicity when compared to plates. More details regarding the U.S Air force and other research groups in the area of cabled structures are discussed in the following subsections of this chapter.

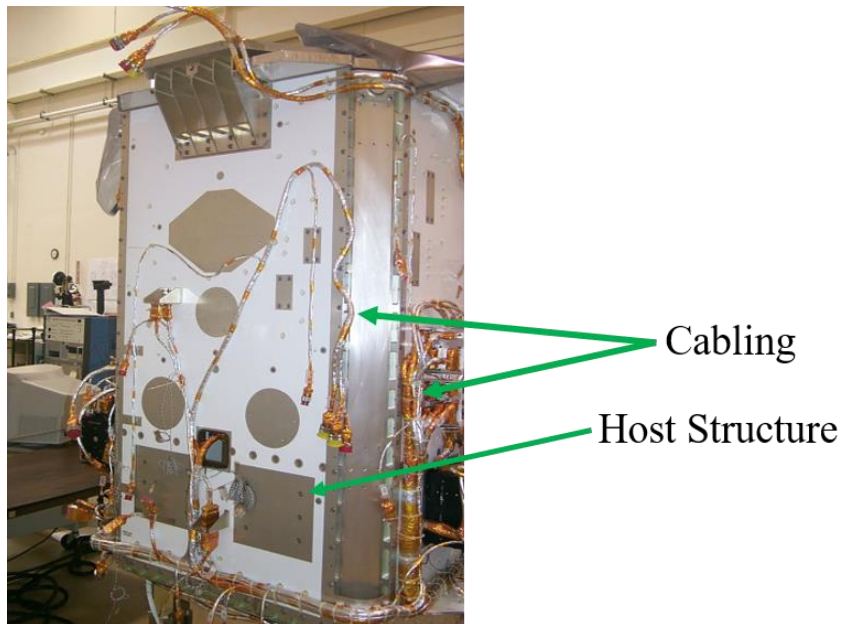


Fig. 1. 1 Cable Harness in NASA satellite structure, Image Courtesy: NASA ICESat Website [13].

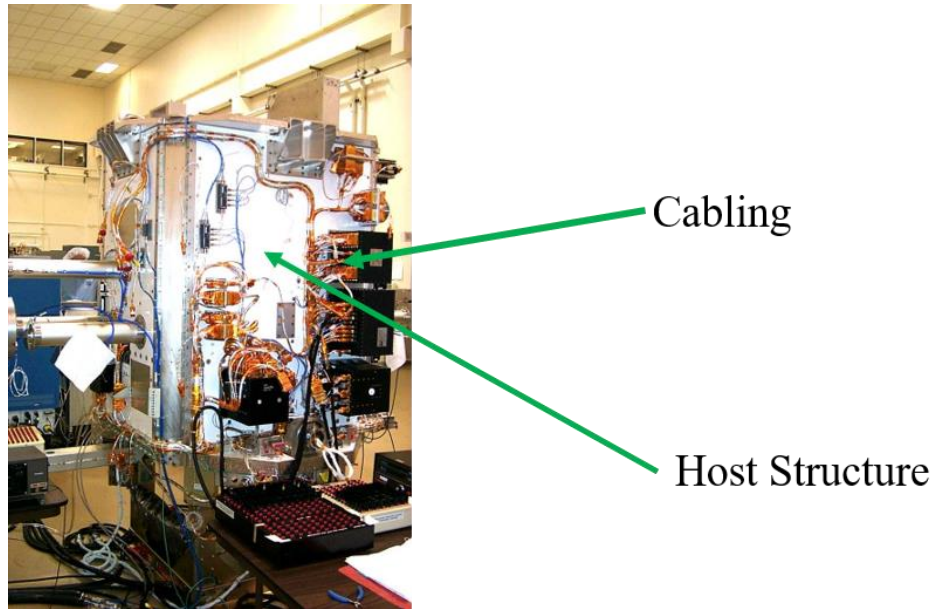


Fig. 1. 2 Cable Harness in NASA satellite structure. Image Courtesy: NASA ICESat Website [13].



Fig. 1. 3 Setup of NASA Satellite structure on shaker for vibration testing, Image Courtesy: NASA LADEE Website [14].

1.1.2 Research by U.S Air force Group in Cable-Harnessed Structures

As a general overview regarding analytical methods, the mathematical model of vibration of physical structure such as a beam or cable is usually obtained using force or energy methods. As the structure gets complicated, it is difficult to account for all the moments or forces in a

structure using force method and in that case, energy methods are preferred. For a distributed parameter structure, the strain and kinetic energy of the structure are computed and the Lagrangian of the system is found out. The final equations of motion are obtained by taking the variation of the time integral of the Lagrangian. This is referred to as the Hamilton's principle. The equation is shown in Eq. (1.1).

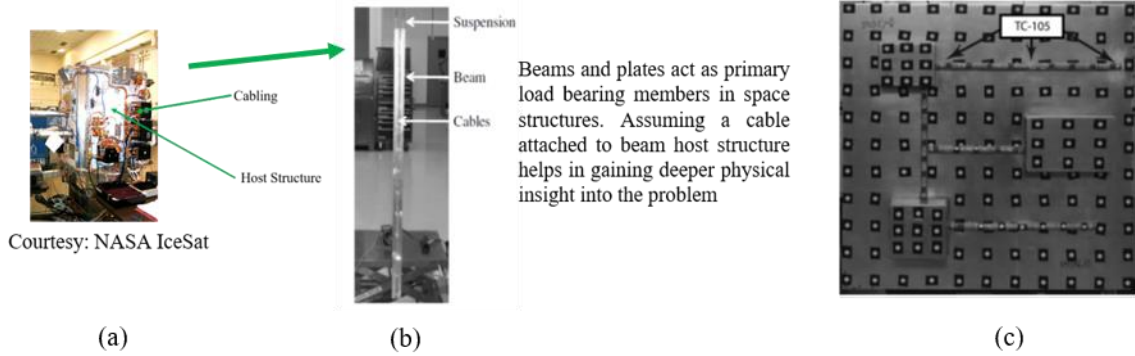


Fig. 1. 4 Cable Harnesses in beam and plate structures by the U.S Air force research laboratory group. Image Courtesy: (a) NASA ICESat; (b) Babuska et al, JSR, 2010 [2]; (c) Coombs et al, JSR, 2011 [1].

$$\delta \int_{t_1}^{t_2} (T - U) dt = 0 \quad (1.1)$$

T and U in Eq. (1.1) stand for kinetic and strain energy of the system respectively. Once the governing partial differential equations are obtained, the vibration characteristics of the structure such as the natural frequencies, mode shapes and the frequency response functions are found out using analytical methods. These analyses give an overall picture of the dynamic response of the structure. Previous research in the area of vibrations of cable-harnessed structures by the U.S Air force research group includes ad hoc techniques that mathematically model these cables as lumped masses attached to the host structure ignoring their stiffness and damping properties [15]. To overcome deficiencies in the earlier models, [1] considers the effect of distributed mass, stiffness and damping effects of cables where added cables are modeled as a beam structure attached to a host specimen. Ref. [1] models the cables using shear-beam theory. Shear beam theory incorporates the effect of shear deformation, which is ignored in the Euler-Bernoulli model. The dynamics of cabled beam is studied using analytical methods. The paper reports bending modes related to the host structure and the cable. It is reported that at higher vibration modes, the cables start to vibrate and induce dissipative effect in the cable-harnessed system. This apparent damping is usually more significant in the higher modes. The shear beam model (for cable) predicts this

apparent damping effect better than the case where the cable is modelled using Euler-Bernoulli beam model. Goodding et al [3] developed methods to attach the cable to the host structures with the help of tie-down structures and performed vibration testing on cabled beam to capture the bending modes for the free-free boundary condition. Comparison of experimental data of bare beam and cabled beam showed significant change. The paper considers two different systems, one is cabled beam with cable at the center line and the other with serpentine configuration. The experimental study between the two different systems concludes that the frequency response functions of the two systems are similar and serpentine configuration shows greater damping for the higher modes. The cabled beam is modeled using beam theory. The paper also developed Finite element models to study the bending vibrations and the natural frequencies of cabled beam dynamic model match well with that of FEA. The bending frequency response functions obtained from the FEA are validated using experiments. The paper reports that at lower modes of bending vibrations, mass effects dominate and at higher modes, the damping effects are dominant. Babuska et al [2] models the host structure and cable using Euler-Bernoulli beam theory. They develop distributed parameter model for transverse vibrations of cable and beam. It is also shown in their work that the stiffness effects are dominant in the lower vibration modes, whereas, the damping effects dominate the higher modes of vibrations. Kauffmann et al [5] developed novel damping model using shear beam theory assumptions. In the lower modes of vibration, the damping ratio almost remains constant and in the higher modes when we see significant shear vibrations, the damping ratio linearly increases with mode number and the model proposed in the paper matches well with the experiment. Remedea et al [7] investigated the effect of cabling on the vibration of cable harnessed honey comb panel. The theory model proposed is simulated using Craig-Bampton stochastic method and provided better result than the full scale monte carlo simulation and the model proposed in the paper is also computationally efficient than the monte carlo simulation. Goodding et al [16] models cable and host structure using beam theory, developed methods to estimate geometric properties of the cable such as the effective area, modulus etc. Goodding et al also developed linear finite element models (FEM) to model the bending vibrations of cable-harnessed beams and validated the FEM model with the help of experiments. Ref. [17] develop a theoretical model for a cable-loaded panel. The host structure considered is a plate and cables are attached to it. The paper develops finite element model to predict the vibration characteristics of the cable loaded panel and the finite element model is validated with experiments. Other papers

on cable or string attached to beam (not related to space structure applications) are: Ref. [18] models the vibrations of two beams elastically connected together using an elastic foundation using Euler-Bernoulli theory. Exact solutions of natural frequency are presented for simply supported boundary conditions. Ref.[19] extended their previous work by performing analysis of beam and string system connected by elastic layers. It was observed that variation of tension in the string significantly changed the bending natural frequency of the structure for simply supported boundary conditions. Other papers of interest in the related area include tensioned string attached to beam near boundaries and the string and beam have different coordinate of out of plane vibrations. The papers [20–24] report non-linear behavior in the structure although the papers lack experimental analysis or validation.

1.1.3 Other Structural Application of Vibration Analysis of Cables

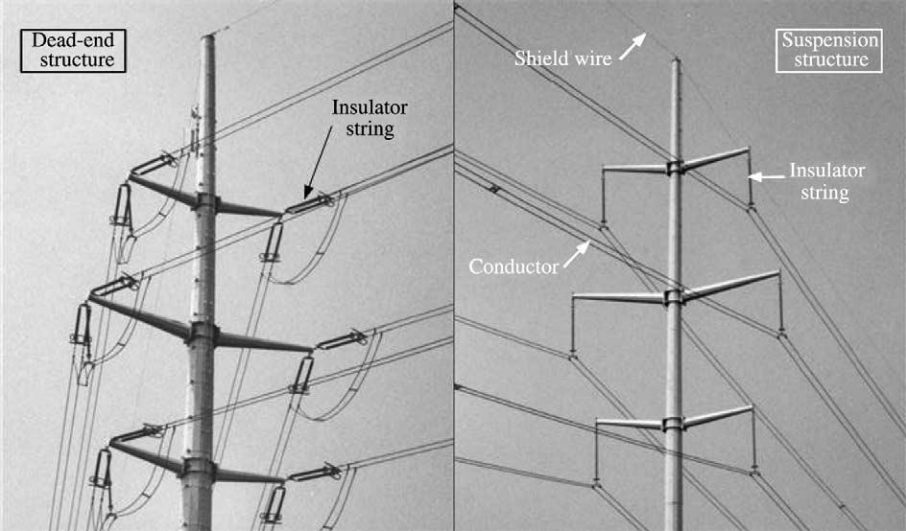


Fig. 1. 5 Applications of cables in power lines. Courtesy: McClure et al, Computers and Structures, 2003 [25]

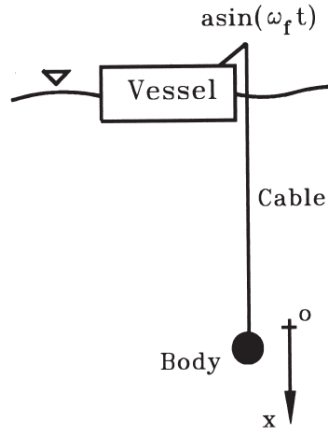


Fig. 1. 6 Marine applications of cables. Courtesy: Huang et al, Appl Sci, 1999 [26]

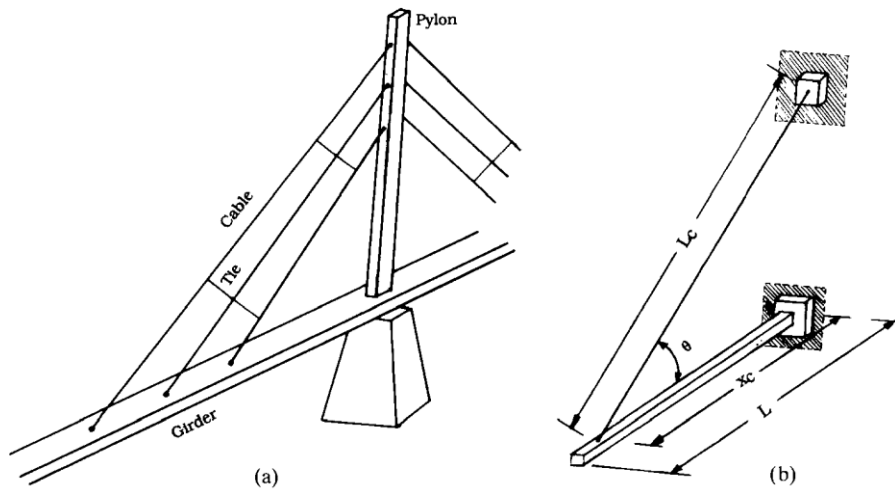


Fig. 1. (a) Cable-stayed bridge; (b) cable-stayed beam.

Fig. 1. 7 Applications of cables in bridge structures. Courtesy: Fujino et al, Appl Sci, 2017 [27]

Apart from space structures, cables also have important structural applications in the areas of (but not limited to) power lines and marine applications. In power lines [25] (Fig. (1.5)) stranded cables are used frequently, where several wires are twisted to form a single cable. Ref. [25] models the dynamic response of power transmission cables when subjected to shock loads. The stranded cables considered in [25] comprise of aluminum and galvanized steel. Ref. [28] develops mathematical models to determine the bending stiffness of stranded cables which have application in power and signal transmission. In marine cables [29] two layers are present. Armor layer is the outer, which provides the mechanical strength, and the inner layer contains optical fibers and conducting wires [29]. Ref. [26] (Fig. (1.6)) states that the marine cables usually cannot withstand

compressive load and operate in tension-slack condition which results in non-linear behavior. In space structure applications, the power cables are attached to the host structures using zip-ties and the cable resonances are usually observed in the higher modes and the presence of cabling significantly effects the dynamics of the host structure [2].

Some of the other areas of applications of cables are in the area of cable-stayed bridges where bridge structures are supported by cables. It is observed that there will be nonlinear effects in cable-stayed bridges and the references are explained in this paragraph. Dallasta et al [30] analyzed bending vibrations of beams pre-stressed by internal cables which are attached to the beam at the boundaries. The beam considered is a thin walled beam pre-stressed by a parabolic cable. It was found that the increase in cable force increased the frequency and the change in the frequency is more significant for higher frequency modes. Fujino et al [27] (Fig. (1.7)) modeled the non-linear vibrations of cable-stayed beam. The structure investigated has similarity to the cable-stayed bridges. The tension effect of cables is considered and the beam structure is assumed to vibrate in the in plane and out of plane direction. The cable is also assumed to vibrate in the horizontal direction and it was observed that auto-parametric resonance exists in the structure and this phenomenon is validated experimentally. Gatulli et al [31] built on the work of Fujino et al and assumed the beam and cable vibrate separately in one direction. Gatulli et al investigated additional non-linear resonances such as 2 to 1 resonance, internal resonance condition and found the existence of period doubling bifurcation condition. Other related references on nonlinear vibrations of cable-stayed vibrations can be found in Refs. [32–36]. Liu et al [32] modeled the vibrations of deck-cable system. The deck-cable system is coupled (separate displacement assumptions of deck and cable which are coupled) and the dynamic model is analyzed for a single cable attached to deck and the results are validated using three-dimensional finite element method. The system has pure cable modes, pure deck modes and coupled cable-deck modes and the presented analytical model is able to accurately predict the coupled cable-deck modes. Kang et al [33] modeled the nonlinear vibrations of cable-deck system. The degrees of freedom considered are the in plane and out of plane bending vibrations of cable and out of plane bending vibrations of deck. The paper reports observation of parametric resonances that 1:1 ratio condition between the out of plane and in-plane bending modes will cause large displacements in the structure. Lepidi et al [34] models quadratic non-linearity in the coupled cable-bridge system. The system is modelled using discrete lumped masses. The degrees of freedom considered are the in plane and

out of plane bending vibration for the cable and the out of plane and torsion vibration for the bridge. When the bending and torsional vibrations of the bridge are subjected to forced excitation, it is found to cause out of plane bending vibrations in the cable through parametric resonance. In Ref. [35], the system considered is a beam with string attached to beam at boundaries and the paper investigates nonlinear and chaotic motion. The case of 1 to 2 resonance between the string and beam is investigated. The equations of motion are solved using the method of multiple scales. It is observed the excitation amplitudes play an important role on the vibrations of the structure.

1.1.4 Research by Other Research Groups in Cable-Harnessed Structures



Fig. 1. 8 Cable harnessed structure experimental setup by Inman research group. Courtesy: Spak, PhD thesis, 2014, Virginia Tech [12]

Apart from the U. S Air force, the research performed by other groups in the area of cable-harnessed structures are, Spak et. al Refs. [12,28,37–43] (Fig. (1.8)) modeled the spaceflight cables using the shear and Timoshenko beam theories and developed theoretical models to determine various effective properties of non-homogenous space flight cables such as density and Young's modulus.



Fig. 1. 9 Cable harnessed structure to validate the spectral element method by Inman research group. Courtesy: Choi et al, JSV 2014 [44]

The initial phase of Spak et al work studies the frequency response of strings and space flight cables. In Ref. [37], the main focus is on the bending vibrations of the cable. The theoretical FRF is plotted using the effective properties determined and is compared with the experimental FRF and the theory showed good match with the experiment. Using the predicted properties, the frequency response characteristics of bending vibrations cable harnessed structures are found out using analytical methods and the predicted frequency response functions are validated using experiments. In Ref. [39,40] Spak et al developed damping models to quantify the damping induced by cabling. The paper concludes that the Timoshenko beam predicts damping and frequencies better than Euler-Bernoulli beam due to rotary inertia and shear deformation effect. Ref. [42] developed distributed transfer function method (DTFM) to predict the damping and other modal parameters in cabled structure and the DTFM model takes into account the cable attachment points and it was found that the DTFM predicts the frequencies and damping better than the distributed mass model. The experimental investigations in Ref. [45] study the bending vibration characteristics of cables (modeled as beams). Spak et al report that as the tension in the string, cables vary, the structure's frequency response shifts slightly, and no major effect of tension is seen. The paper validated the cable models for bending modes that are developed using beam theory (model solved using DTFM approach) with the experiments. Extensive experimental investigations in [12] focus on cabled beams and reports the existence of cable-beam interaction modes and coupled bending-torsion modes. Spak et al report that when host structure is harnessed with thick space flight cables, the presence of interaction and torsional modes is seen experimentally. The analytical model by Ref. [12] neglects the effect of bending torsional coupling in the cabled structure. Ref. [12] compares the analytical model's bending frequency response function with that of experimental frequency response function.

Choi et. al [44,46–48] (Fig. (1.9)) model both the bending vibrations of cable and beam structures using Timoshenko beam theory (TBT). The cable is attached to the beam using tie down structures. The cable-harnessed structure is modeled as a double-beam problem using Timoshenko beam theory. The displacements of host structure and the cable are different. The problem is solved using spectral element method where the displacement functions are defined using standard exponential form. Impact test experiments are performed on the practical structures and the results show good agreement with the theory for the free-free boundary condition tested. The bending vibration coordinates are modeled in these papers and the motion of the structure in other directions

and the coupling effects are neglected. The frequency response functions for the bending mode obtained using the Spectral Element Method (SEM) are compared with the Finite Element Method (FEM). Authors [44] conclude that Spectral Element Method uses significantly lower number of elements when compared to the FEM method. Huang et al [49,50] extends this spectral element approach developed by Choi et al [44] to study the bending vibration characteristics of a cantilevered cable-harnessed beam with a tip mass at the free end. The mathematical model [49,50] also accounts for damping in the structure, apart from extensively studying of tip mass. Huang et al attaches cable to the beam at discrete locations and develops solutions using Cheybshev spectral element method to study the bending vibrations in cable-harnessed structure. In this method, Cheybshev polynomials are used as basis function while finding the natural frequency and the paper reports that more accurate results can be obtained using fewer elements when compared to the other Spectral element methods published in literature.

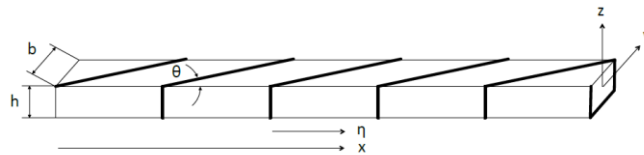


Fig. 1. 10 Periodic wrapped cable-harnessed structure. Courtesy: Martin et al, AIAA 2016 [51]

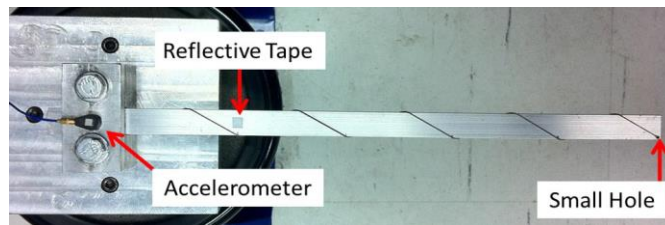


Fig. 1. 11 Experimental setup of periodically wrapped cable-harnessed structure. Courtesy: Martin et al, AIAA 2016 [52]

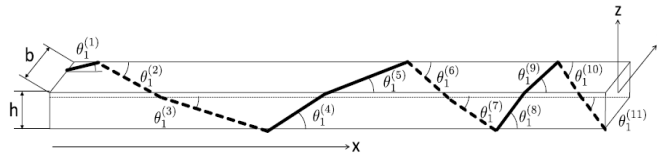


Fig. 1. 12 Non-periodic wrapped cable-harnessed structure. Martin et al, AIAA 2018 [53]

Martin et al [51–60] (Figs. (1.10) to (1.12)) developed analytical models along with their experimental validations for cable-harnessed beam structures with periodic and non-periodic cable patterns. In their work, cables are modeled using both bar and string element assumptions to develop low order, high-fidelity distributed parameter models for bending vibrations of the cable-

harnessed beam structures of periodic patterns. The main goal of Martin et al work is to predict the stiffening and mass effects induced by cabling on the beam structures using decoupled bending vibration model. Ref. [51,52] models the decoupled vibrations of cable harnessed structures with periodic wrapping pattern. The mathematical model takes into account the pre-tension effects of adding cable along with the pre-compressive effect induced in the host structure. The model could predict that by adding cable to host structure there is significant amount of stiffening effect. Numerous simulations are presented by varying parameters such as the number of fundamental elements of wrapping pattern, cable radius and the modulus of the cable to show case the importance of having a mathematical model to predict the stiffening effect. The theory model is validated experimentally in Ref. [52] and the theory shows good agreement with the experiment. Refs. [54–57] are some of the early modeling attempts by Martin et al to study the stiffening effects. The pre-tension effects are neglected in those papers and the cable is modeled using bar model. These models are later built upon and improved in Refs. [51,52]. In Ref. [60], Martin et al solved a stepped beam which periodic elements using Lindstedt-Poincare theory for the decoupled bending vibrations. The coefficients for the stepped beam are variable and the frequencies and mode shapes are calculated using perturbation theory. The theory developed in Ref. [60] is applied to cable harnessed structures with non-periodic wrapping pattern in Ref.[53] by Martin et al. In non-periodic wrapping pattern, the cable has different wrapping angle in each fundamental element. Martin et al modelled the decoupled bending vibrations. In case of zigzag wrapping pattern with inclined side sections, the coefficients of partial differential equations become dependent on the spatial coordinate. The spatially variable partial differential equations (PDEs) are solved using Lindstedt-Poincare approach and the results are experimentally validated. Partial Differential Equations (PDEs) that account for cables' mass, stiffness and tension properties on the system's dynamics are developed. In all the developed models in [51,52,54–57], the out-of-plane bending is of primary interest. The method used employs the homogenization technique for truss structures in [61,62,71,72,63–70] to obtain the PDE's using a linear displacement field through the strain and kinetic energy expressions of a fundamental repeated elements. The asymmetric wrapping pattern in Fig. (1.10) could potentially create mode-coupling effect as the intensity of cabling on the host structure is increased. The coupling induced between various coordinates of vibrations due to the addition of the cables is entirely neglected in their modeling.

1.1.5 Effect of Coupling between Vibration Coordinates in Other Structures.

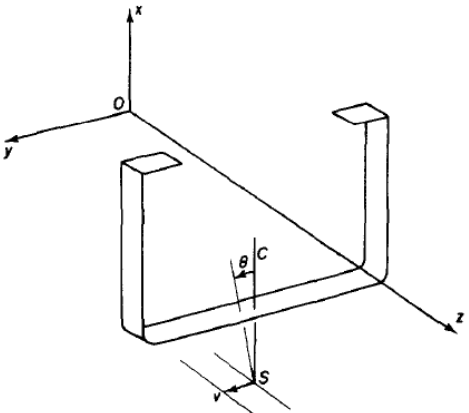


Figure 1. Beam geometry.

Fig. 1. 13 Coupling due to geometry of C cross-section beam. Courtesy: Bishop et al [73]

In the area of cable-harnessed structures, the effect of coupling between various coordinates of motion is not studied before. The other areas/structures in which the mode coupling effects between various coordinates are observed are explained in this section. Dokumaci [74] investigated the coupled bending-torsion vibrations in beams with single-axis symmetry where the shear center and the centroid do not coincide. In this case, because of offset distance between the shear center and the centroid, we see mass coupling between the bending and torsion coordinates. The paper by Dokumaci presents exact results for free-free and clamped-free boundary conditions. Bishop et al [73] (Fig. (1.13)) extended Dokumaci’s theory to incorporate the effect of warping in beams with single axis of symmetry and it was observed that the warping effect becomes significant in beams with open channel cross-sections. The example of a beam structure with single axis symmetry that undergoes coupled-bending torsion vibration is shown in Fig. (1.13) [73]. Banerjee [20,22,23,75] improved Bishop et al work by solving the governing equations of motion using dynamic stiffness method to obtain frequencies from beam with single-axis symmetry. The cases investigated by Banerjee et al also includes the effect of external axial load. The dynamic stiffness proposed in Banerjee et al research resulted in lower computation time and higher accuracy for calculating the natural frequencies. Burlon et al [21] extended the works of Bishop et al and Banerjee et al to include the effect of in-span masses and springs in beams with mono-symmetric cross section and analyzed the coupled bending torsional vibrations.

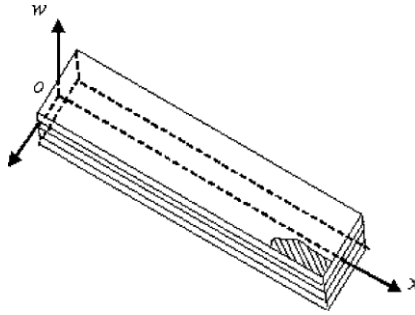


Fig. 1. 14 Material coupling in composite structures. Courtesy: Mei et al, Composite and Structures, 2005 [76].

Lee et al [77,78] analyzed fully coupled vibrations of thin walled composite beams with I section and beams with mono symmetric cross section using Euler-Bernoulli theory. The natural frequencies by Lee et al are found by finite element method by developing the mass and stiffness matrices and solving for eigen-value problem. The variation in frequencies is analyzed for various parameters such as the fiber orientation, boundary conditions. Vo et al [79] analyzed coupled vibrations of thin walled beams with doubly symmetric cross-sections. The natural frequencies are obtained using Finite Element method. The cases analyzed consists of symmetric and asymmetric stacking sequence of the laminates. Vo et al [80] modeled the coupled bending torsion of composite thin walled beams using shear-deformable theory and is able to predict the buckling loads on the structure through the external axial load-frequency analysis. Vo et al [81,82] developed fully coupled vibration model of thin walled composite beams. The coordinates considered include bending in both the directions, axial, twist and both the rotations of cross-section. Vo et al also predicted the loads at which the structure would buckle using the fully coupled model. So far, we have seen coupling between coordinates in beams with mono-symmetric cross section where coupling is because of offset distance between shear center and the centroid.

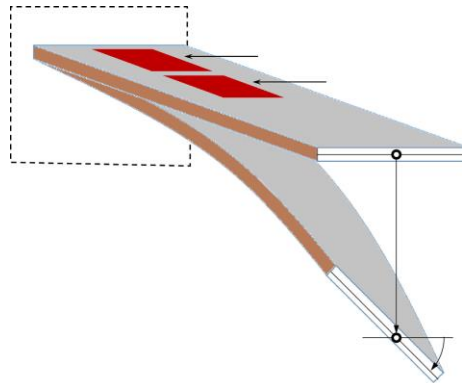


Fig. 1. 15 Coupled Bending-torsion vibrations in piezoelectric composite structure. Courtesy: Xie et al, MSSP, 2018 [83].

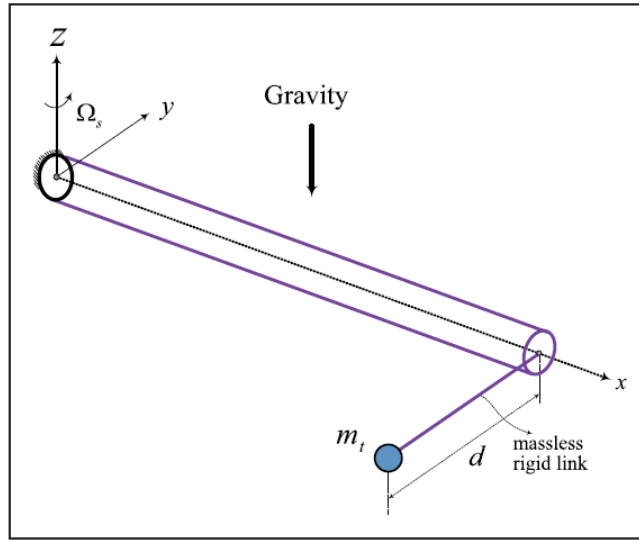


Fig. 1. 16 Coupled bending-torsion vibrations in beams with eccentric tip mass boundary conditions. Courtesy: Al-Solihat et al, 2018 [84]

In Ref. [85], Dennis et al analyzed coupled bending-torsion in tapered beam with C cross section using Galerkin's approach. The papers described so far lack experimental validation. Dennis et al experimentally validated their mathematical model. Normally, in beams with symmetric solid cross-section we do not expect coupling between various coordinates. In Ref. [86] models coupled bending-torsional vibrations in beams with solid rectangular cross-section. The coupled vibrations are because of externally applied torques. The coupled partial differential equations are solved using Green's method and the natural frequencies obtained using proposed method matched with the results obtained from the methods presented in the literature. In Ref. [87] Aldraihem et al studied the coupled bending and torsional vibrations of laminated beams. In the paper, it is mentioned that coupling in the beam structures occurs due to four main cases: due to geometry of the structure, offset mass, stiffness related terms and external loading. Orthotropic PZT layers are attached and the coupled bending-torsion vibrations in the laminated beam with offset mass are actively controlled using the PZT layers. Stoykov et al [88] studied the coupled bending and torsional vibrations in a beam with external load. The load creates coupling between the bending, torsion coordinates, and the paper develops new p-version elements and performs the vibration analyses using finite element method. Bhadbhade et al [89] studies coupled bending torsion vibrations in beam gyroscopes where the base of the cantilever beam is assumed to rotate. The structure is excited using a PZT actuator. Due to rotation, the coupling between the bending and torsion terms occurs due to the gyroscopic terms. The paper concludes that as the angular

velocity of the base rotation is increased, the coupling between the bending and torsion mode gets stronger. Eslimy-Isfahani et al [90] extended the work by Banerjee et al [20] to incorporate the effect of damping to study the coupled bending-torsional vibrations of an aerofoil structure. The coupled term because of damping is also included in the model. In addition, the forced response of the structure under deterministic and random excitation is also studied in the paper. The mean square values of the bending, torsional displacements along the length of the structure are presented for different damping ratios, and the response amplitude is found to decrease for higher damping ratios for both the bending and torsion coordinates. Lenci et al [91] studied the effect of nonlinear coupling between the bending and axial coordinates in the case where the structure is axially restrained. The model neglects damping and investigated into the parameter, which causes hardening and softening behavior backbone curves in the structure. Yang et al [92] models 6 degree of freedom coupled vibrations in rotating Timoshenko beam. The coupling between coordinates is created by the gyroscopic and centrifugal effects induced due to rotation of one end of the structure. The effect of coupling caused by damping is ignored in the work. The phase differences in the motion of different coordinates caused by coupling is investigated in the work. In Ref. [84] Al-Solihat et al (Fig. 1.16) developed a model to study the coupled bending-torsion vibrations in a rotating Timoshenko beam. An off-axis tip mass is attached to the structure. The main contribution in the work is to include and study the effects of tip mass and damping. The coupling term between the bending and torsion mode induced by the damping is also included in the work. Consideration of internal damping in the structure yielded in considerable reduction in the simulation time. Shakya et al [93] studied the flutter characteristics in composite aerofoil with bending-torsion modes coupled. The structure is subjected to aerodynamic loading. Parametric studies are conducted by changing the ply orientation angle in balanced and unbalance laminates. It is shown that the critical flutter speed can be increased by 100 % in the case of blades with asymmetric skin and off-axis fiber angles. Ref. [83] (Fig. 1.15) models the bending torsion vibrations in piezoelectric composite structure. The aim of the paper is study, the effect of mode coupling on energy harvesting capabilities of a structure. It is concluded that the coupling improved the multi-mode energy harvesting capabilities of the piezoelectric structure and the results are experimentally validated. The model ignores the effect of damping. In the recent past, researchers working in the areas of energy harvesting have investigated into effect of coupling between bending and torsion coordinates on the power output of piezoelectric structures, some of them are

[94–98]. Hwang et al [99] investigated the coupling between bending-twist and bending-axial modes in laminated composite structures. The main contribution of the paper lies in investigating the effect of damping on mode coupling. When the fiber orientation angle is at 30 degrees, the damping predicted from the coupled model is dominant for the first three flexural modes. When the fiber orientation angle is at 90 degrees, the damping from the non-coupled model is dominant and when the fiber orientation is 0 degrees, the damping from the torsion coordinate is maximum. Lee et al [100] proposed a spectral element method to find the coupled bending-shear-torsion vibration characteristics of axially loaded composite Timoshenko beams. The model also includes the effect of damping. The observation from the paper is that the spectral element elements gives results with higher accuracy, converge with that of finite element method, and could accurately capture the damping effects. Chortis et al [101] modeled the coupled vibrations in composite blades, which exhibit coupled behavior. The focus of this work is to investigate the effect of coupled damping terms. The model is solved using finite element method. The paper concludes that the inclusion of coupled damping terms significantly improved the damping ratios prediction of the blade and this is demonstrated by comparing the damping ratios obtained from theory and experiment. The references described in this paragraph highlight the importance of having a coupled vibration model to study vibrations of structures where it is expected that coupling significantly affects the dynamics of the system. In the current research, the host structures considered are symmetric and isotropic materials are considered. Normally, such structures do not exhibit mode coupling. After the addition of cabling, the coupling effect between various coordinates will come into picture. For Fig. (1.10), as the cabling increases, the stiffness due to diagonal section members also increase and the coupling effect is in cable-harnessed structures will occur due to the stiffness terms. Due to this, the natural frequency prediction by the decoupled models will not be accurate and the coupling effect needs to be incorporated into the existing mathematical models. The advantage of having coupled model for cable-harnessed beams is it helps in accurately predicting the natural frequency peaks of the cabled structure when compared to the decoupled model assumptions.

1.1.6 Transition Frequency in Timoshenko Beams

It is observed in existing literature that for Timoshenko beam theory there exists a cut-off or transition frequency and the frequency spectra of Timoshenko beams is divided into two parts. The natural frequencies below the cut off frequency belong to the first spectrum where the bending dominant modes are seen and in the natural frequencies above the cut off frequency, both bending dominant and shear dominant modes are seen. Papers [76,102,111–117,103–110], explain the concept of transition frequency in Timoshenko beam theory. Ref. [102] explains that the concept of transition frequency and the second spectrum occurs only in beams with simply-supported boundary condition and concluded that other boundary conditions such as fixed-fixed, free-free and fixed-free etc. does not exhibit the second spectrum. Abbas et al used finite element procedure where higher order element is used. Bhashyam et al [104] used linear element for finite element simulations and observed that the second spectrum exists for boundary conditions other than the simply supported boundary conditions. Levinson et al [105] argues that there is no specific second spectrum of frequencies using Timoshenko beam theory and presented frequencies for simply supported boundary conditions using analytical method. Stephen et al [106,107] explained through his study that the concept of transition frequency is also seen in guided-guided and guided-hinged boundary conditions apart from hinged-hinged boundary conditions. Stephen et al concluded that the concept of second spectrum in Timoshenko beam theory is not practical and can be disregarded. Bhaskar [108] pointed out that the Timoshenko beam theory gives an additional branch of frequencies which correspond to thickness-shear modes and explained that these modes have practical significance and challenged the conclusion in the Stephen et al papers. Oliveto [111] examined the vibrations of axially loaded Timoshenko beams and reported that Timoshenko second spectrum frequencies are observed in the first few structural modes. In-depth analysis for mode shape behavior in Timoshenko beam with simply supported ends is presented by Cazzini et al [109]. The paper [109] concludes that for simply supported boundary condition, the wave numbers corresponding to the mode shapes are decoupled and the first part and second part of the spectrum produces similar mode shapes for both bending and rotation of cross-section coordinates. As per the mathematical expressions presented for the mode shapes by Cazzini et al, at the transition frequency, the structure has pure-shear vibration mode and this divides the frequency spectra into two parts. In the first spectra, we see bending dominant modes and in the second

spectra, we see both bending dominant and shear dominant modes. More mathematical explanation is provided in Chapter. 2. Li [112] analyzed the bending vibrations of functionally graded beams using Timoshenko beam theory for simply supported boundary condition and reported that the second spectra of Timoshenko beam exists in functionally graded beams. Cazzini et al (Ref.[103]) also studied the concept of transition frequency in beams with fixed-fixed and cantilever boundary conditions. Cazzini et al concluded that for boundary conditions other than simply supported boundary condition, the transition frequency is not a part of spectrum. However, by the mathematical nature of the mode shape parameters he divided the behavior of frequencies of Timoshenko beam theory into two spectra and their study concludes that the two spectra exist for all boundary conditions with the thickness shear modes having important practical significance especially when the length to thickness ratio of the structure is very small. Ref. [76] studied the concept of transition frequency in cantilevered composite Timoshenko beams. The composite structure considered in [76] has material coupling between the bending, rotation of cross section and the torsion modes and the study by Mei (Fig. (1.14) concluded that the presence of material coupling has no influence on the cut off or transition frequency. The major contributions of each chapter of this thesis is explained in the further paragraphs.

1.1.7 Key Gaps in the Literature

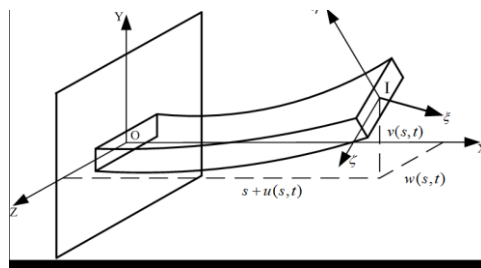


Fig. 1. 17 Coupled bending torsion motion in piezoelectric beam. Courtesy: Shan et al, Appl Sci, 2017 [95].

In the literature, pertaining to the vibrations of cable-harnessed structures published so far, the effect of coupling between various coordinates of vibrations such as the axial, out of plane bending, in-plane bending and torsion is neglected. The analytical models published in the literature only include the vibrations of structure in the out of plane bending direction. An example from the literature of a beam structure undergoing coupled vibration can be seen in Fig. (1.17). The work published in [95] studies the bending-torsional coupling in a piezoelectric beam with eccentric tip mass which creates eccentricity the centroid and the shear center. The work done by U.S Air force, Inman research group addressed a gap in literature by studying the distributed mass,

stiffness and damping effects of cabling. Martin et al [51–53,58] from University of Waterloo developed lower order distributed parameter models with the goal of obtaining deeper physical insight into the mass and stiffening effects of cabling on the host structure. In Martin et al’s work [51–53,58], although the model published gave good match with the experimental results. It remains to be investigated, the accuracy of Martin et al’s model when the cabling becomes more significant on the host structure and could make the existing model inaccurate in predicting the natural frequencies. In this thesis, the effect of coupling between various coordinates is investigated and compared to Martin et al decoupled model [51–53,58] natural frequencies and frequency response functions for structures with more significant cabling.

1.2 Objectives and Scope

The objective of this thesis is to develop analytical models to study the coupled coordinate vibrations in cable-harnessed structures. The theoretical model is to be validated with experiments. Three different systems are investigated. The first one is the beam with straight cable attached at an offset position, beam with periodic cable wrapping pattern and with non-periodic cable wrapping pattern. A main object of the mathematical model is to extend the studies in [51,52,54–57] to investigate the effects of coupling induced in the system due to presence of the cables on the host structure. The system with straight cable at an offset position represents the first attempt on the coupled vibrations analysis for cable-harnessed beams. It is a simpler pattern geometry for the cable and the current work is compared to the previously published work by Martin et al [51,52,54–57] . The straight cable work extends the assumptions of the model that is previously used to study uni-dimensional vibrations in the out-of-plane bending direction to account for the coupling between various coordinates of vibrations such as in-plane bending, out-of-plane bending, torsion and the axial modes. Both Euler Bernoulli (EB) and Timoshenko beam theories (TBT) are used. The effects of several cable parameters such as the cable offset position, radius and pre-tension on the system’s coupled dynamics are investigated. The results are compared to a decoupled model to indicate the importance of including the coupling effects into the system’s dynamics. Then the experimental validation of the analytical models developed in [118] for the coupled vibrations of these cable-harnessed structures is performed.

In case of straight cable, the wavelength is infinite, the continuum model has constant coefficients, and the dynamic behavior observed is for the exact system. For the structure with periodic pattern, each fundamental element has a diagonal element and lumped mass at the end of each fundamental element. In diagonal wrapping pattern, the wavelength is finite and the coupled strain and kinetic energies have variable coefficients and it becomes difficult to solve the exact system of coupled partial differential equations by discretizing the structure at the end of each fundamental element particularly when there are larger number of fundamental elements or when the wavelength of each fundamental element is smaller. Therefore, a constant coefficient coupled PDE model is presented to study the vibrations of cable-harnessed beam with diagonal wrapping pattern. The coupled natural frequencies of the cases: cable-harnessed beam with straight cable at an offset and the periodic wrapping pattern are also compared to give insight into the advantage of having periodic wrapping pattern to reduce the impact of mass and stiffening effects of cabling on the host structure. Sensitivity analysis is presented where the coupled and decoupled models are compared against different values of cable radius and the number of fundamental elements. Then the results obtained from the fully coupled homogenized analytical models (using both Euler-Bernoulli (EB) and Timoshenko beam theories (TBT)) for diagonal wrapping pattern are validated experimentally. In addition, the concept of transition frequency is not studied before for the cable-harnessed structures. For the cable-harnessed structure with diagonal wrapping pattern, the coordinates of motion such as the axial, bending, rotation of cross section and the torsion modes are coupled to each other because of the presence of cabling. For simply supported boundary conditions, a thick cable harnessed beam structure is considered. The findings of the mode shape behavior corresponding to both the first and second frequency spectra along with the transition or cut-off frequency are presented and compared to that of bare beam with simply supported boundary conditions. Cable-wrapped structures in general have applications in space structures where cables can be harnessed in any pattern or configuration around the host structure, which is the motivation behind the work performed in thesis in studying the coupled dynamics behind the cabled structure. Other areas where cable-wrapped structures can have practical applications include: by wrapping cables made of piezoelectric materials around the beam, energy can be harvested from the vibrations of the cabled structure. Cable wrapping can be used to stiffen the structure, as a result, the overall critical buckling load of the structure can be increased. Cable wrapped structures can

have applications in vibration control where by actively controlling the tension of the cable, the desired natural frequency or dynamic characteristics from the structure can be achieved.

For structure with non-periodic cable wrapping pattern, the effect of coupling in cable-harnessed structures with non-periodic wrapping patterns is studied. The coordinates of vibration considered are bending in the out of plane, in plane direction, axial and the torsion coordinates. The exact coupled partial differential equations (PDEs) are presented. The wrapping pattern considered is diagonal. Since the structures under study have multiple fundamental elements and the wrapping pattern is non-periodic (each fundamental element has a different wrapping angle), the equivalent continuum model as in Ref. [119] for periodic wrapping pattern can no longer be derived. Each fundamental element is assumed to have different displacements and continuity conditions are applied at each interface (discretizing the structure at each interface of two fundamental elements) to setup the eigen-value problem and to solve for the natural frequencies and mode shapes of the structure. Due to the diagonal section, some of the coefficients in the exact set of PDEs are spatially variable. Constant coefficient model is developed. The results obtained from the coupled theoretical model from both periodic and non-periodic structures will be validated using experiments and compared to the decoupled assumptions of Martin et al. The samples under investigation in this thesis have more significant cabling wrapped around the host structure and lesser fundamental elements when compared to Martin et al's work. [51–53,58]. The following are the journal and conference paper manuscripts that have been prepared from this thesis.

- [J.1] Yerrapragada, K., and Salehian, A., 2019, “Analytical Study of Coupling Effects for Vibrations of Cable-Harnessed Beam Structures,” *Journal of Vibration and Acoustics*, 141(3), p.031001.
- [J.2] Yerrapragada, K., and Salehian, A., “Coupled Dynamics of Cable-Harnessed Structures: Experimental Validation,” Accepted with Revisions, *Journal of Vibration and Acoustics* (VIB 18 1553).
- [J.3] Yerrapragada, K., and Salehian, A., “Coupled Vibrations in Periodic Cable-Harnessed Structures: Theory and Experimental Validation,” To be Submitted.
- [J.4] Yerrapragada, K., Martin, B., Morris, K., and Salehian, A., 2019, “Theoretical and Experimental Study of Vibrations of Cable-Harnessed Structures with Non-Periodic

Wrapping Pattern: Coupling Effects,” To be Submitted

- [C.1] Yerrapragada, K., and Salehian, A., 2017, “Coupled Axial, In Plane and Out of Plane Bending Vibrations of Cable Harnessed Space Structures,” *International Conference on Applied Mathematics, Modeling and Computational Science*, Springer, pp. 249–257.
- [C.2] Yerrapragada, K., and Salehian, A., 2018, “Coupled Bending, Torsion and Axial Vibrations of a Cable-Harnessed Beam With Periodic Wrapping Pattern,” *IDETC Conference*, ASME, pp. 1–8.

Chapter 2: Mathematical Modeling and Theoretical Analysis of Coupled Vibrations of Cable-Harnessed Structures

This chapter presents several mathematical models to study the coupled vibration characteristics of different systems of cable-harnessed structures such as the structure with straight cable positioned at an offset distance, structure with periodic cable wrapping pattern and structure with non-periodic cable wrapping pattern.

In Section 2.1, the structure with straight cable at an offset distance is considered. The system's configuration, the developed exact mathematical model for the fully coupled cable-harnessed beam and the procedure to find out the natural frequencies are presented. The natural frequencies for the decoupled and coupled vibration models are compared to the finite element results for several boundary conditions such as the fixed-fixed, cantilever and simply supported. Finally, the results for the sensitivity analysis to study the effects of several cable parameters such as cable's geometry, pre-tension and offset position on the natural frequencies are presented. The relation between the system's coupling and the energy transfer between various coordinates of vibrations are also studied.

In Section 2.2, theoretical studies are performed for the structure with periodic cable wrapping pattern. An equivalent coupled continuum model is presented and the coupled natural frequencies are first compared to the decoupled model assumptions from Ref. [51,52] for various system configurations. Sensitivity analysis on the natural frequencies are performed by varying the number of fundamental elements of wrapping pattern and the cable radius. For a given structure, the dynamic behavior of the straight case and periodic pattern are compared to present the advantage of periodic wrapping pattern.

In Section 2.3, the coupled analytical model for the non-periodic wrapping cable pattern is developed by discretizing the structure after each fundamental element and applying continuity conditions, which will result in a complicated mathematical model. The theoretical results obtained are compared to the decoupled model of non-periodic structure by Ref. [53] for three different non-periodic wrapping patterns.

2.1 Coupled Vibrations of Straight Cable Harness at Offset Distance

2.1.1 Mathematical Model

This section presents the mathematical modeling and underlying assumptions for the structure in this study. The structure considered is a beam system with a cable attached along the side of the beam as shown in Fig. (2.1). The coordinate axes are also shown in the Fig. (2.1 a) and Fig. (2.1 b) for Timoshenko and Euler-Bernoulli theories respectively. The cable is positioned at an offset distance along the y-axis.

To develop the continuum model of the cable-harnessed structure, the following assumptions apply:

- 1) The host structure is assumed to be a beam and it is modeled using Euler-Bernoulli and Timoshenko beam theories.
- 2) The cable stays in contact with the beam during vibrations along its length. This is because the electronic cords and power cables are secured in place using cable ties that prevents them from being detached from the host structure during vibrations.
- 3) The cable is in pre-tension at the equilibrium position and will remain in tension during the vibrations. The tension value is assumed to be constant during vibrations.
- 4) The pre-tension in the cable results in the pre-compression in the beam [51].

The fundamental difference between the Euler-Bernoulli and Timoshenko beam models is that the Timoshenko model takes into account the effect of shear deformation and rotary inertia, which the Euler-Bernoulli ignores. In Euler-Bernoulli, it is assumed that the neutral remains perpendicular to the cross-section after the structure bends. In Timoshenko, the effect of rotation of cross-section is taken into consideration. This can be clearly seen in Figs. (2.1 a) and (2.1 b). The stress component assumes uniform shear stress across the cross-section which is not practical and therefore a shear correction factor is used in the Timoshenko theory to correct this assumption [120]. The shear correction factor depends on the cross-section of the structure and accurately takes into account the shear stress across the cross-section. The effect of damping in the structure is neglected in this work.

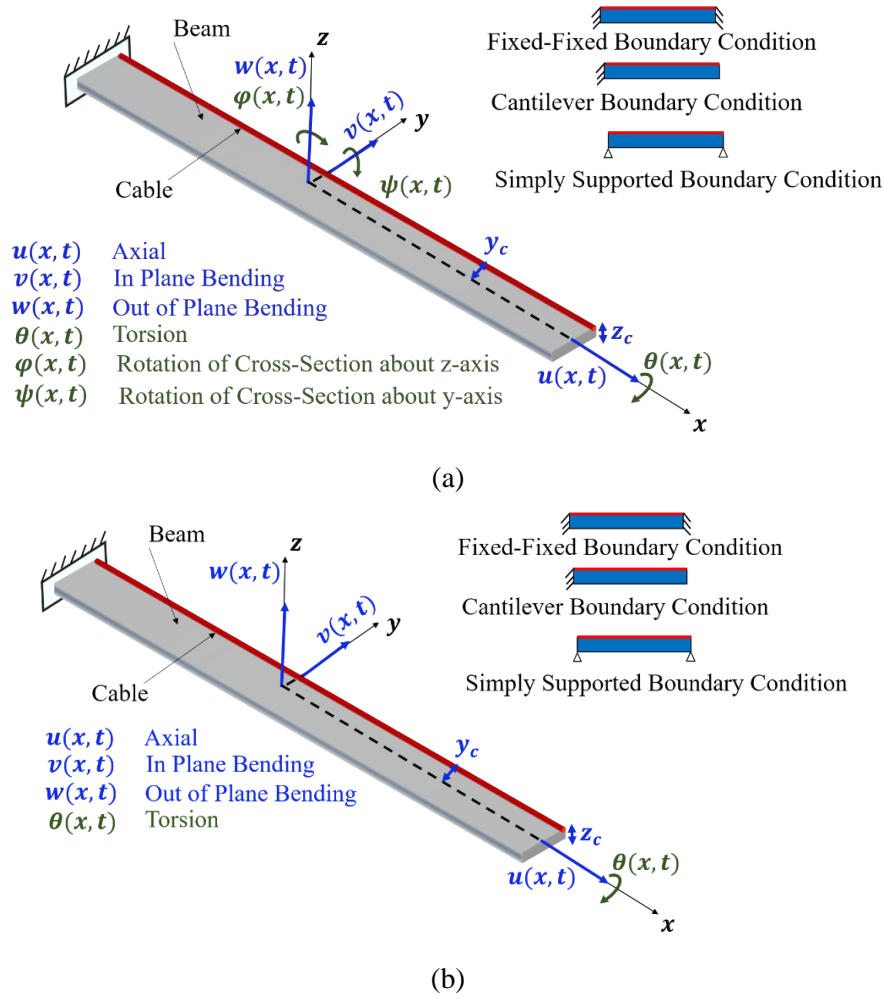


Fig. 2. 1 Representation of the cable harness beam along with the coordinate axes for (a) Timoshenko theory (b) Euler-Bernoulli theory.

The following sections pertain to the vibration analysis of the cable-harnessed beam shown in Fig. (2.1) using a distributed parameter model. The previous work by the authors on the analytical model for the periodically wrapped beam, [51], excludes the coupling effects between various coordinates of vibrations, i.e., bending, axial and torsion. The following steps outline the procedure for an exact fully coupled continuum model development for the system shown in Fig. (2.1) using Euler-Bernoulli and Timoshenko beam theories. The first step in finding an equivalent continuum model is to establish the displacement field relationship and stress-strain components. The linearized three-dimensional displacement fields using Euler-Bernoulli (EB) and Timoshenko beam theories are as follows [88,121–123].

Euler-Bernoulli beam model**Timoshenko beam model**

$$\begin{aligned}
X(x, y, z, t) &= u(x, t) - y \frac{\partial v(x, t)}{\partial x} - z \frac{\partial w(x, t)}{\partial x} \\
Y(x, y, z, t) &= v(x, t) - z\theta(x, t) \\
Z(x, y, z, t) &= w(x, t) + y\theta(x, t)
\end{aligned}
\qquad
\begin{aligned}
X(x, y, z, t) &= u(x, t) - y\varphi(x, t) + z\psi(x, t) \\
Y(x, y, z, t) &= v(x, t) - z\theta(x, t) \\
Z(x, y, z, t) &= w(x, t) + y\theta(x, t)
\end{aligned}
\tag{2.1}$$

where $u(x, t)$, $v(x, t)$, $w(x, t)$, $\theta(x, t)$, $\varphi(x, t)$, $\psi(x, t)$ are the motions in the axial, in-plane bending, out-of-plane bending, torsion, rotation of cross-section about z and y-axes respectively.

$X(x, y, z, t)$, $Y(x, y, z, t)$ and $Z(x, y, z, t)$ are the total displacement of the structure along the x, y and z axes respectively after considering all the coordinates. The next step is to find the stress-strain expressions using the displacement field. Eq. (2.2) gives the relationship between the stress and strain for an isotropic material.

$$\begin{Bmatrix} \sigma_{xx} \\ \sigma_{yy} \\ \sigma_{zz} \\ \tau_{xy} \\ \tau_{yz} \\ \tau_{zx} \end{Bmatrix} = \underbrace{\begin{bmatrix} \frac{E(1-\nu)}{(1+\nu)(1-2\nu)} & \frac{E\nu}{(1+\nu)(1-2\nu)} & \frac{E\nu}{(1+\nu)(1-2\nu)} & 0 & 0 & 0 \\ \frac{E\nu}{(1+\nu)(1-2\nu)} & \frac{E(1-\nu)}{(1+\nu)(1-2\nu)} & \frac{E\nu}{(1+\nu)(1-2\nu)} & 0 & 0 & 0 \\ \frac{E\nu}{(1+\nu)(1-2\nu)} & \frac{E\nu}{(1+\nu)(1-2\nu)} & \frac{E(1-\nu)}{(1+\nu)(1-2\nu)} & 0 & 0 & 0 \\ 0 & 0 & 0 & G & 0 & 0 \\ 0 & 0 & 0 & 0 & G & 0 \\ 0 & 0 & 0 & 0 & 0 & G \end{bmatrix}}_{[D]} \begin{Bmatrix} \varepsilon_{xx} \\ \varepsilon_{yy} \\ \varepsilon_{zz} \\ \gamma_{xy} \\ \gamma_{yz} \\ \gamma_{zx} \end{Bmatrix} \tag{2.2}$$

where $[D]$ is the elasticity matrix, and E and G are the Young's and the Shear Moduli respectively. Eq. (2.3) gives the relationship between the stress and strain for an isotropic material after neglecting the effect of Poisson's ratio [124].

$$\sigma_{xx} = E\varepsilon_{xx}, \tau_{xy} = G\gamma_{xy}, \tau_{zx} = G\gamma_{zx} \tag{2.3}$$

This structure is modelled using beam theory, therefore, the strain components in the y and z directions, (ε_{yy} and ε_{zz}), and the shear strain on the yz plane, (γ_{yz}), can be neglected (Ref. [121]). The expressions for the Green-Lagrange strain tensor for Euler-Bernoulli model are shown in Eq. (2.4 b)-(2.6 b) [88,121] and for Timoshenko model are shown in Eq. (2.4 a)-(2.6 a). The

displacement field (Eq. (2.1)) is substituted into the Green-Lagrange strain tensor expressions to obtain the final expressions for the strain tensor in Eqs. (2.4 a) – (2.6 a) and Eqs. (2.4 b) – (2.6 b).

$$\begin{aligned}\varepsilon_{xx} &= \frac{\partial X}{\partial x} + \frac{1}{2} \left(\frac{\partial X}{\partial x} \right)^2 + \frac{1}{2} \left(\frac{\partial Y}{\partial x} \right)^2 + \frac{1}{2} \left(\frac{\partial Z}{\partial x} \right)^2 \\ &= \left(\frac{\partial u}{\partial x} - y \frac{\partial \varphi}{\partial x} + z \frac{\partial \psi}{\partial x} \right) + \frac{1}{2} \left[\left(\frac{\partial u}{\partial x} - y \frac{\partial \varphi}{\partial x} + z \frac{\partial \psi}{\partial x} \right)^2 + \left(\frac{\partial v}{\partial x} - z \frac{\partial \theta}{\partial x} \right)^2 + \left(\frac{\partial w}{\partial x} + y \frac{\partial \theta}{\partial x} \right)^2 \right]\end{aligned}\quad (2.4 \text{ a})$$

$$\begin{aligned}&= \left(\left(\frac{\partial u}{\partial x} \right) - y \left(\frac{\partial^2 v}{\partial x^2} \right) - z \left(\frac{\partial^2 w}{\partial x^2} \right) \right) \\ &\quad + \frac{1}{2} \left[\left(\left(\frac{\partial u}{\partial x} \right) - y \left(\frac{\partial^2 v}{\partial x^2} \right) - z \left(\frac{\partial^2 w}{\partial x^2} \right) \right)^2 + \left(\frac{\partial v}{\partial x} - z \frac{\partial \theta}{\partial x} \right)^2 + \left(\frac{\partial w}{\partial x} + y \frac{\partial \theta}{\partial x} \right)^2 \right]\end{aligned}\quad (2.4 \text{ b})$$

$$\begin{aligned}\gamma_{xy} &= \frac{\partial X}{\partial y} + \frac{\partial Y}{\partial x} + \frac{\partial X}{\partial x} \frac{\partial X}{\partial y} + \frac{\partial Y}{\partial x} \frac{\partial Y}{\partial y} + \frac{\partial Z}{\partial x} \frac{\partial Z}{\partial y} \\ &= -\sqrt{\kappa} \varphi + \sqrt{\kappa} \frac{\partial v}{\partial x} - z \frac{\partial \theta}{\partial x}\end{aligned}\quad (2.5 \text{ a})$$

$$= -z \frac{\partial \theta}{\partial x}\quad (2.5 \text{ b})$$

$$\begin{aligned}\gamma_{zx} &= \frac{\partial Z}{\partial x} + \frac{\partial X}{\partial z} + \frac{\partial X}{\partial z} \frac{\partial X}{\partial x} + \frac{\partial Y}{\partial z} \frac{\partial Y}{\partial x} + \frac{\partial Z}{\partial z} \frac{\partial Z}{\partial x} \\ &= \sqrt{\kappa} \psi + \sqrt{\kappa} \frac{\partial w}{\partial x} + y \frac{\partial \theta}{\partial x}\end{aligned}\quad (2.6 \text{ a})$$

$$= y \frac{\partial \theta}{\partial x}\quad (2.6 \text{ b})$$

where ε_{xx} is the direct strain in the x direction. γ_{xy} and γ_{zx} are the shear strains in the xy and the yz plane respectively. Here, κ is the shear correction factor and can be found as $\frac{5+5\nu}{6+5\nu}$, [88], where, ν is the Poisson's ratio. The effect of Poisson's ratio on the direct strains of the host structure is neglected. The total strain energy of the unit can be found using the strain energy for each of the beam and cable as,

$$U = \frac{1}{2} \left[\iiint \{\varepsilon\}_b^T \{\sigma\}_b dV + \iiint \{\varepsilon\}_c^T \{\sigma\}_c dV \right] \quad (2.7)$$

where $\{\varepsilon\}_b$ and $\{\varepsilon\}_c$ are the strain components of the beam and cable respectively. $\{\sigma\}_b = [D]_b \{\varepsilon\}_b$ and $\{\sigma\}_c = [D]_c \{\varepsilon\}_c$. After neglecting $\varepsilon_{yy}, \varepsilon_{zz}, \gamma_{yz}$ in Eq. (2.2) due to using a beam theory, the stresses in the beam are found using $\{\sigma_{xx}, \tau_{xy}, \tau_{zx}\}_b^T = \{E_b(\varepsilon_{xx})_b, G_b(\gamma_{xy})_b, G_b(\gamma_{zx})_b\}^T$. The cable is assumed to undergo strain in the x direction only, therefore, $(\sigma_{xx})_c = E_c(\varepsilon_{xx})_c$. Also, the shear modulus effects in the cable are assumed negligible. Additionally, the strains components for the beam and cable include the strain experienced during the vibrations as well as the cable pretension that also induces a pre-compression in the beam. Therefore, the expressions for the direct strains induced in the cable and beam after the incorporating the effect of pre-tension in the cable and pre-compression in the beam are as $(\varepsilon_{xx})_c = T/E_c A_c + \varepsilon_{xx}$ and $(\varepsilon_{xx})_b = -T/E_b A_b + \varepsilon_{xx}$. The negative sign in the equation for $(\varepsilon_{xx})_b$ is due to the pre-compression induced in the beam upon the cable pre-tension. The final energy expressions for the kinetic and strain of the cable-harnessed beam for a Timoshenko beam theory are as follows.

$$\begin{aligned} U_{system} &= \frac{1}{2} \left[\iiint E_b (\varepsilon_{xx})_b^2 + G_b (\gamma_{xy})_b^2 + G_b (\gamma_{zx})_b^2 dV \right] + \frac{1}{2} \left[\iiint E_c (\varepsilon_{xx})_c^2 dV \right] \quad (2.8) \\ &= \frac{1}{2} \int_0^l [c_1 (u')^2 + c_2 (v')^2 + c_3 (w')^2 + c_4 (\theta')^2 + c_5 (\varphi')^2 + c_6 (\psi')^2 + c_7 (\varphi)^2 + \\ &2c_8 (u')(\varphi') + 2c_9 (u')(\psi') + 2c_{10} (\varphi')(\psi') + 2c_{11} (v')(\varphi) + 2c_{12} (v')(\theta') + 2c_{13} (w')(\theta') + \\ &c_{14} (\psi)^2 + 2c_{15} (w')(\psi)] dx \\ T_{system} &= \frac{1}{2} \left[\iiint \rho_b \{\dot{X}, \dot{Y}, \dot{Z}\}^T \{\dot{X}, \dot{Y}, \dot{Z}\} dV + \iiint \rho_c \{\dot{X}, \dot{Y}, \dot{Z}\}^T \{\dot{X}, \dot{Y}, \dot{Z}\} dV \right] \quad (2.9) \\ &= \frac{1}{2} \int_0^l [k_1 (\dot{u})^2 + k_2 (\dot{v})^2 + k_3 (\dot{w})^2 + k_4 (\dot{\theta})^2 + k_5 (\dot{\varphi})^2 + k_6 (\dot{\psi})^2] dx \end{aligned}$$

The constants used in the kinetic and strain energy expressions for the Timoshenko model are presented in Eq. (A.1) in the Appendix A. The terms c_1, c_2, c_3 and c_4 represent the strain energies in the axial, in-plane bending, out of plane bending and torsion modes respectively. c_5, c_7 and c_6, c_{14} represent the coefficients related to the two rotations of cross-sections. The remaining strain energy coefficients are due to coupling terms, which in case of Timoshenko model depend

on the geometry and material properties of the host structure and the radius, pre-tension and position coordinates of the center of the cable.

The energy expressions for Euler-Bernoulli model can be found by neglecting shear deformation and rotary inertia effects. Assuming negligible initial twist, and zero wrapping angle of the cable, the strain and kinetic energy expressions of the system using this theory are found as Ref. [51],

$$U = \frac{1}{2} \int_0^l [b_1(u')^2 + b_2(v'')^2 + b_3(w'')^2 + b_4(\theta')^2 + 2b_5(v'')(w'') + 2b_6(u')(v'') + 2b_7(u')(w'') + 2b_8(w')(\theta') + 2b_9(v')(\theta')] dx \quad (2.10)$$

$$T = \frac{1}{2} \int_0^l [k_1(\dot{u})^2 + k_2(\dot{v})^2 + k_3(\dot{w})^2 + k_4(\dot{\theta})^2] dx \quad (2.11)$$

where superscript ()' denotes partial derivative with respect to spatial coordinate $x(\frac{\partial}{\partial x})$ and superscript ($\dot{}$) denotes partial derivative with respect to time $t(\frac{\partial}{\partial t})$. The constants of the above strain and kinetic energy expressions for Euler-Bernoulli model are presented in Eq. (A.2) in the Appendix A. Here, b_1 to b_4 represent the coupling coefficients in the axial, in-plane bending, out-of-plane bending and torsion modes respectively. The remaining coefficients (b_5 to b_9) represent the coupling coefficients. The coupling coefficients in case of Euler-Bernoulli model depends on the parameters like cable radius, cable pre-tension, young's modulus of the cable and the position coordinates of the center of the cable along the y and z axis. Neglecting dissipative forces, assuming free vibrations and no external loads acting on the system, equations of motion for the cable harnessed structure for the two beam theories may be found using Hamilton's Principle (Eq. (1.1)).

The coupled equations of motion for the six coordinates of vibrations for the Timoshenko beam model are found as,

$$-k_1\ddot{u} + c_1u'' + c_8\varphi'' + c_9\psi'' = 0 \quad (2.12 \text{ a})$$

$$-k_2\ddot{v} + c_2v'' + c_{12}\theta'' + c_{11}\varphi' = 0 \quad (2.12 \text{ b})$$

$$-k_3\ddot{w} + c_3w'' + c_{13}\theta'' + c_{15}\psi' = 0 \quad (2.12 \text{ c})$$

$$-k_4\ddot{\theta} + c_4\theta'' + c_{12}v'' + c_{13}w'' = 0 \quad (2.12 \text{ d})$$

$$-k_5\ddot{\varphi} + c_5\varphi'' - c_7\varphi + c_8u'' - c_{11}v' + c_{10}\psi'' = 0 \quad (2.12 \text{ e})$$

$$-k_6\ddot{\psi} + c_6\psi'' - c_{14}\psi + c_9u'' - c_{15}w' + c_{10}\varphi'' = 0 \quad (2.12 \text{ f})$$

The six coupled partial differential equations obtained after applying Hamilton's principle are presented in Eqs. (2.12 a) - (2.12 f) will require six boundary conditions at each end. The boundary conditions (also obtained from Hamilton's principle) for each of the fixed, simply supported and free ends are as follows. The boundary conditions for the fixed, free and simply supported ends are shown in Eqs. (2.13), (2.14) and (2.15) respectively.

$$u = v = w = \theta = \varphi = \psi = 0|_{x=0 \text{ or } l} \quad (2.13)$$

$$\begin{aligned} c_1 u' + c_8 \varphi' + c_9 \psi' &= 0|_{x=0 \text{ or } l} \\ c_2 v' + c_{11} \varphi + c_{12} \theta' &= 0|_{x=0 \text{ or } l} \\ c_3 w' + c_4 \theta' + c_{15} \psi &= 0|_{x=0 \text{ or } l} \\ c_4 \theta' + c_{12} v' + c_{13} w' &= 0|_{x=0 \text{ or } l} \\ c_5 \varphi' + c_8 u' + c_{10} \psi' &= 0|_{x=0 \text{ or } l} \\ c_6 \psi' + c_9 u' + c_{10} \varphi' &= 0|_{x=0 \text{ or } l} \end{aligned} \quad (2.14)$$

$$\begin{aligned} u = v = w = \theta &= 0|_{x=0 \text{ or } l} \\ c_5 \varphi' + c_8 u' + c_{10} \psi' &= 0|_{x=0 \text{ or } l} \\ c_6 \psi' + c_9 u' + c_{10} \varphi' &= 0|_{x=0 \text{ or } l} \end{aligned} \quad (2.15)$$

A simpler version of Eqs. (2.12 a) - (2.12 f) can be found using assumptions for Euler-Bernoulli beam model in which the shear and rotary inertia effects are excluded. The equations for the Euler-Bernoulli are derived from the displacement field and strain tensor similar to the Timoshenko beam theory. In Euler-Bernoulli, beam theory, Eqs. (2.12 e) and (2.12 f) which correspond to the rotations of cross-sections are not present. The governing equations for Euler Bernoulli beam model are presented in Eqs. (2.16 a)- (2.16 d).

$$-k_1 \ddot{u} + b_1 u'' + b_6 v'''' + b_7 w'''' = 0 \quad (2.16 \text{ a})$$

$$-k_2 \ddot{v} - b_2 v'''' - b_6 u'''' - b_5 w'''' + b_9 \theta'' = 0 \quad (2.16 \text{ b})$$

$$-k_3 \ddot{w} - b_3 w'''' - b_7 u'''' - b_5 v'''' + b_8 \theta'' = 0 \quad (2.16 \text{ c})$$

$$-k_4 \ddot{\theta} + b_4 \theta'' + b_9 v'' + b_8 w'' = 0 \quad (2.16 \text{ d})$$

The associated boundary conditions for the Eqs. (2.16 a) - (2.16 d) for the fixed, free and simply supported ends are shown in Eqs. (2.17), (2.18) and (2.19) respectively.

$$u = v = w = \theta = v' = w' = 0|_{x=0 \text{ or } l} \quad (2.17)$$

$$\begin{aligned} b_1 u' + b_6 v'' + b_7 w'' &= 0|_{x=0 \text{ or } l} \\ b_2 v'' + b_5 w'' + b_6 u' &= 0|_{x=0 \text{ or } l} \\ b_2 v''' + b_5 w''' + b_6 u'' - b_9 \theta' &= 0|_{x=0 \text{ or } l} \\ b_3 w'' + b_5 v'' + b_7 u' &= 0|_{x=0 \text{ or } l} \end{aligned} \quad (2.18)$$

$$\begin{aligned} b_3 w''' + b_5 v''' + b_7 u'' - b_8 \theta' &= 0|_{x=0 \text{ or } l} \\ b_4 \theta' + b_8 w' + b_9 v' &= 0|_{x=0 \text{ or } l} \\ u = v = w = \theta &= 0|_{x=0 \text{ or } l} \\ b_2 v'' + b_5 w'' + b_6 u' &= 0|_{x=0 \text{ or } l} \\ b_3 w'' + b_5 v'' + b_7 u' &= 0|_{x=0 \text{ or } l} \end{aligned} \quad (2.19)$$

Eqs. (2.12 a)- (2.12 f) and (2.16 a) - (2.16 d) are coupled through stiffness terms. All the coordinates of motion are coupled because of the pre-tension in the cable, Young's modulus and radius of the cable. In mathematical terms, the first derivative of displacement represents the slope, second derivative represents moment, third derivative represents shear and the fourth derivative represents the intensity of load. Mathematically, Eqs. (2.16 b) and (2.16 c) corresponding to the in plane and out-of-plane bending coordinates. The axial and torsion coordinates are coupled to these modes because of equivalent shear terms (third derivative of displacement and second derivative of angle). The torsion mode Eq. (2.16 d) is coupled to the in-plane and out-of-bending modes because of equivalent moment terms. The axial mode Eq. (2.16 a) is coupled to the bending coordinates because of equivalent shear terms. Eqs. (2.16 b) and (2.16 c) show that the coupling term related to the in plane and out of plane bending is fourth derivative, which physically corresponds to load. In Timoshenko model, Eqs. (2.12 a)-(2.12 f), the coupling coefficients in addition to depending on the cable parameters like position coordinates along y and z axis, cable radius and cable pre tension, also depends on the geometry of the host structure. In a Timoshenko beam, apart from the cable coupling, the rotation of cross section are geometrically coupled to the bending coordinates. In Eq. (2.12 a), the axial mode is coupled to the rotations of cross-sections through the cable parameters. In Eq. (2.12 b), the in-plane bending mode is coupled to the torsion mode through the cable parameters and to the rotation of cross-section about z axis because of geometry of the beam (c_{11}). Similarly, in Eq. (2.12 c) the out of plane bending mode is coupled to the torsion mode through cable parameters and to the rotation of cross-section through the geometric term. In Eq. (2.12 d), the torsion mode is coupled to the bending terms through the cable

parameters. Similarly, in Eqs. (2.12 e) and (2.12 f), the rotations of cross-section about z and y-axis are coupled to other coordinates through the cable parameters and beam geometry terms. In Timoshenko beam, we can also observe that unlike Euler-Bernoulli, we do not see presence of in-plane bending terms v in the out of plane bending mode equation w (Eq. (2.12 c)) and vice-versa (Eq. (2.12 b)). The two bending terms here are coupled through the rotations of cross-section related terms (Eqs. (2.12 e) and (2.12 f)). After obtaining the governing equations, the next step is to obtain the natural frequencies and mode shapes. In the following steps, the solution procedure for coupled partial differential equations, the Timoshenko model is shown in Eqs. (2.12 a)- (2.12 f). The same procedure is applicable for the Euler-Bernoulli model, which are shown in Eqs. (2.16 a) - (2.16 d). The general form of the solution for the coupled PDE's are shown in Eqs. (2.12 a)- (2.12 f) are as follows,

$$\begin{Bmatrix} u \\ v \\ w \\ \theta \\ \varphi \\ \psi \end{Bmatrix} = \begin{Bmatrix} U \\ V \\ W \\ \Theta \\ \Phi \\ \Psi \end{Bmatrix} e^{\alpha x} e^{i\omega t} \quad (2.20)$$

where U, V, W, Θ, Φ and Ψ are modal vectors. The temporal solution of the PDEs is assumed to be harmonic (represented by the complex exponential $e^{i\omega t}$), and the spatial solution is assumed to be of the form $e^{\alpha x}$, where ω is the frequency and α is the mode shape parameter. Substituting Eq. (2.20) in Eqs. (2.12 a)- (2.12 f), we obtain six simultaneous algebraic equations, which are converted into matrix form as follows,

$$[A]_{6 \times 6} \begin{Bmatrix} U \\ V \\ W \\ \Theta \\ \Phi \\ \Psi \end{Bmatrix}_{6 \times 1} = \{0\}_{6 \times 1} \quad (2.21)$$

where $[A]$ is given by:

$$\begin{bmatrix} c_1\alpha^2 + k_1\omega^2 & 0 & 0 & 0 & c_8\alpha^2 & c_9\alpha^2 \\ 0 & c_2\alpha^2 + k_2\omega^2 & 0 & c_{12}\alpha^2 & c_{11}\alpha & 0 \\ 0 & 0 & c_3\alpha^2 + k_3\omega^2 & c_{13}\alpha^2 & 0 & c_{15}\alpha \\ 0 & c_{12}\alpha^2 & c_{13}\alpha^2 & c_4\alpha^2 + k_4\omega^2 & 0 & 0 \\ c_8\alpha^2 & -c_{11}\alpha & 0 & 0 & c_5\alpha^2 - c_7 + k_5\omega^2 & c_{10}\alpha^2 \\ c_9\alpha^2 & 0 & -c_{15}\alpha & 0 & c_{10}\alpha^2 & c_6\alpha^2 + k_6\omega^2 - c_{14} \end{bmatrix}$$

For non-trivial solution, $|A(\alpha, \omega)|$ should be zero. This results in a polynomial that relates the mode shape parameters α and frequency ω . Solving the above polynomial results in 12 roots for α in terms of ω . The next step is to find the spatial solutions. We know from Eq. (2.21) that

$$A_{61}U + A_{62}V + A_{63}W + A_{64}\Theta + A_{65}\Phi + A_{66}\Psi = 0 \quad (2.22)$$

where A_{6i} ($i \rightarrow 1$ to 6) represent the elements of the sixth row of matrix $[A]$ (any arbitrary row can be used to develop the linear dependency condition. In this case, sixth row is selected). For the linear dependency between U, V, W, Θ, Φ and Ψ to be satisfied, the spatial solutions for different coordinates of motion should be as follows.

$$\begin{aligned} U_n &= |(-1)^{6+1}M_{61}| & V_n &= |(-1)^{6+2}M_{62}| & W_n &= |(-1)^{6+3}M_{63}| & (2.23) \\ \Theta_n &= |(-1)^{6+4}M_{64}| & \Phi_n &= |(-1)^{6+5}M_{65}| & \Psi_n &= |(-1)^{6+6}M_{66}| \end{aligned}$$

where M_{6i} ($i \rightarrow 1$ to 6) represent the minors of the elements A_{6i} for $i \rightarrow 1$ to 6 of matrix $[A]$. The determinant of the co-factor elements presented in Eq. (2.23) gives us the final spatial solution for each coordinates of vibration. Since we have 12 roots for α , subscript n is from 1 to 12. After obtaining α in terms of ω and obtaining the spatial solutions, the general solution of the coupled PDEs is expanded as follows.

$$\begin{pmatrix} u(x, t) \\ v(x, t) \\ w(x, t) \\ \theta(x, t) \\ \varphi(x, t) \\ \psi(x, t) \end{pmatrix} = \sum_{n=1}^{12} d_n \begin{pmatrix} U_n(\alpha = \alpha_n) \\ V_n(\alpha = \alpha_n) \\ W_n(\alpha = \alpha_n) \\ \Theta_n(\alpha = \alpha_n) \\ \Phi_n(\alpha = \alpha_n) \\ \Psi_n(\alpha = \alpha_n) \end{pmatrix} e^{\alpha_n x} e^{i\omega t} \quad (2.24)$$

Here, d_n is a solution constant for $n \rightarrow 1$ to 12. The total of 12 boundary conditions are then used to find the frequencies using the algebraic equations below.

$$[L(\omega)]_{12 \times 12} \{\vec{d}\}_{12 \times 1} = \{0\}_{12 \times 1} \quad (2.25)$$

The non-trivial solution results in $|L(\omega)| = 0$, from which the natural frequencies are found. As the system is fully coupled, the entries of matrices $[A(\alpha, \omega)]_{6 \times 6}$ and $[L(\omega)]_{12 \times 12}$ are very complicated. The characteristic equation obtained by evaluating the determinant of $[A(\alpha, \omega)]$ is found using a computational software. Similarly, the transcendental frequency equation from $[L(\omega)]$ is also found using computational software. The roots of the transcendental frequency equation are found graphically by plotting the $|L(\omega)|$ with respect to the frequency to find the natural frequencies of the system. For the experimental validation, the structure is subjected to harmonic base excitation in the out-of-plane bending direction and the description is shown in Fig. (2.2). The equations of motion (2.12 a) to (2.12 f) and (2.16 a) to (2.16 d) are modified after

including the effect of base excitation as Eq. (2.26) and Eq. (2.29) respectively. Also, $w_b(t)$ is the base excitation (equivalent forcing term) provided to the cantilevered structure in the out of plane bending direction which appears on the right hand side of Eq. (2.26 c) and Eq. (2.29 c) in the equation related to the out of plane bending dominant motion.

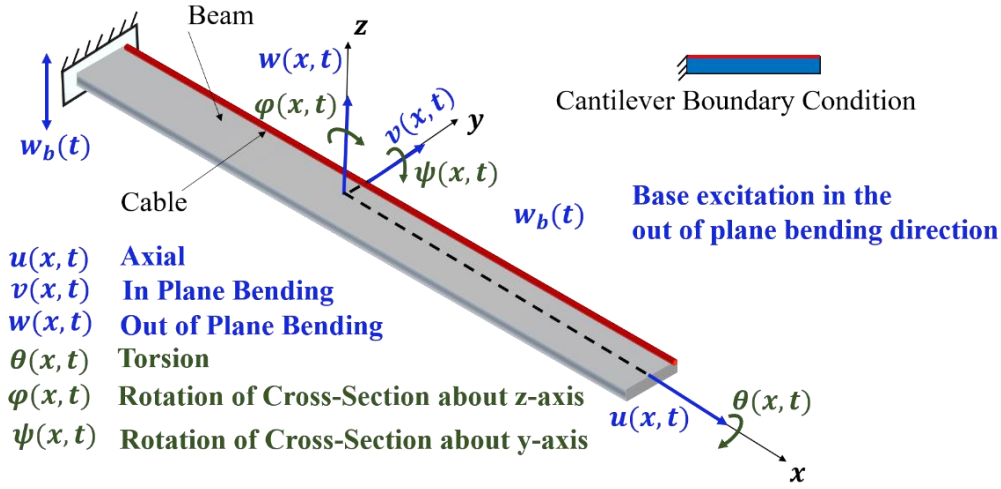


Fig. 2. 2 Schematic of the cable-harnessed beam subjected to harmonic base excitation and the coordinate axes.

For the Euler-Bernoulli model, the equations are as follows: (Eqs. (2.26 a) to (2.26 d)).

$$-k_1 \ddot{u} + b_1 u'' + b_6 v'''' + b_7 w''''_{rel} = 0 \quad (2.26 a)$$

$$-k_2 \ddot{v} - b_2 v'''' - b_6 u'''' - b_5 w''''_{rel} + b_9 \theta'' = 0 \quad (2.26 b)$$

$$-k_3 \ddot{w}_{rel} - b_3 w''''_{rel} - b_7 u'''' - b_5 v'''' + b_8 \theta'' = k_3 \ddot{w}_b \quad (2.26 c)$$

$$-k_4 \ddot{\theta} + b_4 \theta'' + b_9 v'' + b_8 w''_{rel} = 0 \quad (2.26 d)$$

The boundary conditions associated with the fixed and free ends are shown in Eqs. (2.27) and (2.28).

Fixed end

$$u = v = w_{rel} = \theta = v' = w'_{rel} = 0|_{x=0} \quad (2.27)$$

Free end.

$$\begin{aligned} b_1 u' + b_6 v'' + b_7 w''_{rel} &= 0|_{x=l} \\ b_2 v'' + b_5 w''_{rel} + b_6 u' &= 0|_{x=l} \\ b_2 v'''' + b_5 w''''_{rel} + b_6 u'' - b_9 \theta' &= 0|_{x=l} \\ b_3 w''_{rel} + b_5 v'' + b_7 u' &= 0|_{x=l} \\ b_3 w''''_{rel} + b_5 v'''' + b_7 u'' - b_8 \theta' &= 0|_{x=l} \\ b_4 \theta' + b_8 w'_{rel} + b_9 v' &= 0|_{x=l} \end{aligned} \quad (2.28)$$

Therefore, w_{rel} is the relative out of plane bending motion of any point on the structure with respect to the base. Similarly, the governing partial differential equations of motion along with the boundary conditions for the Timoshenko model can be found as, [118].

$$-k_1 \ddot{u} + c_1 u'' + c_8 \varphi'' + c_9 \psi'' = 0 \quad (2.29 \text{ a})$$

$$-k_2 \ddot{v} + c_2 v'' + c_{12} \theta'' + c_{11} \varphi' = 0 \quad (2.29 \text{ b})$$

$$-k_3 \ddot{w}_{rel} + c_3 w''_{rel} + c_{13} \theta'' + c_{15} \psi' = k_3 \ddot{w}_b \quad (2.29 \text{ c})$$

$$-k_4 \ddot{\theta} + c_4 \theta'' + c_{12} v'' + c_{13} w''_{rel} = 0 \quad (2.29 \text{ d})$$

$$-k_5 \ddot{\varphi} + c_5 \varphi'' - c_7 \varphi + c_8 u'' - c_{11} v' + c_{10} \psi'' = 0 \quad (2.29 \text{ e})$$

$$-k_6 \ddot{\psi} + c_6 \psi'' - c_{14} \psi + c_9 u'' - c_{15} w'_{rel} + c_{10} \varphi'' = 0 \quad (2.29 \text{ f})$$

The boundary conditions for the fixed and free ends are,

Fixed end

$$u = v = w_{rel} = \theta = \varphi = \psi = 0|_{x=0} \quad (2.30)$$

Free end

$$\begin{aligned} c_1 u' + c_8 \varphi' + c_9 \psi' &= 0|_{x=l} \\ c_2 v' + c_{11} \varphi + c_{12} \theta' &= 0|_{x=l} \\ c_3 w'_{rel} + c_4 \theta' + c_{15} \psi &= 0|_{x=l} \\ c_4 \theta' + c_{12} v' + c_{13} w'_{rel} &= 0|_{x=l} \\ c_5 \varphi' + c_8 u' + c_{10} \psi' &= 0|_{x=l} \\ c_6 \psi' + c_9 u' + c_{10} \varphi' &= 0|_{x=l} \end{aligned} \quad (2.31)$$

Next, the frequency response functions, for the out-of-plane bending, for experimental validations is shown in Eq. (2.32).

$$W(\omega_f) = \left| \frac{1}{\omega_f^2} + \sum_{i=1}^{\infty} \frac{k_3 \cdot W_{i,rel}(x = x_s) \cdot \int_{x=0}^l W_{i,rel}(x) dx}{\omega_i^2 - \omega_f^2} \right| \quad (2.32)$$

Here, x_s is the sensing location, ω_f is the excitation frequency and ω_i is the natural frequency associated with the i^{th} mode. Also, $W_{i,rel}(x = x_s)$ is the relative mass normalized mode shape value of the i^{th} mode at the sensing location for the out of plane bending.

To better understand, the mathematics behind the coupling effects, a further simplified model is built for the cable-harnessed beam in which only the coupling is assumed to be between the in plane and out-of-plane bending modes. The simulations for the simplified model are presented in the section 2.1.2 after the simulation of the fully coupled model for obtaining in-depth

insight into the problem. Refs.[125,126] developed closed form expressions for natural frequencies of repeated truss structures and beams with initial loads. Following the same approach, closed form expressions for natural frequencies are obtained for the system in the following study for simply supported boundary conditions. The strain and kinetic energy for the simplified model are shown below.

$$U = \frac{1}{2} \int_0^l [b_2(v'')^2 + b_3(w'')^2 + 2b_5(v'')(w'')] dx \quad (2.33)$$

$$T = \frac{1}{2} \int_0^l [k_2(\dot{v})^2 + k_3(\dot{w})^2] dx \quad (2.34)$$

The strain and kinetic energies include decoupled energies in the in plane and out of plane bending directions. The coupling energy between the in plane and out of plane bending is also included. The coupling is due to offset position of the cable and the coupling coefficient b_5 vanishes if the cable is placed along the centerline. If the cable is along the centerline only the decoupled coefficients b_2, b_3, k_2 and k_3 remain.

The reduced order Euler-Bernoulli model for the cable-harnessed beam that includes the bending modes only can be written as follows (reduced from Equations. (2.16 a)- (2.16 d)):

$$-k_2\ddot{v} - b_2v'''' - b_5w'''' = 0 \quad (2.35a)$$

$$-k_3\ddot{w} - b_3w'''' - b_5v'''' = 0 \quad (2.35b)$$

Simply supported boundary condition is considered as an example, therefore,

$$\begin{aligned} v = w = 0|_{x=0 \text{ or } l} \\ b_2v'' + b_5w'' = 0|_{x=0 \text{ or } l} \\ b_3w'' + b_5v'' = 0|_{x=0 \text{ or } l} \end{aligned} \quad (2.36)$$

The last two expressions of Eq. (2.36) correspond to the equivalent bending moment in the in-plane and out-of-plane directions.

Using the assumed form of solution for the bending of a simply supported beam, we get,

$$\begin{aligned} v(x, t) = V \sin\left(\frac{n\pi x}{l}\right) e^{i\omega t} \\ w(x, t) = W \sin\left(\frac{n\pi x}{l}\right) e^{i\omega t} \end{aligned} \quad (2.37)$$

After substituting the general solution in the coupled PDEs (Equations (2.35 a) and (2.35 b)) and converting the simultaneous algebraic equations into the matrix form, we obtain the following equation.

$$\begin{bmatrix} -\frac{b_2 n^4 \pi^4}{l^4} + k_2 \omega^2 & -\frac{b_5 n^4 \pi^4}{l^4} \\ -\frac{b_5 n^4 \pi^4}{l^4} & -\frac{b_3 n^4 \pi^4}{l^4} + k_3 \omega^2 \end{bmatrix} \begin{Bmatrix} V \\ W \end{Bmatrix} = \begin{Bmatrix} 0 \\ 0 \end{Bmatrix} \quad (2.38)$$

For the system to have a non-trivial solution, the determinant of the matrix in Eq. (2.38) should vanish.

$$\frac{b_2 b_3 n^8 \pi^8}{l^8} - \frac{b_5^2 n^8 \pi^8}{l^8} + \left(-\frac{b_3 k_2 n^4 \pi^4}{l^4} - \frac{b_2 k_3 n^4 \pi^4}{l^4} \right) \omega^2 + k_2 k_3 \omega^4 = 0 \quad (2.39)$$

Solving Eq. (2.39) for ω we obtain the expressions for the natural frequencies as follows,

$$\omega_1 = \sqrt{\frac{\frac{b_3 k_2 n^4}{l^4} + \frac{b_2 k_3 n^4}{l^4} - \frac{\sqrt{(b_3 k_2)^2 n^8 - 2b_2 b_3 k_2 k_3 n^8 + 4(b_5)^2 k_2 k_3 n^8 + (b_2 k_3)^2 n^8}}{l^4}}{2k_2 k_3}} \pi^2 \quad (2.40)$$

$$\omega_2 = \sqrt{\frac{\frac{b_3 k_2 n^4}{l^4} + \frac{b_2 k_3 n^4}{l^4} + \frac{\sqrt{(b_3 k_2)^2 n^8 - 2b_2 b_3 k_2 k_3 n^8 + 4(b_5)^2 k_2 k_3 n^8 + (b_2 k_3)^2 n^8}}{l^4}}{2k_2 k_3}} \pi^2$$

For a given value of n one of them corresponds to the out of plane bending dominant mode and the other corresponds to the in-plane dominant mode. As a result, the two natural frequencies obtained from Eq. (2.40) correspond to the same wavenumber. In Section 2.1.2, further explanations for the simplest case are provided through numerical simulations after the simulations for the fully coupled cases. Eq. (2.40) can help in obtaining deeper physical insight into the problem by providing us information how the frequency changes when a parameter is varied. Using analytical solutions as presented in Eq. (2.40) helps us understand the physical behavior that takes place in the system when the offset position of the cable is changed and the simplified coupled partial differential equations along with the results help us explain the phenomenon of coupling better.

2.1.2 Results and Discussion of numerical simulations

Presented in this section are the natural frequencies and mode shapes for the cable-harnessed beam structure shown in Fig. (2.1) using the analytical models developed in the previous section. The results are compared to the decoupled Euler Bernoulli model presented in Ref. [51] for the system parameters shown in Table. (2.1). Further, the presented results help better

understand the dynamics behind the coupling and its effects. In addition, sensitivity analysis such as the effects of the offset position, radius and pre-tension of the cable on the natural frequencies are further presented and discussed using the coupled Euler Bernoulli theory.

The position coordinates of the center of the cable in the y and z directions are given by the expressions, $y_c = \frac{b}{2} - r_c$; $z_c = \frac{h}{2} + r_c$. For the system parameters shown in Table. (2.1), the values (y_c, z_c) are equal to $(0.0043, 0.00145)$ m. The root of transcendental equation $|L(\omega)| = 0$ is used to obtain the natural frequencies of the system for the parameters shown in Table. (2.1) for the coupled system. Results of both Euler-Bernoulli and Timoshenko models are presented for parameters in Table. (2.1). Fixed-fixed, cantilever and simply supported boundary conditions are considered.

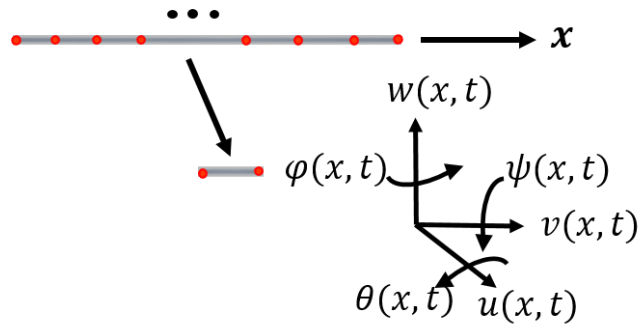


Fig. 2. 3 Finite Element Analysis discretization along with the nodal displacements.

To validate the analytical results, a finite element analysis is performed. The system is discretized by assuming each displacement function to be a third order polynomial in x (where x is the length of the beam, 1D beam element) [51,127] in Eq. (2.41). The discretization and the nodal displacement are shown in Fig. (2.3).

$$\begin{aligned}
 u(x, t) &= g_{11}(t) + g_{21}(t)x + g_{31}(t)x^2 + g_{41}(t)x^3 \\
 v(x, t) &= g_{12}(t) + g_{22}(t)x + g_{32}(t)x^2 + g_{42}(t)x^3 \\
 w(x, t) &= g_{13}(t) + g_{23}(t)x + g_{33}(t)x^2 + g_{43}(t)x^3 \\
 \theta(x, t) &= g_{14}(t) + g_{24}(t)x + g_{34}(t)x^2 + g_{44}(t)x^3 \\
 \varphi(x, t) &= g_{15}(t) + g_{25}(t)x + g_{35}(t)x^2 + g_{45}(t)x^3 \\
 \psi(x, t) &= g_{16}(t) + g_{26}(t)x + g_{36}(t)x^2 + g_{46}(t)x^3
 \end{aligned} \tag{2.41}$$

The degrees of freedom considered for each node are the displacements and the derivatives which are $u, v, w, \theta, \varphi, \psi$ and $\frac{\partial u}{\partial x}, \frac{\partial v}{\partial x}, \frac{\partial w}{\partial x}, \frac{\partial \theta}{\partial x}, \frac{\partial \varphi}{\partial x}, \frac{\partial \psi}{\partial x}$. Using the cubic interpolation polynomials, the displacements of the element are found out using standard procedures in vibration

text books [120]. Using the element displacements, mass and stiffness matrices of the element are constructed from the strain and kinetic energy expressions using the Timoshenko model, Eqs. (2.8)-(2.9) for the cable-harnessed structure using numerical computation software. In this case, since the strain energy and kinetic energy expressions have the effect of cable, the entries in the mass and stiffness matrices have the effect of cable incorporated. The mass matrix is consistent, it is constructed by taking into account the shape functions. The structure was meshed into 200 elements. The total number of nodes in the system are 201 for all the boundary conditions considered. Each node has 12 degrees of freedom which includes the displacement corresponding to the axial, in-plane bending, out of plane bending, torsion and the two rotations of cross-section and their respective derivatives. Once the elemental mass and stiffness matrices are constructed, they are assembled and respective boundary conditions are applied. The eigenvalue problem gives us the natural frequencies and the mode shapes. The mesh size is varied to check that the natural frequency result has converged. The finite element method over-predicts the natural frequencies when compared to the analytical model due to the Rayleigh Ritz criterion. The purpose of finite element analysis adopted in this chapter is to use another method to obtain the natural frequencies from the strain and kinetic energy continuum model. This will help in crosschecking the frequencies obtained using analytical procedure. Ultimately, the analytical models developed in this thesis will be validated against the experiments. The natural frequency errors for each of the models in comparison with the FEA results are presented in the Tables. (2.2)-(2.4). To identify the coordinate of vibration associated with each frequency, the mode shapes are found and plotted in Figs. (2.4)-(2.6). The mass normalization condition for the coupled Timoshenko beam model can found by following the procedure outlined in [128].

$$\int_0^l (k_1 U_n(x)U_n(x) + k_2 V_n(x)V_n(x) + k_3 W_n(x)W_n(x) + k_4 \theta_n(x)\theta_n(x) + k_5 \varphi_n(x)\varphi_n(x) + k_6 \psi_n(x)\psi_n(x)) dx = 1 \quad (2.42)$$

Eq. (2.42) shows the mass normalization condition for a coupled Timoshenko model, the same condition can be easily obtained for an Euler-Bernoulli beam model and is shown in Eq. (2.43).

$$\int_0^l (k_1 U_n(x)U_n(x) + k_2 V_n(x)V_n(x) + k_3 W_n(x)W_n(x) + k_4 \theta_n(x)\theta_n(x)) dx = 1 \quad (2.43)$$

Table 2. 1 Material and geometrical properties of the cable harnessed beam structure.

System parameters	Value
Beam length (l)	0.25 m
Beam width (b)	0.01 m
Beam height (h)	0.0015 m
Beam density (ρ_b)	2,700 Kg/m ³
Beam modulus of elasticity (E_b)	68.9 GPa
Beam Shear modulus (G_b)	26 GPa
Beam Poisson's ratio (ν)	0.34
Cable tension (T)	25 N
Cable radius (r_c)	0.0007 m
Cable density (ρ_c)	1,400 Kg/m ³
Cable modulus of elasticity (E_c)	150 GPa

As an example, the first few mass-normalized mode shapes for the coupled theory using Euler-Bernoulli assumptions for several boundary conditions are shown in Figs. (2.4)-(2.6). For the mode shape analysis, the mass-normalized mode shapes obtained from the coupled Euler Bernoulli model are presented. The results in Fig. (2.4) for fixed-fixed boundary condition indicate that for the 1st, 2nd and 4th modes, the out-of-plane bending is the dominant mode. The 3rd mode is predominantly an in-plane bending mode, and the 5th mode is the torsional mode. The first predominantly axial mode is also shown in this figure, which corresponds to the 22nd mode. To further confirm, the findings of this figure on the dominance of each coordinate of vibrations at a given frequency, a strain energy analysis is performed to find the contribution of each coordinate for the modes shown. Therefore, after obtaining the solution to the coupled PDEs, the strain energy for each of the coordinates is calculated at each frequency.

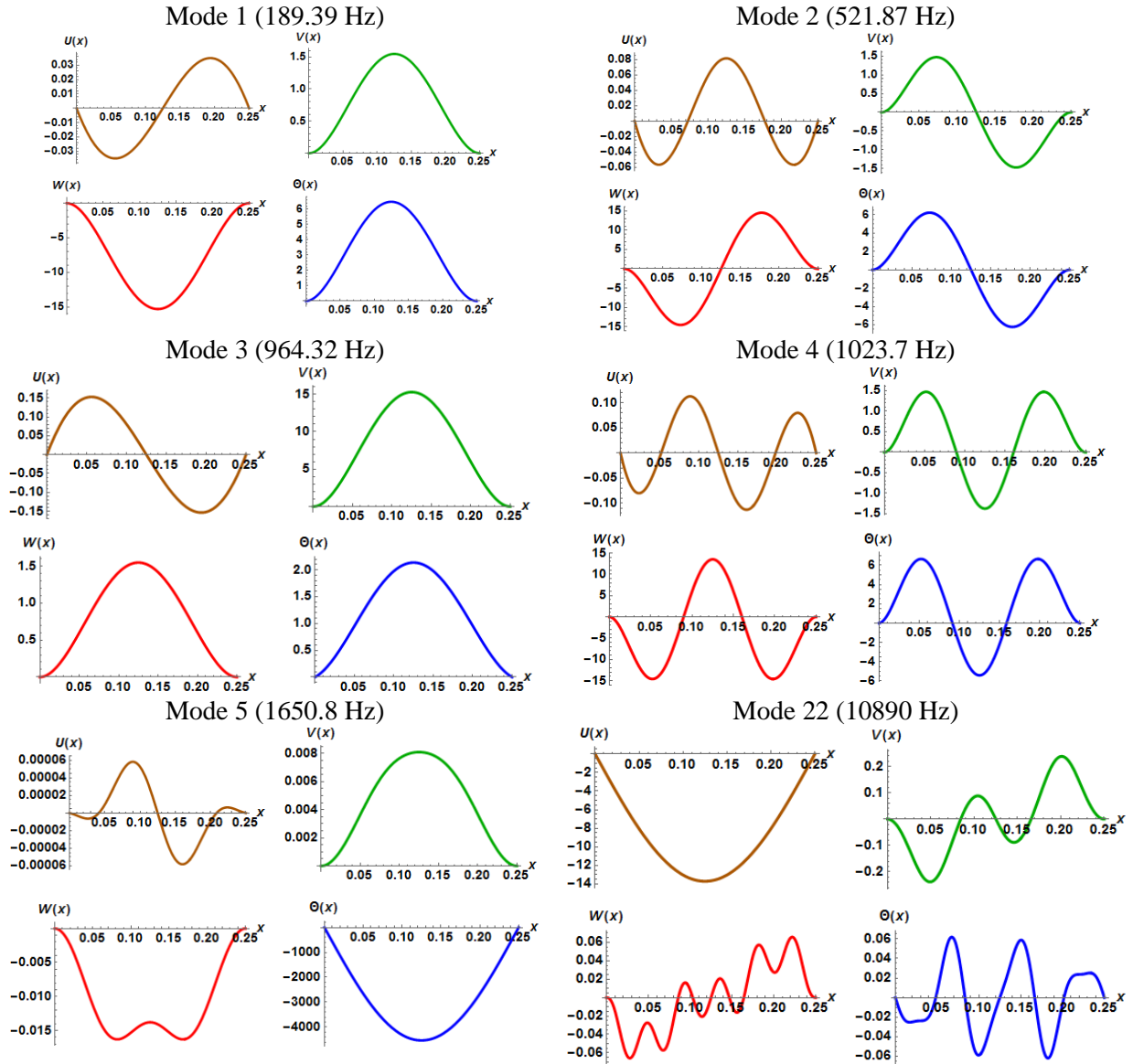


Fig. 2. 4 Vibrations mode shapes for fixed-fixed boundary conditions using coupled EB theory for fixed-fixed boundary conditions using coupled EB theory for Out of plane bending dominant (Modes 1, 2 and 4), In plane bending dominant (Mode 3), Torsion dominant (Mode 5) and Axial dominant (Mode 22).

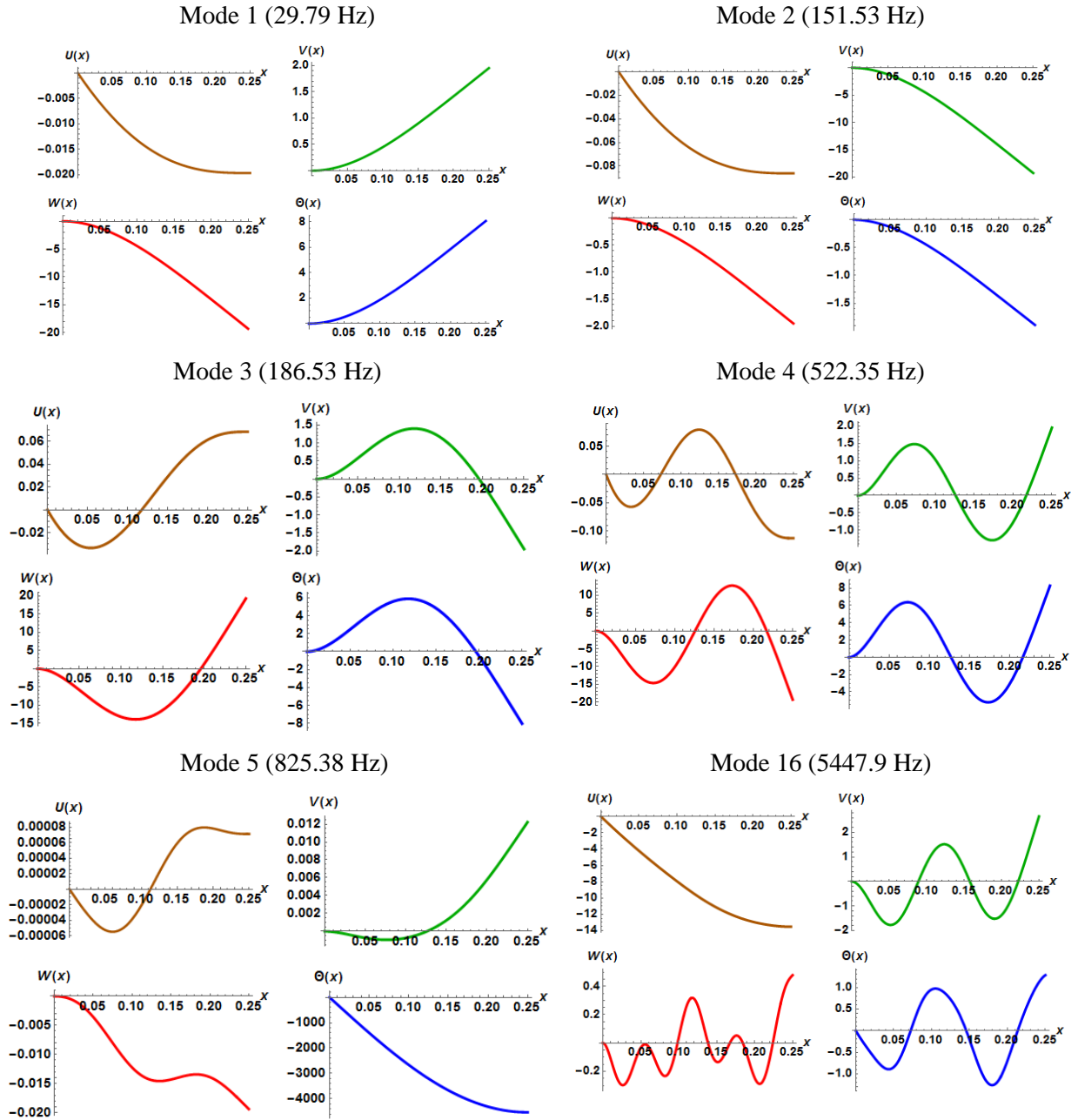


Fig. 2. 5 Vibrations mode shapes for cantilever boundary conditions using coupled EB theory for Out of plane bending dominant (Modes 1, 3 and 4), In plane bending dominant (Mode 2), Torsion dominant (Mode 5) and Axial dominant (Mode 16).

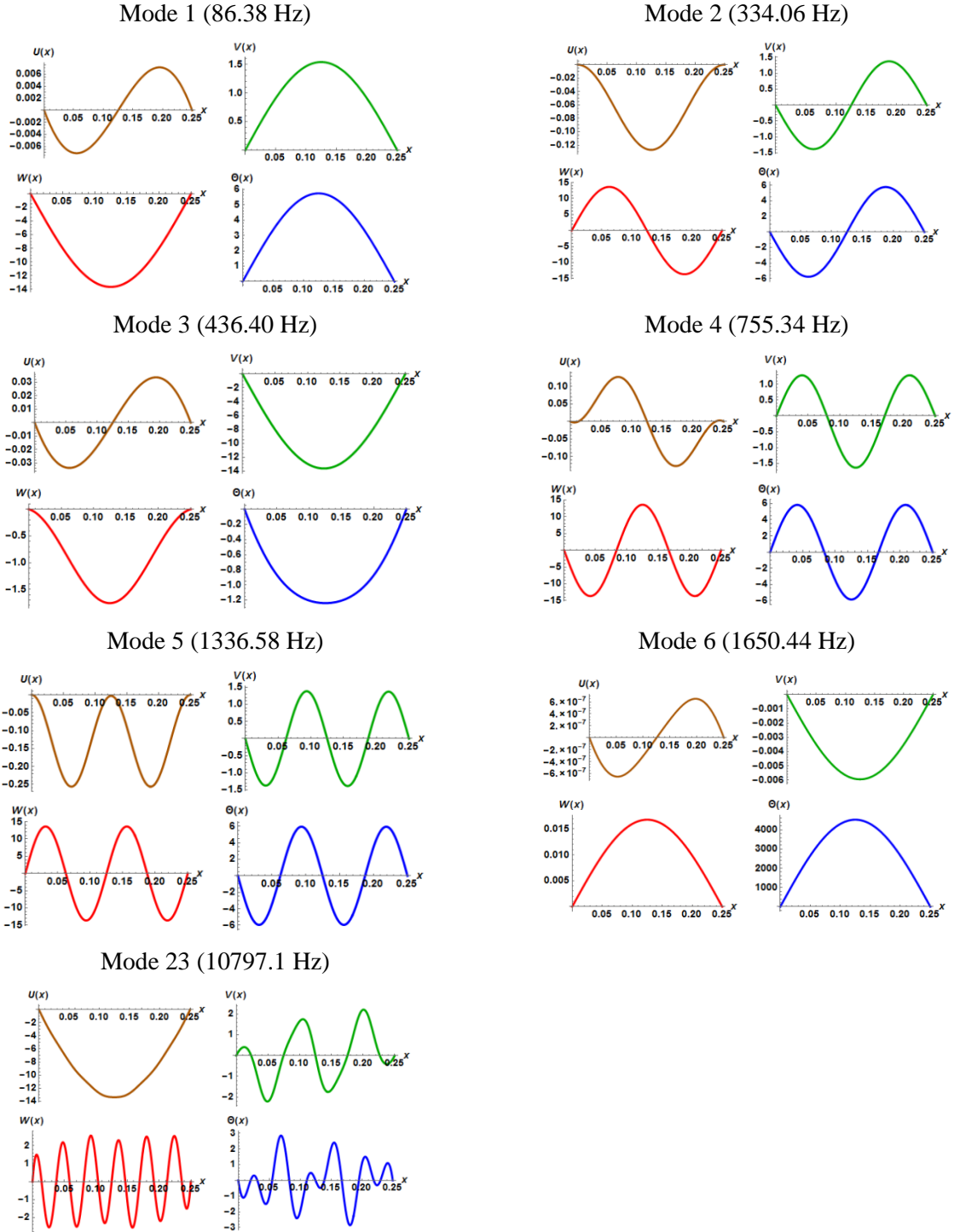


Fig. 2. 6 Vibrations mode shapes for simply supported boundary conditions using coupled EB theory for Out of plane bending dominant (Modes 1, 2 and 5), In plane bending dominant (Mode 3), Torsion dominant (Mode 6) and Axial dominant (Mode 23).

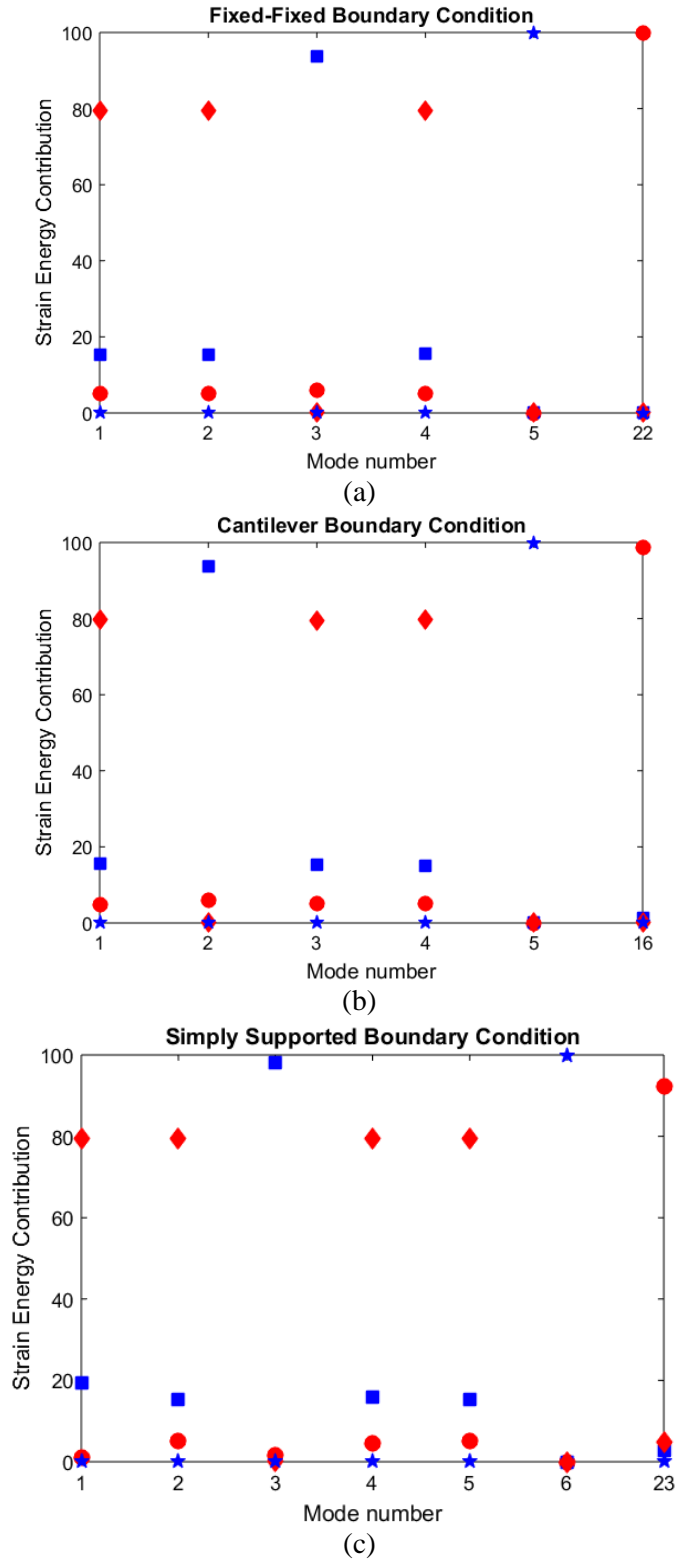


Fig. 2. 7 Percentage for the strain energy contribution of each modal coordinate with respect to mode number ● denotes axial; ■ denotes in plane bending; ◆ denotes out of plane bending; ★ denotes torsion.

Table 2. 2 Natural Frequencies for coupled and decoupled models for fixed-fixed boundary conditions (Hz)

Mode	Decoupled Euler-Ber.	Coupled Euler-Ber.	Coupled Timoshenko	FEA	Error % Decoupled	Error % Coupled Euler-Ber.	Error % Coupled Timoshenko
1	227.36 OP	189.39	189.23	189.75	16.53	-0.16	-0.22
2	626.73 OP	521.87	521.55	522.68	16.60	-0.13	-0.18
3	990.1 IP	964.32	949.51	952.35	3.81	1.20	-0.28
4	1228.6 OP	1023.7	1020.98	1023.63	16.68	0.00	-0.21
5	1650.8 T	1650.8	1650.44	1652.8	-0.12	-0.12	-0.14
6	2031 OP	1691.8	1685.45	1689.91	16.79	0.09	-0.21
7	3034 OP	2527.4	2513.06	2520.45	16.92	0.22	-0.24
8	2729.3 IP	2657.9	2567.17	2576.83	5.58	2.97	-0.35
9	3301.7 T	3301.7	3302.47	3305.59	-0.11	-0.11	-0.09
10	4237.6 OP	3528.5	3504.59	3513.78	17.08	0.34	-0.21
22	10889 A	10890	10886.2	10900.1	-0.10	-0.09	-0.12

*OP, IP, T and A refer to the out-of-plane bending, in-plane bending, torsional and axial modes respectively.

Table 2. 3 Natural Frequencies for coupled and decoupled models for cantilever boundary conditions (Hz)

Mode	Decoupled Euler-Ber.	Coupled Euler-Ber.	Coupled Timoshenko	FEA	Error % Decoupled	Error % Coupled Euler-Ber.	Error % Coupled Timoshenko
1	35.72 OP	29.79	29.63	29.76	16.67	0.07	-0.37
2	155.58 IP	151.53	151.32	151.47	2.63	0.03	-0.09
3	223.91 OP	186.53	186.37	186.65	16.63	-0.05	-0.12
4	626.86 OP	522.35	521.71	522.38	16.66	-0.00	-0.10
5	825.42 T	825.38	825.69	825.91	-0.05	-0.06	-0.02
6	975.07 IP	949.52	938.53	939.92	3.60	0.98	-0.14
7	1228.5 OP	1023.7	1021.46	1022.75	16.74	0.07	-0.10
8	2031 OP	1691.8	1687.04	1688.65	16.85	0.15	-0.07
9	2476.3 T	2476.5	2476.45	2477.73	-0.05	-0.04	-0.05
10	2729.8 IP	2527.4	2516.24	2518.81	7.72	0.31	-0.09
16	5444.5 A	5447.9	5446.28	5449.63	-0.09	-0.03	-0.06

*OP, IP, T and A refer to the out-of-plane bending, in-plane bending, torsional and axial modes respectively.

Table 2. 4 Natural Frequencies for coupled and decoupled models for simply supported boundary conditions (Hz)

Mode	Decoupled Euler-Ber.	Coupled Euler-Ber.	Coupled Timoshenko	FEA	Error % Decoupled	Error % Coupled Euler-Ber.	Error % Coupled Timoshe nko
1	100.29 OP	86.38	86.34	86.32	13.93	0.06	0.01
2	401.18 OP	334.06	334.06	334.03	16.73	0.00	0.00
3	436.76 IP	436.40	434.65	434.98	0.40	0.32	-0.07
4	902.67 OP	755.34	754.07	754.17	16.45	0.13	-0.01
5	1604.75 OP	1336.58	1333.56	1333.87	16.88	0.16	-0.01
6	1650.84 T	1650.44	1650.44	1652.8	-0.11	-0.14	-0.14
7	1747.06 IP	1701.37	1675.90	1677.3	3.99	1.37	-0.08
8	2507.42 OP	2091.3	2083.34	2084.66	16.86	0.26	-0.05
9	3610.69 OP	3008.03	2992.11	2992.51	17.12	0.42	-0.01
10	3301.69 T	3302.47	3302.47	3305.59	-0.11	-0.09	-0.09
23	10889.0 A	10797.1	10766.8	10783.9	0.96	0.12	-0.15

*OP, IP, T and A refer to the out-of-plane bending, in-plane bending, torsional and axial modes respectively.

Finally, the percentages for the energy contributions of each of the coordinates of vibrations for each mode are plotted in Fig. (2.7 a). These values indicate the dominance of each coordinate for a given mode, and further confirm the findings of Fig. (2.4). The same explanation can be extended to cantilever and simply supported boundary conditions. It should be noted that the main assumption behind a decoupled model is that the stiffness values associated with the coordinates of vibrations not included in the analysis are infinitely large, and as a result those coordinates may be neglected. This leads to an overestimation of the frequencies using a decoupled model. Once the effects of these coordinates are included in the coupled analysis, the stiffness values associated with the previously ignored coordinates now become finite that result in a more reasonable natural frequency estimation and improved accuracy. The results shown in Tables. (2.2)-(2.4) further indicate the overestimation of the frequencies for the decoupled model as well as the improved accuracy for the coupled model that is particularly more important for the higher modes. In another words, the coupled model allows for the distribution of strain energy between coordinates of vibrations that is ignored in a decoupled analysis. As the coupled model is more accurate, from a practical perspective this coupling effect can be utilized by positioning the cables at an offset position to reduce the stiffening effect by cabling on the host structure in the out of

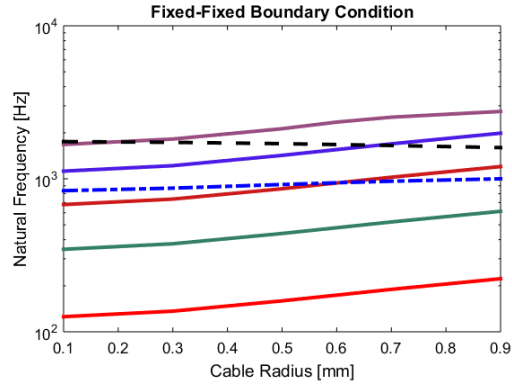
plane bending modes. In addition, it is very important to accurately predict the out of plane bending natural frequency peak of the beam structure, which is better possible by the coupled model.

The mode shape results in Fig. (2.5) pertain to the cantilever boundary conditions. For this boundary condition, it is shown that the out-of-plane bending is dominant in the first, third and the fourth modes; whereas, the in-plane bending is dominant at the second mode. Also, the torsional mode is dominant at the fifth frequency, and the higher mode shown corresponds to the first axial mode. For the simply supported boundary condition, Fig. (2.6), the out-of-plane bending is dominant in the first, second, fourth and the fifth modes. In-plane bending is dominant in the third mode. Torsion is dominant in the sixth mode, and the mode 16 shown relates to the axial dominant mode. In the modes 5, 22 of Fig. (2.4), modes 5, 16 of Fig. (2.5) and modes 5, 23 of Fig. (2.6) respectively, due to the effect of coupling, coordinates of motion related to the in-plane bending, out-of-plane bending and the torsion exhibit different behavior when compared to the decoupled theory. The equation for the displacement of each coordinate of motion is given by Eq. (2.24). Mathematically speaking, the mode shape expression for each coordinate of motion includes the effect of all wave numbers ($\alpha_1 - \alpha_{12}$). For example, in mode 5 of Fig. (2.4), consider the out of plane bending curve $W(x)$, mode 5 is a torsion dominant mode. So, the mode shape parameters α related to torsion also contribute significantly to the out of plane bending response. As a result, we see distinct behavior in the mode shape of out of plane bending for mode 5 of Fig. (2.4) when compared to the decoupled model. The same explanation related to the dominance of the mode shape parameter α can be extended to other modes for all the boundary conditions wherever distinct behavior is seen.

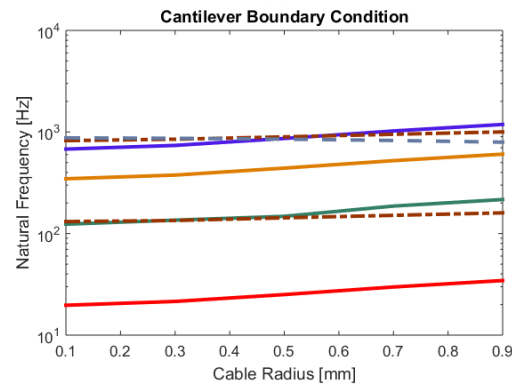
The natural frequencies found using the decoupled and coupled models are presented and compared to the FEA results in Tables. (2.2)-(2.4). Comparing the errors in the natural frequency estimations for each of these methods clearly indicates the advantage of the coupled analysis over the decoupled. In particular, significant improvement in the accuracy can be observed for the out-of-plane bending dominant modes. It is shown that the decoupled model tends to overestimate the frequencies compared to the coupled model due to overestimating the overall stiffness of the system. This is because the decoupled model only allows for the out of plane bending, hence, it ignores the flexibility of the system in other directions and their vibrations. In addition, it can be seen that the Timoshenko model predicts the frequencies better when compared to the Euler

Bernoulli. This is particularly noticeable for the higher in-plane bending modes due to the length to thickness ratio in that direction and the shear effects becoming more important.

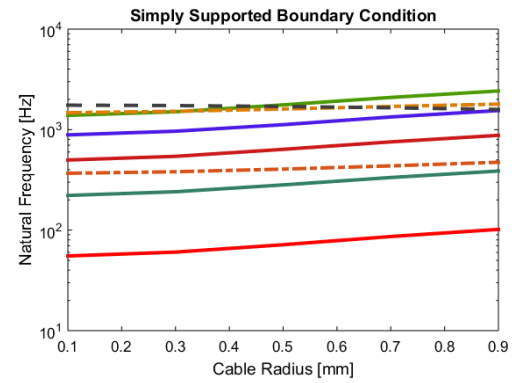
Finally, to obtain more insight into the coupling effects, a sensitivity analysis is performed by varying several parameters such as radius of the cable, the offset position, and the tension in the cable. For simplicity, these analyses are performed using the coupled EB analytical model as the shear effects become important for structures with larger length to thickness ratios. Fig. (2.8) shows, the effects of cable radius on natural frequencies for each mode while keeping other system parameters constant. As the cable radius increases, the frequencies pertaining to the modes for which out of plane bending is dominant increase, while the frequencies for the dominantly torsional modes decrease. This is because as the radius of the cable increases, the strain energy increases at a faster rate than the kinetic energy for the out of plane bending dominant mode and its frequency increases; however, the kinetic energy increases at a faster rate than the strain energy for the torsion dominant modes as the cable radius becomes larger, that results in smaller torsional frequencies.



(a)



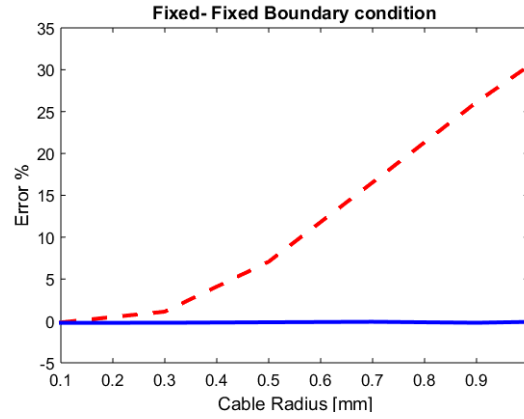
(b)



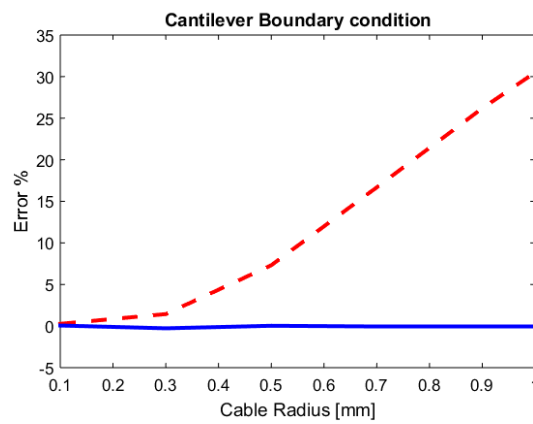
(c)

Fig. 2. 8 Effects of cable radius on the coupled natural frequencies. Solid lines denote Out of plane dominant modes; Dash dot lines denote In plane bending dominant; Dashed line denote Torsion dominant.

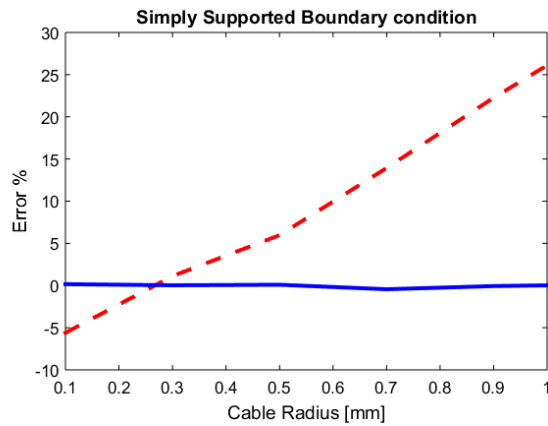
In Fig. (2.9), the errors between the natural frequencies of coupled and decoupled EB models compared to the FEA are plotted against the cable radius for different boundary conditions. As expected, when the cable radius increases, the coupling between different coordinates of vibrations gets stronger.



(a)



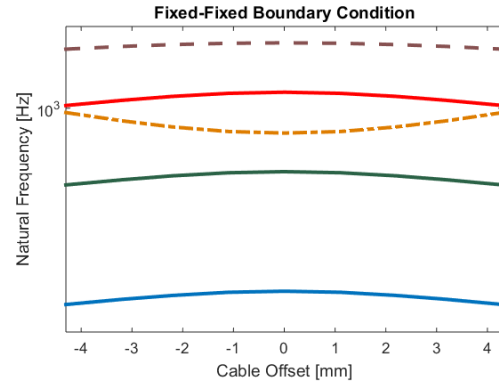
(b)



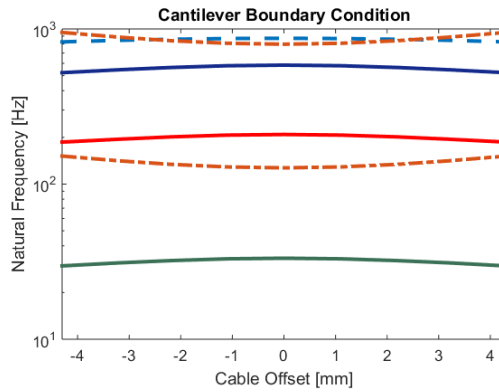
(c)

Fig. 2. 9 Error comparisons for natural frequencies between the coupled and decoupled models and the FEA. **---** denotes error between decoupled analytical and FEA and **—** error between coupled analytical and FEA.

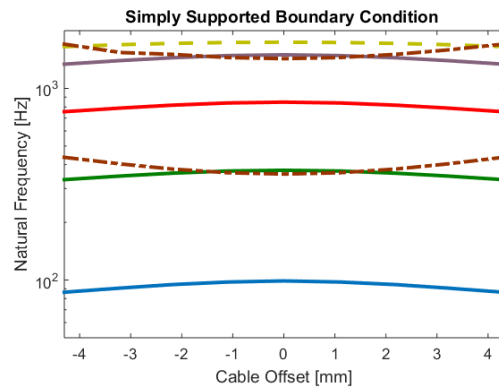
It is shown that the error for the decoupled model with respect to the FEA becomes significantly larger when compared to the coupled model due to ignoring the coupling effects that are particularly important for larger cable radius values due to greater coupling.



(a)



(b)



(c)

Fig. 2. 10 Effect of cable offset position on the coupled natural frequencies. Solid lines denote Out of plane dominant modes; Dash dot lines denote In plane bending dominant; Dashed line denote Torsion dominant.

The results for several cable-offset positions are presented in Fig. (2.10). The natural frequency results shown in this figure further indicate the strain energy transfer between the in plane and out of plane bending modes as the system coupling increases. As the cable is placed further from the center, the coupling effects are more pronounced that result in an energy transfer between the in plane and out of plane bending modes subsequently causing the smaller frequencies for the out-of-plane bending dominant modes and larger frequencies for the in-plane modes. In addition, the frequency patterns show a symmetric behavior for offset positions on either side of the beam as expected.

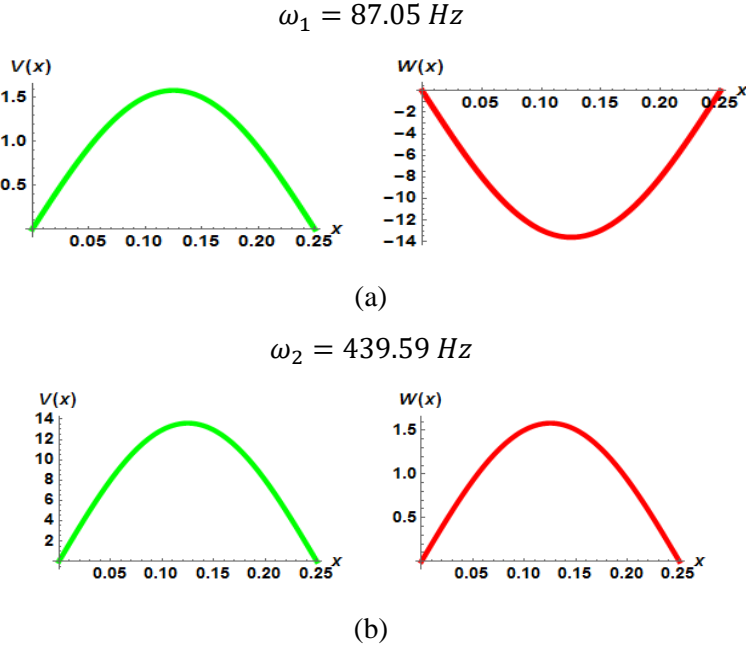
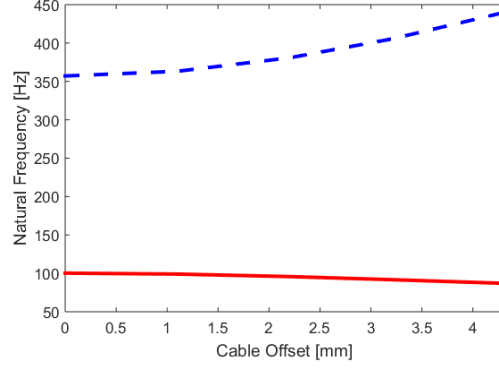
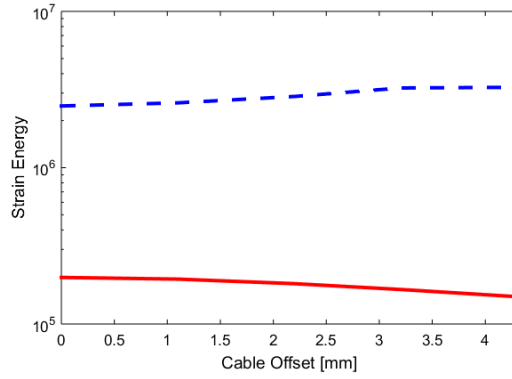


Fig. 2. 11 Mode shapes corresponding to $n=1$ for the system with coupled bending at 0.0043 m cable offset position

The analysis of the natural frequencies of the simplest coupling case from Eq. (2.40) is presented in Fig. (2.12 a). The system parameters are assumed the same as Table. (2.1). The value of n is taken to be one. For $n = 1$, we get two frequencies from Eq. (2.40). The next step is to plot the mode shapes.



(a)



(b)

Fig. 2. 12 Strain energy and natural frequency with respect to cable offset position. — denotes out of plane bending dominant mode. - - denotes in plane bending dominant mode.

The spatial solutions can be obtained by satisfying the linear dependency criterion for the following equation.

$$\left(-\frac{b_2 n^4 \pi^4}{l^4} + k_2 \omega^2\right) V + \left(-\frac{b_5 n^4 \pi^4}{l^4}\right) W = 0 \quad (2.44)$$

Therefore, the coupled mode shapes for $n = 1$ of the system are as follows.

$$V(x) = b_m \left(\frac{b_5 \pi^4}{l^4}\right) \sin\left(\frac{\pi x}{l}\right) \quad W(x) = b_m \left(-\frac{b_2 \pi^4}{l^4} + k_2 \omega^2\right) \sin\left(\frac{\pi x}{l}\right) \quad (2.45)$$

The mode shape constant b_m can be found out by using the following mass normalization criterion.

$$\int_0^l (k_2 V_n(x) V_n(x) + k_3 W_n(x) W_n(x)) dx = 1 \quad (2.46)$$

The coupled mode shapes corresponding to the lower and higher natural frequency roots of Eq. (2.40) are plotted in Fig. 2.11 (a) and 2.11 (b) respectively. In Fig. 2.11 (a), the mode shapes corresponding to the out of plane bending and in plane bending are out of phase with each other. The magnitudes for the mass normalized mode shapes shown in this figure indicates that the lower

root corresponds to the out-of-plane bending dominant mode, and the other corresponds to the in-plane bending. Fig. (2.12) shows the variations for the strain energy and the fundamental natural frequency for these two bending modes as the cable offset changes. Zero offset in the plot denotes the system is decoupled at that point and at zero offset, the solutions pertaining to the decoupled system are presented. It is shown that as the offset distance increases, both the frequency and strain energy corresponding to the out-of-plane bending dominant mode drop while they both increase for the in-plane bending mode. This indicates an energy transfer between the two modes as the coupling increases due to the offset position.

Another interesting aspect to study is the effect of the cable tension on the natural frequencies. For this purpose both rectangular and I-beam cross-sections are further considered in this paper. Fig. (2.13) shows the natural frequency variations for the first in-plane and out-of-plane bending and torsional modes with respect to the cable pre-tension for the system parameters shown in Table. (2.1). From this figure, it can be understood that the pre-tension has negligible effect on the system's natural frequencies. This is because of the relatively large bending stiffness that makes it less susceptible to the effects of tension. Therefore, to better study this effect, the system

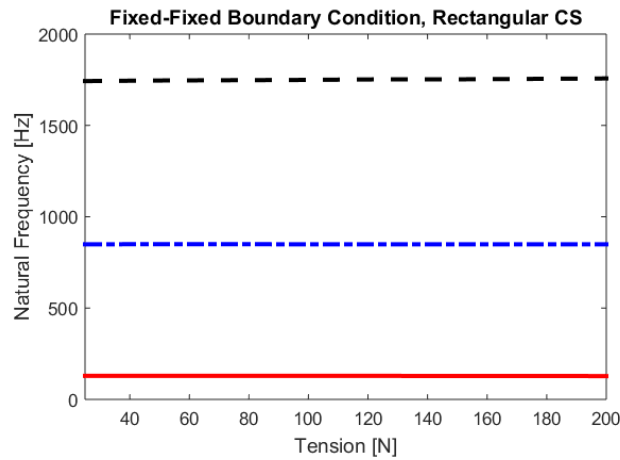


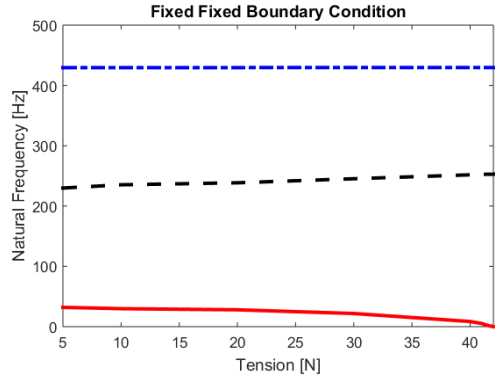
Fig. 2. 13 Effect of cable pre-tension on the natural frequencies for first in-plane bending, out-of-plane bending and torsional mode using the system parameters of Table (2.1). — denotes out of plane bending dominant mode. - - denotes torsion dominant mode. - - denotes in plane bending dominant mode.

parameters in Table. (2.5) are additionally considered for a rectangular cross section. The position coordinates of the center of the cable (y_c, z_c) are equal to (0.0098, 0.00095) m. From Fig. (2.14), we can see that as the cable pre-tension increases, the fundamental natural frequency for the out-of-plane bending drops to zero as the system undergoes buckling. As expected, the buckling load

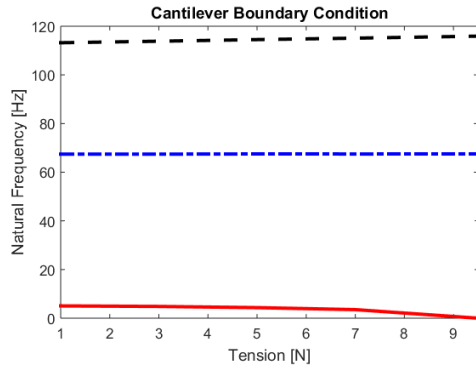
for the fixed-fixed boundary condition is the largest, then the simply supported, and finally the cantilever beam has the smallest critical loading. The strain energy distribution (bar graph) for beams with system parameters from Tables. (2.1) and (2.5) for fixed-fixed boundary condition for the first mode (which corresponds to the out of plane bending dominant mode) are shown in Figs. (2.15 a) and (2.15 b) respectively. In Fig. (2.15 a), the strain energy contributions from the axial, in-plane bending, out of plane bending and torsion coordinates are 5.08 %, 15.43 %, 79.48 % and 0.008 % respectively. In Fig. (2.15 b), the strain energy contributions in the axial, in-plane bending, out-of-plane bending and torsion coordinates are 0.005 %, 0.023 %, 71.75 % and 28.21 % respectively. As explained earlier for Fig. (2.7 a), in Fig. (2.15 a), the out of plane and in plane bending coordinates are strongly coupled to each other (for beam with parameters from Table. (2.1)). In Fig. (2.15 b), the out of plane bending coordinate is strongly coupled to the torsion mode when compared to axial and in-plane bending as a beam with lower young's modulus and wider geometry is more flexible in the torsional direction. By increasing the value for the cable pre-tension, the system's coupling gets stronger that results in strain energy transfer between the out of plane bending mode and other coordinates of motion as shown in Fig. (2.14). As similarly observed for the offset case study, for the modes associated with the same wave number, the mode with lower natural frequency transfers energy into the modes with the higher frequency. In this case, there is noticeable increase in the frequency for the torsion dominant mode when compared to the in plane due to the nature of the coupling between these three modes.

Table 2. 5 Material and geometrical properties for the tension case study, rectangular cross-section beam.

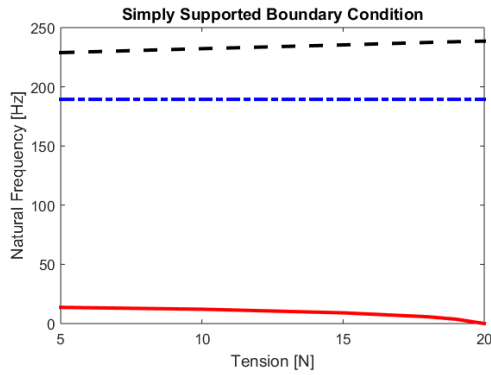
System parameters	Value
Beam length	0.25 m
Beam width	0.02 m
Beam height	0.0015 m
Beam density	1,300 Kg/m ³
Beam modulus of elasticity	2.2 GPa
Beam shear modulus	0.785 GPa
Beam Poisson's ratio	0.4
Cable radius	0.0002 m
Cable density	1,200 Kg/m ³
Cable modulus of elasticity	2 GPa



(a)



(b)

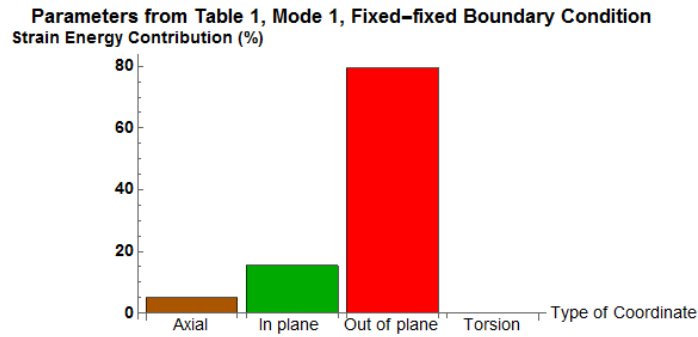


(c)

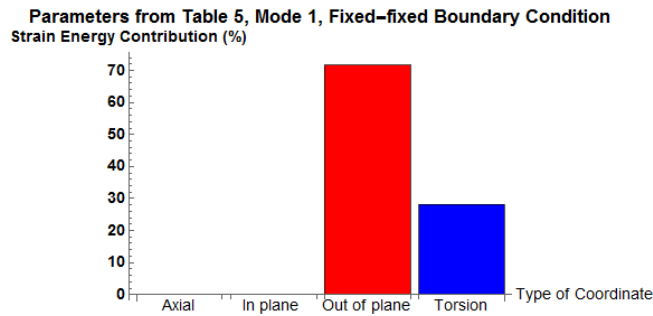
Fig. 2. 14 Effect of cable pre-tension on the natural frequencies for first in-plane bending, out-of-plane bending and torsional mode using the system parameters of Table. (2.5). — denotes out of plane bending dominant mode. - - denotes torsion dominant mode. - - denotes in plane bending dominant mode.

Table 2. 6 Material and geometrical properties for the tension case study, I-cross section beam

System parameters	Value
Beam length	0.25 m
Beam density	1,300 Kg/m ³
Beam modulus of elasticity	1 GPa
Beam shear modulus	0.35 GPa
Beam Poisson's ratio	0.4
Cable radius	0.0002 m
Cable density	1,200 Kg/m ³
Cable modulus of elasticity	1.1 GPa



(a)



(b)

Fig. 2. 15 Bar graph of strain energy contributions for mode 1 for beam with parameters from a) Table (2.1); b) Table (2.5) for fixed-fixed boundary condition.

To further, study the impact of tension on the natural frequencies, an I-beam cross-section shown in Figure. (2.16) (Front View) with the numerical parameters presented in Table. (2.6) is also considered. The position coordinates of the center of the cable in this case are $(y_c, z_c) = (0.0048, 0.0052) m$.

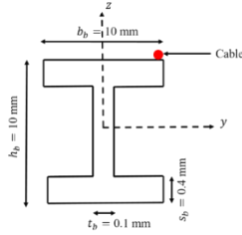
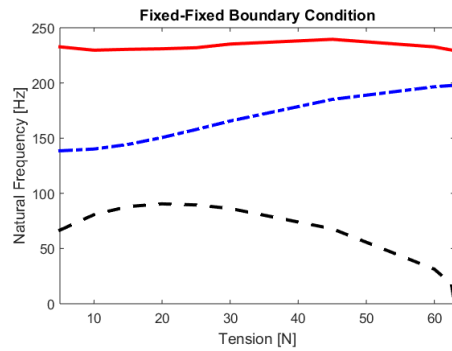
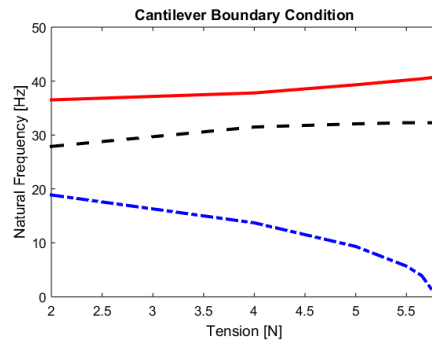


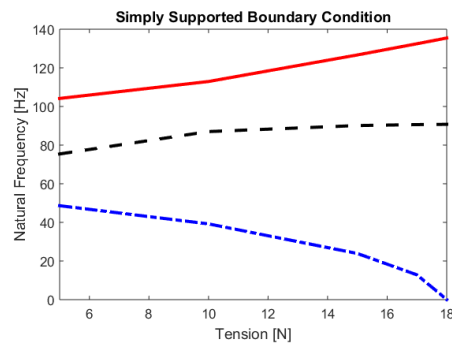
Fig. 2. 16 I-beam cross section and dimensions



(a)



(b)



(c)

Fig. 2. 17 Effect of cable pre-tension on the natural frequencies of first in plane bending, out-of-plane bending and torsional mode using the system parameters of Table (2.6) for an I-cross section beam. — denotes out of plane bending dominant mode. - - - denotes torsion dominant mode. - - - denotes in plane bending dominant mode.

This geometry was chosen due to its smaller torsional stiffness. As shown in Figure (2.17 a), the fundamental mode for the fixed-fixed boundary condition corresponds to the torsional dominant mode. In Figures (2.17 b) and (2.17 c), for cantilever and simply supported boundary conditions, the fundamental mode corresponds to the in plane bending dominant mode. As expected for the I cross-section, the in-plane bending has much smaller critical loading compared to the out-of plane bending due to the smaller moment of inertia in that direction. Therefore, the in-plane bending is shown to be more prone to buckling in Figures (2.17 b) and (2.17 c). Also, the critical loading for the simply supported is shown to be larger than the cantilever beam as expected. For fixed-fixed boundary condition, because the torsion mode is the fundamental one, the I section beam experiences torsional buckling. For cantilver and simply supported boundary conditions, the system experiences buckling in the in-plane direction.

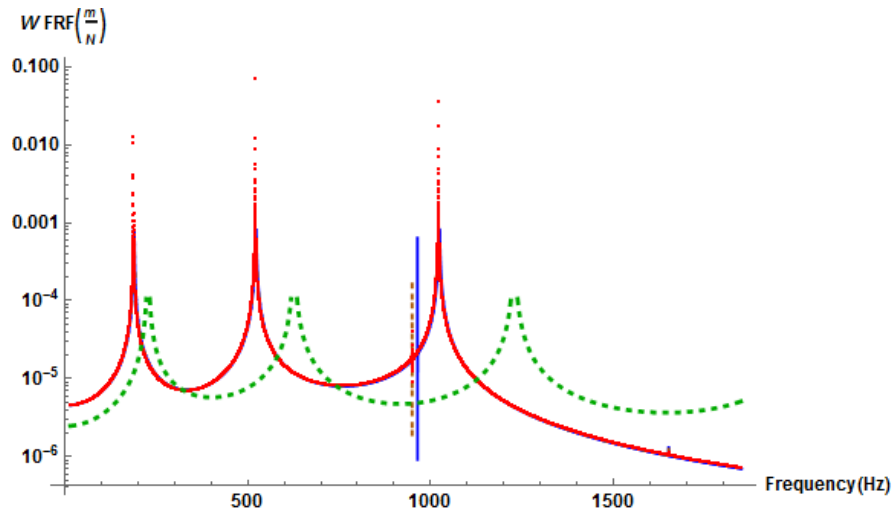
Finally, to clearly show the effect of coupling, a case study where forced excitation is applied to the structure in the out of plane bending direction and the resulting frequency response functions for the coupled Euler-Bernoulli analytical, coupled Timoshenko model, FEA and decoupled Euler Bernoulli model are presented in Fig. (2.18).

The numerical parameters used are from Table. (2.1). The frequency response function for the coupled analytical model is calucated from Eq. (2.46).

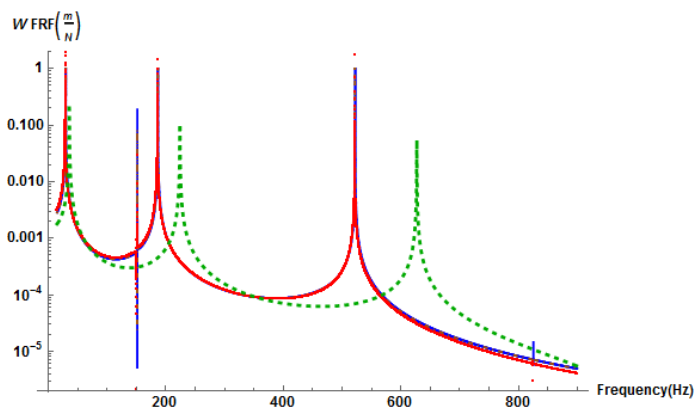
$$W(\omega) = \sum_{i=1}^{\infty} \frac{W(x = x_s).W(x = x_a)}{\omega_i^2 - \omega_f^2} \quad (2.46)$$

where $W(x = x_s)$ represents the mass-normalized coupled out-of-plane bending displacement at the sensing location and $W(x = x_a)$ represents the mass-normalized coupled out-of-plane bending displacement at the actuation location. ω_f is the forcing frequency. ω_i is the natural frequency corresponding to the mode i . The natural frequencies for fixed-fixed, cantilever and simply supported boundary conditions are presented in Tables. (2.2)- (2.4) respectively. The mass normalized coupled mode shapes are calculated and presented in Figs. (2.4)- (2.6) for fixed-fixed, cantilever and simply supported boundary conditions respectively.

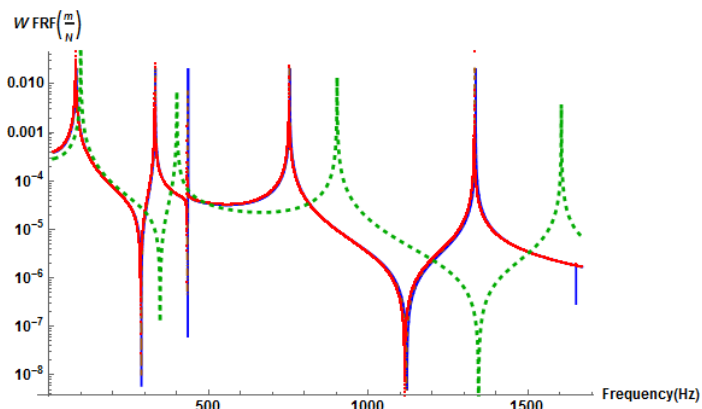
Here, $x_s = 0.2276 \text{ m}$ & $x_a = 0.0498 \text{ m}$, $x_s = 0.25 \text{ m}$ & $x_a = 0.0952 \text{ m}$, $x_s = 0.199 \text{ m}$ & $x_a = 0.136 \text{ m}$ are the sensing and actuation locations respectively for fixed-fixed, cantilever, simply supported boundary condition respectively. Similarly, the frequency response functions for the decoupled and FEA models are calculated and plotted in Fig. (2.18). The significant peaks in the plots correspond to the out of plane bending direction and the first sharp peak corresponds to



(a)



(b)



(c)

Fig. 2. 18 Frequency response functions for a) Fixed-fixed b) Cantilever c) Simply Supported boundary conditions. — denotes cabled beam analytical (Euler Bernoulli coupled) - - - denotes cabled beam analytical (Timoshenko coupled) ··· denotes FEA (coupled) - - - Cabled beam analytical (decoupled).

the in-plane bending dominant mode and the second sharp peak corresponds to the torsional dominant mode. In Fig. (2.18 a), for the fixed-fixed boundary condition, for the in-plane bending dominant mode, it can be seen that the coupled Timoshenko beam model predicts the frequency better than the coupled Euler-bernoulli beam model. As we can clearly observe from Fig. (2.18), the frequency response function of both coupled Euler-Bernoulli and coupled Timoshenko models match very well with that of FEA when compared to the decoupled model. Therefore, the coupled model provides a better picture of the dynamics when compared to a decoupled model.

2.2 Coupled Vibrations in Structure with Periodic Wrapping Pattern

2.2.1 Mathematical Model

The cable-harnessed structure with periodic wrapping pattern is shown in Fig. (2.19 a) with the different coordinates of motion such as the axial, in plane bending, out of plane bending, torsion and both the rotations of cross-sections about y and z-axes. The cable is wrapped around the beam in a diagonal manner. The fundamental element of the wrapping pattern is shown in Fig. (2.19 b). Each fundamental element of the wrapping pattern consists of a diagonal section of the cable and the cable wrapping at the end of each fundamental element act as lumped masses.

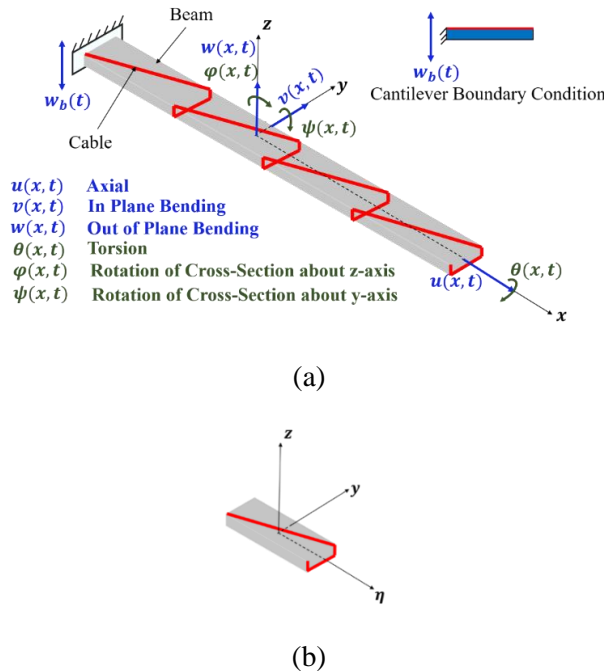


Fig. 2. 19 (a) Representation of the cable harnessed structure with periodic wrapping pattern along with the coordinates of motion. (b) Fundamental element of wrapping pattern.

In case of straight cable in Section. (2.1), the model developed is exact and in case of periodic pattern it is difficult to develop exact model due to diagonal section and also multiple fundamental elements. An equivalent continuum model is presented to study the vibrations of structures with periodic pattern. The total strain and kinetic energies of the cable-harnessed structure for Timoshenko model are shown in Eqs. (2.47) and (2.48).

$$U_{system} = \frac{1}{2} \left[\iiint E_b (-T \cos \mu / E_b A_b + \varepsilon_{xx})^2 + G_b (\gamma_{xy})_b^2 + G_b (\gamma_{zx})_b^2 dA dx \right] + \frac{1}{2} \left[\iiint E_c (T / E_c A_c + \varepsilon_{xx} \cos^2 \mu + \gamma_{xy} \cos \mu \sin \mu)^2 dA \frac{dx}{\cos \mu} \right] \quad (2.47)$$

$$= \frac{1}{2} \int_0^L [c_1(u')^2 + c_2(v')^2 + c_3(w')^2 + c_4(\theta')^2 + c_5(\varphi')^2 + c_6(\psi')^2 + c_7(\varphi)^2 + 2c_8(u')(\varphi') + 2c_9(u')(\psi') + 2c_{10}(\varphi')(\psi') + 2c_{11}(v')(\varphi) + 2c_{12}(\varphi)(\theta') + 2c_{13}(v')(\theta') + 2c_{14}(w')(\theta') + 2c_{15}(u')(\varphi) + 2c_{16}(\psi')(\varphi) + 2c_{17}(u')(v') + 2c_{18}(u')(\theta') + 2c_{19}(v')(\varphi') + 2c_{20}(\theta')(\varphi') + 2c_{21}(v')(\varphi') + 2c_{22}(\psi')(\theta') + c_{23}(\psi)^2 + 2c_{24}(\psi)(w')] dx$$

$$T_{system} = \frac{1}{2} \left[\iiint \rho_b \{\dot{X}, \dot{Y}, \dot{Z}\}^T \{\dot{X}, \dot{Y}, \dot{Z}\} dA dx + \iiint \rho_c \{\dot{X}, \dot{Y}, \dot{Z}\}^T \{\dot{X}, \dot{Y}, \dot{Z}\} dA \frac{dx}{\cos \mu} \right] \quad (2.48)$$

$$= \frac{1}{2} \int_0^L [k_1(\dot{u})^2 + k_2(\dot{v})^2 + k_3(\dot{w})^2 + k_4(\dot{\theta})^2 + k_5(\dot{\varphi})^2 + k_6(\dot{\psi})^2] dx$$

where ε_{xx} is the direct strain in the x direction. γ_{xy} and γ_{zx} are the shear strains in the xy and the yz plane respectively. The constants used in the kinetic and strain energy expressions Eq. (2.47) and Eq. (2.48) are shown in Eq. (B.1) of Appendix B. L is the length of each fundamental element of the periodic pattern. where superscript $(\)'$ denotes partial derivative with respect to spatial coordinate $x(\frac{\partial}{\partial x})$ and superscript $(\dot{\ })$ denotes partial derivative with respect to time $t(\frac{\partial}{\partial t})$. The strain and kinetic energy coefficients depend on the material and geometric properties of the cable and the beam.

Similarly, the strain and kinetic energy expressions for the cable harnessed beam with diagonal wrapping pattern for the Euler-Bernoulli model [51] are shown in Eqs. (2.49) and (2.50).

$$U = \frac{1}{2} \int_0^L [b_1(u'')^2 + b_2(v'')^2 + b_3(w'')^2 + b_4(\theta'')^2 + 2b_5(w'')(v'') + 2b_6(u'')(\theta'') + 2b_7(v'')(\theta'') + 2b_8(w'')(\theta'') + 2b_9(u'')(v'') + 2b_{10}(u'')(w'') + 2b_{11}(w'')(v'') + 2b_{12}(v'')(v'') + 2b_{13}(v'')(w'')] dx \quad (2.49)$$

$$T = \frac{1}{2} \int_0^L [k_1(\dot{u})^2 + k_2(\dot{v})^2 + k_3(\dot{w})^2 + k_4(\dot{\theta})^2] dx \quad (2.50)$$

The constants of the above strain and kinetic energy expressions for the Euler-Bernoulli strain and kinetic energy are shown in Eq. (B.2) of Appendix B.

Let ηyz be the local coordinate system of a single fundamental element (Fig. (2.19 b)). Then position of the cable where the strains are evaluated can be defined as $(y_c, z_c) = (\eta \tan \mu - \frac{b}{2}, \frac{h}{2})$.

The wrapping angle μ can be defined as $\tan^{-1}(\frac{b}{L})$. The advantage of periodicity of wrapping pattern can be taken and the equivalent continuum model including the effect of lumped masses at the end of each fundamental element can be obtained using the homogenization method [51]. The strain and kinetic energy per unit length of the fundamental element are calculated and are assumed the same through the length of the fundamental element. Since the wrapping pattern is periodic, the homogenized strain and kinetic energy is assumed the same across all the other fundamental elements. After applying the Hamilton's principle, $\delta \int_{t_1}^{t_2} (T - U) dt = 0$, the governing equations for the Timoshenko and Euler-Bernoulli model after including the effect of harmonic base excitation are shown in Eqs. (2.51) and (2.53). The boundary conditions for the fixed and free ends are shown in Eqs. (2.52, 2.55) and (2.54, 2.56) respectively.

Timoshenko model

$$-k_1 \ddot{u} + c_1 u'' + c_8 \varphi'' + c_9 \psi'' + c_{15} \varphi' + c_{17} v'' + c_{18} \theta'' = 0 \quad (2.51 \text{ a})$$

$$-k_2 \ddot{v} + c_2 v'' + c_{13} \theta'' + c_{19} \varphi'' + c_{21} \psi'' + c_{11} \varphi' + c_{17} u'' = 0 \quad (2.51 \text{ b})$$

$$-k_3 \ddot{w}_{rel} + c_3 w_{rel}'' + c_{14} \theta'' + c_{16} \theta' + c_{24} \psi' = k_3 \ddot{w}_b \quad (2.51 \text{ c})$$

$$-k_4 \ddot{\theta} + c_4 \theta'' + c_{13} v'' + c_{14} w_{rel}'' + c_{12} \varphi' - c_{16} w_{rel}' + c_{18} u'' + c_{22} \psi'' + c_{20} \varphi'' = 0 \quad (2.51 \text{ d})$$

$$-k_5 \ddot{\varphi} + c_5 \varphi'' - c_7 \varphi + c_8 u'' - c_{11} v' + c_{10} \psi'' - c_{12} \theta' - c_{15} u' - c_{16} \psi' + c_{19} v'' + c_{20} \theta'' = 0 \quad (2.51 \text{ e})$$

$$-k_6 \ddot{\psi} + c_6 \psi'' - c_{23} \psi + c_9 u'' - c_{24} w_{rel}' + c_{10} \varphi'' + c_{21} v'' + c_{22} \theta'' + c_{16} \varphi' = 0 \quad (2.51 \text{ f})$$

Fixed end

$$u = v = w_{rel} = \theta = \varphi = \psi = 0|_{x=0 \text{ or } l} \quad (2.52)$$

Free end

$$c_1 u' + c_8 \varphi' + c_9 \psi' + c_{15} \varphi + c_{17} v' + c_{18} \theta' = 0|_{x=0 \text{ or } l}$$

$$c_2 v' + c_{11} \varphi + c_{13} \theta' + c_{17} u' + c_{19} \varphi' + c_{21} \psi' = 0|_{x=0 \text{ or } l}$$

$$c_3 w_{rel}' + c_{14} \theta' + c_{16} \theta + c_{24} \psi = 0|_{x=0 \text{ or } l}$$

$$c_4 \theta' + c_{12} \varphi + c_{13} v' + c_{14} w_{rel}' + c_{18} u' + c_{20} \varphi' + c_{22} \psi' = 0|_{x=0 \text{ or } l} \quad (2.53)$$

$$c_5 \varphi' + c_8 u' + c_{10} \psi' + c_{19} v' + c_{20} \theta' = 0|_{x=0 \text{ or } l}$$

$$c_6 \psi' + c_9 u' + c_{10} \varphi' + c_{16} \varphi + c_{21} v' + c_{22} \theta' = 0|_{x=0 \text{ or } l}$$

Euler-Bernoulli model

$$-k_1\ddot{u} + b_1u'' + b_9v'''' + b_{10}w_{rel}'' + b_6\theta'' = 0 \quad (2.54 \text{ a})$$

$$-k_2\ddot{v} - b_2v'''' - b_9u'''' - b_5w_{rel}'''' + b_{13}w_{rel}'' - b_7\theta'''' + b_{12}\theta'' = 0 \quad (2.54 \text{ b})$$

$$-k_3\ddot{w}_{rel} - b_3w_{rel}'''' - b_{10}u'''' - b_5v'''' - b_{13}v'''' - b_8\theta'''' + b_{11}\theta'' = k_3\ddot{w}_b \quad (2.54 \text{ c})$$

$$-k_4\ddot{\theta} + b_4\theta'' + b_6u'' + b_7v'' + b_{12}v'' + b_8w_{rel}'' + b_{11}w_{rel}'' = 0 \quad (2.54 \text{ d})$$

Fixed end

$$u = v = w_{rel} = \theta = v' = w_{rel}' = 0|_{x=0 \text{ or } l} \quad (2.55)$$

Free end

$$b_1u' + b_6\theta' + b_9v'' + b_{10}w_{rel}'' = 0|_{x=0 \text{ or } l}$$

$$b_2v'' + b_5w_{rel}'' + b_6u' + b_7\theta' = 0|_{x=0 \text{ or } l}$$

$$b_2v'' + b_5w_{rel}'' + b_9u'' + b_7\theta'' - b_{12}\theta' - b_{13}w_{rel}' = 0|_{x=0 \text{ or } l}$$

$$b_3w_{rel}' + b_5v'' + b_8\theta' + b_{10}u' + b_{13}v' = 0|_{x=0 \text{ or } l} \quad (2.56)$$

$$b_3w_{rel}'' + b_5v'''' + b_{10}u'' + b_8\theta'' - b_{11}\theta' + b_{13}v'' = 0|_{x=0 \text{ or } l}$$

$$b_4\theta' + b_6u' + b_7v'' + b_8w_{rel}' + b_{11}w_{rel}' + b_{12}v' = 0|_{x=0 \text{ or } l}$$

where $w_b(t)$ is the base displacement in the out of plane direction. $w_{rel}(x, t)$ is the relative out of plane bending displacement of the structure with respect to the base excitation. In Timoshenko model Eq. (2.51), coefficients c_{12} , c_{13} and c_{15} to c_{22} and for the Euler-Bernoulli model, in Eq. (2.54) coefficients b_6 to b_8 are the additional coupling terms that are not seen in the case of straight cable pattern. Therefore, the mathematical model in this paper covers a more general case when the wrapping angle is non-zero. In Eq. (2.51 a), the axial coordinate is coupled to the two rotations of cross-section, in-plane bending and the torsion mode. In Eq. (2.51 b), the in-plane bending mode is coupled to the two rotations of cross-section, axial and the torsion mode. In Eq. (2.51 c), the out of plane bending is coupled to the rotation of cross-section about y-axis and the torsion mode. In Eq. (2.51 d), the torsion mode is coupled with the all the coordinates. In Eq. (2.51 e), the rotation of cross-section about z-axis is coupled with all the coordinates except the out of plane bending. In Eq. (2.51 f), the rotation of cross-section about y-axis is coupled to all the other coordinates. In Eq. (2.54 a), the axial mode is coupled to all the other coordinates. Similarly, in Eqs. (2.54 b), (2.54 c) and (2.54 d), the in-plane, out-of-plane and torsion modes are coupled to all the other coordinates. The coupled partial differential equations, Eqs. (2.51) and (2.54) are second order in time and the temporal solution of the PDEs can be assumed harmonic. In the first step, the unforced coupled system is solved for the natural frequencies and mode shapes. The solution procedures for obtaining the natural frequencies, mode shapes for the PDEs of the

type Eqs. (2.51) and (2.54) are shown in the previous works [118,129,130] and are presented in Section. 2.1 of this chapter.

2.2.2 Numerical Simulations and Analysis

In the Section. 2.2.2, theoretical case studies related to the periodic wrapping pattern are performed. Firstly, the frequency response functions obtained from the coupled EB and TBT models are compared with the frequency response function obtained from the EB decoupled model for three different samples. Then, the sensitivity analysis is performed by varying parameters such as the cable radius and the number of fundamental elements of the wrapping pattern and the frequencies of the periodically wrapped structure are compared with the frequencies of straight cable to highlight the change in dynamic behavior between the two patterns.

Table 2. 7 System parameters for the samples 1, 2 and 3.

System parameters	Sample 1 Values	Sample 2 Values	Sample 3 Values
Beam length (l)	250 mm	260 mm	252 mm
Beam width (b)	10 mm	11 mm	9.5 mm
Beam thickness (t)	1.5 mm	0.975 mm	1.20 mm
Beam density (ρ_b)	2,700 Kg/m ³	2,768 Kg/m ³	2,768 Kg/m ³
Beam modulus of elasticity (E_b)	68.9 GPa	68.9 GPa	68.9 GPa
Beam Shear modulus (G_b)	26 GPa	25.7 GPa	25.7 GPa
Pre-tension of the cables (T)	25 N	40 N	20 N
Cable radius (r_c)	0.7 mm	0.21 mm	0.21 mm
Cable density (ρ_c)	1,400 Kg/m ³	1,400 Kg/m ³	1,400 Kg/m ³
Cable modulus of elasticity (E_c)	150 GPa	128.04 GPa	128.04 GPa
Number of fundamental elements	8	10	9
Number of Cables	1	5	10
Sensing location	250 mm	53 mm	250 mm

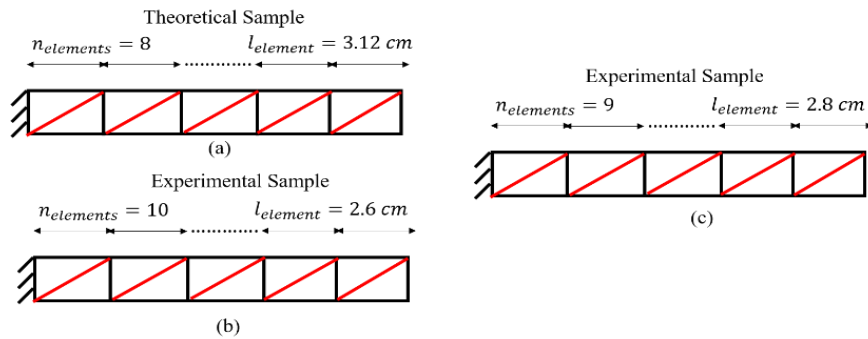
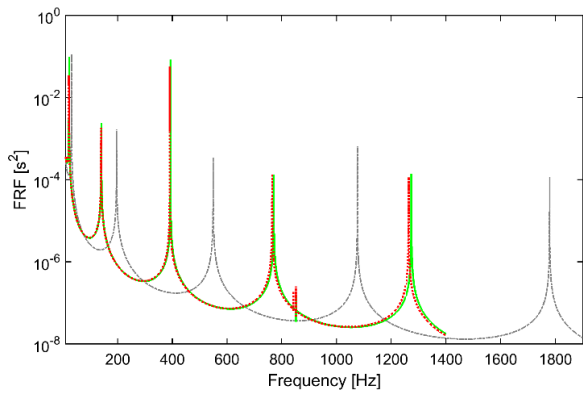
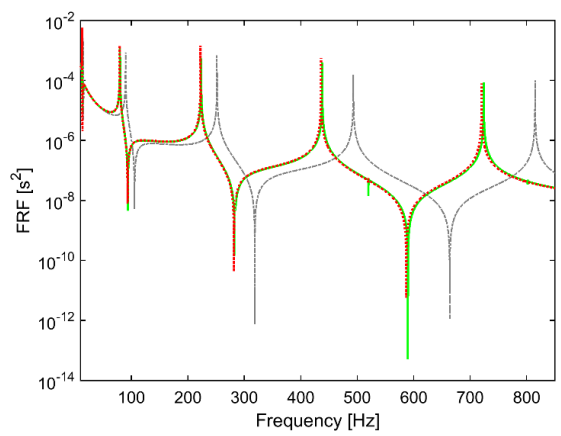


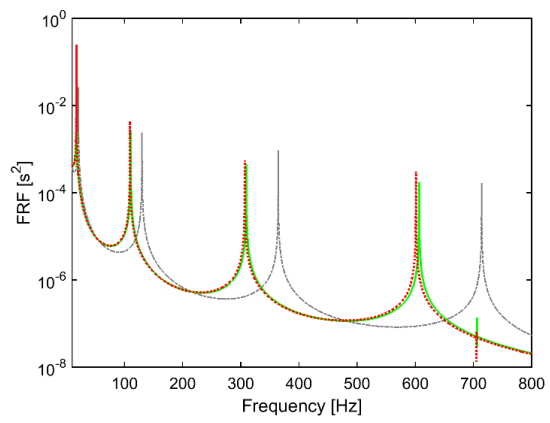
Fig. 2. 20 Representation of the top view cable harnessed structure with periodic wrapping pattern along with the dimensions. (a) Sample 1 (b) Sample 2 (c) Sample 3.



(a)



(b)



(c)

Fig. 2. 21 Comparison of theoretical frequency response functions for coupled (EB and TBT) and decoupled models for (a) Sample 1 (b) Sample 2 (c) Sample 3.
 ----- Cabled Analytical (Decoupled)
 ————— Cabled Analytical (coupled EB)
 Cabled Analytical (coupled Timoshenko).

The layout and dimensions of wrapping pattern of the three different periodic designs studied are presented in Fig. (2.20). In Fig. (2.21), the frequency response functions (FRF) of the fully coupled Euler-Bernoulli, Timoshenko models are compared to the frequency response function of the Martin et al [51,52] decoupled model for the samples 1,2 and 3 whose parameters are presented in Table. (2.7). The boundary condition assumed is cantilever as shown in Fig. (2.19) and the structure is subjected to harmonic base excitation. It is assumed that the cable will have same strain values as the top fiber of the beam. The sensing locations for the simulations are at $x = 250, 53$ and 250 mm for samples 1, 2 and 3 respectively. Physically, out of the three samples, sample 1 has the highest length to thickness ratio followed by samples 3 and 2. Sample 1 has the largest cable radius of 0.7 mm, sample 3 has 10 cables with each cable having a radius of 0.21 mm and sample 2 has 5 cables each having a diameter of 0.21 mm. From Figs. (2.21 a), (2.21 b) and (2.21 c), it can be seen that the out of plane bending peaks from the decoupled model over-predict the frequencies when compared to the corresponding peaks from the fully coupled EB and TBT models for all the samples. Since, the structure is excited in the out of plane bending direction, the significant peaks in coupled FRF correspond to the out-of-plane bending dominant mode and certain sharp peaks which correspond to the torsion and in-plane bending mode can also be noticed. The natural frequencies from the coupled and decoupled models are tabulated and shown in Tables. (2.8), (2.9) and (2.10) along with the percentage difference in the frequencies between the coupled and decoupled models. In sample 1, where the cable radius is the largest, we see greater difference between the coupled and decoupled model. When the cable radius is large, the strain energy is highly over-predicted by the decoupled model when compared to the coupled model for the out of plane bending modes. At larger values of cable radius, the coupling coefficients also increase in magnitude. This increase in coupling effect means that the structure is more flexible in multiple directions, which the decoupled model ignores. In decoupled model, the structure is assumed flexible in one direction and rigid in the other directions, so, the decoupled FRF curve does not predict the modes in the other coordinates of motion. Therefore, in the coupled model the strain energy is re-distributed amongst different coordinates from the out of plane direction because of this the frequencies are lower for coupled model. Later on, in this Section. 2.2.2, the simulation result of the variation of natural frequency with respect to the cable radius is presented. For the modes analyzed for the three samples, from Table. (2.8) we see two in-plane bending modes and one torsion mode in addition to the five out of plane bending modes for the fully coupled models for sample 1. Similarly, for samples 2 and 3, we see two in-plane bending dominant modes and one torsion dominant mode (Tables. (2.9) and (2.10)). In the higher modes in the FRF plot (Fig. (2.21)), the coupling effect can be significantly seen. The Timoshenko model also under predicts the frequencies when compared to the Euler-Bernoulli model. This is because, in Timoshenko model we consider two more additional coordinates namely the rotations of cross-section

therefore the coupled Timoshenko model allows more flexibility for the structure when compared to the coupled Euler-Bernoulli model.

Table 2. 8 Coupled and Decoupled Natural Frequencies for sample 1.

Mode No	Decoupled EB [Hz]	Coupled EB [Hz]	Coupled TBT [Hz]	% Decoupled EB and Coupled EB	% Decoupled EB and Coupled TBT
1	31.29	22.40 (OP)	22.27 (OP)	28.41	28.82
2	-	135.71 (IP)	135.53 (IP)	-	-
3	196.13	140.43(OP)	139.55 (OP)	28.39	28.84
4	549.23	393.19(OP)	390.6 (OP)	28.41	28.88
5	1076.21	770.45(OP)	764.93 (OP)	28.41	28.92
6	-	850.52(IP)	842.40 (IP)	-	-
7	-	852.17 (T)	851.78 (T)	-	-
8	1779.02	1253.58(OP)	1263.62 (OP)	28.41	28.97

*OP, IP and T stand for Out of plane bending, In-plane bending and Torsion dominant modes respectively

Table 2. 9 Coupled and Decoupled Natural Frequencies for sample 2.

Mode No	Decoupled EB [Hz]	Coupled EB [Hz]	Coupled TBT [Hz]	% Decoupled EB and Coupled EB	% Decoupled EB and Coupled TBT
1	14.16	12.66 (OP)	12.61	10.59 %	10.94 %
2	88.81	79.25 (OP)	79.03	10.76 %	11.01 %
3	-	133.74 (IP)	133.54	-	-
4	248.7	222.28 (OP)	221.26	10.62 %	11.03 %
5	487.32	435.59 (OP)	433.49	10.67 %	11.04 %
6	-	497.93 (T)	497.52	-	-
7	805.56	720.02 (OP)	716.40	10.61 %	11.06 %
8	-	838.12 (IP)	829.69	-	-

*OP, IP and T stand for Out of plane bending, In-plane bending and Torsion dominant modes respectively

Table 2. 10 Coupled and Decoupled Natural Frequencies for sample 3.

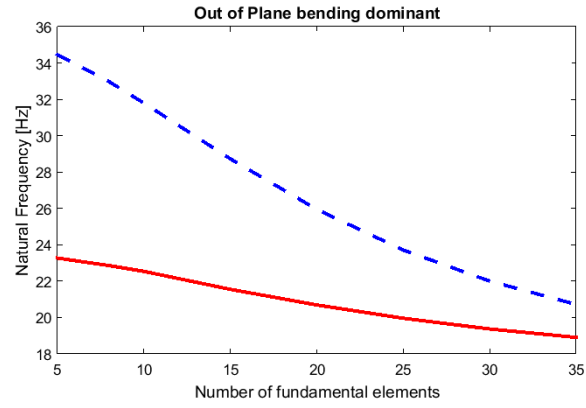
Mode No	Decoupled EB [Hz]	Coupled EB [Hz]	Coupled TBT [Hz]	% Decoupled EB and Coupled EB	% Decoupled EB and Coupled TBT
1	20.76	17.63 (OP)	17.49	15.07 %	15.75 %
2	130.13	110.56 (OP)	109.62	15.03 %	15.76 %
3	-	126 (IP)	125.85	-	-
4	364.41	309.55 (OP)	306.86	15.05 %	15.79 %
5	714.06	606.53 (OP)	601.07	15.05 %	15.82 %
6	-	705.97 (T)	705.22	-	-
7	-	789.70 (IP)	783.02	-	-

*OP, IP and T stand for Out of plane bending, In-plane bending and Torsion dominant modes respectively

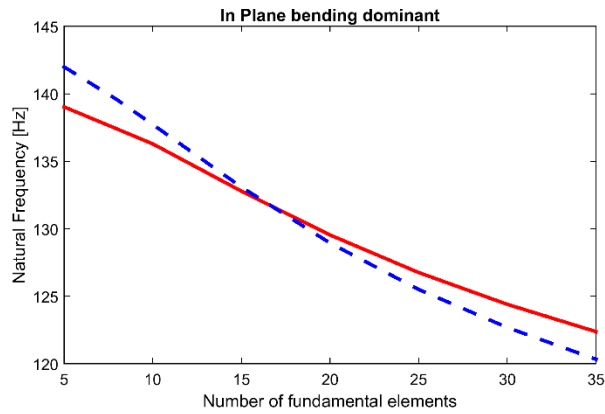
Table 2. 11 System parameters for the sensitivity analysis

System parameters	Values
Beam length (l)	250 mm
Beam width (b)	10 mm
Beam thickness (t)	1.5 mm
Beam density (ρ_b)	2,700 Kg/m ³
Beam modulus of elasticity (E_b)	68.9 GPa
Beam Shear modulus (G_b)	26 GPa
Pre-tension of the cables (T)	25 N
Cable radius (r_c)	0.7 mm (variable)
Cable density (ρ_c)	1,400 Kg/m ³
Cable modulus of elasticity (E_c)	150 GPa
Number of Cables	9 (variable)

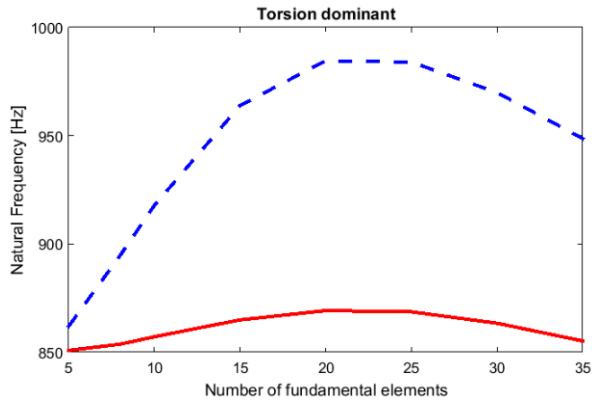
In Figs. (2.22) and (2.23), the effect of parameters like cable radius and number of fundamental elements on the natural frequency are presented. Fig. (2.22) presents the variation of natural frequency of the structure with respect to the number of fundamental elements of wrapping pattern along the x-axis. The parameters used for this simulation are from Table. (2.11). The natural frequencies of the out of plane bending dominant, in-plane bending dominant and the torsion dominant are plotted in Figs. (2.22 a), (2.22 b) and (2.22 c) respectively. Frequencies obtained from the coupled model presented in this paper and Martin et al [51] model are plotted on the same figure. For the results pertaining to the coupled curve, coupled Euler-Bernoulli is used, as the structure considered in the simulation is slender and the effect of rotation of cross-section degree of freedom will be minimal. In Fig. (2.22 a), when the number of fundamental elements are lower, there is large difference between the coupled and the decoupled models and as the number of fundamental elements increase, the coupling effect reduces and we see the gap between the coupled and decoupled getting smaller. The coupling in the structure is maximum when the wrapping angle is smaller and as the wrapping becomes tighter, the coupling decreases. More analysis related to this is presented in Table. (2.13) and the discussion related to this will be touched upon at that point. From Fig. (2.22 b), it can be observed that the coupling in the in plane bending dominant modes is lesser than the out-of-plane bending mode. From Fig. (2.22 c), the torsion dominant mode increases until 20 elements and starts decreasing when the number of elements increase beyond 25. This suggests that the strain energy is re-distributed from the out-of-plane bending into the torsional mode until when the number of fundamental elements are 25. This



(a)



(b)



(c)

Fig. 2. 22 Effect of variation in number of fundamental elements vs the fundamental natural frequency of a) Out of plane dominant mode b) In-plane bending dominant mode c) Torsion dominant mode.
— Present work (Coupled) - - - Martin et al [51].

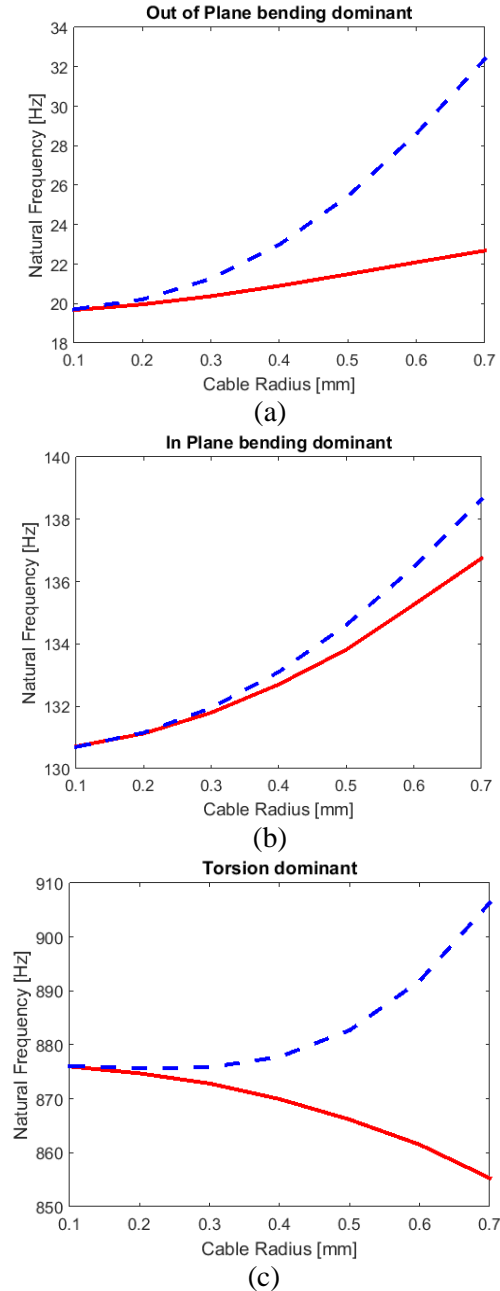


Fig. 2. 23 Effect of variation in cable radius vs the fundamental natural frequency of a) Out of plane dominant mode b) In-plane bending dominant mode c) Torsion dominant mode. — Present work (Coupled); — Martin et al [51].

is because of the coupling effect between various coordinates. The stiffening effects dominate the response of the structure when the number of fundamental elements are less than 20 because of smaller wrapping angle and the mass effects start becoming more significant when the number of fundamental elements of wrapping start increasing beyond 25 elements.

Table 2. 12 System parameters for the sensitivity analysis in Table. 2.13

System parameters	Values
Beam length (l)	250 mm
Beam width (b)	10 mm
Beam thickness (t)	1.2 mm
Beam density (ρ_b)	2,768 Kg/m ³
Beam modulus of elasticity (E_b)	68.9 GPa
Beam Shear modulus (G_b)	25.7 GPa
Pre-tension of the cables (T)	25 N
Cable radius (r_c)	0.21 mm
Cable density (ρ_c)	1,400 Kg/m ³
Cable modulus of elasticity (E_c)	128.04 GPa
Number of Cables	9

Table 2. 13 Sensitivity analysis for multiple frequencies with respect to the straight and periodic pattern cases

Mode No	Bare Beam [Hz]	Straight Cable No offset [Hz]	Straight Cable at offset [Hz]	n=5 [Hz]	n=9 [Hz]	n=15 [Hz]	n=20 [Hz]	n=30 [Hz]	n=50 [Hz]
1	15.47	18.4	17.39	18.1	17.6	16.82	16.18	15.24	14.30
2	96.96	115.2	109.76	113.5	110.7	105.28	101.22	95.92	88.71
3	128.93	125.67	147.20 (IP)	135.8	133.7	130.07	127.37	122.70	116.43
4	271.54	322.6	307.48	317	309.2	295.07	284.25	267.53	248.44
5	532.09	632.3	602.87	621.2	606.2	578.20	556.88	524.09	486.77
6	702.16	683.88	660.50 (T)	678.6	681.8	688.02	690.57	689.07	658.42
7	808.09	787.64	923.25 (IP)	850.7	838.1	815.82	798	769	729.64
8	879.57	1045.3	996.94	1027.5	1001.9	956.04	920.23	866.31	804.52

*OP, IP and T stand for Out of plane bending, In-plane bending and Torsion dominant modes respectively

Fig. (2.23 a), (2.23 b) and (2.23 c) represents the variation of the first out-of-plane, in-plane and torsion dominant modes with respect to the cable radius respectively. In Fig. (2.23 a) and Fig. (2.23 b), the natural frequencies increase as the cable radius increases for the out-of-plane and in-plane dominant modes as the strain energy increases at a faster rate when compared to kinetic energy. The natural frequency of the coupled curve increases at a slower rate when compared to the decoupled curve. As the radius of the cable radius increases, the coupling coefficients, which depend on the area of cross-section, also become stronger. Stronger coupling means the structure is flexible in multiple directions, which the decoupled model does not take into account, and as a result the decoupled model over predicts the frequencies at larger values of cable radius for bending dominant modes. In Fig. (2.23 c), the frequency associated with the torsion dominant

mode decreases as the cable radius increases. The torsional kinetic energy increases at a faster rate when compared to the strain energy in the torsional direction.

In Table. (2.13), the natural frequencies associated with the case where the cable is positioned at the centerline (no offset) [118] , case where the cable is at an offset position [118], bare beam and cases where the number of fundamental elements are varied are compared to each other. The parameters used for this simulation are from Table. (2.13). In Table. (2.13), the frequencies presented in the third row correspond to the first in-plane bending mode. The frequencies presented in the sixth row correspond to the first torsion dominant mode and the frequencies presented in the seventh row correspond to the second in plane bending dominant mode. To analyze further, the case with straight cable at offset shows more coupling than the case of periodic wrapping pattern. This can be noticed when we look at the coupled natural frequencies of the two different systems under comparison with their respective decoupled counterparts. For out-of-plane bending modes, in case of straight cable with offset case, the percentage difference between the coupled and the decoupled model in Martin et al [51] for the first three modes are 19.56%,19% and 18.97% and the difference between the coupled and decoupled models for the structure with five diagonal elements for the first three modes are 14.29%, 14.26% and 14.51%. As the coupling effect in case of periodic pattern is lower, the coupled out of plane bending dominant frequencies did not drop as much as the straight cable case and therefore we see more stiffening effect in case of structure with periodic wrapping pattern until when the number of fundamental elements are equal to 9. The case where straight cable is positioned at the centerline (no offset case) shows lesser coupling and more stiffening effect (by also comparing with the frequencies from bare beam) when compared to the case where the cable is positioned at an offset distance. When the number of fundamental elements of wrapping pattern are increased beyond 9 elements, the natural frequency of the periodic wrapped structure decreases and approaches the bare beam. As the number of fundamental elements of wrapping pattern increase, the natural frequencies drop in periodic structure as more mass is added to the structure and also when the more fundamental elements of wrapping pattern are increased, the wrapping angle also increases. As the wrapping angle is increased, the stiffening effect reduces, and therefore we see a drop in the natural frequencies as the number of fundamental elements are increased. Therefore, to minimize the effect of stiffening and mass effects of cabling on the host structure, it is better to wrap the cable around the host structure in periodic pattern. From the case study presented in

Table. (2.13), if number of fundamental elements are around 30 we see minimal effect of mass and stiffening effects of cabling on the host structure. The optimal number of fundamental elements depends on the parameter under study and from the mathematical models presented in this section, coupled analytical models give better picture of the dynamics of the system when compared to the decoupled model.

Another interesting aspect to study in the cable-harnessed beam with periodic wrapping pattern is the concept of cut off or transition frequency in Timoshenko beam theory. The relevant literature regarding this is described in Chapter 1. In Timoshenko beams with simply supported boundary conditions [109], we see a mode with pure-shear mode vibrations which is referred to as cut off or transition frequency an interesting concept which has received considerable attention in the recent past. For frequencies below this transition frequency, we see bending mode vibrations and for frequencies above the transition frequency, we see both shear dominant mode and also some modes with bending dominant vibrations. This concept may be of practical interest in structures where the transition frequency and shear dominant modes start to appear in the lower modes of vibration. For a simple beam, this aspect has been studied thoroughly through various papers for simply supported boundary condition and it is concluded there that the transition frequency is a part of frequency spectrum for simply supported boundary conditions. For other boundary conditions, it is not part of the frequency spectrum. However, we still see the appearance of shear dominant modes in the structure for all the boundary conditions. For a simple Timoshenko beam, the modes that are coupled are the bending and the rotation of cross-section modes. The governing partial differential equations for Timoshenko bare beam can be obtained from Ref. [120]. The mathematical form of the mode shape parameter α_i is shown in Eqs. (2.57)- (2.59) as follows:

Table 2. 14 System parameters for transition frequency case study

System parameters	Values
Beam length (l)	200 mm
Beam width (b)	11 mm
Beam thickness (t)	10 mm
Beam density (ρ_b)	2,768 Kg/m ³
Beam modulus of elasticity (E_b)	68.9 GPa
Beam Shear modulus (G_b)	25.7 GPa
Pre-tension of the cables (T)	25 N
Cable radius (r_c)	3 mm
Cable density (ρ_c)	1,400 Kg/m ³
Cable modulus of elasticity (E_c)	128.04 GPa
Number of fundamental elements	10

$$\begin{cases} \alpha_1 \\ \alpha_2 \\ \alpha_3 \\ \alpha_4 \end{cases} = \begin{cases} +a \\ -a \\ +ib \\ -ib \end{cases} \quad (2.57)$$

$$\begin{cases} \alpha_1 \\ \alpha_2 \\ \alpha_3 \\ \alpha_4 \end{cases} = \begin{cases} 0 \\ 0 \\ +ib \\ -ib \end{cases} \quad (2.58)$$

$$\begin{cases} \alpha_1 \\ \alpha_2 \\ \alpha_3 \\ \alpha_4 \end{cases} = \begin{cases} +ia \\ -ia \\ +ib \\ -ib \end{cases} \quad (2.59)$$

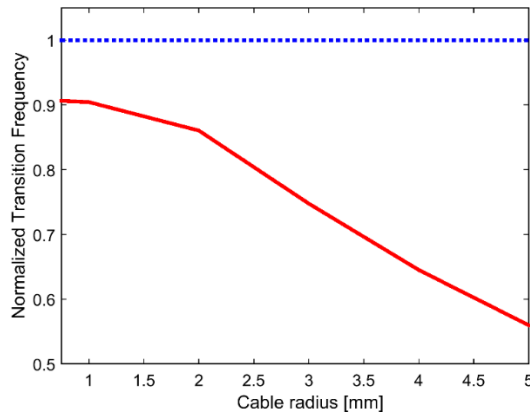


Fig. 2. 24 Variation of normalized transition frequency of cabled beam with respect to the radius of the cable. ■■■■■ Bare beam ■■■■■ Cabled beam.

Eq. (2.57)-(2.59) shows the mode shape parameters for frequencies below the cut off frequencies, at the transition frequency and above the transition frequencies. The form of couple of α_i 's changes from real to zero to imaginary. In the literature, for a given structure the transition frequency was constant and even in composite structures with coupling between multiple coordinates, this frequency was found to be unaffected [76]. In this Chapter, the effect of wrapping a cable around the host structure in a periodic manner on the transition frequency and mode shapes is investigated for simply supported boundary condition. For this analysis, the continuum model for the Timoshenko beam theory applies here. This study is the first in the area of cable-harnessed structures. Initially, a case study is investigated where the effect of cable radius is studied on the transition frequency. In Fig. (2.24), the radius of the cable is varied along the x-axis and the normalized frequency is plotted along the y-axis. The system parameters for this study are shown

in Table. (2.15). The transition frequency of the cabled beam is normalized with respect to the transition frequency of bare to clearly obtain an idea of the behavior of cabled beam with respect to the bare beam. The transition frequency of bare beam is independent of cable radius and will remain constant [109]. In Fig. (2.24), the transition frequency of the cabled beam is plotted using coupled vibration model (Eq. (2.51 a) to Eq. (2.51 f)). As it can be seen in Fig. (2.24), the transition frequency of cabled beam decreases with increase in cable radius. This shows that at the transition frequency, the kinetic energy effects of cabling will be more dominant than the strain energy, which is why the frequency decreases.

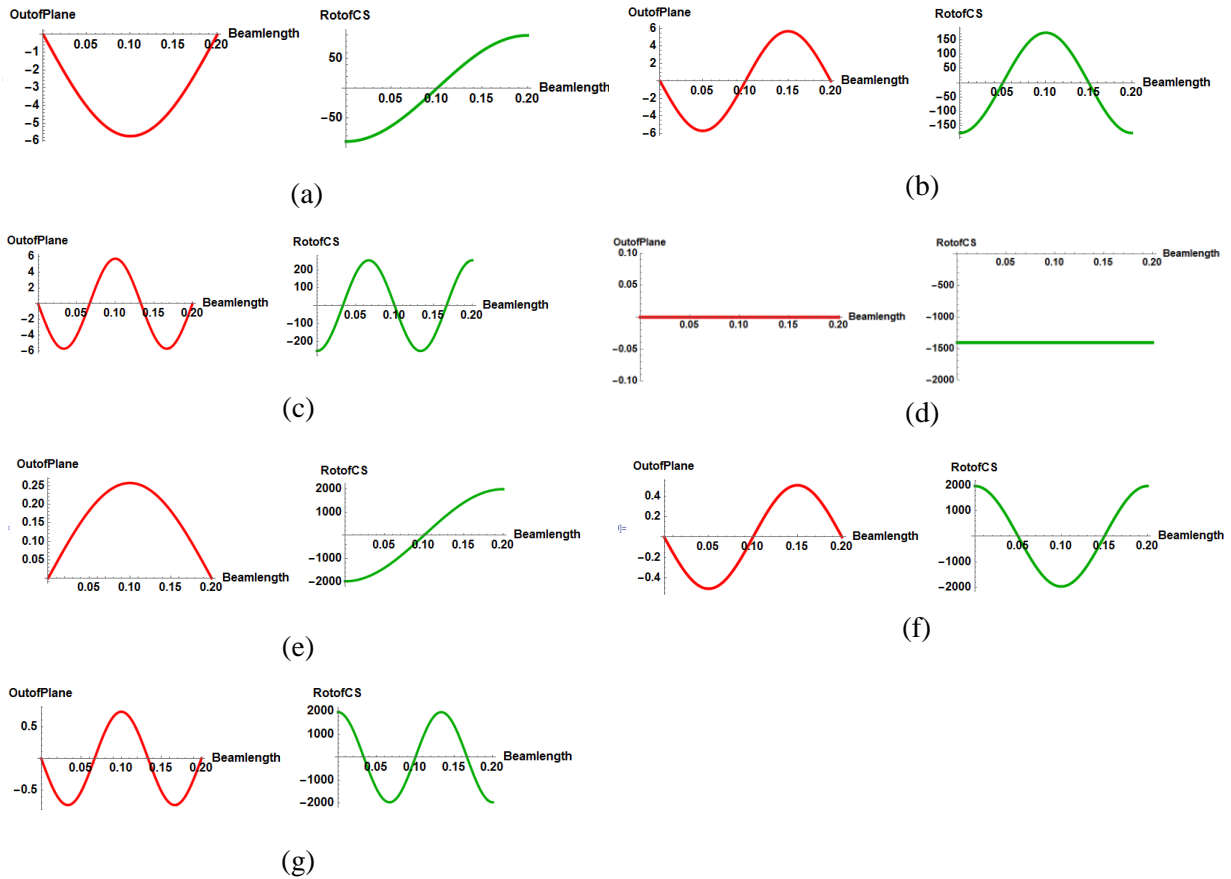


Fig. 2. 25 Mode shapes for (a)-(c) frequencies in first spectrum; (d) transition frequency; (e)-(g) frequencies in the second spectrum.

Table 2. 15 Natural Frequencies for bare and cabled beam for both first and second spectra using TBT

Mode No	Bare beam	Cabled beam
First Spectra [Hz]		
1a	563.09	660.88 (OP)
2a	2224.98	2348.01 (OP)
3a	4910.40	5190.35 (OP)
4a		5990.59
5a	8506.83	8785.35 (OP)
6a		11861.26
7a		12372.76
8a	12891.39	13368.92 (OP)
Transition Frequency [kHz]		
	156.70	117.13
Second Spectra [kHz]		
1b		117.62
2b	157.36	118.02 (SD)
3b		118.88
4b	159.29	120.63 (SD)
5b		123.12
6b		124.26
7b	162.33	124.84 (SD)
8b		128.64
9b		129.41
10b		130.31
11b	166.63	130.62 (SD)
12b		135.37
13b		136.35
14b	171.72	137.17 (SD)

For the bare beam model, the mode shapes are plotted in Fig. (2.25). The mode shapes are explained in detail in the published literature for the simply supported boundary condition [109]. While solving the partial differential equations for a bare beam, it is assumed that the mode shapes for simply supported are sinusoidal. We see a pure shear vibration mode in Fig. (2.25 d). Figs. 2.25 (a)-(c) are the mode shapes in the first spectrum which are bending dominant modes. Figs. 2.25 (e)-(g) are shear dominant modes and some bending dominant modes in between the shear dominant modes. The natural frequencies corresponding to the bare beam and cabled beam for both spectra are shown in Table. (2.15).

In a similar way, the natural frequencies for the cabled beam are calculated using the theory proposed in this Chapter 2. For the cabled beam simulations of Table. (2.15), the coordinates considered are the axial, out of plane bending, torsion and the rotation of cross section. The governing equations of motion along with the simply supported boundary conditions are shown in Eqs. (2.60) and (2.61).

$$-k_1\ddot{u} + c_1u'' + c_9\psi'' + c_{18}\theta'' = 0 \quad (2.60 \text{ a})$$

$$-k_3\ddot{w} + c_3w'' + c_{14}\theta'' + c_{16}\theta' + c_{24}\psi' = 0 \quad (2.60 \text{ b})$$

$$-k_4\ddot{\theta} + c_4\theta'' + c_{14}w'' - c_{16}w' + c_{18}u'' + c_{22}\psi'' = 0 \quad (2.60 \text{ c})$$

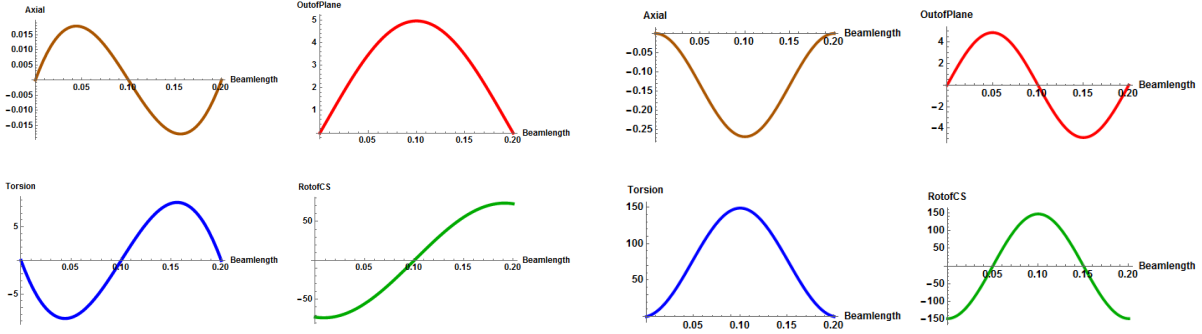
$$-k_6\ddot{\psi} + c_6\psi'' - c_{23}\psi + c_9u'' - c_{24}w' + c_{22}\theta'' = 0 \quad (2.60 \text{ d})$$

$$u = 0|_{x=0 \text{ or } l}$$

$$w = 0|_{x=0 \text{ or } l}$$

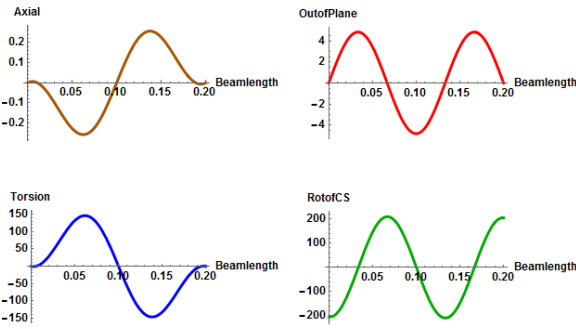
$$\theta = 0|_{x=0 \text{ or } l}$$

$$c_6\psi' + c_9u' + c_{22}\theta' = 0|_{x=0 \text{ or } l} \quad (2.61)$$



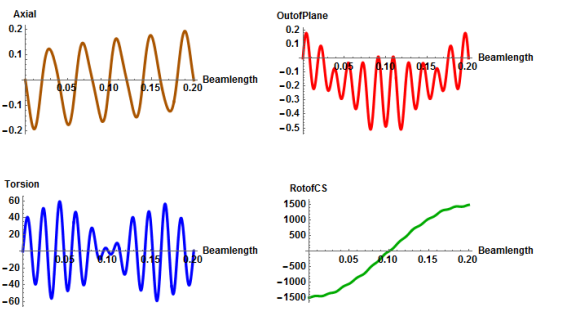
(a)

(b)



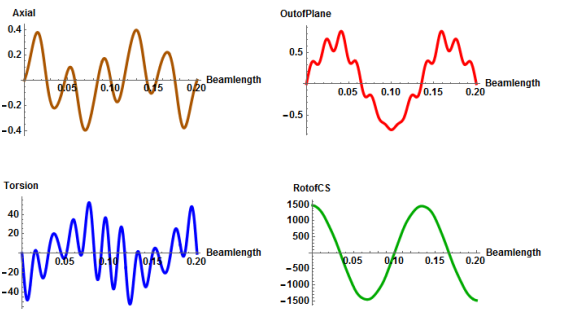
(c)

(d)



(e)

(f)



(g)

Fig. 2. 26 Mode shapes for (a)-(c) frequencies in first spectrum; (d) transition frequency; (e)-(g) frequencies in the second spectrum.

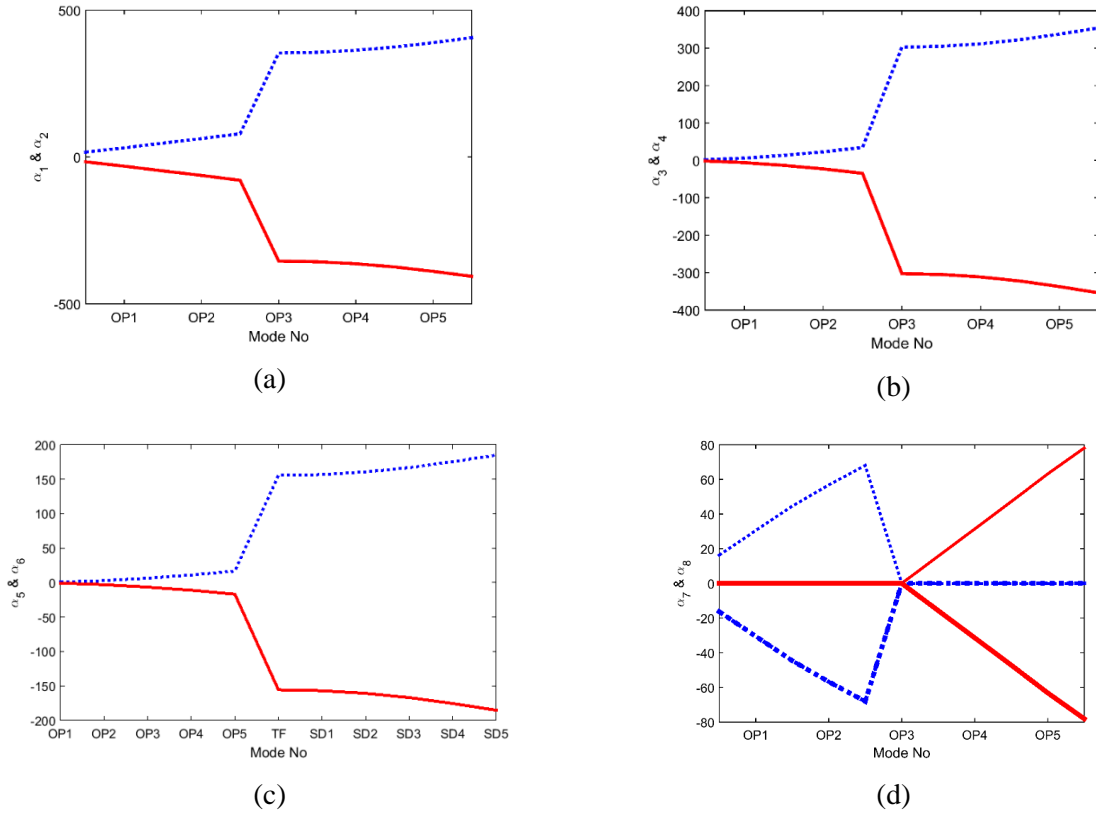


Fig. 2. 27 The nature of mode shape parameters of out of plane dominant modes in spectra 1 and shear dominant modes in spectra 2. ■■■■■ Im [α_1], Im [α_3], Im [α_5], Re [α_7] ——— Im [α_2], Im [α_4], Im [α_6], Im [α_7] ■■■■■ Re [α_8] ——— Im [α_8].

The natural frequencies are tabulated in the third column of Table. (2.15) and the mode shapes of the cabled beam for both the spectra are presented in Fig. (2.26). The focus of Table. (2.15) is to compare the frequencies of bending and shear dominant mode for both the spectra with that of bare beam. In the first spectra for bending dominant mode, we see stiffening effect as predicted in the all the results presented earlier in this Chapter 2. For the transition frequency, we see that the frequency has decreased after the addition of cable. It can also seen in Fig. (2.24) that the transition frequency for the cabled beam is less than that of bare beam. From this, it can be analyzed that the addition of cable will push the shear modes into the lower modes for cabled beam when compared to bare beam. In the second spectrum frequencies shown in Table. (2.15), the shear dominant modes frequencies are lower than that of bare beam. The slenderness ratio of the structure considered for this simulation is 20. Practically, when the slenderness ratio decreases further, we see the transition frequency appearing in the lower modes and have significant role on the overall dynamics of the structure. This concept may be used for reducing the bending vibrations

of thick structures by adding cables to bare beam structure to increase the vibrations of structure in the thickness shear direction.

Coming to the nature of mode shapes in Fig. (2.26), for the transition frequency in Fig. (2.26 d), we see pure shear vibration mode for the simply supported boundary condition for the cable-harnessed structure as well. The nature of the mode shape parameter (α_i) for bare beam is explained in Eqs. (2.57) to (2.59). Similarly, the mode shape parameters for cabled beam are plotted in Fig. (2.27). In Fig. (2.27), on the x-axis OP stands for Out of Plane bending dominant mode and SD stands for shear dominant mode. In Figs. (2.27 a) to (2.27 c), the mode shape parameter is imaginary for both the spectra and the transition frequency. In Fig. (2.27 d), the pair of mode shape parameters are real for the out of plane bending dominant modes in the first spectra. At the transition frequency, they approach to zero and in the second spectra, the pair of mode shape parameters turn imaginary. In the second spectra, only the α_i associated with the shear dominant modes are presented. For the shear dominant modes, for bare beam in simply supported boundary conditions we see symmetric solutions of the mode shape [109] that is the profile of the shapes for both the spectra a similar (symmetric behavior). For example, we observe that the shapes of the first, second bending dominant (Fig. (2.25 a) and Fig. (2.25 b)) and shear dominant modes (Fig. (2.25 e) and Fig. (2.25 f)) are similar although the magnitudes are different due to dominance of each direction in each spectrum. For the cable-harnessed structure, we see complicated shape of the first, second shear dominant modes and the bending coordinate also shows complicated shapes different from the shapes for bare beam for the second spectra. From the boundary conditions in Eq. (2.61), we can observe that the modal shape for cable-harnessed structure will not be as simple as that of bare beam even for simply supported boundary conditions. For a bare beam, the mode shape is simply a sinusoidal function. In case of cable-harnessed structure, when there is coupling, the mode shapes from axial and torsion coordinate, contribute to the bending and rotation of cross section displacements. All α_i 's contribute to the response of all the coordinates. As a result, we see complicated mode shapes for the second spectra where we see lesser bending vibrations and more shear vibrations. This suggests that the symmetry of having similar shapes in both spectrum for bare beam is broken in case of cable-harnessed structure with periodic wrapping pattern for a simply supported condition due to effect of coupling between various coordinates of vibration.

2.3 Coupled Vibrations in Structure with Non-Periodic Wrapping Pattern

This section presents the coupled vibrations of cable-harnessed structures with non-periodic wrapping pattern. In Section. 2.3.1, exact set of coupled PDEs for the non-periodic wrapped structure are presented. The solution procedure to solve the system of PDEs by applying boundary and continuity conditions to find the natural frequencies is presented. In Section. 2.3.1, theoretical studies are performed. The frequency response functions of decoupled and coupled models are analyzed. The findings obtained of this Section will be submitted to [131].

2.3.1 Mathematical Model

The cable-harnessed structure with non-periodic wrapping pattern along with the coordinates of motion is shown in Fig. (2.28). In case of periodic wrapping pattern, all the fundamental elements had same wrapping angle and equivalent continuum is developed. Unlike in the case of Periodic wrapping pattern [119,124], here the wrapping angle is different across each fundamental element and represents a more complicated case of study than compared to the periodic wrapping pattern. To analyze non-periodic wrapping structures, it is important to discretize the structure into multiple sub-substructures (at the end of each fundamental element) and assume the displacement function is continuous by applying continuity conditions. The coordinates of motion considered are Axial $u(x, t)$, In plane bending $v(x, t)$, Out of plane bending $w(x, t)$ and Torsion $\theta(x, t)$. The cable is assumed to wrapped in a diagonal manner and there is a lumped mass section at the end of each fundamental element.

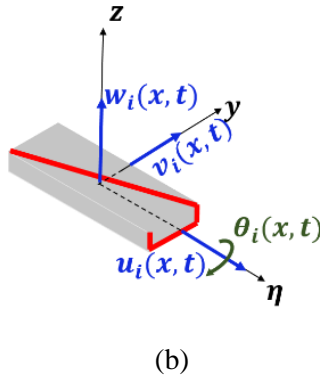
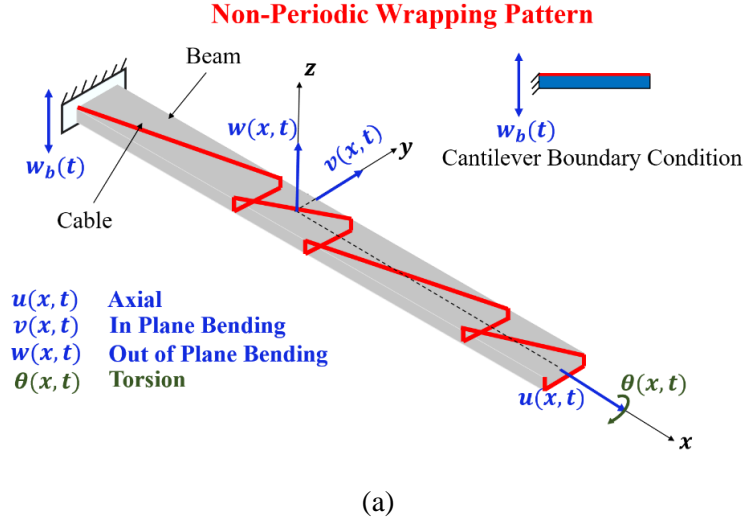


Fig. 2. 28 Representation of non-periodically wrapped cable harnessed structure pattern along with the coordinates of motion.

Each fundamental element of wrapping is assumed to have different displacement. The fundamental element along with the local coordinates is described in Fig. 2.28(b). where $u_i(x, t)$, $v_i(x, t)$, $w_i(x, t)$ and $\theta_i(x, t)$ in the Fig. 2.28(b) are the displacements in the axial, in-plane bending, out of plane bending and the torsion coordinates of the i^{th} fundamental element. In this Section. 2.3, the procedure to obtain the governing exact partial differential equations using energy methods is described. Then the mathematical steps to set up the eigen value problem and obtaining the natural frequency from the partial differential equations are derived. The assumptions made in the continuum model development are as follows:

The strain and kinetic energy of the cable-harnessed structure for Euler-Bernoulli model are shown in Eqs. (2.62) and (2.63).

$$\begin{aligned}
U_i &= \frac{1}{2} \left[\iiint E_b (-T \cos \psi_i / E_b A_b + \varepsilon_{xx})^2 + G_b (\gamma_{xy})_b^2 + G_b (\gamma_{zx})_b^2 dA dx \right] \\
&\quad + \frac{1}{2} \left[\iiint E_c (T / E_c A_c + \varepsilon_{xx} \cos^2 \psi_i + \gamma_{xy} \cos \psi_i \sin \psi_i)^2 dA \frac{dx}{\cos \psi_i} \right] \\
&= \frac{1}{2} \int_0^{l_i} [c_{1i}(\dot{u}_i)^2 + c_{2i}(\dot{v}_i'')^2 + c_{3i}(\dot{w}_i'')^2 + c_{4i}(\dot{\theta}_i')^2 + 2c_{5i}(\dot{w}_i'')(\dot{v}_i'') + 2c_{6i}(\dot{u}_i)(\dot{\theta}_i') \\
&\quad + 2c_{7i}(\dot{v}_i'')(\dot{\theta}_i') + 2c_{8i}(\dot{w}_i'')(\dot{\theta}_i') + 2c_{9i}(\dot{u}_i)(\dot{v}_i'') + 2c_{10i}(\dot{u}_i)(\dot{w}_i'') + 2c_{11i}(\dot{w}_i')(\dot{\theta}_i') \\
&\quad + 2c_{12i}(\dot{v}_i')(\dot{\theta}_i') + 2c_{13i}(\dot{v}_i')(\dot{w}_i'')] dx
\end{aligned} \tag{2.62}$$

$$\begin{aligned}
T_i &= \frac{1}{2} \left[\iiint \rho_b \{\dot{X}, \dot{Y}, \dot{Z}\}^T \{\dot{X}, \dot{Y}, \dot{Z}\} dA dx + \iiint \rho_c \{\dot{X}, \dot{Y}, \dot{Z}\}^T \{\dot{X}, \dot{Y}, \dot{Z}\} dA \frac{dx}{\cos \psi_i} \right] \\
&= \frac{1}{2} \int_0^{l_i} [k_{1i}(\dot{u}_i)^2 + k_{2i}(\dot{v}_i)^2 + k_{3i}(\dot{w}_i)^2 + k_{4i}(\dot{\theta}_i)^2] dx
\end{aligned} \tag{2.63}$$

where superscript ()' denotes partial derivative with respect to spatial coordinate $x(\frac{\partial}{\partial x})$ and superscript () $\dot{}$ denotes partial derivative with respect to time $t(\frac{\partial}{\partial t})$. where l_i is the length of the i^{th} fundamental element. where ψ_i is the wrapping angle of the i^{th} fundamental element and given by $\tan^{-1}(\frac{b}{l_i})$. The coefficients of Eqs. (2.62) and (2.63) are presented in Eq. (D.1). Once the strain and kinetic energy expressions are obtained, Hamilton's principle is applied: $\delta \int_{t_1}^{t_2} (T - U) dt = 0$ to obtain the fully coupled partial differential equations of equations along with the boundary conditions. This paper does not consider the damping induced by the cabling and the focus is on the mass and stiffness effects of cables. Although the structure is subjected to harmonic base excitation, the free vibration characteristics of the system such as the natural frequency and the mode shapes remain unaffected. The following mathematical steps show the procedure to calculate the natural frequency and mode shapes from the unforced system. At the end of Section. 2.3.1, the partial differential equations are shown for the structure subjected to base excitation along with the formula to find the frequency response function. The exact coupled set of governing equations of motion obtained after applying the extended Hamilton's principle for the non-periodically wrapped structure are shown in Eqs. (2.64 a)-(2.64 d).

$$\hat{k}_{1i}\ddot{u}_i - \hat{c}_{1i}u_i'' - \hat{c}_{6i}\theta_i'' - \hat{c}_{10i}w_i''' - (\hat{c}_{9i}(\hat{x})v_i'')' = 0 \quad (2.64 \text{ a})$$

$$\hat{k}_{2i}\ddot{v}_i + (\hat{c}_{2i}(\hat{x})v_i'')'' + (\hat{c}_{5i}(\hat{x})w_i'')'' + (\hat{c}_{7i}(\hat{x})\theta_i'')' + (\hat{c}_{9i}(\hat{x})u_i'')' - \hat{c}_{12i}\theta_i'' - \hat{c}_{13i}w_i''' = 0 \quad (2.64 \text{ b})$$

$$\hat{k}_{3i}\ddot{w}_i + \hat{c}_{3i}w_i'''' + \hat{c}_{8i}\theta_i''' + \hat{c}_{10i}u_i''' - (\hat{c}_{11i}(\hat{x})\theta_i')' + (\hat{c}_{5i}(\hat{x})v_i'')'' + \hat{c}_{10i}u_i''' + \hat{c}_{13i}v_i''' = 0 \quad (2.64 \text{ c})$$

$$\hat{k}_{4i}(\hat{x})\ddot{\theta}_i - (\hat{c}_{4i}(\hat{x})\theta_i')' - \hat{c}_{6i}u_i'' - \hat{c}_{8i}w_i''' - (\hat{c}_{11i}(\hat{x})w_i')' - (\hat{c}_{7i}(\hat{x})v_i'')' - \hat{c}_{12i}v_i'' = 0 \quad (2.64 \text{ d})$$

In Eq. (2.64), we can observe that the coefficients \widehat{c}_{2i} , \widehat{c}_{4i} , \widehat{c}_{5i} , \widehat{c}_{7i} , \widehat{c}_{9i} and \widehat{c}_{11i} are spatially variable. This would make solving the Eq. (2.64) complicated with the spatially varying PDEs. The coefficients that are variable are averaged in Eq. (2.65) over the length of the fundamental element to develop constant coefficient coupled PDEs. The constant coefficient coupled PDEs can be solved using the standard procedure adopted in the previous works by the authors [118,130]. The y and z coordinates of the cross-section of the cable in terms of local coordinate η are $(y_c, z_c) = (\eta \tan \psi_i - \frac{b}{2}, \frac{h}{2})$.

$$\begin{aligned} c_{2i} &= \frac{\int_0^{l_i} \widehat{c}_{2i}(\eta) d\eta}{\int_0^{l_i} d\eta} & c_{4i} &= \frac{\int_0^{l_i} \widehat{c}_{4i}(\eta) d\eta}{\int_0^{l_i} d\eta} & c_{5i} &= \frac{\int_0^{l_i} \widehat{c}_{5i}(\eta) d\eta}{\int_0^{l_i} d\eta} \\ c_{7i} &= \frac{\int_0^{l_i} \widehat{c}_{7i}(\eta) d\eta}{\int_0^{l_i} d\eta} & c_{9i} &= \frac{\int_0^{l_i} \widehat{c}_{9i}(\eta) d\eta}{\int_0^{l_i} d\eta} & c_{11i} &= \frac{\int_0^{l_i} \widehat{c}_{11i}(\eta) d\eta}{\int_0^{l_i} d\eta} \end{aligned} \quad (2.65)$$

The form of the constant coefficient PDEs for each fundamental element of the structure are as follows.

$$k_{1i}\ddot{u}_i - c_{1i}u_i'' - c_{6i}\theta_i'' - c_{10i}w_i''' - c_{9i}v_i''' = 0 \quad (2.66 \text{ a})$$

$$k_{2i}\ddot{v}_i + c_{2i}v_i'''' + c_{5i}w_i'''' + c_{7i}\theta_i''' + c_{9i}u_i''' - c_{12i}\theta_i'' - c_{13i}w_i''' = 0 \quad (2.66 \text{ b})$$

$$k_{3i}\ddot{w}_i + c_{3i}w_i'''' + c_{8i}\theta_i''' + c_{10i}u_i''' - c_{11i}\theta_i'' + c_{5i}v_i'''' + c_{13i}v_i''' = 0 \quad (2.66 \text{ c})$$

$$k_{4i}\ddot{\theta}_i - c_{4i}\theta_i'' - c_{6i}u_i'' - c_{8i}w_i''' - c_{11i}w_i'' - c_{7i}v_i'' - c_{12i}v_i'' = 0 \quad (2.66 \text{ d})$$

From the form Eqs. (2.66 a) - (2.66 d), in each equation we can see that each coordinate is coupled to all the other coordinates. For example, in Eq. (2.66 a), the axial is coupled to all other coordinates such as the in plane bending, out of plane bending and the torsion mode. In Eq. (2.66 a), the axial coordinate is coupled to other coordinates through equivalent shear terms. In Eq. (2.66 b), the in-plane bending is coupled to the out of plane bending through the fourth derivative and shear (cable tension related) term, to the torsion through the second (tension related term) and third derivative term, to the axial coordinate through equivalent shear term. In Eq. (2.66 c), the out of plane bending is coupled to in-plane bending term through fourth derivative term and tension related shear term, to the axial coordinate through shear related term and to the torsion coordinate through

the third derivative term and tension related second derivative term. In Eq. (2.66 d), the torsion coordinate is coupled to the axial coordinate through moment related term, to the out of plane bending coordinate through shear and moment related terms, to the in plane bending coordinate through shear and moment related terms.

The PDEs in Eq. (2.66 a)-(2.66 d) have constant coefficients and the general form of the PDE solution is assumed as shown in Eq. (2.67).

$$\begin{pmatrix} u_i(x, t) \\ v_i(x, t) \\ w_i(x, t) \\ \theta_i(x, t) \end{pmatrix} = \begin{pmatrix} U_i \\ V_i \\ W_i \\ \Theta_i \end{pmatrix} e^{\alpha_i x} e^{j\omega t} \quad (2.67)$$

where α_i is the mode shape parameter. ω is the natural frequency. $j = \sqrt{-1}$. Substituting the general form of solution Eq. (2.67) into Eq. (2.66) we obtain,

$$-k_{1i}U_i\omega^2 - c_{1i}U_i\alpha_i^2 - c_{6i}\Theta_i\alpha_i^2 - c_{10i}W_i\alpha_i^3 - c_{9i}V_i\alpha_i^3 = 0 \quad (2.68 a)$$

$$-k_{2i}V_i\omega^2 + c_{2i}V_i\alpha_i^4 + c_{5i}W_i\alpha_i^4 + c_{7i}\Theta_i\alpha_i^3 + c_{9i}U_i\alpha_i^3 - c_{12i}\Theta_i\alpha_i^2 - c_{13i}W_i\alpha_i^3 = 0 \quad (2.68 b)$$

$$-k_{3i}W_i\omega^2 + c_{3i}W_i\alpha_i^4 + c_{8i}\Theta_i\alpha_i^3 + c_{10i}U_i\alpha_i^3 - c_{11i}\Theta_i\alpha_i^2 + c_{5i}V_i\alpha_i^4 + c_{13i}V_i\alpha_i^3 = 0 \quad (2.68 c)$$

$$-k_{4i}\Theta_i\omega^2 - c_{4i}\Theta_i\alpha_i^2 - c_{6i}U_i\alpha_i^2 - c_{8i}W_i\alpha_i^3 - c_{11i}W_i\alpha_i^2 - c_{7i}V_i\alpha_i^3 - c_{12i}V_i\alpha_i^2 = 0 \quad (2.68 d)$$

The boundary conditions at the fixed end are as follows: ($x = 0$). (Eq. (2.69))

$$U_1(0) = \Theta_1(0) = W_1(0) = W_1'(0) = V_1(0) = V_1'(0) = 0 \quad (2.69)$$

The boundary conditions at the free end are as follows: ($x = l$). (Eq. (2.70))

$$\begin{aligned} c_{1i}U_n' + c_{6i}\Theta_n' + c_{10n}W_n'' + c_{9n}V_n'' + m_1\omega^2U_n &= 0 \\ c_{2n}V_n'' + c_{5n}W_n'' + c_{7n}\Theta_n' + c_{9n}U_n' &= 0 \\ c_{2n}V_n''' + c_{5n}W_n''' + c_{7n}\Theta_n'' + c_{9n}U_n'' - c_{13n}W_n'' - c_{12n}\Theta_n' + m_1\omega^2V_n &= 0 \\ c_{3n}W_n'' + c_{8n}\Theta_n' + c_{10n}U_n' + c_{5n}V_n'' + c_{13n}V_n' &= 0 \\ c_{3n}W_n''' + c_{8n}\Theta_n'' + c_{10n}U_n'' + c_{5n}V_n''' + c_{13n}V_n'' - c_{11n}\Theta_n' + m_1\omega^2W_n &= 0 \\ c_{4n}\Theta_n' + c_{6n}U_n' + c_{8n}W_n'' + c_{12n}V_n' + c_{7n}V_n'' + c_{11n}W_n' + m_2\omega^2\Theta_n &= 0 \end{aligned} \quad (2.70)$$

At the interface of the two fundamental elements, the displacement, slope, moment and shear functions should be continuous. The continuity conditions for all the coordinates of motion at the interface are as follows ($x = x_i$): (Eq. (2.71)). m_1 is associated with the lumped mass at the end of each fundamental element in the bending in the in plane and out of plane direction and axial direction. m_2 is the lumped mass associated with the torsional direction.

$$\begin{aligned}
& \text{i. } U_i = U_{(i+1)} \\
& c_{1i}U_i' + c_{6i}\theta_i' + c_{10i}W_i'' + c_{9i}V_i'' = c_{1(i+1)}U_{(i+1)}' + c_{6(i+1)}\theta_{(i+1)}' + c_{10(i+1)}W_{(i+1)}'' + \\
& c_{9(i+1)}V_{(i+1)}'' - m_1\omega^2U_{(i+1)} \\
& \text{ii. } V_i = V_{(i+1)} \\
& V_i' = V_{(i+1)}' \\
& c_{2i}V_i'' + c_{5i}W_i'' + c_{7i}\theta_i' + c_{9i}U_i' \\
& \quad = c_{2(i+1)}V_{(i+1)}'' + c_{5(i+1)}W_{(i+1)}'' + c_{7(i+1)}\theta_{(i+1)}' + c_{9(i+1)}U_{(i+1)}' \\
& c_{2i}V_i''' + c_{5i}W_i''' + c_{7i}\theta_i'' + c_{9i}U_i'' - c_{13i}W_i'' - c_{12i}\theta_i' = c_{2i}V_{(i+1)}''' + c_{5i}W_{(i+1)}''' + c_{7i}\theta_{(i+1)}'' + \\
& c_{9i}U_{(i+1)}'' - c_{13i}W_{(i+1)}'' - c_{12i}\theta_{(i+1)}' - m_1\omega^2V_{(i+1)} \\
& \text{iii. } W_i = W_{(i+1)} \\
& W_i' = W_{(i+1)}' \\
& c_{3i}W_i'' + c_{8i}\theta_i' + c_{10i}U_i' + c_{5i}V_i'' + c_{13i}V_i' \\
& \quad = c_{3(i+1)}W_{(i+1)}'' + c_{8(i+1)}\theta_{(i+1)}' + c_{10(i+1)}U_{(i+1)}' + c_{5(i+1)}V_{(i+1)}'' + c_{13(i+1)}V_{(i+1)}' \\
& c_{3i}W_i''' + c_{8i}\theta_i'' + c_{10i}U_i'' + c_{5i}V_i''' + c_{13i}V_i'' - c_{11i}\theta_i' = \\
& c_{3(i+1)}W_{(i+1)}''' + c_{8(i+1)}\theta_{(i+1)}'' + c_{10(i+1)}U_{(i+1)}'' + c_{5(i+1)}V_{(i+1)}''' + c_{13(i+1)}V_{(i+1)}'' - \\
& c_{11(i+1)}\theta_{(i+1)}' - m_1\omega^2W_{(i+1)} \\
& \text{iv. } \theta_i = \theta_{(i+1)} \\
& c_{4i}\theta_i' + c_{6i}U_i' + c_{8i}W_i'' + c_{12i}V_i' + c_{7i}V_i'' + c_{11i}W_i' = c_{4(i+1)}\theta_{(i+1)}' + c_{6(i+1)}U_{(i+1)}' + \\
& c_{8(i+1)}W_{(i+1)}'' + c_{12(i+1)}V_{(i+1)}' + c_{7(i+1)}V_{(i+1)}'' + c_{11(i+1)}W_{(i+1)}' - m_2\omega^2\theta_{(i+1)}
\end{aligned} \tag{2.71}$$

The expressions for the lumped masses are: $m_1 = \rho_c A_c [4\bar{h} + 2\bar{b}]$ and $m_2 = \rho_c A_c \left(4\bar{b}^2\bar{h} + \frac{4\bar{h}^3}{3} + \frac{2\bar{b}^3}{3} + 2\bar{b}\bar{h}^2 \right)$. For continuity conditions, In Eqs. (2.71 i) and (2.71 iv), the axial and torsional, displacement and slope are assumed to be continuous. In Eqs. (2.71 ii) and (2.71 iii), the in plane and out of plane bending, displacement, slope, moment and shear are assumed to be continuous. where m_1 and m_2 in Eqs. (2.70) and (2.71) are the lumped mass parameters due to cable section at the end of each fundamental elements. Converting Eqs. (2.68 a)-(2.68 d) into matrix form we obtain Eq. (2.72).

$$[A_i]_{4 \times 4} \begin{Bmatrix} U_i \\ V_i \\ W_i \\ \theta_i \end{Bmatrix}_{4 \times 1} = \{0\}_{4 \times 1} \quad (2.72)$$

where $[A_i]$ is given by:

$$\begin{bmatrix} -c_{1i}\alpha_i^2 - k_{1i}\omega^2 & -c_{9i}\alpha_i^3 & -c_{10i}\alpha_i^3 & -c_{6i}\alpha_i^2 \\ c_{9i}\alpha_i^3 & c_{2i}\alpha_i^4 - k_{2i}\omega^2 & c_{5i}\alpha_i^4 - c_{13i}\alpha_i^3 & c_{7i}\alpha_i^3 - c_{12i}\alpha_i^2 \\ c_{10i}\alpha_i^3 & c_{5i}\alpha_i^4 + c_{13i}\alpha_i^3 & c_{3i}\alpha_i^4 - k_{3i}\omega^2 & c_{8i}\alpha_i^3 - c_{11i}\alpha_i^2 \\ -c_{6i}\alpha_i^2 & -c_{7i}\alpha_i^3 - c_{12i}\alpha_i^2 & -c_{8i}\alpha_i^3 - c_{11i}\alpha_i^2 & -c_{4i}\alpha_i^2 - k_{4i}\omega^2 \end{bmatrix}$$

By setting $|A_i(\alpha_i, \omega)| = 0$, we obtain non-trivial solution to Eq. (2.72). The determinant gives a 12th degree polynomial in terms of mode shape parameter α_i and frequency ω . Solving the above polynomial, we get 12 roots for α_i in terms of ω . In the next step to find the spatial solutions U_i, V_i, W_i and θ_i , we write from Eq. (2.72).

$$a_{41i}U_i + a_{42i}V_i + a_{43i}W_i + a_{44i}\theta_i = 0 \quad (2.73)$$

where a_{4wi} for $w \rightarrow 1$ to 4 represent the elements of the fourth row of matrix $[A_i]$ (any row can be selected at this step). The spatial solutions should be as follows to satisfy the condition in Eq. (2.73).

$$\begin{aligned} U_{ki} &= |(-1)^{4+1}M_{41i}| & V_{ki} &= |(-1)^{4+2}M_{42i}| & W_{ki} &= |(-1)^{4+3}M_{43i}| & (2.74) \\ \theta_{ki} &= |(-1)^{4+4}M_{44i}| \end{aligned}$$

where M_{4wi} ($w \rightarrow 1$ to 4) represent the minors of the elements a_{4wi} for $i \rightarrow 1$ to 4 of matrix $[A_i]$. The determinant of the co-factor elements presented in Equation. (2.74) gives us the final spatial solution for each coordinates of vibration. The general form of the spatial solution of the PDEs can be expanded to be of the following form.

$$\begin{Bmatrix} u_i(x, t) \\ v_i(x, t) \\ w_i(x, t) \\ \theta_i(x, t) \end{Bmatrix} = \sum_{k=1}^{12} d_{ki} \begin{Bmatrix} U_{ki}(\alpha = \alpha_{ki}) \\ V_{ki}(\alpha = \alpha_{ki}) \\ W_{ki}(\alpha = \alpha_{ki}) \\ \theta_{ki}(\alpha = \alpha_{ki}) \end{Bmatrix} e^{\alpha_{ki}x} e^{i\omega t} \quad (2.75)$$

The next step is to setup the eigen-value problem and find the natural frequencies. Karami et al [132] and Ansari et al [133] in papers related to vibrations of zigzag structure for energy harvesting purposes used matrix method for applying continuity and boundary conditions to set up the eigen-value problem for the zigzag structure. The matrix method has advantages in that it results smaller determinant values when compared to traditional methods. This is advantageous

for solving systems where different coordinates of motion are coupled to each other. Similar procedure is used in this paper to set up eigen-value problem from the coupled set of PDEs. Substitute Eq. (2.75) into the continuity conditions Eq. (2.71) and convert into matrix form, we obtain,

$$[M]_i \{d_{1(i)} \quad d_{2(i)} \cdots \cdots d_{11(i)} \quad d_{12(i)}\}^T = [N]_{i+1} \{d_{1(i+1)} \quad d_{2(i+1)} \cdots \cdots d_{11(i+1)} \quad d_{12(i+1)}\}^T \quad (2.76)$$

Repeating Eq. (2.76) type analysis for all the segments, we obtain

$$\{d_{1(n)} \quad d_{2(n)} \cdots d_{11(n)} \quad d_{12(n)}\}^T = [N]_n^{-1} [M]_{n-1} \{d_{1(1)} \quad d_{2(1)} \cdots d_{11(1)} \quad d_{12(1)}\}^T \quad (2.77)$$

Combining all the matrices we get the following form

$$\begin{bmatrix} [M]_0 \\ [M]_l [N]_n^{-1} [M]_{n-1} \cdots \cdots \end{bmatrix} \{d_{1(1)} \quad d_{2(1)} \cdots d_{11(1)} \quad d_{12(1)}\}^T = \{0\}_{12 \times 1} \quad (2.78)$$

$[M]_0$ and $[M]_l$ are the matrices obtained from the boundary conditions; $[M]_i$ and $[N]_i$ for $i \neq 0$ or l are the matrices obtained from the continuity conditions. Setting the determinant of the 12X12 matrix in Eq. (2.78) to zero would lead us to the frequency equation, the roots of which can be found numerically and would lead to the natural frequency of the structure. The form of the constant coefficient PDEs after including the effect of base excitation are shown in Eq. (2.79).

$$k_{1i} \ddot{u}_i - c_{1i} u_i'' - c_{6i} \theta_i'' - c_{10i} w_{i,rel}''' - c_{9i} v_i''' = 0 \quad (2.79 \text{ a})$$

$$k_{2i} \ddot{v}_i + c_{2i} v_i'''' + c_{5i} w_{i,rel}'''' + c_{7i} \theta_i'''' + c_{9i} u_i'''' - c_{12i} \theta_i'' - c_{13i} w_{i,rel}''' = 0 \quad (2.79 \text{ b})$$

$$\begin{aligned} k_{3i} \ddot{w}_{i,rel} + c_{3i} w_{i,rel}'''' + c_{8i} \theta_i'''' + c_{10i} u_i'''' - c_{11i} \theta_i'' + c_{5i} v_i'''' + c_{10i} u_i'''' + c_{13i} v_i'''' \\ = - \left(k_{3i} + \sum_{i=1}^{n-1} m_1 \delta(x - x_i) + m_1 \delta(x - l) \right) \ddot{w}_b \end{aligned} \quad (2.79 \text{ c})$$

$$k_{4i} \ddot{\theta}_i - c_{4i} \theta_i'' - c_{6i} u_i'' - c_{8i} w_{i,rel}''' - c_{11i} w_{i,rel}'' - c_{7i} v_i'''' - c_{12i} v_i'' = 0 \quad (2.79 \text{ d})$$

where w_b is the base excitation and $w_{i,rel}$ is the relative displacement of the structure in the out of plane bending direction with respect the base. The boundary and the continuity conditions can be modified accordingly. The mass normalization condition for the fully coupled non-periodic cable-harnessed structure is as follows: (Eq. (2.80)).

$$\begin{aligned} \sum_{i=1}^n \left(\int_0^l (k_{1i} U_{gi}^2 + k_{2i} V_{gi}^2 + k_{3i} W_{gi}^2 + k_{4i} \theta_{gi}^2) dx \right) \\ + \sum_{i=1}^{n-1} m_1 (U_{gi}^2(x_i) + V_{gi}^2(x_i) + W_{gi}^2(x_i) + \frac{m_2}{m_1} \theta_{gi}^2(x_i)) + m_1 (U_{gn}^2(x_n) \\ + V_{gn}^2(x_n) + W_{gn}^2(x_n) + \frac{m_2}{m_1} \theta_{gn}^2(x_n)) = 1 \end{aligned} \quad (2.80)$$

x_i in Eqs. (2.79) and (2.80) is the location of i^{th} lumped mass. where U_{gi}, V_{gi}, W_{gi} and θ_{gi} denotes the axial, in plane bending, out of plane bending and torsion mode shapes respectively corresponding to the g^{th} mode and i^{th} fundamental element. The formula for the frequency response function after incorporating the effect of base excitation is shown in Eq. (2.81).

$$W(\omega_f) = \left| \frac{1}{\omega_f^2} + \sum_{g=1}^{\infty} \frac{k_{3i} \cdot W_{g,rel}(x = x_s) \cdot Q}{\omega_g^2 - \omega_f^2} \right| \quad (2.81)$$

$$Q = \sum_{i=1}^n \left(\int_0^l (W_{gi}) dx \right) + \sum_{i=1}^{n-1} m_1 W_{gi}(x_i) + m_1 W_{gn}(x_n) \quad (2.82)$$

where k_{3i} is the kinetic energy coefficient in the out-of-plane bending direction. x_s is the sensing location. ω_f is the forcing frequency. ω_g is the natural frequency associated with the g^{th} mode. $W_{g,rel}(x = x_s)$ is the relative mass-normalized mode shape value of the g^{th} mode at the sensing location, $x = x_s$, with respect to the base motion in the out-of-plane bending direction. where Q is defined in Eq. (2.82).

2.3.2 Numerical Results

In Section. 2.3.2, the theoretical frequency response functions obtained from coupled and decoupled [53] models are compared for the three samples analyzed. The top view of wrapping pattern for the three samples considered are shown in Figs. (2.29 a) - (2.29 c). In Fig. (2.29), the solid line represents the diagonal section and the dotted line represents the lumped mass section. Clear isometric view of the structure can be seen in Fig. (2.28).

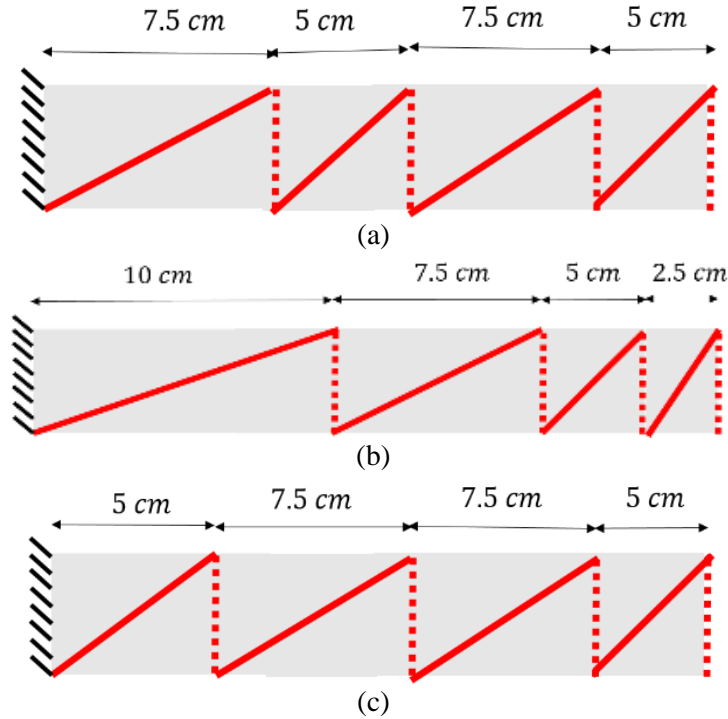
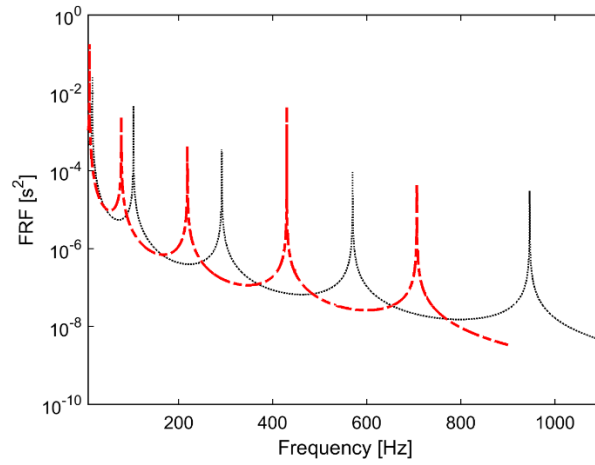


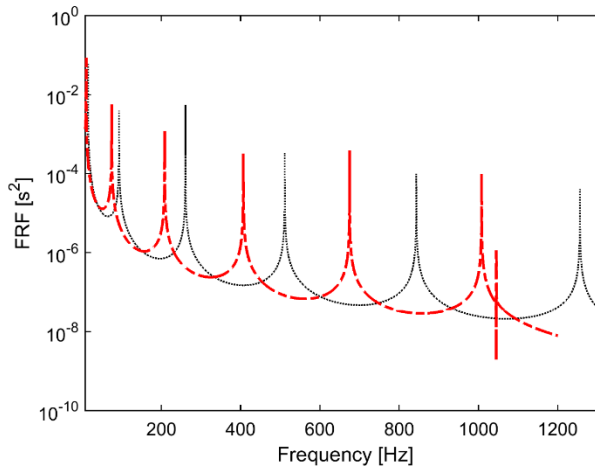
Fig. 2. 29 Top view representation of (a) Sample 1; (b) Sample 2; (c) Sample 3

Table 2. 16 System parameters for the samples 1, 2 and 3.

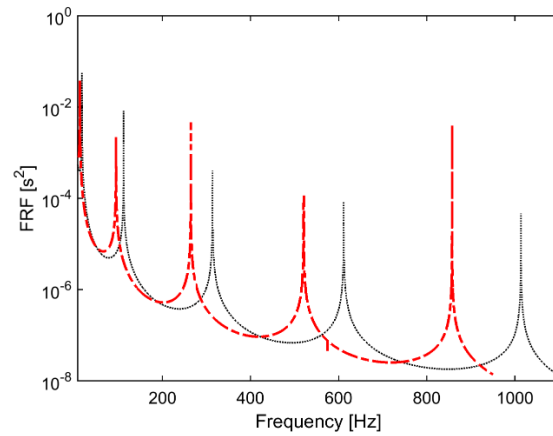
System parameters	Sample 1 Values	Sample 2 Values	Sample 3 Values
Beam length (l)	250 mm	250 mm	250 mm
Beam width (b)	10 mm	13.1 mm	10 mm
Beam thickness (t)	0.782 mm	0.782 mm	1 mm
Beam density (ρ_b)	2,768 Kg/m ³	2,768 Kg/m ³	2,768 Kg/m ³
Beam modulus of elasticity (E_b)	68.9 GPa	68.9 GPa	68.9 GPa
Beam Shear modulus (G_b)	25.7 GPa	25.7 GPa	25.7 GPa
Pre-tension of the cables (T)	14 N	14 N	15 N
Cable radius (r_c)	0.00021 m	0.00021 m	0.00021 m
Cable density (ρ_c)	1,400 Kg/m ³	1,400 Kg/ m ³	1,400 Kg/ m ³
Cable modulus of elasticity (E_c)	128.04 GPa	128.04 GPa	128.04 GPa
Number of Cables	9	8	7
Number of fundamental elements	4	4	4
Sensing Location (x_s)	23.8 cm	24.8 cm	24 cm



(a)



(b)



(c)

Fig. 2. 30 Frequency response functions of coupled and decoupled models for (a) Sample 1; (b) Sample 2; (c) Sample 3. Cabled Analytical (Decoupled) Cabled Analytical (Coupled).

Table 2. 17 Coupled and Decoupled Natural Frequencies for Sample 1

Mode No	Coupled EB [Hz]	Decoupled EB [Hz]	% Coupled EB and Decoupled
1	10.78 (OP)	16.65	35.22 %
2	78.45 (OP)	104.18	24.69 %
3	140.29 (IP)	-	-
4	218.85 (OP)	291.93	25.03 %
5	429.9 (OP)	570.06	24.58 %
6	447.07 (T)	-	-
7	706.47 (OP)	946.33	25.34 %
8	878.21 (IP)	-	-

*OP stands for out of plane bending, IP stands for in plane bending and T stands for Torsion dominant modes

Table 2. 18 Coupled and Decoupled Natural Frequencies for Sample 2

Mode No	Coupled EB [Hz]	Decoupled EB [Hz]	% Coupled EB and Decoupled
1	10.27 (OP)	14.92	31.13 %
2	74.62 (OP)	93.32	20.04 %
3	179.65 (IP)	-	-
4	208.32 (OP)	260.69	20.09 %
5	335.52 (T)	-	-
6	406.96 (OP)	511.52	20.44 %
7	674.98 (OP)	843.36	19.96 %
8	1007.98 (OP)	1256.05	19.75 %
9	1045.29 (T)	-	-
10	1120.34 (IP)	-	-

*OP stands for out of plane bending, IP stands for in plane bending and T stands for Torsion dominant modes

Table 2. 19 Coupled and Decoupled Natural Frequencies for Sample 3

Mode No	Coupled EB [Hz]	Decoupled EB [Hz]	% Coupled EB and Decoupled
1	13.03 (OP)	17.81	26.83 %
2	94.85 (OP)	112	15.31 %
3	136.03 (IP)	-	-
4	264.60 (OP)	313.83	15.68 %
5	520.55 (OP)	611.54	14.87 %
6	574.60 (T)	-	-
7	857.4 (OP)	1013.67	15.51 %

*OP stands for out of plane bending, IP stands for in plane bending and T stands for Torsion dominant modes

In Fig. (2.29 a), alternate elements have the same wrapping angle as we go from the element from the clamp to the tip, in Fig. (2.29 b), the wrapping angle increases as we go from one element to the other starting from the clamp and in Fig. (2.29 c), semi-periodic wrapping pattern is considered. Using the procedure derived in Section. 2.3.1, the natural frequencies and mode shapes

are calculated for cantilever boundary condition as shown in Fig. (2.28). The structure is subjected to harmonic base excitation and the frequency response function are plotted in Fig. (2.30) for all the three samples. The strain values of the cable are assumed the same as the top fiber of the host structure. The frequency response function of the decoupled curve is plotted using the assumptions of Martin et al [53] for pure out of plane bending coordinate. The frequency response function for the coupled model proposed in this paper considering the effect of coupling between the out of plane, in-plane bending, torsion and the axial coordinates is plotted in the same Fig. (2.30). The significant peaks denote the frequencies corresponding to the out of plane bending coordinate and the sharp peaks denote the torsional and in-plane coordinates. For clarity, the frequencies are listed in Tables. (2.18)-(2.20) for the samples 1, 2 and 3 respectively. The dominance of each mode is decided by looking at the mode shapes. The mode shapes corresponding to the torsion and the in-plane bending dominant modes for the samples 1 and 2 are shown in the Chapter 3. Since for the structures considered, the axial dominant mode is associated with very high frequency, that particular mode will not be in the range considered for finding the frequency response functions. From Fig. (2.30), in all the samples considered, the decoupled model consistently over-predicted the natural frequency. The decoupled model assumes the structure only vibrates in the out-of-plane direction and assumes the stiffness of other coordinates to be infinity. The coupled model takes into account the flexibility of multiple coordinates, as a result the coupled model assumes the out-of-plane bending coordinates is less stiffer than the decoupled model. As a result, the coupled model gives lower frequency for the out of plane bending when compared to the decoupled model. Samples 1 and 2 have lower length to thickness ratio when compared to sample 3. The effect of coupling will be more prominent in samples 1 and 2 due to greater effect of stiffness related terms and the coupling in the structure in turn comes from the stiffness terms. From the percentage difference between coupled and decoupled in Tables. (2.17)-(2.19) we can see that the sample 3 has the least coupling effect. Sample 1 has the largest number of cables, therefore we expect that sample 1 has maximum coupling effect amongst samples 1 and 2. In terms of wrapping pattern, samples 1 and 2 have largest sections near the clamp. The fundamental element with largest length will have the least wrapping angle. Sections with least amount of wrapping angle contribute more to stiffness effect. Since the largest elements are located near the clamp for samples 1 and 2, this line of thought has also some contribution to the argument that samples 1 and 2 exhibit more coupling when compared to sample 3 which has the smallest element is located near the clamp. In

addition to the out of plane bending modes, all the samples also have sharp peaks in the frequency range of interest. Sample 1 has two in-plane and one torsion dominant mode. Sample 2 two in-plane bending and torsion dominant modes. Sample 3 has one in-plane bending and torsion dominant mode. The frequencies are tabulated in Tables. (2.18)-(2.20) for samples 1,2 and 3 respectively.

2.4 Conclusions of the Chapter

In Chapter 2, analytical models are presented to study the free vibrations characteristics of cable-harnessed beam structures motivated by space applications with straight cable pattern, periodic pattern and non-periodic pattern. A distributed parameter model that accounts for the effect of coupling in cable-harnessed structures is developed. Kinetic and strain energy derivations are found using the Green-Lagrange strain field and Hamilton's principle is used to obtain both partial differential equations for the system. The natural frequencies of the decoupled vibration model adopted in the literature were compared against the coupled vibration model used in this paper. The coupling effects between various coordinates of vibrations due to the presence of the cable are studied for all systems. The results demonstrate the importance of using a coupled vibration model to accurately predict the vibration behavior of the cable-harnessed structure. For straight pattern, several cable parameters are studied for their effects on the system's frequencies, coupling and the energy transfer between the modes. It is observed that at larger cable radius, and if the cable is placed at an offset position, the coupling effect is greater and the coupled analytical model predicts the natural frequencies better than the decoupled model.

For periodic pattern, theoretical simulations were presented to compare the frequency response function of Euler-Bernoulli and Timoshenko fully coupled models and the decoupled Euler-Bernoulli model in the literature. Sensitivity analysis were performed by varying the number of fundamental elements of wrapping pattern and the cable radius. It was seen that the coupling effect was maximum for lower fundamental elements and larger cable radii. The natural frequencies obtained from the straight cable case (cable positioned at an offset distance from the centerline) are also compared to the periodic wrapping pattern for a given host structure and cable parameters and it was found that the cable effects on the host structure are minimized when the cable is wrapped in a periodic manner particularly when the number of fundamental elements are larger as

opposed to the case when the cable is positioned at an offset distance. In the concept of transition frequency for cable-harnessed structure, we have seen that for larger cable radius, the transition frequency decreases. It is also observed for simply supported boundary condition that the symmetrical behavior of mode shapes in both spectra is broken due to effect of coupling between various coordinates.

For non-periodic pattern, the structure was modelled by assuming that each fundamental element has different displacement. The system of coupled partial differential equations were solved using analytical method. Displacement, slope, moment and shear continuity conditions were applied at the interface of two fundamental elements to obtain the coupled natural frequencies and mode shapes. Analyses were performed on three different samples with different non-periodic wrapping patterns. The theoretical results suggested that it is important to incorporate the coupling effects in the mathematical model, which the recently published literature on cable-harnessed structures with non-periodic wrapping patterns has ignored.

Chapter 3: Experimental Validation of Coupled Vibrations of Cable-Harnessed Structures

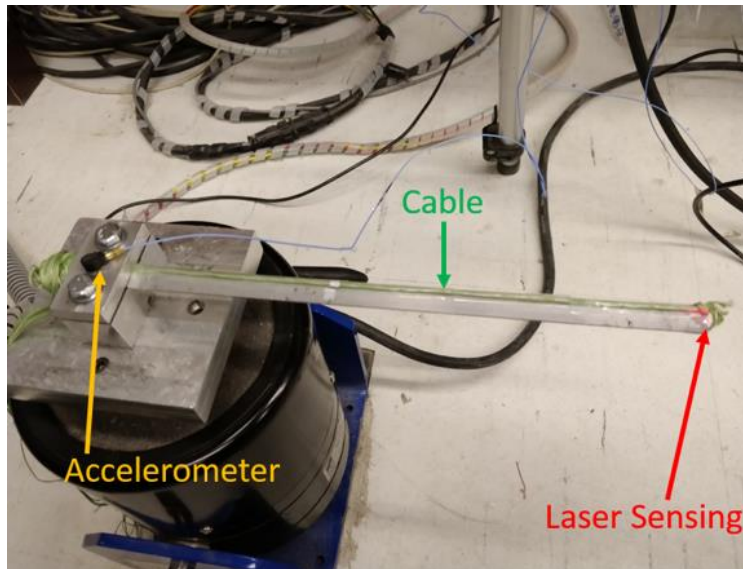
In the Chapter 3 experimental validation of the mathematical models developed in Chapter 2 for the cases of beam structure with straight cable pattern at offset distance, periodic and non-periodic wrapping patterns are performed. In Section. 3.1, the coupled vibration model in Section. 2.1 for straight cable pattern at offset distance is experimentally validated. The sample is subjected to harmonic base excitation using a vibration shaker to obtain the experimental frequency response function. The experimental frequency response function is compared to the coupled Euler-Bernoulli, Timoshenko and the decoupled Euler-Bernoulli models. In plane impact tests are performed to confirm the presence of in plane bending dominant modes. In Chapters 3.2 and 3.3, the experimental validation for the models related to the periodic and non-periodic wrapping patterns are performed respectively by using shaker and impact tests. Experimental mode shape deflection snapshots are also presented to confirm the modes related to the in plane bending and torsion coordinates.

3.1 Experimental Validation of Straight Cable Pattern with Offset Distance

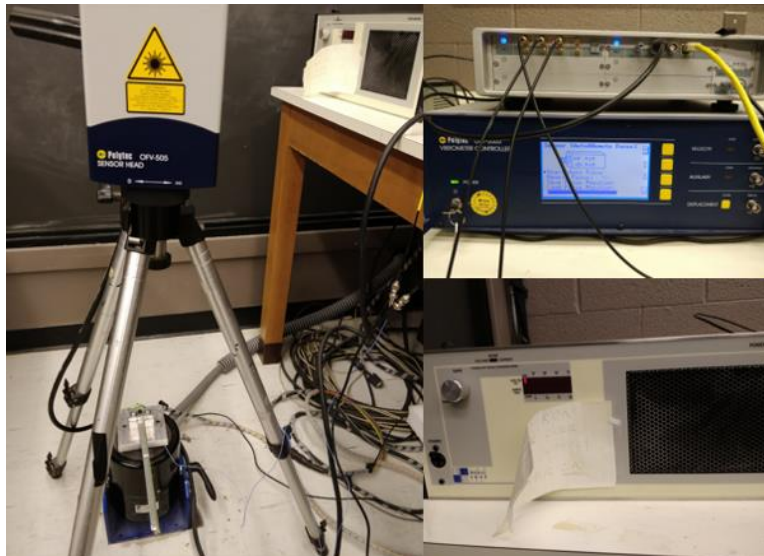
In Fig. (3.1), the experimental setup for the cable harnessed system under the base excitations is shown. The system consists of 10 pre-tensioned cables attached to the host structure as shown at an offset distance in a straight pattern. The host structure is a beam made of Aluminum 6061 alloy and the cable is an 80-pound strength Power Pro Super 8 Slick fishing line. The material and geometrical properties are presented in Table. (3.1). This research is built on Martin et al work in AIAA Journal [52] where they have developed lower order decoupled distributed parameter models. In this research, coupled mathematical models are developed. In the current thesis, the amount of cabling in the experiments is more significant than Martin et al work and as observed in Chapter 2, this will lead to increase in the mode coupling effects. For the experimental testing, exactly same type of cable [52] is used to perform experiments in this thesis. The material and geometrical properties for the cable can be found in [52,53]. In terms of beam host structure dimensions, the lengths are similar to the ones used by Martin et al and other researchers with slight variation in width and thickness. Extremely thick substrates are difficult to clamp in

cantilever boundary condition so relatively slender substrates are used to perform experiments. The length of the host substrates have been selected in such a way that the beam structure does not create dynamic moments on the shaker particularly when there are large displacements of the host structure near the resonance. Since this work compares coupled model with the decoupled model, for selecting cable pre-tension values guidance is taken from the experimental analysis papers of the decoupled model [52,53,58]. Before conducting experiments, it has been physically checked that there is no permanent deformation in the structure after attaching pre-tensioned cables and it has been ensured that the pre-tension is large enough that the cables do not rattle.

A 2075E TMS electrodynamic shaker and a 2050E09 TMS power amplifier both by modal shop are used to provide the excitations. To control the acceleration profile for the shaker base excitations, a PCB accelerometer 352A24 and an LMS SCM 05 SCADAS data acquisition unit are used. This data acquisition system is also used to obtain the frequency response functions. A Polytec OFV-5000 laser vibrometer controller and an OFV-505 sensor head are used for vibration measurements. The structure is mounted on the shaker as shown in Fig. (3.1 a) and is subjected to the sine sweep base excitations in the out-of-plane bending direction (z-axis) from 5 to 500 Hz using the LMS Sine Control Module. The frequency response functions are measured in the out-of-plane bending direction as well. In order to make sure that the added tape to attach the cables to the beam has not resulted in any noticeable dynamic effects, the experimental frequency response functions for the substrate beam without any cables both before and after adding the tape are measured and shown in Fig. (3.2). It has to be noted that there is no cabling in the structure in Fig. (3.2) and the purpose of Fig. (3.2) is just to observe the effect of tape on the natural frequencies of the structure. The FRFs comparison for the two systems clearly indicates that the added tape has no noticeable effect on the substrate's dynamics. It is, therefore, expected that the tape used for attaching the cables in Fig. (3.1) will have no measurable dynamic impact on the natural frequencies of the cable-harnessed system in the future experimental analysis.



(a)



(b)

Fig. 3. 1 Base excitation experimental setup for the cantilevered cable harnessed beam, (a) beam structure, accelerometer and shaker, (b) laser vibrometer controller, sensor head, power amplifier, and LMS data acquisition system.

Table 3. 1 Material and geometrical properties of the cable harnessed beam structure.

System parameters	Value
Beam length	0.25 m
Beam width	0.01243 m
Beam thickness	0.00144 m
Beam density	2,768 Kg/m ³
Beam modulus of elasticity	68.9 GPa
Beam Shear modulus	25.7 GPa
Pre-tension of the cables	17.22 N
Cable radius (per cable)	0.00021 m
Cable density	1400 Kg/m ³
Cable modulus of elasticity	128.04 GPa
Number of Cables	10

Next step involves obtaining the experimental frequency response functions for the cable-harnessed beam structure with pre-tensioned cables. Modular weights are used to apply the cable pre-tension while the unit is fabricated. The cables are attached at an offset distance along the y-axis as shown in Fig. (3.1 a). The total pre-tension applied is 17.22 N for the 10 cables attached. The base excitations for the cable-harnessed beam to obtain the FRFs are performed at two different sensing locations, 95 mm and 248 mm. In Fig. (3.3), an overall picture of the theoretical and experimental frequency response functions are presented. The experimental and theory FRFs of the bare beam match very well. As a sanity check, the experimental frequency response function for the substrate beam with the added tape (no cable) is compared to the analytical results for the substrate beam with no tape or cable. The good match between the two shown in Fig. (3.3) further proves that the added tape has no noticeable effect on the substrate beam's dynamics and, therefore, it can be ignored in the rest of the analysis for the cable harnessed beam structure as well. The Fig. (3.3) also presents the results of the cabled analytical (coupled EB and decoupled models) and cabled experimental. From the plot, it can be observed that addition of cables to the host structure causes stiffening effect in the system and it also observed experimentally by shift in the natural frequency peaks going from bare beam to cabled beam. Once it is observed that the cabling induces stiffening effect, the next step is to compare coupled and decoupled models to the experiment. Further analysis of coupled and decoupled models to the cabled experimental is presented in Figs. (3.5) and (3.6). Shown in Fig. (3.4) is the cross-sectional area of the n cables bundled together; here $n=10$. The total cross-sectional area of the n cables can be found using Eq. (3.1). This area is equivalent to that of a circle with $\sqrt{n} \cdot r_c$ radius as shown in Fig. (3.4). Using this

diagram, it can be easily understood how y_c and z_c coordinates of the point of attachment of the cable to the beam are found. This is the point where the strain value for the cables is evaluated. It is assumed that the cables remain attached to the top surface of the beam at all times and, therefore, will have the same strain values as the beam top fiber. It is also assumed that the entire bundle of cables experiences the same strain values. This assumption includes further corrections to Martin et al. [51] where the strain was previously evaluated at the center of the cable using the beam strain distribution function.

$$A = n \cdot \pi r_c^2 = \pi(\sqrt{n} \cdot r_c)^2 \quad (3.1)$$

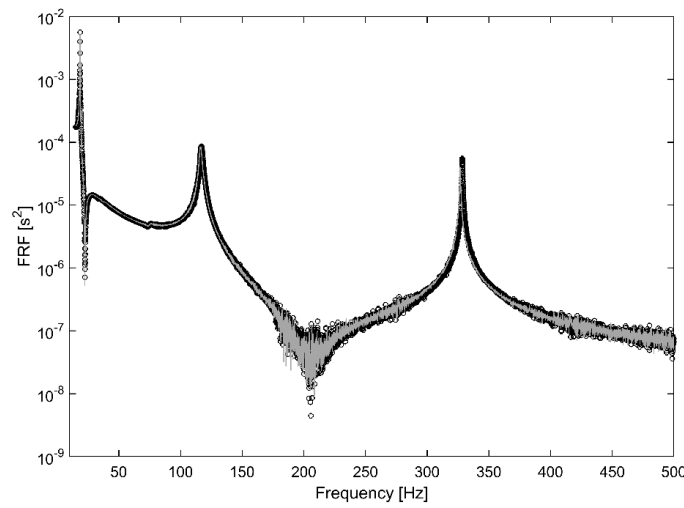


Fig. 3. 2 Experimental frequency response functions from shaker tests for substrate beam + tape and no cables and substrate beam without tape at $x_s=95$ mm sensing location. \circ Bare beam experimental (Uncabled). — Bare beam + Tape experimental (Uncabled).

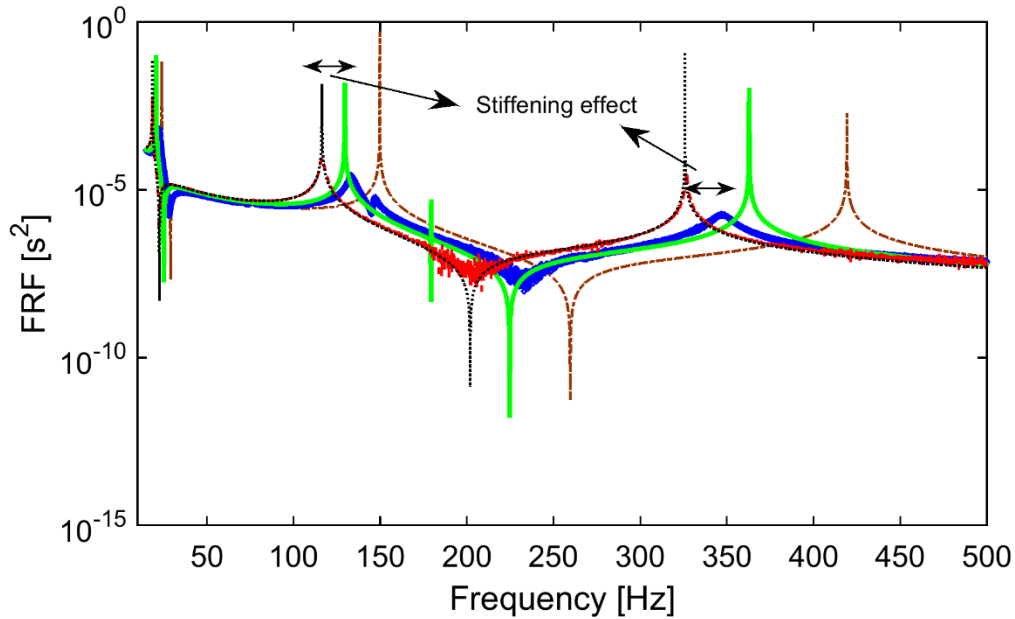


Fig. 3.3 Comparison between the frequency response functions at $x_s=95$ mm sensing location; $-\cdot-\cdot-$ Martin et al ; \blacksquare Cabled Experimental; — Cabled Analytical (Coupled EB); $-\cdot-\cdot-$ Bare beam Experimental; \cdots Bare beam analytical;

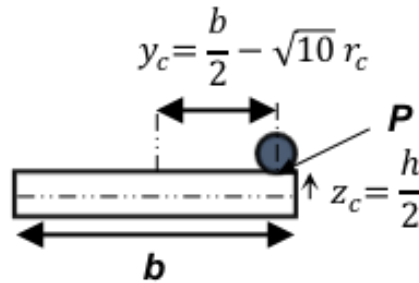


Fig. 3.4 Schematic of beam width view and cable offset position.

The frequency response functions obtained from the experiments are compared to the theoretical results for each of the Euler Bernoulli and Timoshenko coupled models presented in this Chapter as well as the previously decoupled Euler Bernoulli model, [51]. The results for the two sensing locations are shown in Figures. (3.5) and (3.6). As clearly demonstrated in these figures, significant improvement is observed for the proposed coupled model in comparison to the previous decoupled model particularly for the higher modes. In addition, in the frequency range shown, apart from the three significant peaks corresponding to the out-of-plane bending dominant

modes, there exists a small peak at around 147.1 Hz. This peak corresponds to the in-plane bending that is well predicted by the coupled modeling approach while the decoupled system is only capable of predicting the out-of-plane bending modes.

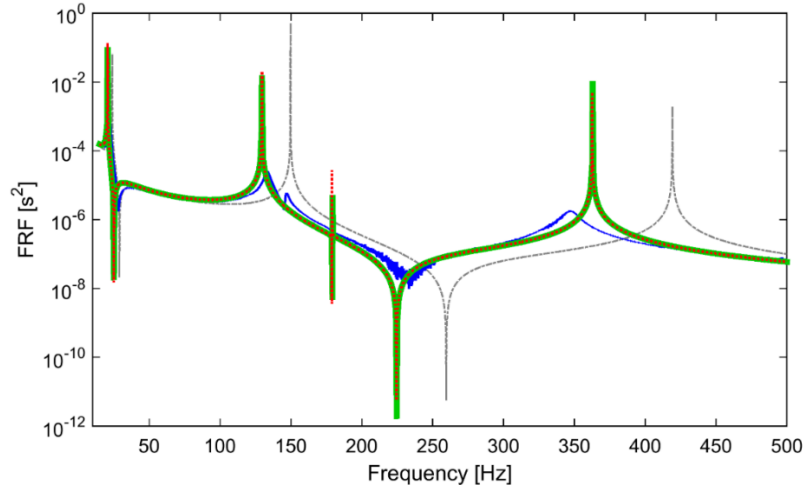


Fig. 3. 5 Comparison of the cable harnessed frequency response functions from shaker experiment, decoupled and coupled analytical models for $x_s=95$ mm. ----- Cabled Analytical (Decoupled EB) — Cabled Experimental — Cabled Analytical (Coupled EB) Cabled Analytical (Coupled Timoshenko)

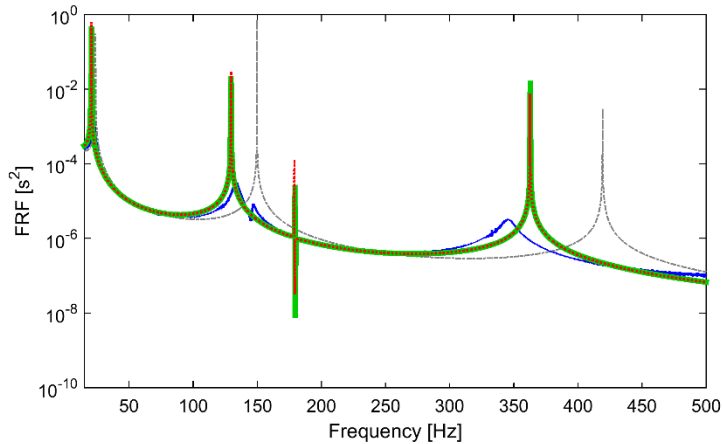
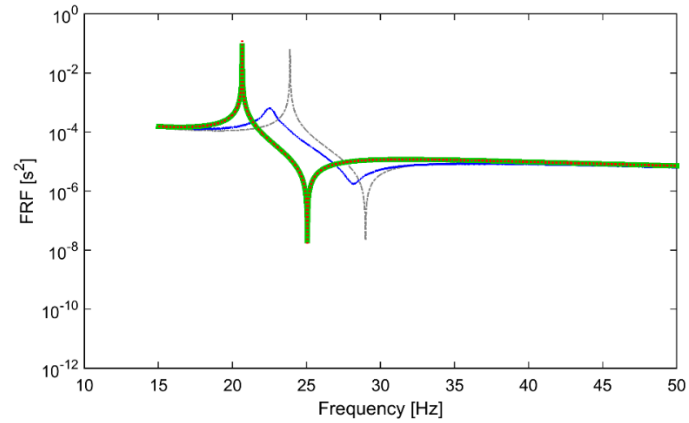


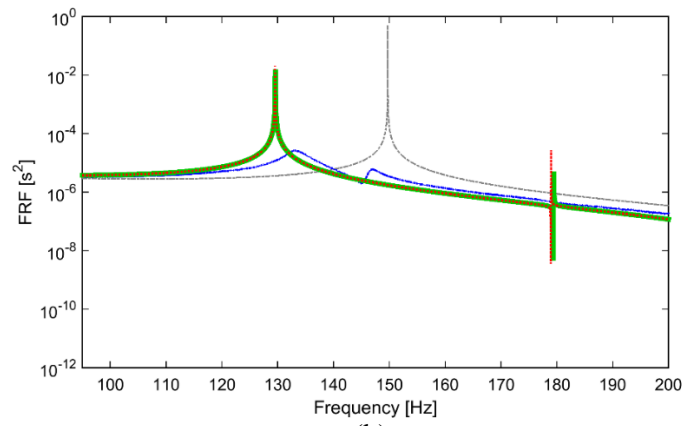
Fig. 3. 6 Comparison of the cable harnessed frequency response functions from shaker experiment, decoupled and coupled analytical models for $x_s=248$ mm. ----- Cabled Analytical (Decoupled EB) — Cabled Experimental — Cabled Analytical (Coupled EB) Cabled Analytical (Coupled Timoshenko).

The mode coupling occurs because of the addition of the cable through stiffness terms. The intensity of coupling depends on the various cable parameters such as the number of cables, offset position etc. For a bare rectangular aluminum beam, as the cross-section is symmetric, all the coordinates of vibration are decoupled. In general, for certain uncabled structures, mode coupling

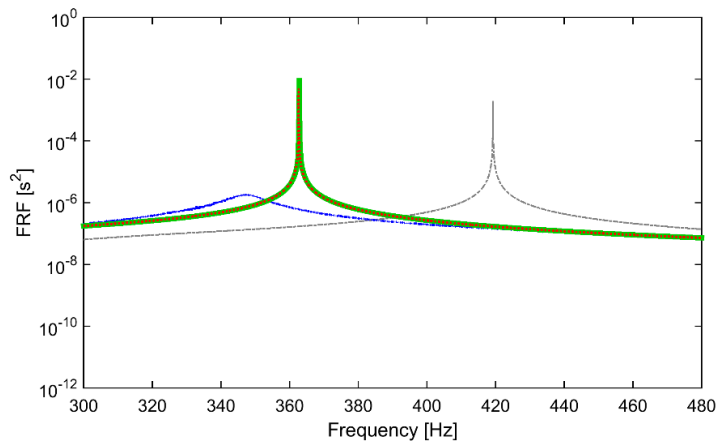
depends on geometry, boundary condition and material properties etc. For example, the difference between coupled and uncoupled models largely depends on the values of parameters causing coupling such as the fiber orientation angle in case of composite structure. To better observe the details of the FRFs comparisons, the zoom-in plots around each mode are shown in Figs. (3.7) and (3.8) for both sensing locations. The reason for overestimating the natural frequencies by the previous decoupled model, [51], is due to ignoring the compliance in the other coordinates of vibrations as also discussed by Yerrapragada et al [118]. Since in the decoupled model only the out-of-plane bending coordinate is considered, this implies that the structure is assumed to be rigid in all the other directions of motion preventing it from vibrating in those directions. This overestimation of the overall stiffness of the structure results in the frequencies to be overestimated as well. Therefore, introducing the other coordinates of vibrations in the model is a more realistic assumption that results in a more accurate representation of the system's overall stiffness and natural frequencies compared to their experimental values. Additionally, the coupled model accounts for the energy transfer between various coordinates of vibrations that ultimately results in lowering the out-of-plane bending frequency estimations compared to the decoupled system, [118]. The magnitude of peaks near the resonance are different for experiment and theory as the effect of damping is neglected in this thesis. The main goal of the thesis is to present fully coupled mathematical model that can accurately find the natural frequencies of the cabled structure. Incorporating damping related mode coupling terms into the mathematical model can be taken up as a future work as is outlined in Chapter 4. Also shown in the experimental FRFs for the out-of-plane measurement is a small peak at 147.1 Hz. This mode pertains to the in-plane bending coordinate, which is difficult to observe in the out-of-plane direction of measurement. To further investigate this mode, the in-plane bending tests are also performed for the two sets of actuation and sensing locations shown in Fig. (3.9) and the FRFs are presented in Fig. (3.10). Subscripts 'a' and 's' denote the actuation and sensing in Fig. (3.9) respectively. An impact hammer model number PCB 086C01 with a metal tip is used for this test. Both the impact excitation and sensing are made in the in-plane direction shown. A total number of 5 averages are taken for the impact test for which the coherence plots are also presented in Figure. (3.11). The very dominant peak shown at about 147 Hz frequency for both these FRF plots further indicates of this mode corresponding to an in-plane bending mode.



(a)



(b)



(c)

Fig. 3. 7 Zoom in plots for frequency response functions for shaker experiment, coupled and decoupled models of $x_s=95$ mm for a) Mode 1 b) Modes 2 and 3 and c) Mode 4.
 ----- Cabled Analytical (Decoupled EB)
 — Cabled Experimental
 — Cabled Analytical (Coupled EB)
 Cabled Analytical (Coupled Timoshenko).

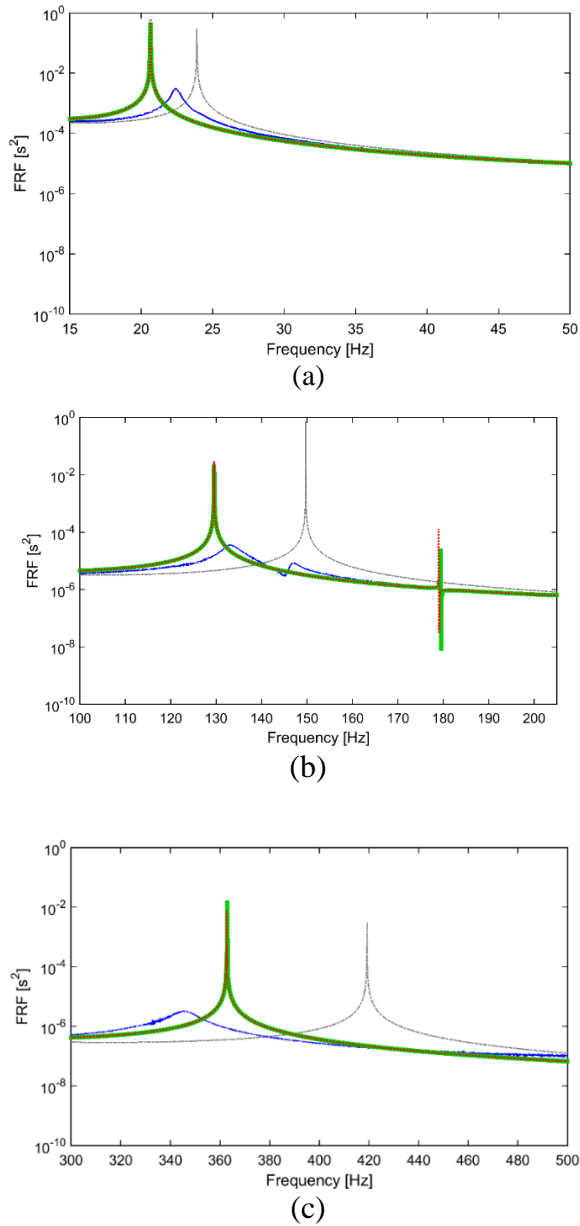


Fig. 3. 8 Zoom in plots for frequency response functions for shaker experiment, coupled and decoupled models of $x_s=248 \text{ mm}$ for a) Mode 1 b) Modes 2 and 3 and c) Mode 4. . - - - - - Cabled Analytical (Decoupled EB) — Cabled Experimental — Cabled Analytical (Coupled EB) - - - - - Cabled Analytical (Coupled Timoshenko).

Also, shown in these plots are the small peaks at about 22 Hz and 133 Hz, both corresponding to the out-of-plane bending modes that are not as obvious due to being in the other direction. Both experimental and their corresponding theoretical frequency values for all the modes are tabulated and shown in Table. (3.2) for comparison. Also, the sharp peak at around 178 Hz in the FRFs from the model corresponds to the coupled model estimation for the in-plane bending frequency. To

further prove this, the theoretical mode shapes are also plotted at this frequency and shown in Figure. (3.12).

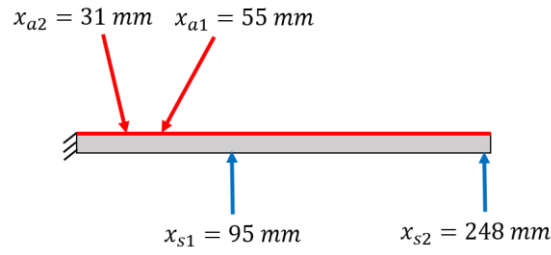
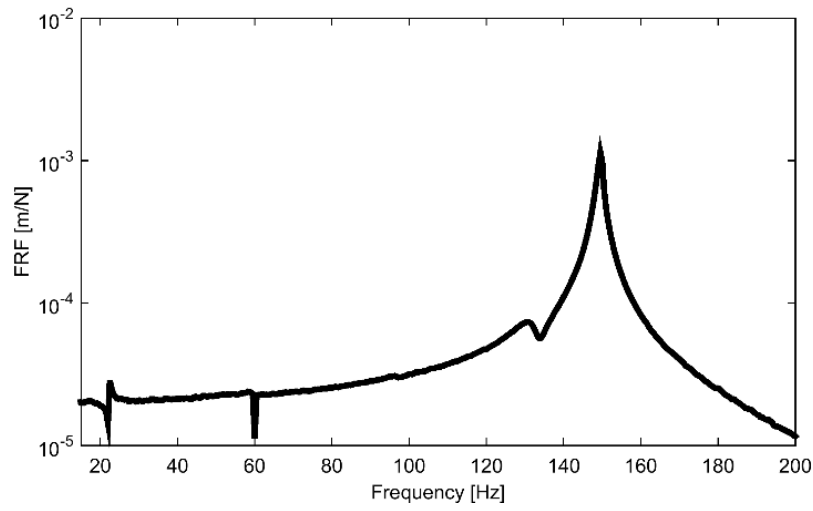
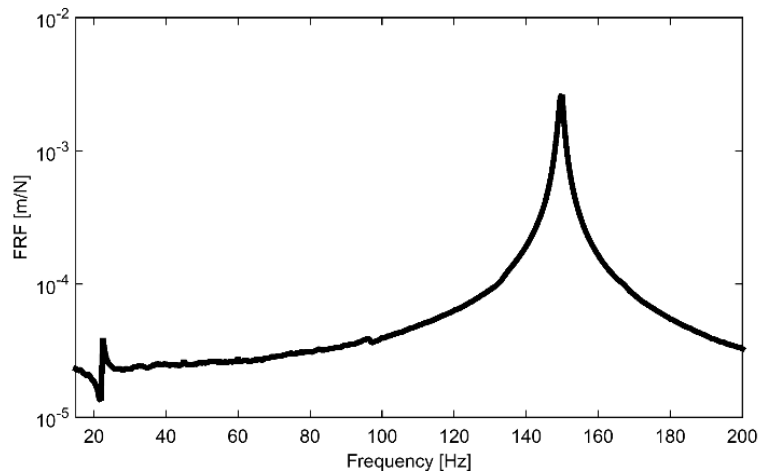


Fig. 3. 9 Sensing and actuation locations for the two in-plane impact hammer tests.

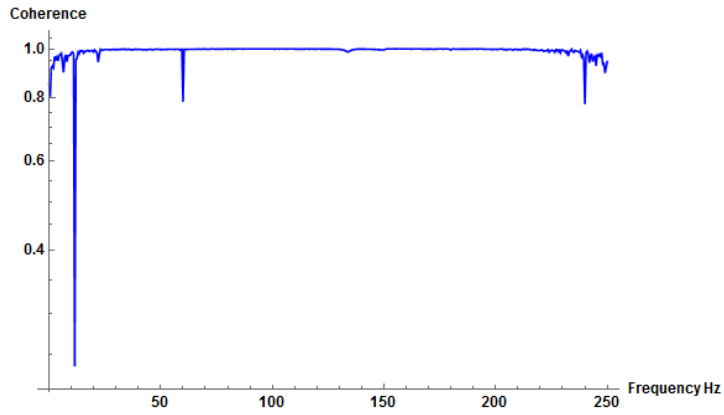


a)

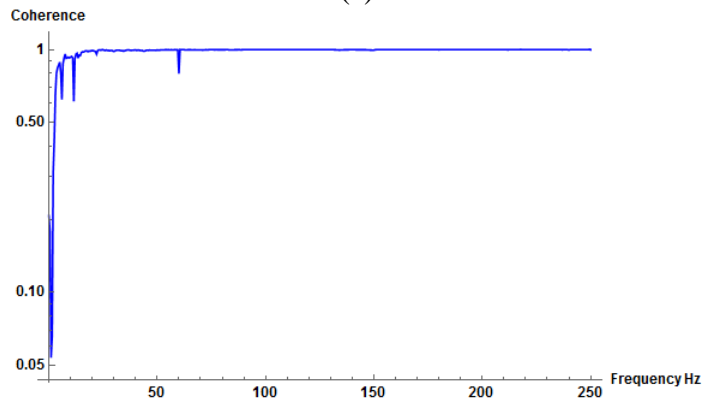


b)

Fig. 3. 10 Frequency response functions for in-plane impact tests. a) impact test for $(x_{a1}, x_{s1}) = (55, 95)$ mm, b) impact test for $(x_{a2}, x_{s2}) = (31, 248)$ mm.



(a)



(b)

Fig. 3. 11 Coherence plots for the in-plane impact hammer tests. (a) $(x_{a1}, x_{s1}) = (55, 95)$ mm, (b) $(x_{a2}, x_{s2}) = (31, 248)$ mm.

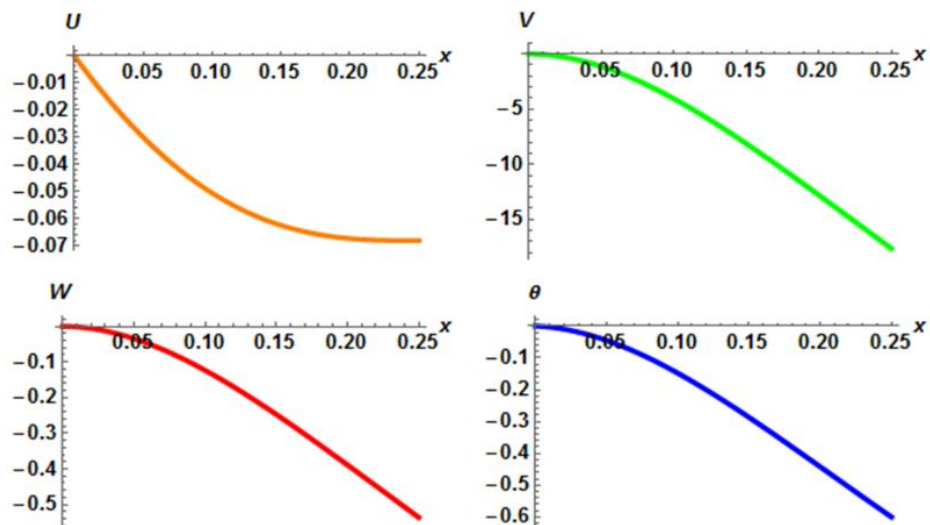


Fig. 3. 12 First in plane bending dominant mode shape from the coupled analytical model. U, V, W, θ denote the axial, in-plane bending, out-of-plane bending and torsional mode shapes at the first in-plane dominant mode respectively.

From the mass normalized values for each of these coordinates' mode shapes at this frequency, it can be observed that this mode is clearly an in-plane dominant mode. The mode shape also indicates the first in-plane bending mode. The error values shown in Table. (3.2) further indicate the improvement made for using the coupled model when compared to the previous decoupled model. Also, the Euler-Bernoulli and Timoshenko results line up perfectly showing that for the system parameters considered in this case study, there is no need for including the Timoshenko beam assumptions to obtain better accuracy. The testing performed at two different locations yielded same natural frequencies. In addition, the cables were removed and re-attached to the host structure and tested again. Similar natural frequencies are obtained and are presented in Table. (3.3). This suggests the repeatability of the tests is very good after re-wrapping of the host structure with cables. The percentage difference in the out of plane bending modes is less than 1 %. For the testing of future samples on periodic and non-periodic wrapping pattern, repeatability test results are not included.

Table 3. 2 Natural frequencies for analytical and experimental models for cabled harnessed beam.

Mode	Decoupled Euler-Ber.	Coupled Euler- Ber.	Coupled Timoshenko	Experiment	Error % Decoupled	Error % Coupled Euler-Ber.	Error % Coupled Timoshenko
1	23.88	20.65	20.65	22.35 (OP)	6.84 %	-7.60 %	-7.60 %
2	149.70	129.56	129.53	133.2 (OP)	12.38 %	-2.73 %	-2.75 %
3	-	179.42	178.99	147.1 (IP)	-	21.97 %	21.67 %
4	419.23	362.85	362.65	345.6 (OP)	21.30 %	4.99 %	4.93 %

*OP and IP refer to the out of plane and in plane bending modes respectively.

Table 3. 3 Natural frequencies for two different experiment sets for cabled harnessed beam.

Mode	Experiment 1 [Hz]	Experiment 2 [Hz]	% Difference
1	22.35 (OP)	22.30 (OP)	0.22 %
2	133.2 (OP)	134.30 (OP)	0.82 %
3	147.1 (IP)	145.25 (IP)	1.25 %
4	345.6 (OP)	345.80 (OP)	0.057 %

*OP and IP refer to the out of plane and in plane bending modes respectively.

Table 3. 4 Effect of product of inertia terms on the natural frequencies.

Mode	Coupled Timoshenko [Hz]	Coupled Timoshenko (including product of inertia terms) [Hz]	% Difference
1	20.65	20.65 (OP)	0 %
2	129.53	129.53 (OP)	0 %
3	178.99	178.98 (IP)	0.005 %
4	362.65	362.66 (OP)	0.002 %

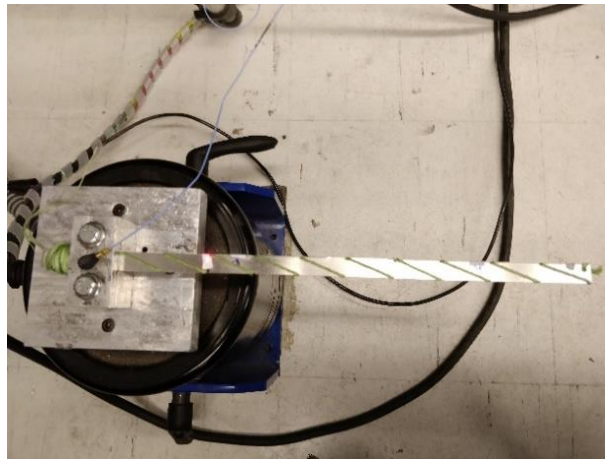
*OP and IP refer to the out of plane and in plane bending modes respectively.

In addition the following provides justification of ignoring the product of inertia terms in the kinetic energy expression in Eq. (2.9). To obtain more insight, the kinetic energy after including the terms related to the product of inertia between various coordinates are shown below in Eq. (3.2).

$$T = \frac{1}{2} \int_0^l \left[k_1(\dot{u})^2 + k_2(\dot{v})^2 + k_3(\dot{w})^2 + k_4(\dot{\theta})^2 + k_5(\dot{\phi})^2 + k_6(\dot{\psi})^2 + 2\rho_c A_c y(\dot{u})(\dot{\phi}) + 2\rho_c A_c z(\dot{u})(\dot{\psi}) - 2\rho_c A_c yz(\dot{\psi})(\dot{\phi}) - 2\rho_c A_c z(\dot{v})(\dot{\theta}) + 2\rho_c A_c y(\dot{w})(\dot{\theta}) \right] dx \quad (3.2)$$

After incorporating the above additional terms in the governing partial differential equations and the resulting frequencies from the model that contains the effect of these additional terms is compared to the model which neglects these terms. The system parameters are used are the same as the experimental sample. The natural frequency comparison is shown in Table (3.4). From the Table (3.4) it is clear that the product of inertia terms in the kinetic energy do not play a role on the natural frequencies associated with the cable-harnessed structure and can be ignored in the analysis of future samples.

3.2 Experimental Validation of Periodic Wrapping Pattern



(a)



(b)

Fig. 3. 13 Experimental setup of the cable harnessed structure (a) Sample 2 (b) Sample 3.

The experimental setup is shown in Fig. (3.13). Two samples for host structure are considered and multiple pre-tensioned cables are wrapped in a diagonal manner around the structure. One end of the cable is attached to the host structure through a small hole at the tip of the cantilever. The cable pre-tension is applied using modular weights while the structure is being wrapped. Two of the three samples for periodic pattern presented in Chapter 2.2 are experimentally validated namely the samples 2 and 3. The system parameters for the host structure and cables for samples 2 and 3 are shown in the third and fourth columns of Table. (2.7) respectively. In the first sample, the cable system parameters are chosen on the similar lines as theoretical paper on periodic wrapping pattern by Martin et al [51]. The purpose of sample 1 is to first theoretically demonstrate the differences in the peaks between the coupled model proposed in thesis for periodic wrapping

pattern and the decoupled one published by Martin et al. The system parameters for the cable for the next two samples are chosen on the similar lines as experimental paper [52] as the same cable is used to perform experiments. In this thesis, more cables when compared to [52] are used as the effective increase in the cable wrapping area to showcase the increase in the mode coupling effect. The cable considered is an 80 pound strength Power pro Super 8 Slick fishing line whose material properties are as [52,130]. The equipment used to perform experiments is the same as described in Section 3.1. In the first set of tests, the structures are subjected to harmonic base excitation in the out of plane bending direction and the experimental frequency response function (FRF) is recorded at a given sensing location in the out of plane bending direction using the laser vibrometer. To help identify the type of coordinate associated with the sharp peaks in the experimental FRF, mode shape animation studies are performed by sensing at multiple locations. To animate the torsion mode experimentally, the structure is discretized into three columns, with two columns at each edge and one along the centerline. At each column, the sensing is performed at every 1 cm. Similarly, to animate the in-plane bending modes, the structure is excited in the in-plane bending direction using a PCB 086C01 impact hammer with a metal tip and is sensed in the in-plane bending direction using laser vibrometer at multiple sensing locations.

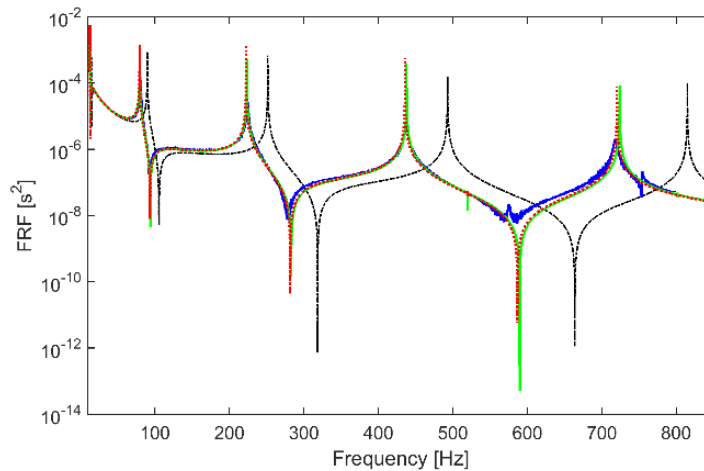
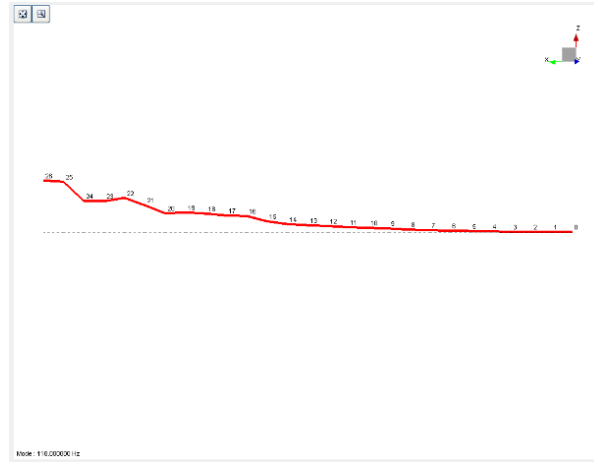


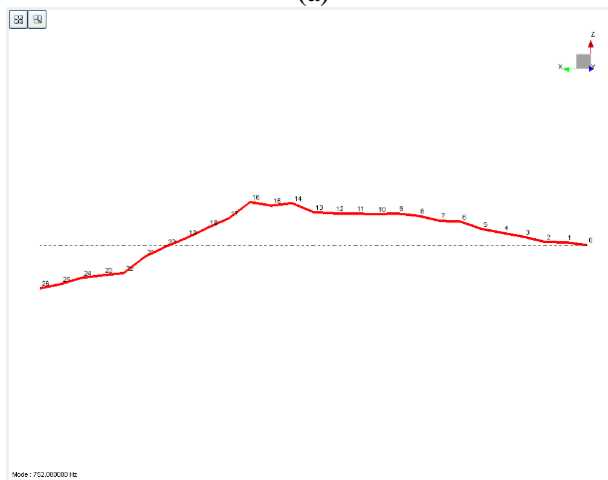
Fig. 3. 14 Comparison of experimental frequency response function with theoretical frequency response function for Sample 2.
 ----- Cabled Analytical (Decoupled EB) ——— Cabled Experimental
 ——— Cabled Analytical (Coupled EB) Cabled Analytical (Coupled Timoshenko)

The frequency response function comparison results for sample 2 are presented in Fig. (3.14). The coupled analytical frequency function (both Euler-Bernoulli and Timoshenko theory) match well with that of the experimental frequency function when compared to the decoupled

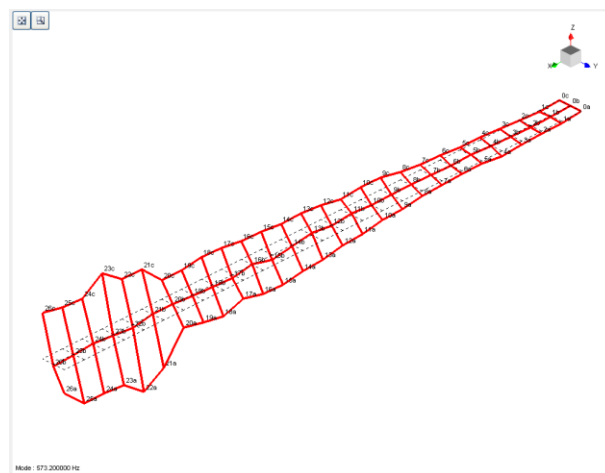
model. The frequency response function from bending decoupled model of Martin et al [52] is also shown in Fig. (3.14). Previous work by the authors in Ref. [130] includes further correction to Martin et al assumptions and the strain values the cable experiences are assumed the same as the strain values of the top fiber of the beam and the assumptions are used in this paper. The significant peaks denote the modes associated with the out-of-plane bending coordinate. The experimental natural frequencies associated with the first two in-plane bending dominant modes and the torsion dominant mode are 118, 752 and 573.7 Hz respectively. The FRF obtained from the test where the actuation is performed using an impact hammer in the in-plane direction and the sensing also performed in the in-plane direction is presented in Fig. (3.20 a). The plot in Fig. (3.20 a) clearly gives the frequencies associated with the in plane bending dominant mode. The natural frequencies obtained from both theoretical models and experiment for this sample along with the error percentage with respect to the experimental natural frequencies are presented in Table. (3.5). To confirm the experimental frequencies associated with the in-plane bending and torsion dominant mode, the deflection shapes are plotted in Fig. (3.15). Fig. (3.15 a) shows the first in plane bending dominant shape and Fig. (3.15 b) shows the second in plane bending dominant peak. Fig. (3.7 c) shows the first torsion dominant mode shape. In Fig. (3.15 c) we can clearly see that the displacement of points at the two opposite edges in the same row are out of phase, which clearly confirms that it is a torsion dominant mode. As explained earlier in the first paragraph of Section. 3.2, these shapes are obtained by sensing at multiple locations. The corresponding theoretical mode shapes from the coupled EB model for the two in-plane dominant modes and the torsion dominant mode are plotted in Figs. (3.16 a), (3.16 b) and (3.16 c) respectively.



(a)



(b)



(c)

Fig. 3. 15 Experimental snapshot mode shapes for (a) first in-plane dominant (b) second in-plane dominant (c) first torsion dominant modes for sample 2.

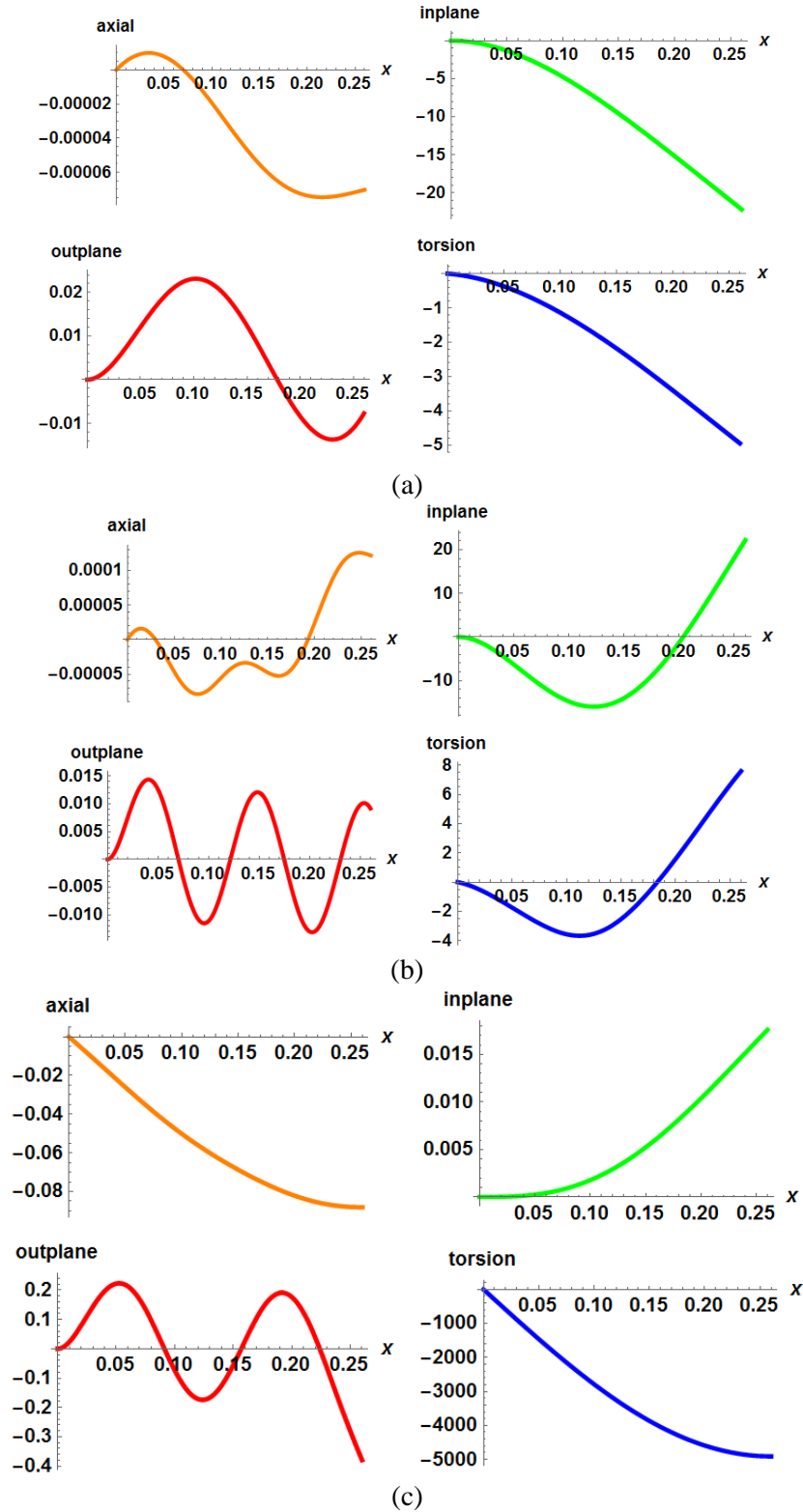


Fig. 3. 16 Theoretical mode shapes for (a) First in-plane bending dominant; (b) Second in-plane bending dominant; (c) First torsion dominant for sample 2

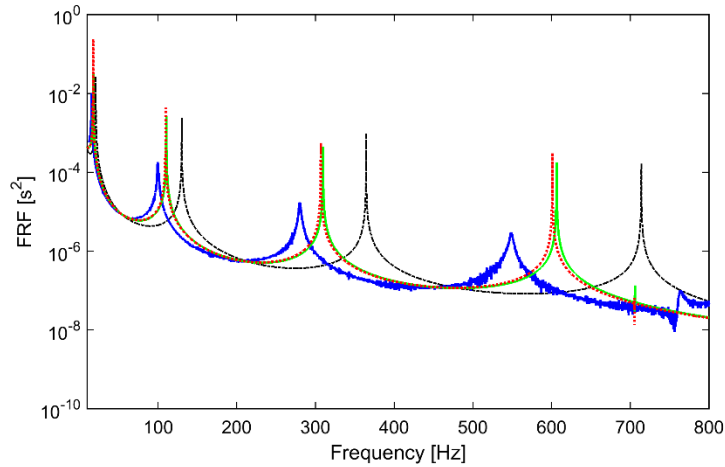
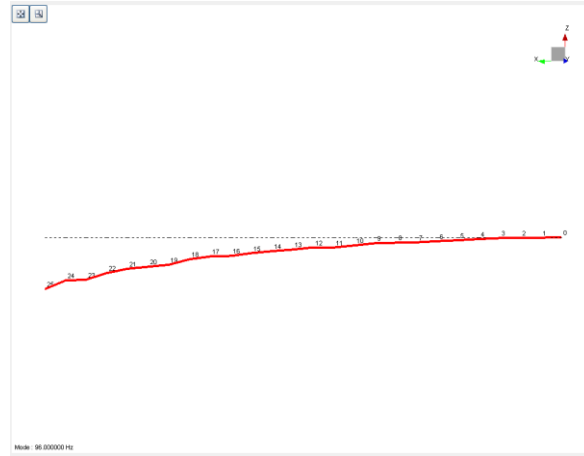
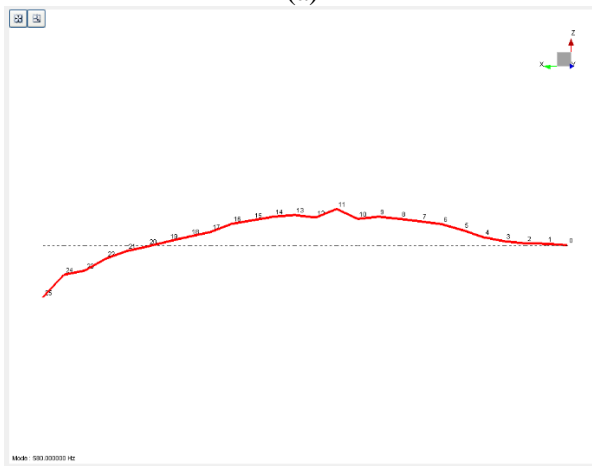


Fig. 3. 17 Comparison of experimental frequency response function with theoretical frequency response function for Sample 3.
 ----- Cabled Analytical (Decoupled EB) ——— Cabled Experimental
 ——— Cabled Analytical (Coupled EB) Cabled Analytical (Coupled Timoshenko)

The theoretical natural frequencies associated with the first, second in-plane modes and the first torsional mode are 133.74, 838.12 and 497.93 Hz respectively. Overall, the coupled model proposed for periodic wrapping pattern shows significant improvement with good match with the experimental FRF when compared to the decoupled model presented in the existing literature. As explained earlier, the coupled model accounts for the stiffness of the structure in all the coordinates whereas the decoupled considers the stiffness only in one direction as a result over predicts the stiffness by more than the coupled model.



(a)



(b)



(c)

Fig. 3. 18 Experimental snapshot mode shapes for (a) first in-plane dominant (b) second in-plane dominant (c) first torsion dominant modes for sample 3.

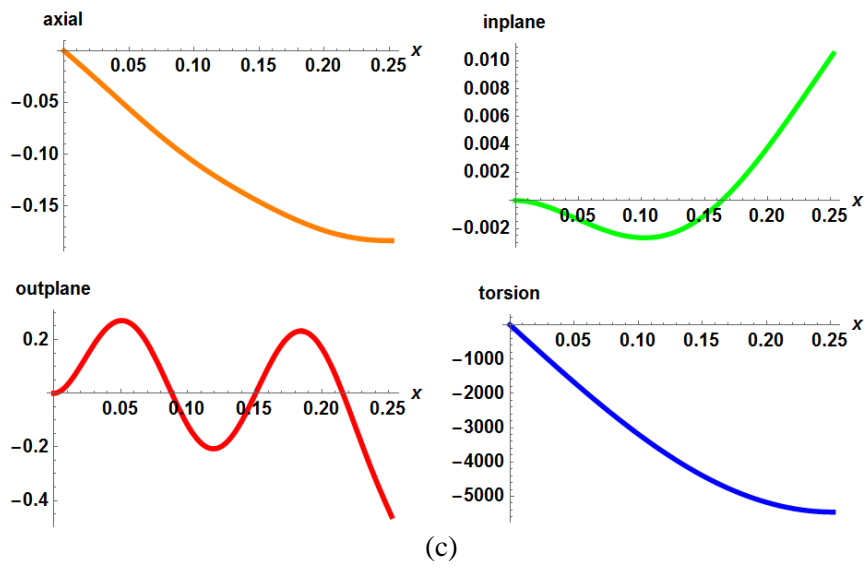
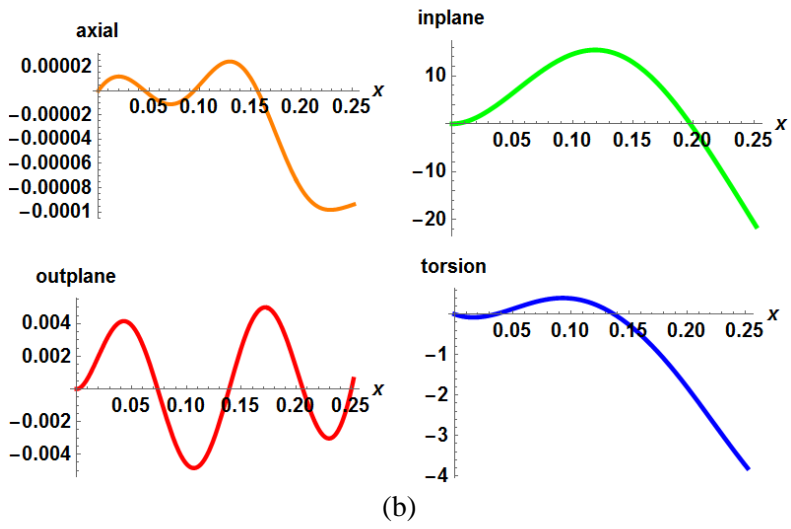
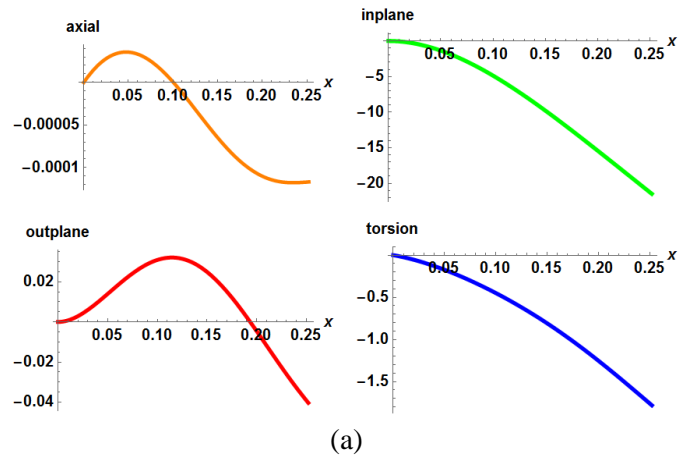


Fig. 3. 19 Theoretical mode shapes for (a) First in-plane bending dominant; (b) Second in-plane bending dominant; (c) First torsion dominant for sample 3.

Table 3. 5 Comparison of Theoretical Natural Frequencies with Experiment for Sample 2.

Mode No	Experiment [Hz]	Coupled EB [Hz]	Coupled TBT [Hz]	Decoupled EB [Hz]	Error % Coupled EB	Error % Coupled TBT	Error % Decoupled EB
1	13.20 (OP)	12.66 (OP)	12.61	14.16	-4.09 %	4.46 %	7.27 %
2	81.1 (OP)	79.25 (OP)	79.03	88.81	-2.28 %	2.55 %	9.50 %
3	118 (IP)	133.74 (IP)	133.54	-	13.33 %	13.16 %	-
4	224.50 (OP)	222.28 (OP)	221.26	248.7	-0.98 %	1.44 %	10.77 %
5	438 (OP)	435.59 (OP)	433.49	487.32	-0.55 %	1.02 %	11.26 %
6	573.70 (T)	497.93 (T)	497.52	-	-13.20 %	13.27 %	-
7	718.60 (OP)	720.02 (OP)	716.40	805.56	0.197 %	0.30 %	12.10 %
8	752 (IP)	838.12 (IP)	829.69	-	11.45 %	10.33 %	-

*OP, IP and T stand for Out of plane bending, In-plane bending and Torsion dominant modes respectively. EB stands for Euler-Bernoulli. TBT stands for Timoshenko theory and errors are computed with respect to the experiment

Table 3. 6 Comparison of Theoretical Natural Frequencies with Experiment for Sample 3.

Mode No	Experiment [Hz]	Coupled EB [Hz]	Coupled TBT [Hz]	Decoupled EB [Hz]	Error % Coupled EB	Error % Coupled TBT	Error % Decoupled EB
1	15.60 (OP)	17.63 (OP)	17.49	20.76	13.01 %	12.11 %	33.07 %
2	99.6 (OP)	110.56 (OP)	109.62	130.13	11.00 %	10.06 %	30.65 %
3	96 (IP)	126 (IP)	125.85	-	31.25 %	31.09 %	-
4	280.2 (OP)	309.55 (OP)	306.86	364.41	10.47 %	9.51 %	30.05 %
5	548.6 (OP)	606.53 (OP)	601.07	714.06	10.55 %	9.56 %	30.16 %
6	764.5 (T)	705.97 (T)	705.22	-	-7.65 %	7.75 %	-
7	580 (IP)	789.70 (IP)	783.02	-	36.15 %	35 %	-

*OP, IP and T stand for Out of plane bending, In-plane bending and Torsion dominant modes respectively. EB stands for Euler-Bernoulli. TBT stands for Timoshenko theory and errors are computed with respect to the experiment

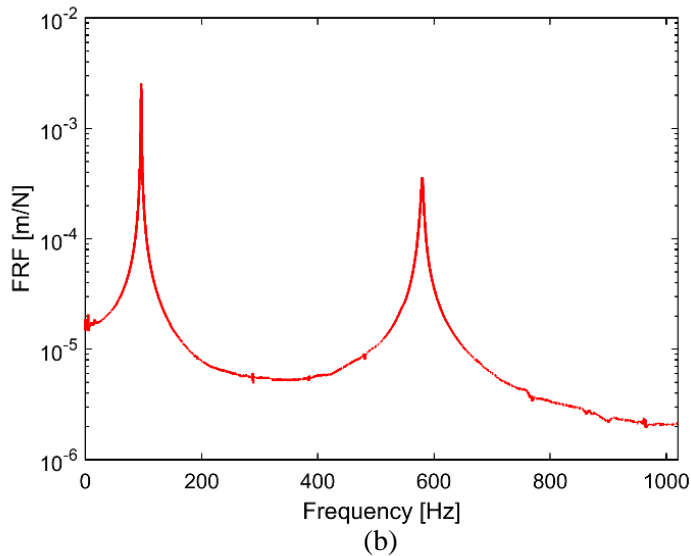
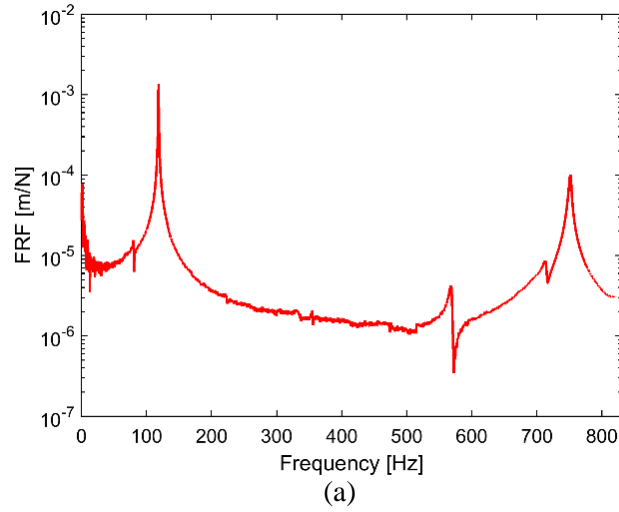


Fig. 3. 20 Frequency response function obtained from in-plane impact test (a) Sample 2 (b) Sample 3.

Similarly, in the FRF comparison for sample 3 in Fig. (3.17), the coupled model shows significant improvement when compared to the decoupled model from the existing literature. The case of sample 3 considered has more coupling when compared to sample 2 due to larger number of cables considered. The significant peaks again represent the out of plane bending modes. The natural frequency results from the theory and experiment along with the error percentages are tabulated in Table. (3.6). Fig. (3.20 b) shows the FRF for the in-plane actuation-sensing case to clearly identify the natural frequencies associated with the in plane bending dominant modes. To further confirm, the type of each mode, experimental deflection shapes for sample 3 are presented in Fig. (3.18). The first two in-plane bending dominant mode shapes are presented in Figs. (3.18

a) and (3.18 b) and the first torsion dominant mode shape is presented in Fig. (3.18 c). The corresponding theoretical mode shapes for the first two in plane bending dominant modes are presented in Figs. (3.19 a) and (3.19 b) and the torsion dominant mode is presented in Fig. (3.19 c). Similar to experimental sample 2, from the overall analysis of the FRF plots in Fig. (3.17), the coupled EB and TBT models give better matches when compared to the decoupled model. For both samples 2 and 3, the in plane bending dominant mode gives higher errors when compared to the other coordinates of motion. The theory over-predicts the natural frequencies for the in-plane bending dominant modes.

Table 3. 7 Natural Frequencies after updating the width parameter

Mode No	Experiment [Hz]	Coupled EB Analytical [Hz] (Parameter Updating)	Error % Coupled EB and Experiment
1	13.20 (OP)	12.73 (OP)	-3.56 %
2	81.1 (OP)	79.83 (OP)	-1.59 %
3	118 (IP)	127.94 (IP)	8.42 %
4	224.50 (OP)	223.45 (OP)	-0.46 %
5	438 (OP)	437.99 (OP)	0 %
6	573.70 (T)	519.95 (T)	-9.36 %
7	718.60 (OP)	723.99 (OP)	0.75 %
8	752 (IP)	801.82 (IP)	6.62 %

For sample 2, the width parameter is updated from 11 mm to 10.5 mm. The new natural frequencies are presented in Table. (3.10), the error percentages have improved when compared to Table. (3.7). The in-plane bending and torsional dominant errors are now lower.

The natural frequencies for sample 3, are presented in Table. (3.6). As the cabling becomes more significant for sample 3, the out of plane bending mode is slightly over-predicted when compared to sample 2. The coupled model proposed in this thesis shows improvement over the model published by Martin et al [52,54] for periodic pattern. As the cabling becomes more significant, the shear effects due to cable also increases which is ignored in the current coupled model. As a future work, the model may be improved incorporating the shearing effect at the top of the cross-section of the cable as its value is minimum at the top of the cable. Due to this, the natural frequency prediction will be lower and may provide better match with the experiment. This can be investigated by interested readers as a future work. Also, the natural frequencies for the in plane bending dominant mode from the theoretical model are on the higher side. To obtain more

insight, the experimental in plane bending dominant natural frequencies of the bare beam for sample 3 are found. The FRF in the in plane bending direction for the experimental data of bare beam is shown in Fig. (3.21). The results are tabulated in Table. (3.8) and are compared with the bare beam analytical frequencies along with the error percentages. The error for the in-plane bending modes between the bare beam theory and experimental is higher. This is because the analytical model treats the fixed end as rigid (infinite stiffness). In reality, the fixed end has some finite stiffness, which becomes more important while modeling the in-plane bending modes for thicker substrates. When larger number of cables are added to host structure (in case of sample 3 they are 10 cables when compared to 5 cables in sample 2). The error that existed in the bare beam will also increase due to increase in effective thickness of the structure to be clamped. In addition to this, for larger number of cables, the diagonal section of the cables are not in proper contact with the host structure when it vibrates in the in-plane direction. For clarity, the system configuration is shown in Fig. (3.22). When the cable does not stay in contact, both the inertia and stiffening effect due to cabling will be lower when compared to the situation where the cable is perfectly in contact. Mathematically, this case can be modelled by assuming distinct in-plane displacements for the host structure and the cable for the system in Fig. (3.22). Practically, in the in-plane bending direction, the compressive axial force acting on the host structure due to pre-tension in the cable will be dominant. Because of this compressive effect, the resulting frequencies will be lower than the bare beam. The equation to study this effect is shown in Eq. (3.2).

Table 3. 8 Comparison of theoretical and experimental in plane bending dominant natural frequencies for bare beam of Sample 3.

Mode No	Analytical Frequencies [Hz]	Experiment [Hz]	Error (%) Analytical and experiment
1	120.55 (IP)	103.6 (IP)	16.36
2	755.55 (IP)	619.20 (IP)	22.02

$$(\rho_b A_b + \frac{\rho_c A_c}{L} [4\bar{h} + 2\bar{b}])\ddot{v} + E_b I_{zz} v'''' + P_T v'' = 0 \quad (3.2)$$

where P_T is the compressive force acting on the host structure due to pre-tension of the cable. The kinetic energy mass term also contains the cable lumped masses. The lumped masses stay in contact with the host structure. The mathematical form of Eq. (3.2) is a standard equation in

vibration text books [120] when a structure is subjected to compressive axial load and can be easily solved for natural frequency by applying boundary conditions.

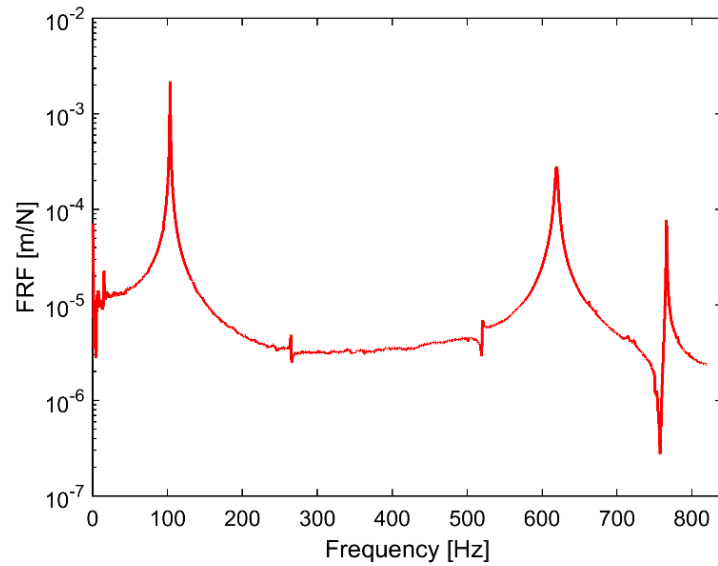


Fig. 3. 21 Frequency response function of in-plane bending vibration of bare beam of sample 3

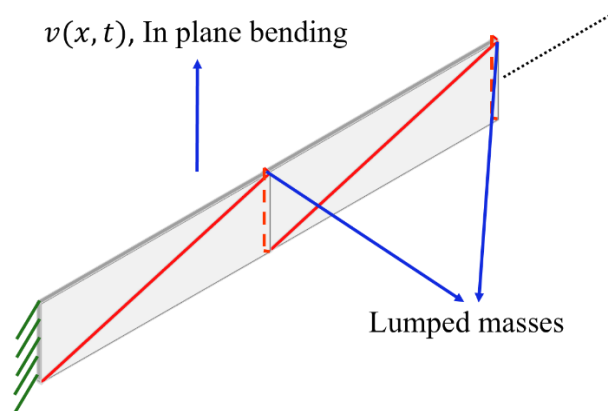


Fig. 3. 22 Top isometric view of the cable-harnessed structure undergoing in plane bending vibration

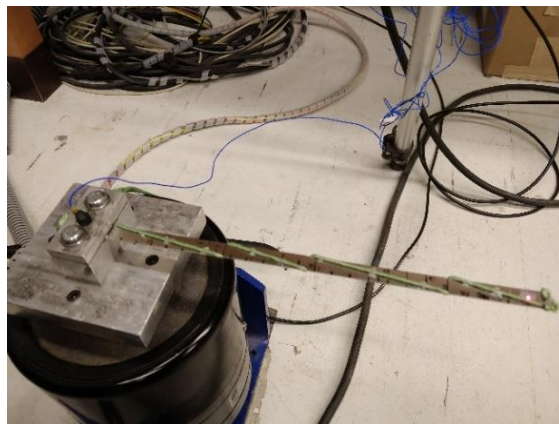
Eq. (3.2) is valid only when the cable is not properly attached to the host structure, which happens only in the in-plane bending direction when the structure has larger number of cables as in sample 3. By using the system parameters of sample 3, the natural frequencies of the first two in-plane bending dominant modes are 114.05 Hz and 739.59 Hz. The errors w.r.t cabled experimental are 18.80 % and 27.5 %. The errors are still on the higher side. For further explanation, these errors are when the clamped end is assumed perfectly rigid. As seen in Table. (3.8) for the bare beam of sample 3, the error for the first two modes are in the range of 16.26 and

22.02 %. Large part of resulting error after solving Eq. (3.2) can be related to error propagating into the cabled structure from bare beam structure.

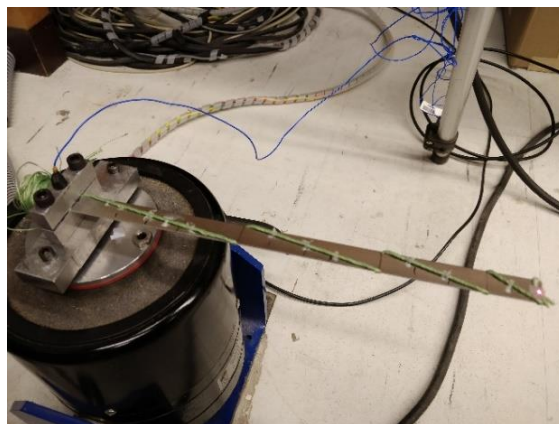
In addition, the Timoshenko coupled model curve shows some more improvement over coupled Euler-Bernoulli model as the Timoshenko model allows for additional degrees of freedom (rotation of cross-section coordinates). To conclude from the theory and experimental observations, in order to accurately study the dynamic behavior of cable-harnessed structure with periodic wrapping pattern, coupled vibration model is a better choice when compared to the decoupled vibration model.

3.3 Experimental Validation of Non-Periodic Wrapping Pattern

The non-periodic samples along with experimental setup are shown in Figs. (3.23 a) and (3.23 b). The top view of the wrapping is clearly described in Figs. (3.24 a) and (3.24 b) respectively.



(a)



(b)

Fig. 3. 23 Experimental setup of a) Sample 1 b) Sample 2 for non-periodic wrapping pattern

The numerical parameters of the samples are shown in Table. (2.16). The structures are fixed at one end (cantilever boundary condition). Both the samples have four fundamental elements. The wrapping pattern of samples 1 and 2 are described in Chapter 2.3. Multiple pre-tensioned cables are wrapped around the host structure. After the structure is wrapped and clamped tightly at one end, super glue is applied at discrete locations to make sure the cables stay in contact with the structure while the structure vibrates. The cable is an 80 lb. strength Power Pro fishing line. The substrates are made of Al 6061 alloys. The material and geometrical properties of the host structure and the cable are presented in Table. (2.16) for samples 1 and 2.

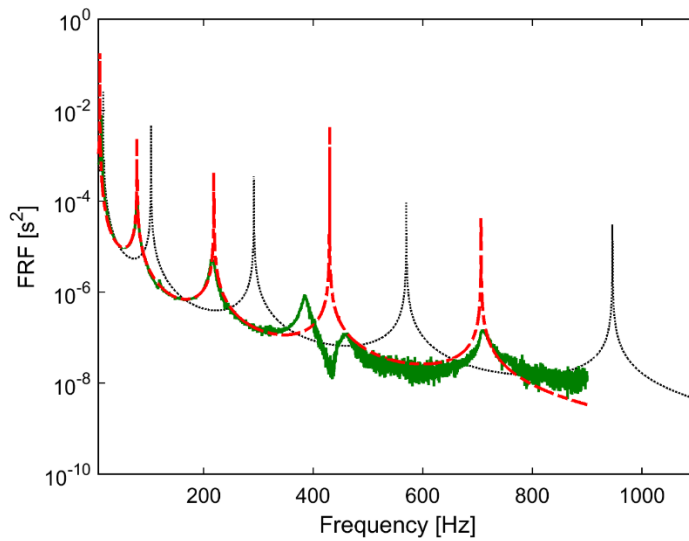


Fig. 3. 24 FRF comparison between the coupled, decoupled analytical models and the experiment for sample 1. Cabled Analytical (Decoupled) —— Cabled Experimental - - - Cabled Analytical (Coupled).

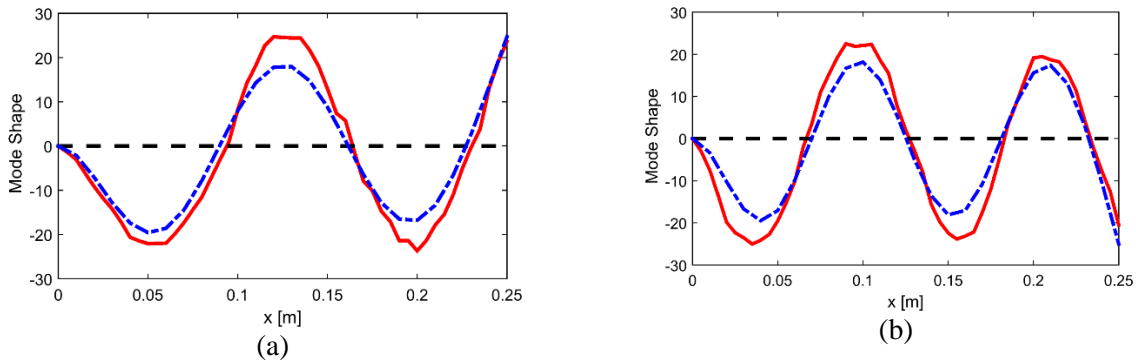


Fig. 3. 25 Comparison of experimental and theoretical out of plane bending mode shapes for (a) Mode 4 (b) Mode 5. —— Experimental —— Centerline - - - Analytical.

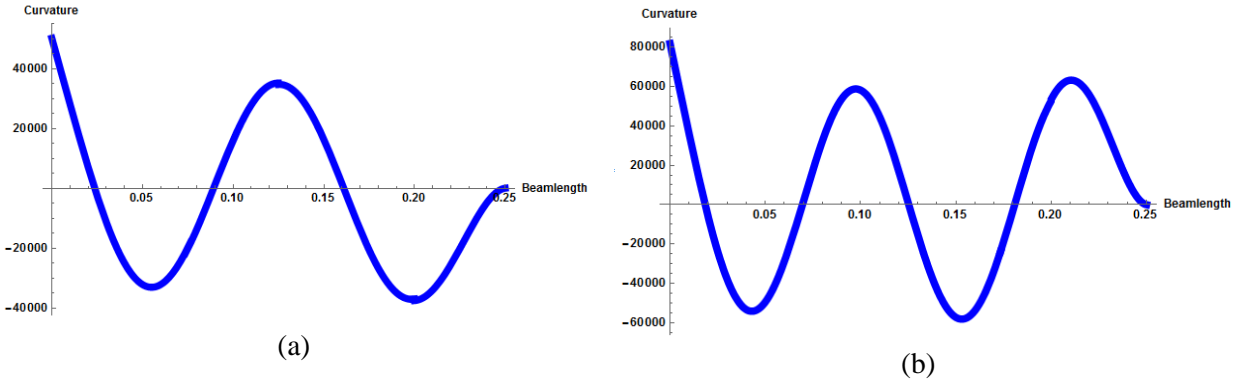
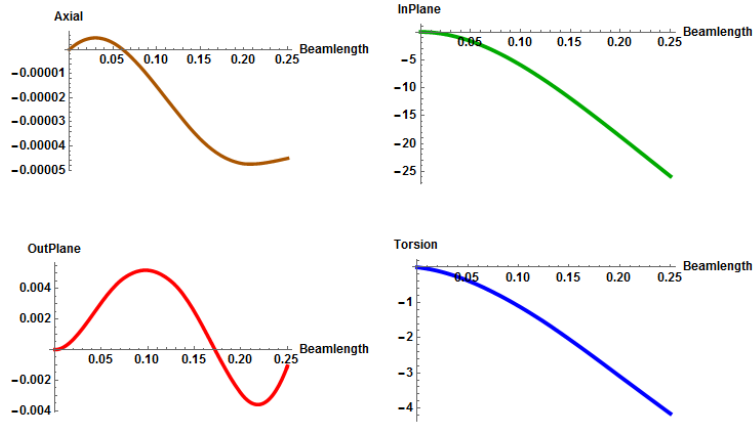


Fig. 3. 26 Theoretical plots for curvature for (a) Mode 4 (b) Mode 5 for sample 1

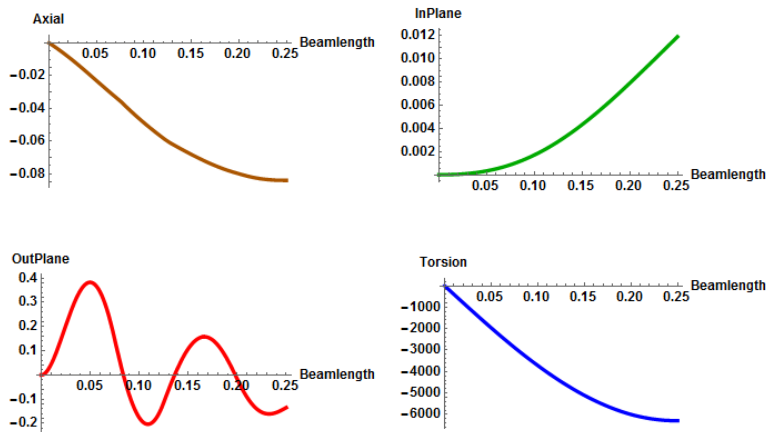
Table 3. 9 Coupled and Decoupled Natural Frequencies for Sample 1

Mode No	Experiment [Hz]	Coupled EB [Hz]	Decoupled EB [Hz]	% Coupled EB and Experiment	% Decoupled EB and Experiment
1	13.2	10.78 (OP)	16.65	18.33 %	26.13 %
2	78.6	78.45 (OP)	104.18	0.19 %	32.54 %
3	121 (IP)	140.29 (IP)	-	15.94 %	-
4	215.7	218.85 (OP)	291.93	1.46 %	35.34 %
5	384.8	429.9 (OP)	570.06	11.72 %	48.14 %
6	459.5 (T)	447.07 (T)	-	2.70 %	-
7	709.1	706.47 (OP)	946.33	0.37 %	33.45 %
8	752.8 (IP)	878.21 (IP)	-	16.65 %	-

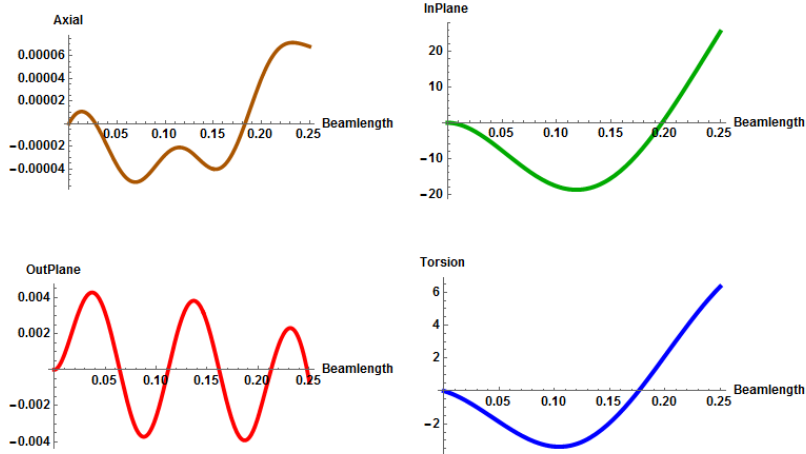
*OP stands for out of plane bending, IP stands for in plane bending and T stands for Torsion dominant modes



(a)



(b)



(c)

Fig. 3. 27 Coupled theoretical mode shapes (a) First in plane bending dominant (b) First torsion dominant (c) Second in-plane bending dominant for sample 1

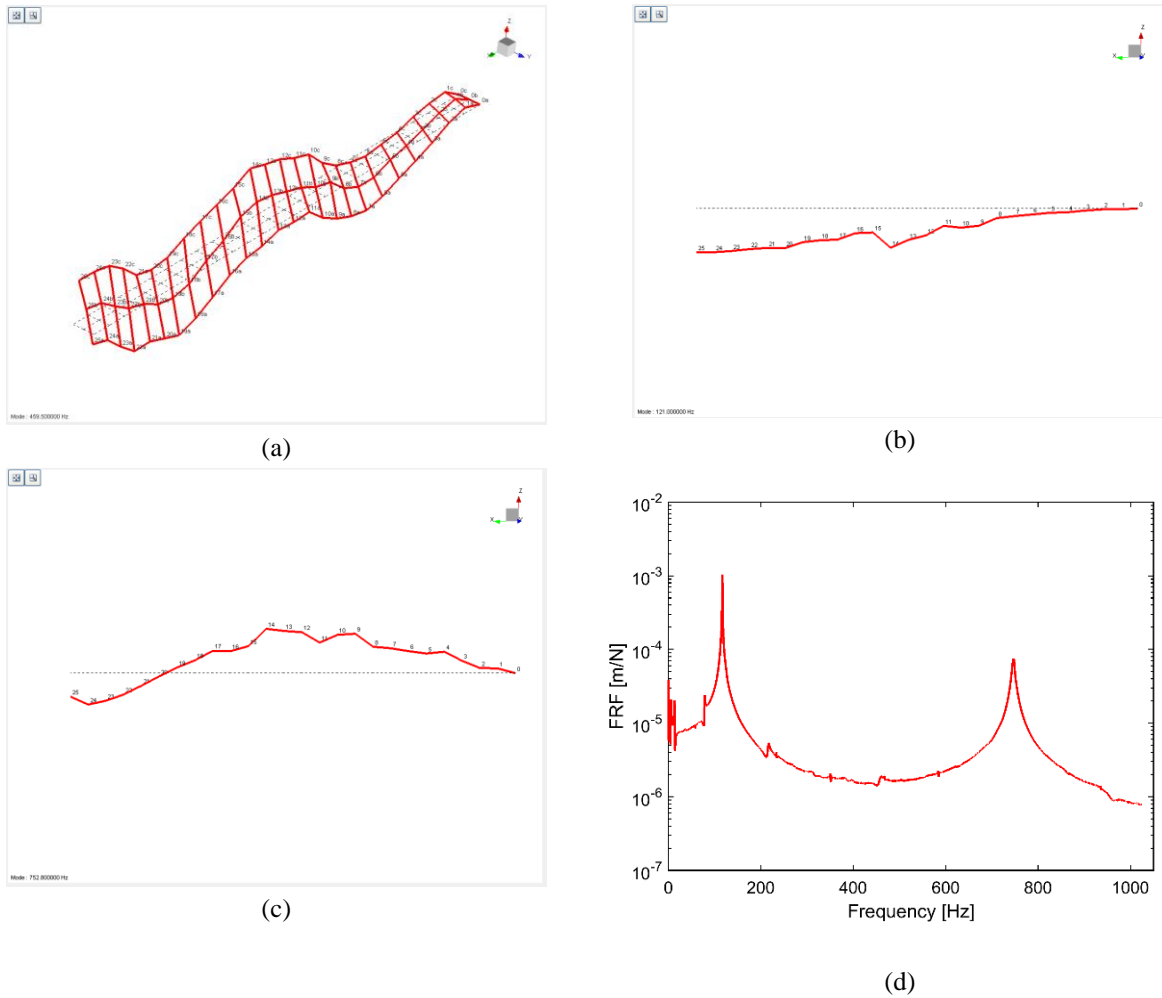


Fig. 3. 28 Experimental snapshot mode shapes for (a) First torsion dominant mode (b) First in-plane bending dominant mode (c) Second in-plane bending dominant mode (d) FRF obtained from impact testing for sample 1

In Fig. (3.24), the FRF comparison between the coupled, decoupled models and experiment are presented for sample 1. The schematic of the wrapping pattern for the sample can be seen in Fig. (2.29 a). The coupled model shows significant improvement over decoupled model for all modes and overall the coupled curve matches well with the experiment. In Fig. (3.24), the coupled theory over-predicts the fourth bending mode. To analyze further, the theoretical and experimental mode shapes are compared for out of plane bending dominant modes 4 and 5 and the plots are shown in Figs. (3.25 a) and (3.25 b). To animate the experimental mode shapes in the out of plane bending direction, the centerline has been selected and the sensing is done every 0.5 cm starting from the clamp. The node locations of the out of plane bending dominant modes 4 and 5 of theory and experiment are close to each other. To obtain more insight into the mismatch into one of the

out of plane bending dominant mode 4, the theoretical curvature ($\frac{\partial^2 w}{\partial x^2}$) is plotted for the modes 4 (mismatched mode) and modes 5 (mode with good match). The coupled mode shape $W(x)$ is selected for plotting the curvature. The structure under consideration (sample 1) has four fundamental elements of wrapping pattern. The length of the elements in the order starting from the clamp are $x = 7.5$ cm, 5 cm, 7.5 cm and 5 cm. From Fig. (3.25 a), for the fourth out of plane bending dominant mode, the second and the third peak locations of the curvature line up with the interface location of the two fundamental elements and the first interface location is fairly closer to the first node of the curvature. The structure has lumped mass section at the interface of two different fundamental elements. The bending stiffness is proportional to the curvature. In Fig. (3.25 a), the close proximity of two peaks of the curvature to the lumped mass locations would mean that the stiffening effect for the fourth mode will be practically lower and mass effect will be higher. Therefore, it is expected that the practically measured natural frequency for this mode will be lower and the theory over-predicted the frequency for this mode more than the other out of plane bending modes. This can be also observed in Table. (3.9), where the frequencies of the coupled theory proposed in the paper and the experiment are compared to each other. In Fig. (3.25 b), for the fifth bending dominant mode, the three interface locations are away from the peak locations of the curvature and therefore we do not see the type of behavior seen in the fourth out of plane bending dominant mode. Some more explanation regarding this is provided while discussing Table. (3.12) later in this section. To identify the modes in the other direction for both theory and experiment, mode shape analysis is performed. The theoretical mode shapes for the first in plane bending dominant, first torsion dominant and the second in-plane bending dominant mode shapes are plotted in Figs. (3.27 a) - (3.27 c) respectively. The experimental first torsion dominant, first and second in-plane bending dominant modes are plotted in Figs. (3.28 a) - (3.28 c) respectively. Practically speaking, the in plane bending dominant mode is weakly coupled to the out of plane bending mode, we do not clearly see the sharp peaks associated with the in plane bending dominant mode in the experimental curve of Fig. (3.24). To accurately identify the frequencies associated with the in plane bending dominant mode, in-plane impact tests are performed and in Fig. (3.28 d), the FRF for the case where the structure is excited in the in plane bending direction is presented and the significant peaks in Fig. (3.28 d) correspond to the in plane bending dominant modes. The error percentages of the coupled and decoupled model with respect to the experiment are presented in Table. (3.9). As explained in Chapter 2.3, the decoupled model

proposed in [53] over-predicts the natural frequencies when compared to the coupled model and gives large errors. The out of plane bending modes from the coupled model match well with the experiment when compared to Martin et al model [53] . In Table (3.9), the in-plane bending dominant modes are over predicted by the coupled theory and show larger errors when compared to other coordinates. This means that the theory assumes larger stiffness in that direction than the practical stiffness of the structure in the in-plane direction.

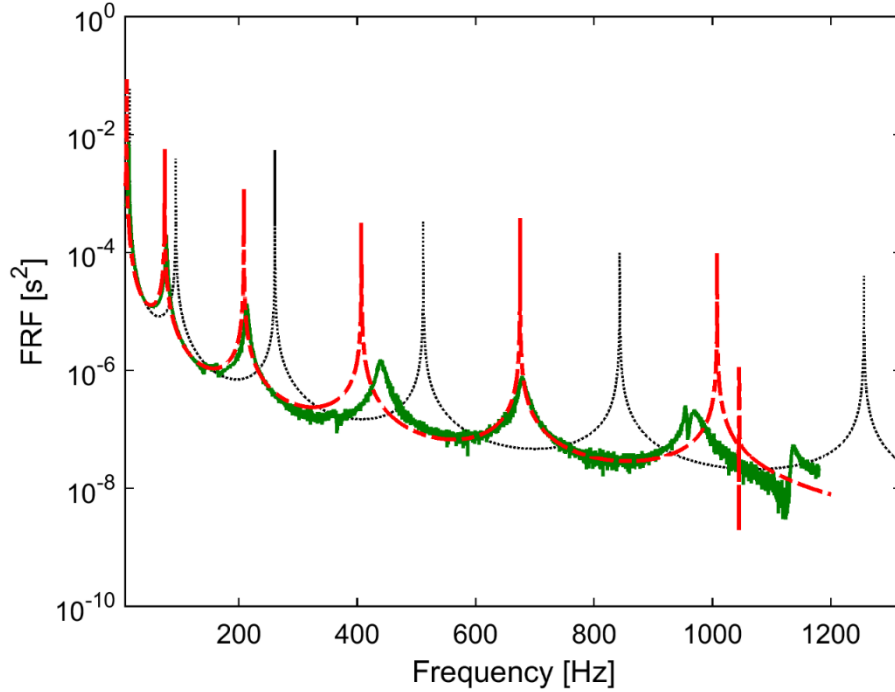


Fig. 3. 29 FRF comparison between the coupled, decoupled analytical models and the experiment for sample 2. Cabled Analytical (Decoupled) — Cabled Experimental - - - Cabled Analytical (Coupled).

In Ref. [119] (Chapter 3.2), for the sample 3 tested for periodic wrapping pattern, the errors for the in plane bending dominant are on the higher side. In this Section 3.3, the number of cables in samples 1 and 2 are of similar range in sample 3 of Ref. [119] but the substrates used have higher slenderness ratio ($\frac{l}{h}$). Large part of the error in the in-plane bending mode for cabled beam in Ref. [119] for sample 3 is attributed to the error existing in bare beam due to clamping in the in-plane direction. Since the substrates used in this paper are thinner than sample 3 of Ref. [119], we could observe that the structures are now better clamped than the thicker substrate in Ref.[119]. For the testing of structures, traditional type clamp for cantilever beam testing is used. The structure is constrained in the thickness (z direction) and from the discussions from Section 3.2,

for thicker substrates, the fixed end will have some finite stiffness in the in-plane direction which gives lower frequencies than the theory can predict. For the thinner samples, this issue should not be as significant as thinner structures can be better clamped. This is also one of the reason why the overall in-plane errors are lower in this non-periodic wrapping pattern when compared to sample 3 of periodic wrapping pattern. In addition, glue is applied to the samples 1 and 2 in this paper at discrete cable locations. This is more practical representation of cable-harnessed structure where the cables are attached at discrete locations to the host structure in the research by U.S Air force [16,44,45]. The assumptions in the theoretical model are now more realistic.

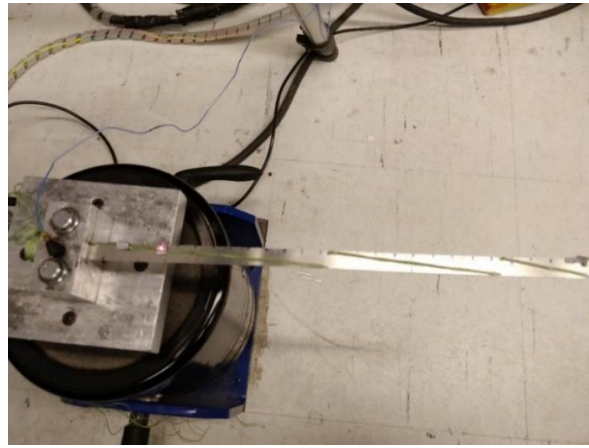


Fig. 3. 30 Experimental testing of preliminary sample

Table 3. 10 System parameters for the sample for preliminary testing

System parameters	Value
Beam length	270 mm
Beam width	11 mm
Beam thickness	0.975 mm
Beam density	2,768 Kg/m ³
Beam modulus of elasticity	68.9 GPa
Beam Shear modulus	25.7 GPa
Pre-tension of the cables	20 N
Cable radius	0.00021 m
Cable density	1,400 Kg/m ³
Cable modulus of elasticity	128.04 GPa
Number of Cables	5
Sensing Location	$x = l$ tip sensing
Number of fundamental elements	3 (non-periodic)

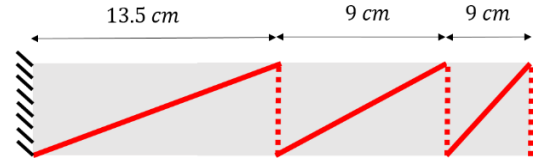


Fig. 3. 31 Top view of the preliminary sample

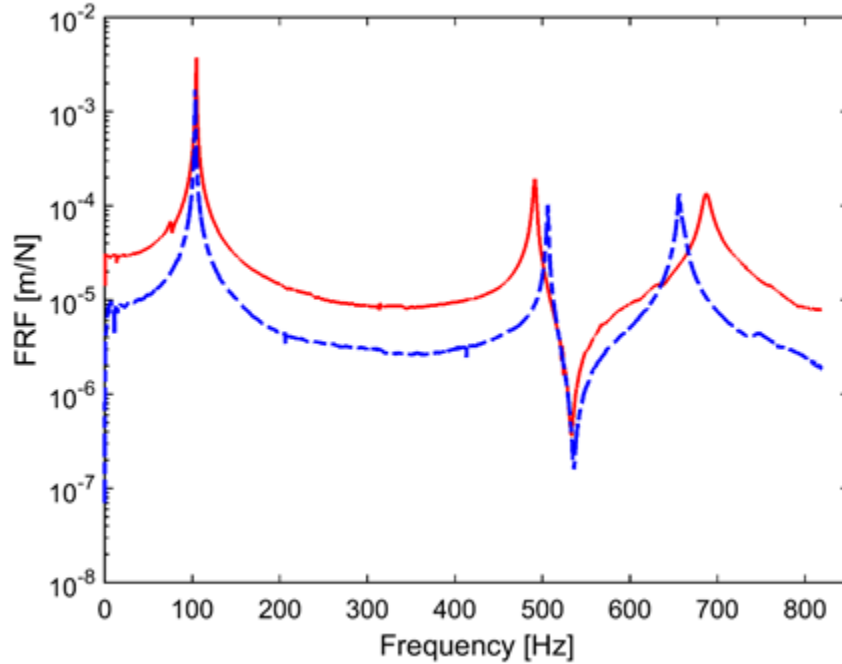


Fig. 3. 32 Comparison of in plane impact FRFs for experiment of cabled beam of preliminary sample with and without glue. — cabled beam without glue — cabled beam with glue

To obtain more insight into the in plane bending dominant modes, the experimental setup of preliminary sample is presented in Fig. (3.30). It consists of three non-periodic elements and the wrapping angle increases after each section. The system parameters are presented in Table. (3.10) and the top view of the wrapping pattern is shown in Fig. (3.31). The purpose of this analysis is to find out the effect of adding glue at discrete locations to the natural frequencies of the in plane bending dominant mode. The result is presented in Fig. (3.32). It can be seen that there is not much change for the first in-plane bending dominant mode and the frequency is slightly reduced for the second in-plane bending dominant mode. For the in plane bending dominant modes in non-periodic wrapping pattern, the cable is in better contact with the host structure when compared to the periodic wrapping pattern case [119]. When the cable is in better contact with the host structure, the inertia effect due to cabling increases along with the stiffening effect. Since the bending stiffness of the cables considered in this paper is negligible, the plane in which the host structure

vibrates is parallel to the plane in which the pre-tensioned cable is attached for in plane bending vibrations. In this case, overall, the pre-compressive effect on the host structure due to cabling dominates the stiffening effect due to cabling in the in-plane bending direction; because of this, we do not practically see significant stiffening effect in the in-plane bending direction. To conclude, the reason for over-prediction of the in plane bending dominant modes is because of combination of three reasons. First, the clamping issue, which in this paper is not as high as Ref. [119] due to using thinner substrates. Second, the dominance of pre-compressive effect of on host structure over the pre-tension effect of cable in the in-plane bending direction. Third, in this non-periodic wrapping pattern experiments, additional inertia effect due to better contact of cables with the host structure. The same reason can also be extended to the next sample for in-plane bending explanation.

Fig. (3.29) shows the comparison of the frequency response functions between the coupled, decoupled model [53] and the experiment for sample 2, the schematic of wrapping pattern for this sample is shown in Fig. (2.29 b). The significant peaks denote the out of plane dominant modes and the sharp peaks denote the modes in the in plane and the torsional direction. Similar to sample 1, the decoupled model over-predicts the natural frequencies. The coupled model shows good agreement with the experimental curve when compared to the decoupled model. In the frequency range tested, the structure has 6 out of plane bending, 2 in-plane bending and 2 torsion dominant modes. For the out of plane bending modes, the match between coupled theory and experiment is good for all the modes when compared to the decoupled theory. For the fourth out of plane bending dominant mode, the theory slightly under-predicts the natural frequency and for the sixth out of plane bending dominant mode, the theory slightly over-predicts the natural frequency. Similar to sample 1, the mode shapes corresponding to the 4th, 5th and the 6th out of plane bending dominant modes are simulated using experiments and compared to theory in Figs. (3.33 a)-(3.33 c).

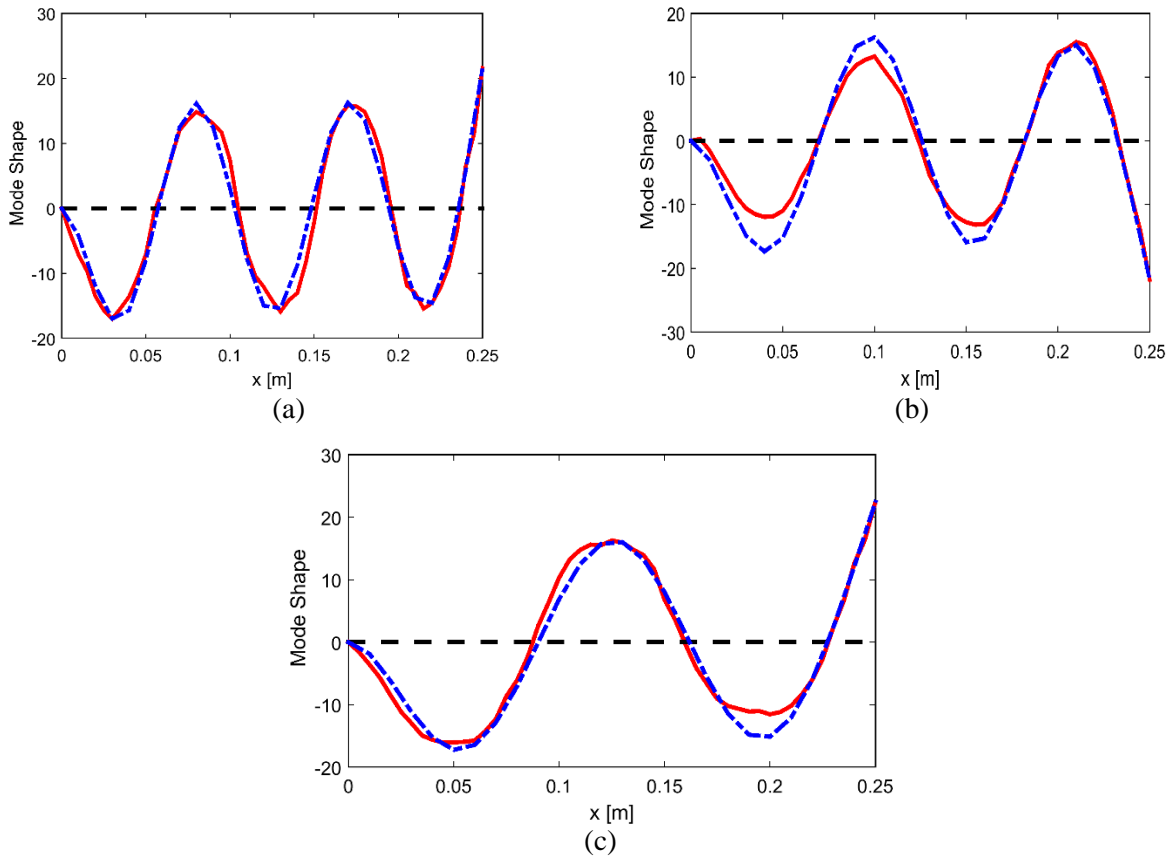


Fig. 3.33 Comparison of experimental and theoretical out of plane bending mode shapes for (a) Mode 4 (b) Mode 5 (c) Mode 6 for sample 2. — Experimental - - - Centerline - - - Analytical.

The curvature plots for the same modes are presented in Figs. (3.34 a)-(3.34 c). For the sixth out of plane bending mode similar to the fourth mode of sample 1, the theory over-predicts the natural frequency. From Fig. (3.34 c), first interface location of the structure is near the second node of the curvature plot. The next two interface locations are near the peaks of the curvature plot. For the modes, that have interface locations near the peak of curvature particularly near the tip of the cantilever, practically we see less stiffening effect but in this case the first interface location is near the node of the curvature, this should add some stiffening effect into the system. Overall, the measured frequency for the sixth bending mode is slightly lower than the frequency predicted by the coupled model. In Fig. (3.34 a), the curvature plot for the fourth out of plane bending dominant mode, the interface locations of the structure are near the node locations of the curvature. This means, practically at the fourth mode for this sample, the stiffness measured

from the experiment is more than the stiffness predicted by the coupled theory when compared to all the other out of plane bending modes. In the work on periodic wrapping pattern [119] (Chapter 2.2 and 3.2), the experimental samples considered there has larger number of fundamental elements (9 and 10 for the two samples). It was observed there that all the out of plane bending modes has consistent error for all the out of plane bending modes in case of periodic wrapping pattern. Based on the observations from this Section 3.3, in structures with lower number of non-periodic elements, the error percentage between the theory and experiment is not consistent for certain modes depending on the

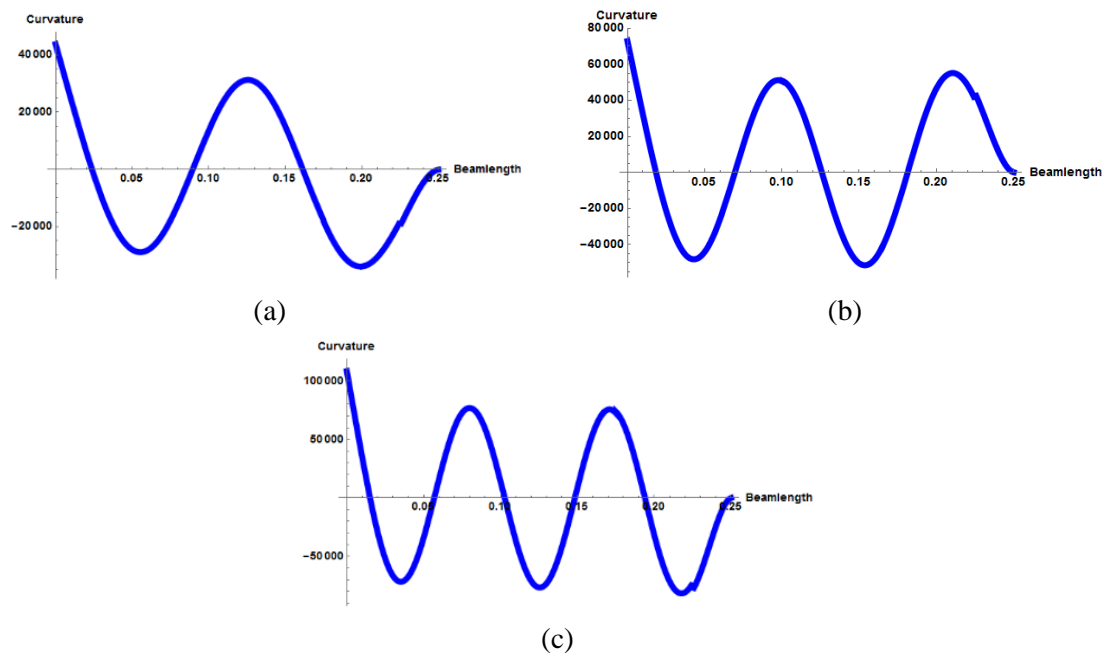


Fig. 3. 34 Theoretical plots for curvature for (a) Mode 4 (b) Mode 5 (c) Mode 6 for sample 2

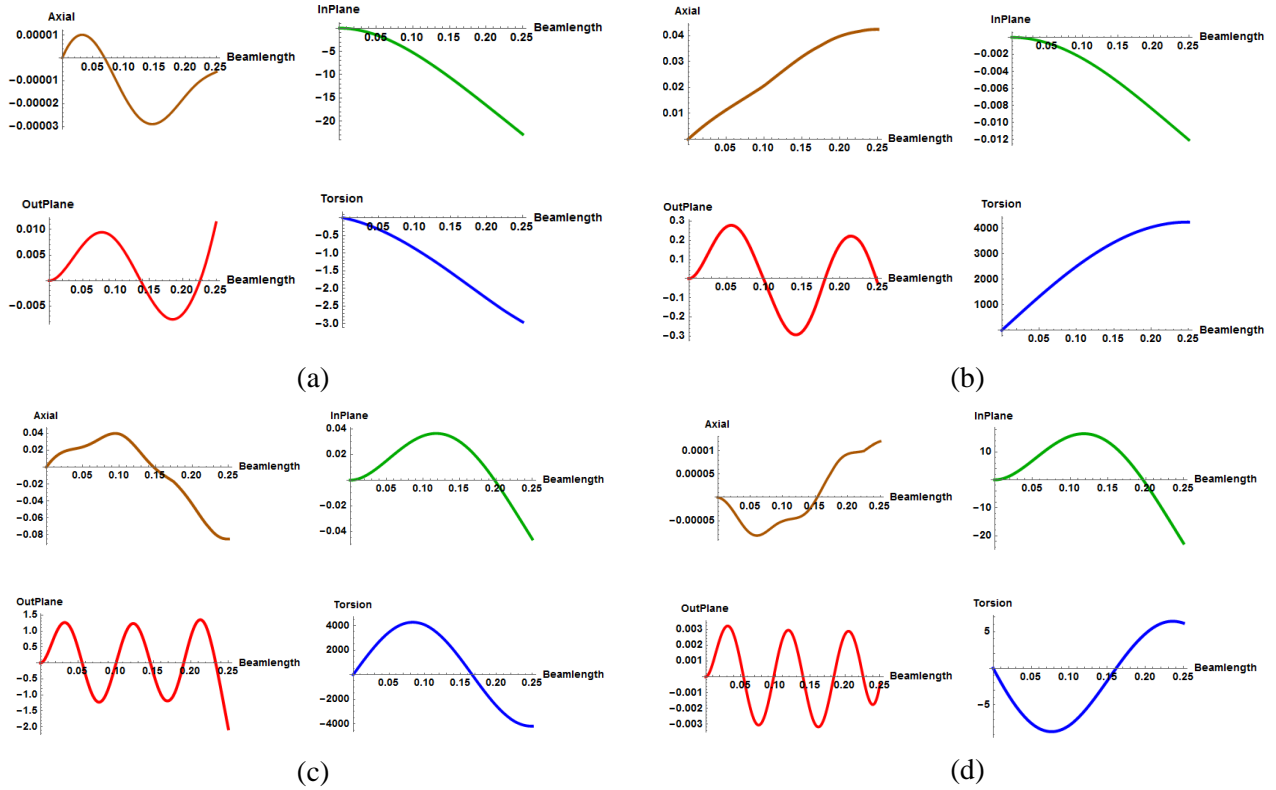
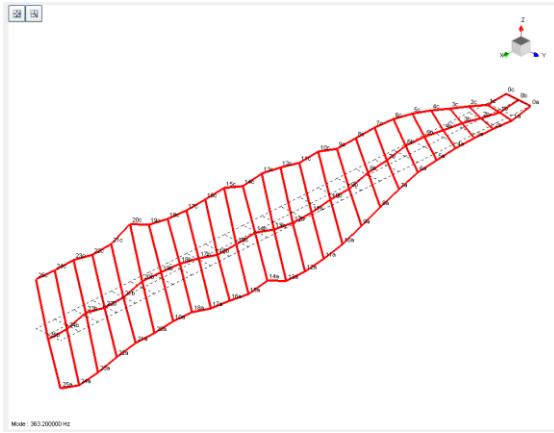
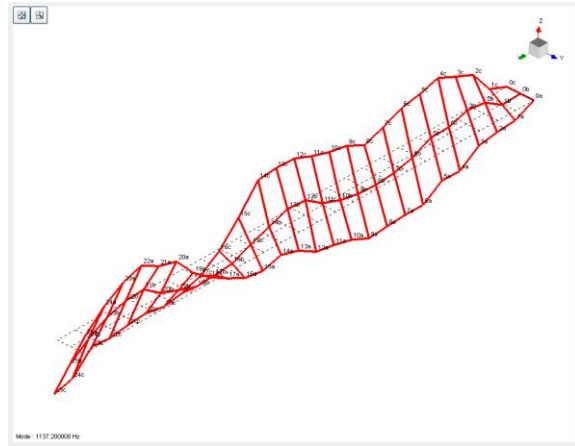


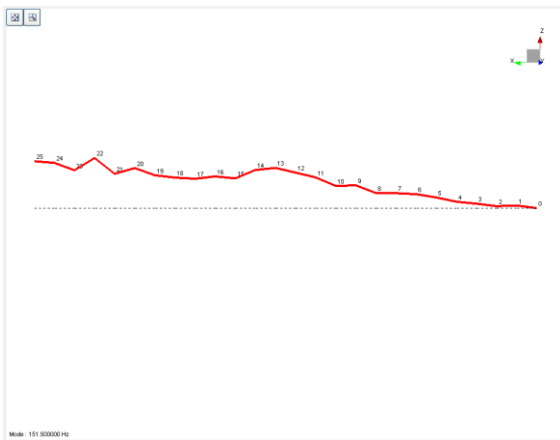
Fig. 3.35 Coupled theoretical mode shapes (a) First in plane bending dominant (b) First torsion dominant (c) Second torsion dominant (d) Second in-plane bending dominant for sample 2



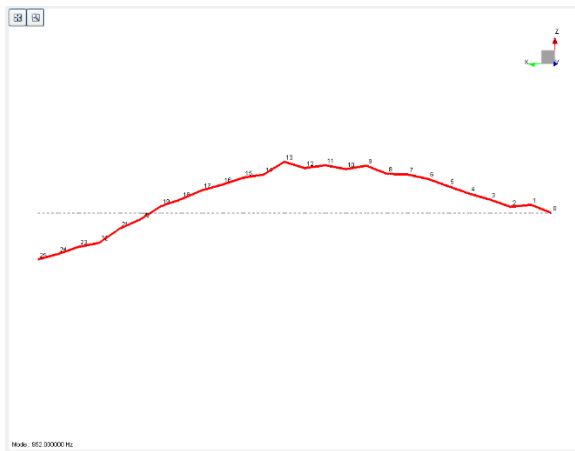
(a)



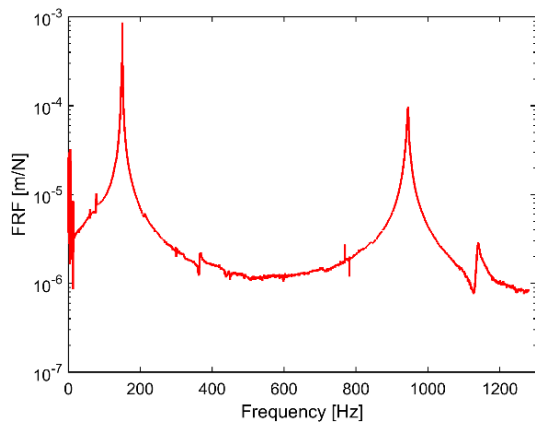
(b)



(c)



(d)



(e)

Fig. 3.36 Experimental snapshot mode shapes for (a) First torsion dominant mode; (b) Second torsion dominant mode; (c) First in-plane bending dominant mode; (d) Second in-plane bending dominant mode; (e) FRF obtained from impact testing for sample 2

locations of curvature peak and node with respect to the interface location between two different fundamental elements. To minimize the cabling stiffening effects in a certain mode, the interface locations and number of fundamental elements on non-periodic pattern can be carefully selected based on estimate on the curvature peak and node location and the structure can be wrapped accordingly. The theoretical mode shapes for the two torsion and in plane bending dominant are presented in Figs. (3.35 a) - (3.35 d) for sample 2. The corresponding experimental mode shapes are presented in Figs. (3.36 a) - (3.36 d) and the FRF from the in-plane bending is presented in Fig. (3.36 e) to accurately find the natural frequencies associated with the in plane bending dominant modes. The host structure in the sample 2 is wider than the first sample; hence, sample 2 is more flexible in torsional direction as we see two torsion dominant modes in the frequency range of interest tested (Table. (3.11)). Similar to sample 1, the natural frequencies associated with the in plane bending dominant mode are higher than the experiment.

Table 3. 11 Coupled and Decoupled Natural Frequencies for Sample 2

Mode No	Experiment [Hz]	Coupled EB [Hz]	Decoupled EB [Hz]	% Coupled EB and Experiment	% Decoupled EB and Experiment
1	13.7	10.27 (OP)	14.92	25.03 %	8.90 %
2	76.9	74.62 (OP)	93.32	2.96 %	21.35 %
3	151.5 (IP)	179.65 (IP)	-	18.58 %	-
4	213.4	208.32 (OP)	260.69	2.38 %	22.16 %
5	363.2 (T)	335.52 (T)	-	7.62 %	-
6	438.9	406.96 (OP)	511.52	7.27 %	16.54 %
7	679	674.98 (OP)	843.36	0.59 %	24.20 %
8	965.7	1007.98 (OP)	1256.05	4.37 %	30.06 %
9	1137.2 (T)	1045.29 (T)	-	8.08 %	-
10	952 (IP)	1120.34 (IP)	-	17.68 %	-

*OP stands for out of plane bending, IP stands for in plane bending and T stands for Torsion dominant modes

In Table. (3.12), the ratio of the natural frequencies between the two successive modes are presented, for example $\frac{\text{Mode 2}}{\text{Mode 1}}$, $\frac{\text{Mode 3}}{\text{Mode 2}}$ etc. for different models such as the bare beam, coupled cabled harnessed model for samples 1 and 2, experiment for samples 1 and 2 and also the frequencies from the periodic wrapping pattern [119] (Chapter 2.2). For a bare beam model, the frequency ratio between the successive modes for a cantilever beam can be calculated using the standard formulae [120]. The ratios are shown in the first row of Table. (3.12). The frequency ratios for the coupled model of samples 1 and 2 of non-periodic are presented in the rows 2 and 4 of Table. (3.12) and the frequency ratios of the coupled model of sample 1 of periodic wrapping

pattern are presented in the row 6. The frequency ratios for the experiment are presented in rows 3, 5 and 7. From the Table. (3.12), we can see that the frequency ratios of the coupled models for cable-harnessed structure follow similar trend to that of standard models particularly the ratios of Modes 3, 4 and 5 where there was some mismatch in Mode 4 for both the samples in Figs. (3.24) and (3.29). For the experiment related to the periodic wrapping pattern, the trend of the frequency ratios is similar to the coupled theory and the bare beam especially in the columns 4 and 5. However, for the experiment data of non-periodic wrapping pattern, the ratios $\frac{\text{Mode 4}}{\text{Mode 3}}$, $\frac{\text{Mode 5}}{\text{Mode 4}}$ are follow a different trend than the expected and this is more noticeable for sample 1. This is an interesting phenomena observed practically in the structures with non-periodic wrapping pattern structures with larger number of cables and lesser number of fundamental elements when compared to the parameters used in Martin et al paper [53].

Table 3. 12 Ratio of the natural frequencies for different models

	$\omega_{OP} \left(\frac{\text{Mode 2}}{\text{Mode 1}} \right)$	$\omega_{OP} \left(\frac{\text{Mode 3}}{\text{Mode 2}} \right)$	$\omega_{OP} \left(\frac{\text{Mode 4}}{\text{Mode 3}} \right)$	$\omega_{OP} \left(\frac{\text{Mode 5}}{\text{Mode 4}} \right)$	$\omega_{OP} \left(\frac{\text{Mode 6}}{\text{Mode 5}} \right)$
Bare beam	6.26	2.8	1.95	1.65	1.49
Coupled (Sample 1)	7.27	2.78	1.96	1.63	-
Experiment (Sample 1)	5.95	2.74	1.78	1.84	-
Coupled (Sample 2)	7.26	2.79	1.95	1.65	1.49
Experiment (Sample 2)	5.61	2.77	2.05	1.54	1.42
Coupled (Periodic [119])	6.25	2.80	1.95	1.64	-
Experiment (Periodic[119])	6.14	2.76	1.95	1.64	-

In non-periodic structures, the fundamental elements have different wavelength as opposed to the periodic wrapping pattern where each fundamental element has the same wavelength. Therefore, in non-periodic structures, because of variable wavelengths, we see different mode spacing ratios when compared to the periodic structure and this effect will be more noticeable if the nodes of the curvature overlap with the interface of two fundamental elements as observed in sample 1. This concept may be built upon to wrap the cables in a non-periodic manner to minimize the stiffening effect across some modes of interest. Overall, the coupled model proposed in this

paper for the cable-harnessed structures with non-periodic wrapping pattern gives good match with the experiment when compared to the existing models in the literature. For non-periodic wrapping pattern, the host structure and cables considered have similar dimensions for all the three samples with the difference being in wrapping pattern. The first two samples are validated to demonstrate the accuracy of theoretical model. Once the model is validated, a third sample, which has semi-periodic wrapping pattern, is also theoretically investigated in Section 2.2.

3.4 Conclusions of the Chapter

In this chapter, experimental validations for the mathematical models presented in Chapter 2 are performed. For straight cable pattern, the system tested consisted of a bundle of pre-tensioned cables attached along the length of the host structure at an offset position. Base excitations are provided to the structure in the out-of-plane bending direction to obtain the FRFs. The frequency response functions for both the coupled and decoupled analytical models are then compared to the experimental values. The results for the coupled model are shown to be in good agreement with the experimental results when compared to the decoupled vibration model clearly indicating the need for including the coupling effects between various coordinates of vibrations in the model. For the periodic and non-periodic wrapping pattern, experiments were performed on two samples and the FRFs obtained from the coupled EB and TBT models give better match with the experimental FRF when compared to the decoupled EB FRF. Mode shape animation snapshots of the in-plane bending and torsion dominant modes are presented to accurately identify the type of vibration associated with each mode. To conclude the objective that the coupled mathematical models presented in the thesis show significant improvement in the natural frequency results when compared to the model published in the literature by Martin et al with respect to the experimental frequencies is achieved.

Chapter 4

Conclusion and Future Work

4.1 Conclusions

This thesis investigated the phenomenon of coupling between different coordinates of vibrations in cable-harnessed structures. The effect of coupling is ignored in the published literature in this field. The main goal of thesis is to perform the coupled vibration analysis using analytical methods. The distributed parameter analytical models presented in this thesis are validated through experiments. The governing partial differential equations of motion are derived through energy methods by applying Hamilton's principle. The coupled results are compared to the decoupled results to highlight the importance of modeling the coupling effect. In Chapter 2a, the coupled partial differential equations for the cable-harnessed structure are developed using both Euler-Bernoulli and Timoshenko beam theories. The system consists of a straight cable positioned at an offset distance along the width axis on a beam. The theoretical studies pointed that the natural frequencies from the coupled model are lower than the decoupled model due to the structure being more compliant after the coupling effects were considered. Sensitivity analyses were performed by finding the effect of varying the offset position and radius of the cable on the natural frequencies. It is found that the coupling effects are maximum when the offset distance increases. Increased strain energy transfer from the out of plane bending mode to the in-plane bending mode is also observed as the offset distance is increased. In Chapter 2b, cable-harnessed structure with periodic wrapping pattern is studied. The coupled partial differential equations are derived using Euler-Bernoulli and Timoshenko models. The coupled equivalent continuum model is presented to model the complicated periodic structure. The coupled model gives lower frequencies when compared to the decoupled models published in the literature for the periodic structure. It is observed in this chapter that for larger number of periodic elements, the frequency of the cabled structure from the coupled model will be smaller and approaches bare beam thereby minimizing the effect of cabling on the host structure. This is an advantage over the structure with straight cable pattern at an offset distance. In straight cable with offset position, the structure still has a larger stiffening effect when compared to bare beam. The concept of transition frequency is also investigated in this chapter for cable-harnessed structure with periodic wrapping pattern. In

the published literature, the transition frequency is mainly studied for bare Timoshenko beams for simply supported boundary conditions. In this chapter, for cable-harnessed structure it is observed that the transition frequency decreases as the radius of the cable increases. Pure shear vibration mode is seen for cable-harnessed structure with simply supported boundary conditions. For the mode shapes in the second spectrum, the profile of shapes corresponding to the shear dominant modes are not identical to the first spectrum which is the case in bare beam with simply supported boundary condition. This concept of transition frequency in cabled structures may have application in vibration control. For a cabled structure, the transition frequency and shear dominant modes start to appear in lower modes of vibration when compared to that of bare beam. The modal participation factor contribution for a structure is usually more from the lower vibration modes when compared to the higher modes. Presence of transition frequency mode and the shear dominant modes in the lower vibration modes of cabled beam will ensure that the structure has lesser amplitude vibrations in the out of plane bending direction when compared to the bare beam counterpart. In chapter 2c, coupled vibrations for structures with non-periodic wrapping pattern are analyzed. The structure has different wrapping angles for each fundamental element, which makes it difficult to obtain an equivalent continuum model like periodic wrapping structure. The structure is discretized at the interface of each fundamental element by applying interface continuity conditions along with the boundary conditions resulting in a complicated model. Structures with three different wrapping patterns are investigated for the theoretical studies for cantilever boundary condition. It is observed that for some vibration modes, the decoupled model published by Martin et al significantly over predicts the natural frequencies.

In Chapter 3, experimental investigations are performed for the structure with straight cable, periodic and non-periodic wrapping patterns. In Chapter 3a, straight cable along the offset is attached to the host structure. Practically, the structure is excited in the out of plane direction using a shaker and the presence of sharp in plane bending dominant mode peak is confirmed by performing the impact test in the in plane bending direction. The theoretical frequency response functions from the coupled model match well with the experimental frequency response function when compared to that of decoupled Martin et al model thereby showing the importance of having a coupled model for structure with straight cable pattern placed at an offset distance from the centerline. In Chapter 3b, for the periodic wrapping pattern structure, in addition to the shaker base excitation test in the out plane bending direction, mode shape animations are also performed to

practically confirm the in-plane bending and the torsion dominant modes. In Chapter 3c, for the non-periodic wrapping pattern structure experimental results are presented. Similar to periodic wrapping pattern, animation plots are presented for the in plane and torsion dominant modes to confirm the respective modes in those directions. To conclude, in this thesis, the importance of having a mathematical model to study the coupling effects in cable-harnessed structures is shown. The results of mathematical models proposed in this thesis matched very well with the experiments for all the designs investigated when compared to the existing decoupled models published in the literature for the three different systems investigated such as the cabled harnessed structure with straight pattern at offset, periodic and non-periodic patterns.

4.2 Future Work

For future work, the research may be extended in the following directions:

- 1) The analytical model investigated in this thesis can be built upon by including the effect of damping and the coupling it creates between various coordinates of vibrations. Mathematically, the Rayleigh dissipation function for the cabled structure needs to be found out for the cabled structure by considering the coupling effects. After Rayleigh dissipation function is included in the Hamilton's principle, the final distributed parameter model will contain damping related terms. Through numerical and experimental investigations, interested readers can further explore the effect of coordinate coupling created by damping related terms and their effect on the peaks of the frequency response function.
- 2) It is seen in this thesis, at larger values of cable diameter the coordinate coupling effects become important. The space flight cables are very thick and have significant bending stiffness. The effect of coupling, in beams harnessed with thick space flight cables can be investigated by developing a coupled analytical model by incorporating the bending stiffness of cables and comparing the results with the existing models by Spak et al or Choi et al and the experimental data.
- 3) Another aspect ignored in the literature is to investigate any potential non-linear phenomena in the cable-harnessed structure. For thicker cables, if the attachment points of cable to the host structures are at the boundaries, then significant cable resonance could be seen which may induce non-linear phenomena in the structure like multi-period oscillations, quasi-periodic or chaotic behavior. This can be initially investigated experimentally and depending on the

behavior of the structure in the experiments, the nonlinear effects can be incorporated in the mathematical model at least for the out of plane bending vibrations to accurately model any potential non-linear effects observed from the experiment.

- 4) Space structures are made of lightweight composite materials. Another aspect to investigate would be cable-harnessed composite structures subjected to thermal loading. Thermal loading will also affect the dynamic characteristics of the structure, which will be interesting aspect to investigate in the field of cable-harnessed structures.

References

- [1] Coombs, D. M., Goodding, J. C., Babuška, V., Ardelean, E. V., Robertson, L. M., and Lane, S. A., 2011, “Dynamic Modeling and Experimental Validation of a Cable-Loaded Panel,” *Journal of Spacecraft and Rockets*, **48**(6), pp. 958–974.
- [2] Babuska, V., Coombs, D. M., Goodding, J. C., Ardelean, E. V., Robertson, L. M., and Lane, S. A., 2010, “Modeling and Experimental Validation of Space Structures with Wiring Harnesses,” *Journal of Spacecraft and Rockets*, **47**(6), pp. 1038–1052.
- [3] Goodding, J., Babuska, V., Griffith, D. T., Ingram, B., and Robertson, L., 2007, “Studies of Free-Free Beam Structural Dynamics Perturbations Due to Mounted Cable Harnesses,” *48th AIAA/ASME/ASCE/AHS/ASC Structures, Structural Dynamics, and Materials Conference*, p. 2390.
- [4] Coombs, D., Glaese, R., Babuška, V., Robertson, L., and Ingram, B., 2008, “Structural Dynamic Effects of Cables on a Sparse Aperture Deployable Optical Telescope,” *49th AIAA/ASME/ASCE/AHS/ASC Structures, Structural Dynamics, and Materials Conference, 16th AIAA/ASME/AHS Adaptive Structures Conference, 10th AIAA Non-Deterministic Approaches Conference, 9th AIAA Gossamer Spacecraft Forum, 4th AIAA Multidisciplinary Des*, p. 2266.
- [5] Kauffman, J. L., Lesieutre, G. A., and Babuška, V., 2013, “Damping Models for Shear Beams with Applications to Spacecraft Wiring Harnesses,” *Journal of Spacecraft and Rockets*, **51**(1), pp. 16–22.
- [6] McPherson, B., 2017, “Timoshenko Beam Viscous Damping Model for Spacecraft Cabling Dynamics.”, Masters Thesis, University of Central Florida.
- [7] Remedias, M., Aglietti, G. S., and Richardson, G., 2015, “Modelling the Effect of Electrical Harness on Microvibration Response of Structures,” *Acta Astronautica*, **109**, pp. 88–102.
- [8] Ardelean, E. V., Babuška, V., Goodding, J. C., Coombs, D. M., Robertson III, L. M., and Lane, S. A., 2014, “Cable Effects Study: Tangents, Rabbit Holes, Dead Ends, and Valuable Results,” *Journal of Spacecraft and Rockets*, **52**(2), pp. 569–583.
- [9] Lesieutre, G. A., and Kauffman, J. L., 2014, “Damping Models for Shear-Deformable Beam with Applications to Spacecraft Wiring Harness ”, Pennsylvania State Univ State College.

- [10] Goodding, J. C., 2008, "Spacecraft Electrical Cable Harness Structural Test and Analysis Methods," *IMAC: Conference and Exposition on Structural Dynamics*, pp. 437–443.
- [11] Ardelean, E., Goodding, J., Mehle, G., Coombs, D., Babuska, V., Robertson, L., Lane, S., Ingram, B., and Hansen, E., 2007, "Dynamics of Cable Harnesses on Large Precision Structures," *48th AIAA/ASME/ASCE/AHS/ASC Structures, Structural Dynamics, and Materials Conference*, p. 2388.
- [12] Spak, K. S., 2014, "Modeling Cable Harness Effects on Spacecraft Structures.," PhD Thesis., Virginia Tech.
- [13] "<https://icesat.gsfc.nasa.gov/icesat/photogallery/space2000gallery.php>."
- [14] "<https://sservi.nasa.gov/articles/ladee-vibration-testing-complete/>."
- [15] Robertson, L., Lane, S., Ingram, B., Hansen, E., Babuska, V., Goodding, J., Mimovich, M., Mehle, G., Coombs, D., and Ardelean, E., 2007, "Cable Effects on the Dynamics of Large Precision Structures," *48th AIAA/ASME/ASCE/AHS/ASC Structures, Structural Dynamics, and Materials Conference*, p. 2389.
- [16] Goodding, J. C., Ardelean, E. V, Babuska, V., Robertson, L. M., and Lane, S. A., 2011, "Experimental Techniques and Structural Parameter Estimation Studies of Spacecraft Cables," *Journal of Spacecraft and Rockets*, **48**(6), pp. 942–957.
- [17] Ardelean, E., Goodding, J., Coombs, D., Griffiee, J., Babuška, V., Robertson, L., and Lane, S., 2010, "Cable Effects Study: Tangents, Rat Holes, Dead Ends, and Valuable Results," *51st AIAA/ASME/ASCE/AHS/ASC Structures, Structural Dynamics, and Materials Conference 18th AIAA/ASME/AHS Adaptive Structures Conference 12th*, p. 2806.
- [18] Oniszczyk, Z., 2000, "Free Transverse Vibrations of Elastically Connected Simply Supported Double-Beam Complex System," *Journal of sound and vibration*, **232**(2), pp. 387–403.
- [19] Oniszczyk, Z., 2002, "Free Transverse Vibrations of an Elastically Connected Complex Beam–String System," *Journal of Sound and Vibration*, **254**(4), pp. 703–715.
- [20] Banerjee, J. R., and Williams, F. W., 1994, "Coupled Bending-Torsional Dynamic Stiffness Matrix of an Axially Loaded Timoshenko Beam Element," *International Journal of Solids and Structures*, **31**(6), pp. 749–762.
- [21] Burlon, A., Failla, G., and Arena, F., 2017, "Coupled Bending and Torsional Free Vibrations of Beams with In-Span Supports and Attached Masses," *European Journal of*

- Mechanics-A/Solids, **66**, pp. 387–411.
- [22] Banerjee, J. R., and Fisher, S. A., 1992, “Coupled Bending–Torsional Dynamic Stiffness Matrix for Axially Loaded Beam Elements,” *International journal for numerical methods in engineering*, **33**(4), pp. 739–751.
- [23] Banerjee, J. R., and Williams, F. W., 1992, “Coupled Bending-Torsional Dynamic Stiffness Matrix for Timoshenko Beam Elements,” *Computers & Structures*, **42**(3), pp. 301–310.
- [24] Hegazy, U. H., 2010, “3: 1 Internal Resonance of a String-Beam Coupled System with Cubic Nonlinearities,” *Communications in Nonlinear Science and Numerical Simulation*, **15**(12), pp. 4219–4229.
- [25] McClure, G., and Lapointe, M., 2003, “Modeling the Structural Dynamic Response of Overhead Transmission Lines,” *Computers & Structures*, **81**(8–11), pp. 825–834.
- [26] Huang, S., 1999, “Stability Analysis of the Heave Motion of Marine Cable-Body Systems,” *Ocean Engineering*, **26**(6), pp. 531–546.
- [27] Fujino, Y., Warnitchai, P., and Pacheco, B. M., 1993, “An Experimental and Analytical Study of Autoparametric Resonance in a 3DOF Model of Cable-Stayed-Beam,” *Nonlinear dynamics*, **4**(2), pp. 111–138.
- [28] Spak, K., Agnes, G., and Inman, D., 2014, “Parameters for Modeling Stranded Cables as Structural Beams,” *Experimental Mechanics*, **54**(9), pp. 1613–1626.
- [29] Witz, J. A., and Tan, Z., 1992, “On the Axial-Torsional Structural Behaviour of Flexible Pipes, Umbilicals and Marine Cables,” *Marine Structures*, **5**(2–3), pp. 205–227.
- [30] Dall’Asta, A., and Leoni, G., 1999, “Vibrations of Beams Prestressed by Internal Frictionless Cables,” *Journal of Sound and Vibration*, **222**(1), pp. 1–18.
- [31] Gattulli, V., and Lepidi, M., 2003, “Nonlinear Interactions in the Planar Dynamics of Cable-Stayed Beam,” *International Journal of Solids and Structures*, **40**(18), pp. 4729–4748.
- [32] Liu, M.-Y., Zuo, D., and Jones, N. P., 2013, “Analytical and Numerical Study of Deck-Stay Interaction in a Cable-Stayed Bridge in the Context of Field Observations,” *Journal of Engineering Mechanics*, **139**(11), pp. 1636–1652.
- [33] Kang, Z., Xu, K., and Luo, Z., 2012, “A Numerical Study on Nonlinear Vibration of an Inclined Cable Coupled with the Deck in Cable-Stayed Bridges,” *Journal of Vibration and control*, **18**(3), pp. 404–416.
- [34] Lepidi, M., and Gattulli, V., 2016, “Non-Linear Interactions in the Flexible Multi-Body

- Dynamics of Cable-Supported Bridge Cross-Sections,” *International Journal of Non-Linear Mechanics*, **80**, pp. 14–28.
- [35] Amer, Y. A., and Hegazy, U. H., 2012, “Chaotic Vibration and Resonance Phenomena in a Parametrically Excited String-Beam Coupled System,” *Meccanica*, **47**(4), pp. 969–984.
- [36] Wei, M. H., Lin, K., Jin, L., and Zou, D. J., 2016, “Nonlinear Dynamics of a Cable-Stayed Beam Driven by Sub-Harmonic and Principal Parametric Resonance,” *International Journal of Mechanical Sciences*, **110**, pp. 78–93.
- [37] Spak, K., Agnes, G., and Inman, D., 2014, “Cable Parameters for Homogenous Cable-Beam Models for Space Structures,” *Dynamics of Civil Structures, Volume 4*, Springer, pp. 7–18.
- [38] Spak, K. S., Agnes, G. S., and Inman, D. J., 2014, “Bakeout Effects on Dynamic Response of Spaceflight Cables,” *Journal of Spacecraft and Rockets*, **51**(5), pp. 1721–1734.
- [39] Spak, K., Agnes, G., and Inman, D., 2013, “Comparison of Damping Models for Space Flight Cables,” *Topics in Dynamics of Civil Structures, Volume 4*, Springer, pp. 183–194.
- [40] Spak, K., Agnes, G., and Inman, D., 2013, “Cable Modeling and Internal Damping Developments,” *Applied Mechanics Reviews*, **65**(1), p. 10801.
- [41] Spak, K. S., Agnes, G. S., and Inman, D., 2014, “Inclusion of Shear Effects, Tension, and Damping in a DTF Beam Model for Cable Modeling,” *55th AIAA/ASME/ASCE/AHS/SC Structures, Structural Dynamics, and Materials Conference*, p. 491.
- [42] Spak, K. S., Agnes, G. S., and Inman, D. J., 2015, “Modeling Vibration Response and Damping of Cables and Cabled Structures,” *Journal of Sound and Vibration*, **336**, pp. 240–256.
- [43] Spak, K. S., Agnes, G. S., and Inman, D. J., 2015, “Experimental and Theoretical Analysis of Cabled Beams,” *56th AIAA/ASCE/AHS/ASC Structures, Structural Dynamics, and Materials Conference*, p. 690.
- [44] Choi, J., and Inman, D. J., 2014, “Spectrally Formulated Modeling of a Cable-Harnessed Structure,” *Journal of sound and vibration*, **333**(14), pp. 3286–3304.
- [45] Spak, K. S., Agnes, G. S., and Inman, D., 2013, “Towards Modeling of Cable-Harnessed Structures: Cable Damping Experiments,” *54th AIAA/ASME/ASCE/AHS/ASC Structures, Structural Dynamics, and Materials Conference*, p. 1889.
- [46] Choi, J., and Inman, D., 2013, “Development of Predictive Modeling for Cable Harnessed Structure,” *54th AIAA/ASME/ASCE/AHS/ASC Structures, Structural Dynamics, and*

- Materials Conference*, p. 1888.
- [47] Choi, J., 2014, “Investigation of the Dynamic Behavior of a Cable-Harnessed Structure.”, PhD Thesis, Virginia Tech.
- [48] Choi, J., and Inman, D. J., 2014, “Spectral Element Method for Cable Harnessed Structure,” *Topics in Modal Analysis, Volume 7*, Springer, pp. 377–387.
- [49] Huang, Y.-X., Tian, H., and Zhao, Y., 2016, “Effects of Cable on the Dynamics of a Cantilever Beam with Tip Mass,” *Shock and Vibration*, **2016**.
- [50] Huang, Y.-X., Tian, H., and Zhao, Y., 2017, “Dynamic Analysis of Beam-Cable Coupled Systems Using Chebyshev Spectral Element Method,” *Acta Mechanica Sinica*, **33**(5), pp. 954–962.
- [51] Martin, B., and Salehian, A., 2016, “Mass and Stiffness Effects of Harnessing Cables on Structural Dynamics: Continuum Modeling,” *AIAA Journal*, pp. 2881–2904.
- [52] Martin, B., and Salehian, A., 2016, “Homogenization Modeling of Periodically Wrapped String-Harnessed Beam Structures: Experimental Validation,” *AIAA Journal*, pp. 3965–3980.
- [53] Martin, B., and Salehian, A., 2018, “Continuum Modeling of Nonperiodic String-Harnessed Structures: Perturbation Theory and Experiments,” *AIAA Journal*, pp. 1–16.
- [54] Martin, B., and Salehian, A., 2013, “Dynamic Modelling of Cable-Harnessed Beam Structures with Periodic Wrapping Patterns: A Homogenization Approach,” *International Journal of Modelling and Simulation*, **33**(4), pp. 185–202.
- [55] Martin, B., and Salehian, A., 2013, “Cable-Harnessed Space Structures: A Beam-Cable Approach,” *24th International Association of Science and Technology for Development International Conference on Modelling and Simulation*, ACTA Press Calgary, AB, Canada, pp. 280–284.
- [56] Martin, B., and Salehian, A., 2013, “Vibration Analysis of String-Harnessed Beam Structures: A Homogenization Approach,” *54th AIAA/ASME/ASCE/AHS/ASC Structures, Structural Dynamics, and Materials Conference*, p. 1892.
- [57] Martin, B., and Salehian, A., 2014, “Vibration Modelling of String-Harnessed Beam Structures Using Homogenization Techniques,” *ASME 2014 International Mechanical Engineering Congress and Exposition*, American Society of Mechanical Engineers, p. V04BT04A074-V04BT04A074.

- [58] Martin, B., 2017, “Continuum Modelling and Vibration Analysis of String-Harnessed Structures.”, PhD Thesis, University of Waterloo.
- [59] Martin, B., and Salehian, A., 2017 “String-Harnessed Beam Structures: An Inverse Problem Approach for Model Approximation.” In Proceedings of the 9th International Conference on Inverse Problems in Engineering.
- [60] Martin, B., and Salehian, A., 2018, “Reference Value Selection in a Perturbation Theory Applied to Nonuniform Beams,” *Shock and Vibration*, **2018**.
- [61] Salehian, A., and Inman, D. J., 2008, “Dynamic Analysis of a Lattice Structure by Homogenization: Experimental Validation,” *Journal of Sound and Vibration*, **316**(1–5), pp. 180–197.
- [62] Salehian, A., Cliff, E. M., and Inman, D. J., 2006, “Continuum Modeling of an Innovative Space-Based Radar Antenna Truss,” *Journal of Aerospace Engineering*, **19**(4), pp. 227–240.
- [63] Salehian, A., Seigler, T. M., and Inman, D. J., 2007, “Dynamic Effects of a Radar Panel Mounted on a Truss Satellite,” *AIAA journal*, **45**(7), pp. 1642–1654.
- [64] Salehian, A., and Chen, Y., 2012, “On Strain-Rate Dependence of Kinetic Energy in Homogenization Approach: Theory and Experiment,” *AIAA journal*, **50**(10), pp. 2029–2033.
- [65] Salehian, A., Inman, D. J., and Cliff, E. M., 2006, “Natural Frequency Validation of a Homogenized Model of a Truss,” *Proceedings of the XXIV-International Modal Analysis Conference*.
- [66] Salehian, A., and Inman, D. J., 2010, “Micropolar Continuous Modeling and Frequency Response Validation of a Lattice Structure,” *Journal of Vibration and Acoustics*, **132**(1), p. 11010.
- [67] Salehian, A., and Inman, D., “A Reduced Order Micro-Polar Model of a Space Antenna with Torsional Joints,” *49th AIAA/ASME/ASCE/AHS/ASC Structures, Structural Dynamics, and Materials Conference, 16th AIAA/ASME/AHS Adaptive Structures Conference, 10th AIAA Non-Deterministic Approaches Conference, 9th AIAA Gossamer Spacecraft Forum, 4th AIAA Multidisciplinary Des*, p. 1954.
- [68] Salehian, A., Ibrahim, M., and Seigler, T. M., 2014, “Damping in Periodic Structures: A Continuum Modeling Approach,” *AIAA journal*, **52**(3), pp. 569–590.
- [69] Salehian, A., Cliff, E. M., and Inman, D. J., 2005, “Continuum Modeling of a Slewing ISAT

- (Innovative Space Antenna Technology),” *ASME 2005 International Design Engineering Technical Conferences and Computers and Information in Engineering Conference*, American Society of Mechanical Engineers, pp. 1971–1977.
- [70] Salehian, A., Inman, D., and Cliff, E., 2006, “Natural Frequencies of an Innovative Space Based Radar Antenna by Continuum Modeling,” *47th AIAA/ASME/ASCE/AHS/ASC Structures, Structural Dynamics, and Materials Conference 14th AIAA/ASME/AHS Adaptive Structures Conference 7th*, p. 2101.
- [71] Salehian, A., Seigler, T. M., and Inman, D. J., 2006, “Control of the Continuum Model of a Large Flexible Space Structure,” *ASME 2006 International Mechanical Engineering Congress and Exposition*, American Society of Mechanical Engineers, pp. 561–570.
- [72] Salehian, A., 2008, “Micropolar Continuum Modeling of Large Space Structures with Flexible Joints and Thermal Effects: Theory and Experiment.”, PhD Thesis, Virginia Tech.
- [73] Bishop, R. E. D., Cannon, S. M., and Miao, S., 1989, “On Coupled Bending and Torsional Vibration of Uniform Beams,” *Journal of sound and vibration*, **131**(3), pp. 457–464.
- [74] Dokumaci, E., 1987, “An Exact Solution for Coupled Bending and Torsion Vibrations of Uniform Beams Having Single Cross-Sectional Symmetry,” *Journal of Sound and Vibration*, **119**(3), pp. 443–449.
- [75] Banerjee, J. R., Guo, S., and Howson, W. P., 1996, “Exact Dynamic Stiffness Matrix of a Bending-Torsion Coupled Beam Including Warping,” *Computers & structures*, **59**(4), pp. 613–621.
- [76] Mei, C., 2005, “Effect of Material Coupling on Wave Vibration of Composite Timoshenko Beams,” *Journal of vibration and acoustics*, **127**(4), pp. 333–340.
- [77] Lee, J., and Kim, S.-E., 2002, “Flexural–Torsional Coupled Vibration of Thin-Walled Composite Beams with Channel Sections,” *Computers & structures*, **80**(2), pp. 133–144.
- [78] Lee, J., and Kim, S.-E., 2002, “Free Vibration of Thin-Walled Composite Beams with I-Shaped Cross-Sections,” *Composite Structures*, **55**(2), pp. 205–215.
- [79] Vo, T. P., and Lee, J., 2008, “Free Vibration of Thin-Walled Composite Box Beams,” *Composite Structures*, **84**(1), pp. 11–20.
- [80] Vo, T. P., and Lee, J., 2009, “Flexural–Torsional Coupled Vibration and Buckling of Thin-Walled Open Section Composite Beams Using Shear-Deformable Beam Theory,” *International Journal of Mechanical Sciences*, **51**(9–10), pp. 631–641.

- [81] Vo, T. P., Lee, J., and Ahn, N., 2009, “On Sixfold Coupled Vibrations of Thin-Walled Composite Box Beams,” *Composite structures*, **89**(4), pp. 524–535.
- [82] Vo, T. P., and Lee, J., 2009, “On Sixfold Coupled Buckling of Thin-Walled Composite Beams,” *Composite Structures*, **90**(3), pp. 295–303.
- [83] Xie, M., Zhang, Y., Krašny, M. J., Rhead, A., Bowen, C., and Arafa, M., 2018, “Energy Harvesting from Coupled Bending-Twisting Oscillations in Carbon-Fibre Reinforced Polymer Laminates,” *Mechanical Systems and Signal Processing*, **107**, pp. 429–438.
- [84] Al-Solihat, M. K., Nahon, M., and Behdinan, K., 2018, “Three-Dimensional Nonlinear Coupled Dynamic Modeling of a Tip-Loaded Rotating Cantilever,” *Journal of Vibration and Control*, **24**(22), pp. 5366–5378.
- [85] Dennis, S. T., and Jones, K. W., 2017, “Flexural-Torsional Vibration of a Tapered C-Section Beam,” *Journal of Sound and Vibration*, **393**, pp. 401–414.
- [86] Han, H., Cao, D., and Liu, L., 2017, “Green’s Functions for Forced Vibration Analysis of Bending-Torsion Coupled Timoshenko Beam,” *Applied Mathematical Modelling*, **45**, pp. 621–635.
- [87] Aldraihem, O. J., and Wetherhold, R. C., 1997, “Mechanics and Control of Coupled Bending and Twisting Vibration of Laminated Beams,” *Smart materials and structures*, **6**(2), p. 123.
- [88] Stoykov, S., and Ribeiro, P., 2010, “Nonlinear Forced Vibrations and Static Deformations of 3D Beams with Rectangular Cross Section: The Influence of Warping, Shear Deformation and Longitudinal Displacements,” *International Journal of Mechanical Sciences*, **52**(11), pp. 1505–1521.
- [89] Bhadbhade, V., Jalili, N., and Mahmoodi, S. N., 2008, “A Novel Piezoelectrically Actuated Flexural/Torsional Vibrating Beam Gyroscope,” *Journal of Sound and Vibration*, **311**(3–5), pp. 1305–1324.
- [90] Eslimy-Isfahany, S. H. R., Banerjee, J. R., and Sobey, A. J., 1996, “Response of a Bending–Torsion Coupled Beam to Deterministic and Random Loads,” *Journal of Sound and Vibration*, **195**(2), pp. 267–283.
- [91] Lenci, S., and Rega, G., 2016, “Axial–Transversal Coupling in the Free Nonlinear Vibrations of Timoshenko Beams with Arbitrary Slenderness and Axial Boundary Conditions,” *Proceedings of the Royal Society A: Mathematical, Physical and Engineering*

- Sciences, **472**(2190), p. 20160057.
- [92] Yang, X.-D., Wang, S.-W., Zhang, W., Yang, T.-Z., and Lim, C. W., 2018, “Model Formulation and Modal Analysis of a Rotating Elastic Uniform Timoshenko Beam with Setting Angle,” *European Journal of Mechanics-A/Solids*, **72**, pp. 209–222.
- [93] Shakya, P., Sunny, M. R., and Maiti, D. K., 2019, “A Parametric Study of Flutter Behavior of a Composite Wind Turbine Blade with Bend-Twist Coupling,” *Composite Structures*, **207**, pp. 764–775.
- [94] Abdelkefi, A., Najar, F., Nayfeh, A. H., and Ayed, S. Ben, 2011, “An Energy Harvester Using Piezoelectric Cantilever Beams Undergoing Coupled Bending–Torsion Vibrations,” *Smart Materials and Structures*, **20**(11), p. 115007.
- [95] Shan, X., Deng, J., Song, R., and Xie, T., 2017, “A Piezoelectric Energy Harvester with Bending–Torsion Vibration in Low-Speed Water,” *Applied Sciences*, **7**(2), p. 116.
- [96] Sharpes, N., Abdelkefi, A., and Priya, S., 2015, “Two-Dimensional Concentrated-Stress Low-Frequency Piezoelectric Vibration Energy Harvesters,” *Applied Physics Letters*, **107**(9), p. 93901.
- [97] Abdelkefi, A., Nayfeh, A. H., Hajj, M. R., and Najar, F., 2012, “Energy Harvesting from a Multifrequency Response of a Tuned Bending–Torsion System,” *Smart Materials and Structures*, **21**(7), p. 75029.
- [98] Karami, M. A., Yardimoglu, B., and Inman, D. J., 2010, “Coupled out of Plane Vibrations of Spiral Beams for Micro-Scale Applications,” *Journal of Sound and Vibration*, **329**(26), pp. 5584–5599.
- [99] Hwang, S. J., and Gibson, R. F., 1993, “Influence of Bending-Twisting and Extension-Bending Coupling on Damping of Laminated Composites,” *Journal of materials science*, **28**(1), pp. 1–8.
- [100] Lee, U., and Jang, I., 2010, “Spectral Element Model for Axially Loaded Bending–Shear–Torsion Coupled Composite Timoshenko Beams,” *Composite Structures*, **92**(12), pp. 2860–2870.
- [101] Chortis, D. I., Varelis, D. S., and Saravanos, D. A., 2012, “Prediction of Material Coupling Effect on Structural Damping of Composite Beams and Blades,” *Composite Structures*, **94**(5), pp. 1646–1655.
- [102] Abbas, B. A. H., and Thomas, J., 1977, “The Second Frequency Spectrum of Timoshenko

- Beams,” *Journal of Sound and vibration*, **51**(1), pp. 123–137.
- [103] Cazzani, A., Stochino, F., and Turco, E., 2016, “On the Whole Spectrum of Timoshenko Beams. Part II: Further Applications,” *Zeitschrift für angewandte Mathematik und Physik*, **67**(2), p. 25.
- [104] Bhashyam, G. R., and Prathap, G., 1981, “The Second Frequency Spectrum of Timoshenko Beams,” *Journal of Sound and Vibration*, **76**(3), pp. 407–420.
- [105] Levinson, M., and Cooke, D. W., 1982, “On the Two Frequency Spectra of Timoshenko Beams,” *Journal of Sound and Vibration*, **84**(3), pp. 319–326.
- [106] Stephen, N. G., 2006, “The Second Spectrum of Timoshenko Beam Theory—Further Assessment,” *Journal of sound and vibration*, **292**(1–2), pp. 372–389.
- [107] Stephen, N. G., 1982, “The Second Frequency Spectrum of Timoshenko Beams,” *Journal of Sound Vibration*, **80**, pp. 578–582.
- [108] Bhaskar, A., 2009, “Elastic Waves in Timoshenko Beams: The ‘Lost and Found’ of an Eigenmode,” *Proceedings of the Royal Society of London A: Mathematical, Physical and Engineering Sciences*, The Royal Society, pp. 239–255.
- [109] Cazzani, A., Stochino, F., and Turco, E., 2016, “On the Whole Spectrum of Timoshenko Beams. Part I: A Theoretical Revisitation,” *Zeitschrift für angewandte Mathematik und Physik*, **67**(2), p. 24.
- [110] Gopalakrishnan, S., Martin, M., and Doyle, J. F., 1992, “A Matrix Methodology for Spectral Analysis of Wave Propagation in Multiple Connected Timoshenko Beams,” *Journal of Sound and Vibration*, **158**(1), pp. 11–24.
- [111] Oliveto, G., 1992, “Dynamic Stiffness and Flexibility Functions for Axially Strained Timoshenko Beams,” *Journal of sound and vibration*, **154**(1), pp. 1–23.
- [112] Li, X.-F., 2008, “A Unified Approach for Analyzing Static and Dynamic Behaviors of Functionally Graded Timoshenko and Euler–Bernoulli Beams,” *Journal of Sound and vibration*, **318**(4–5), pp. 1210–1229.
- [113] Manevich, A. I., 2015, “Dynamics of Timoshenko Beam on Linear and Nonlinear Foundation: Phase Relations, Significance of the Second Spectrum, Stability,” *Journal of Sound and Vibration*, **344**, pp. 209–220.
- [114] Mahapatra, D. R., and Gopalakrishnan, S., 2003, “A Spectral Finite Element Model for Analysis of Axial–Flexural–Shear Coupled Wave Propagation in Laminated Composite

- Beams,” *Composite Structures*, **59**(1), pp. 67–88.
- [115] Elishakoff, I., Kaplunov, J., and Nolde, E., 2015, “Celebrating the Centenary of Timoshenko’s Study of Effects of Shear Deformation and Rotary Inertia,” *Applied Mechanics Reviews*, **67**(6), p. 60802.
- [116] Tang, A.-Y., Wu, J.-X., Li, X.-F., and Lee, K. Y., 2014, “Exact Frequency Equations of Free Vibration of Exponentially Non-Uniform Functionally Graded Timoshenko Beams,” *International Journal of Mechanical Sciences*, **89**, pp. 1–11.
- [117] Chan, K. T., Wang, X. Q., So, R. M. C., and Reid, S. R., 2002, “Superposed Standing Waves in a Timoshenko Beam,” *Proceedings of the Royal Society of London A: Mathematical, Physical and Engineering Sciences*, The Royal Society, pp. 83–108.
- [118] Yerrapragada, K., and Salehian, A., 2019, “Analytical Study of Coupling Effects for Vibrations of Cable-Harnessed Beam Structures,” *Journal of Vibration and Acoustics*, **141**(3), p. 031001.
- [119] Yerrapragada, K., and Salehian, A., “Coupled Vibrations in Periodic Cable-Harnessed Structures: Theory and Experimental Validation,” To be Submitted.
- [120] Rao, S. S., 2007, *Vibration of Continuous Systems*, John Wiley & Sons.
- [121] Stoykov, S., and Ribeiro, P., 2013, “Vibration Analysis of Rotating 3D Beams by the P-Version Finite Element Method,” *Finite Elements in Analysis and Design*, **65**, pp. 76–88.
- [122] Stoykov, S., and Margenov, S., 2014, “Nonlinear Vibrations of 3D Laminated Composite Beams,” *Mathematical Problems in Engineering*, **2014**.
- [123] Fonseca, J. R., and Ribeiro, P., 2006, “Beam P-Version Finite Element for Geometrically Non-Linear Vibrations in Space,” *Computer methods in applied mechanics and engineering*, **195**(9–12), pp. 905–924.
- [124] Yerrapragada, K., and Salehian, A., 2018, “Coupled Bending, Torsion and Axial Vibrations of a Cable-Harnessed Beam With Periodic Wrapping Pattern,” *IDETC Conference*, ASME, pp. 1–8.
- [125] Stephen, N. G., and Zhang, Y., 2006, “Coupled Tension–Torsion Vibration of Repetitive Beam-like Structures,” *Journal of sound and vibration*, **293**(1–2), pp. 253–265.
- [126] Vörös, G. M., 2009, “On Coupled Bending–Torsional Vibrations of Beams with Initial Loads,” *Mechanics Research Communications*, **36**(5), pp. 603–611.
- [127] Tanaka, M., and Bercin, A. N., 1997, “Finite Element Modelling of the Coupled Bending

- and Torsional Free Vibration of Uniform Beams with an Arbitrary Cross-Section,” *Applied Mathematical Modelling*, **21**(6), pp. 339–344.
- [128] Song, O., Ju, J.-S., and Librescu, L., 1998, “Dynamic Response of Anisotropic Thin-Walled Beams to Blast and Harmonically Oscillating Loads,” *International Journal of Impact Engineering*, **21**(8), pp. 663–682.
- [129] Yerrapragada, K., and Salehian, A., 2017, “Coupled Axial, In Plane and Out of Plane Bending Vibrations of Cable Harnessed Space Structures,” *International Conference on Applied Mathematics, Modeling and Computational Science*, Springer, pp. 249–257.
- [130] Yerrapragada, K., and Salehian, A., “Coupled Dynamics of Cable-Harnessed Structures: Experimental Validation,” Accepted with Minor Revisions, *Journal of Vibration and Acoustics* (VIB 18 1553).
- [131] Yerrapragada, K., Martin, B., Morris, K., and Salehian, A., “Theoretical and Experimental Study of Vibrations of Cable-Harnessed Structures with Non-Periodic Wrapping Pattern: Coupling Effects,” To be Submitted.
- [132] Karami, M. A., and Inman, D. J., 2011, “Analytical Modeling and Experimental Verification of the Vibrations of the Zigzag Microstructure for Energy Harvesting,” *Journal of Vibration and Acoustics*, **133**(1), p. 11002.
- [133] Ansari, M. H., and Karami, M. A., 2016, “Modeling and Experimental Verification of a Fan-Folded Vibration Energy Harvester for Leadless Pacemakers,” *Journal of Applied Physics*, **119**(9), p. 94506.

Appendix A

Strain and Kinetic Energy Coefficients for Straight Cable at Offset Pattern

$$\begin{aligned}
 c_1 &= E_b A_b + E_c A_c & c_{12} &= -z_c T \\
 c_2 &= \kappa A_b G_b & c_{13} &= y_c T \\
 c_3 &= \kappa A_b G_b & c_{14} &= \kappa A_b G_b \\
 c_4 &= G_b J + T(y_c^2 + z_c^2) - \frac{TJ}{A_b} & c_{15} &= \kappa A_b G_b \\
 c_5 &= E_c A_c y_c^2 + T y_c^2 + E_b I_{zz} - \frac{T I_{zz}}{A_b} & k_1 &= \rho_b A_b + \rho_c A_c \\
 c_6 &= E_c A_c z_c^2 + T z_c^2 + E_b I_{yy} - \frac{T I_{yy}}{A_b} & k_2 &= \rho_b A_b + \rho_c A_c \\
 c_7 &= \kappa A_b G_b & k_3 &= \rho_b A_b + \rho_c A_c \\
 c_8 &= -E_c A_c y_c - T y_c & k_4 &= \rho_b I_{xx} + \rho_c A_c (y_c^2 + z_c^2) \\
 c_9 &= E_c A_c z_c + T z_c & k_5 &= \rho_b I_{zz} + \rho_c A_c (y_c^2) \\
 c_{10} &= (E_c A_c + T)(-y_c z_c) & k_6 &= \rho_b I_{yy} + \rho_c A_c (z_c^2) \\
 c_{11} &= -\kappa A_b G_b
 \end{aligned} \tag{A.1}$$

$$\begin{aligned}
 b_1 &= E_b A_b + E_c A_c & b_8 &= T y_c \\
 b_2 &= E_b I_{zz} + E_c A_c y_c^2 + T y_c^2 - \frac{T I_{zz}}{A_b} & b_9 &= -T z_c \\
 b_3 &= E_b I_{yy} + E_c A_c z_c^2 + T z_c^2 - \frac{T I_{yy}}{A_b} & k_1 &= \rho_b A_b + \rho_c A_c \\
 b_4 &= G_b J + T(y_c^2 + z_c^2) - \frac{TJ}{A_b} & k_2 &= \rho_b A_b + \rho_c A_c \\
 b_5 &= E_c A_c y_c z_c + T y_c z_c & k_3 &= \rho_b A_b + \rho_c A_c \\
 b_6 &= (E_c A_c + T)(-y_c) & k_4 &= \rho_b I_{xx} + \rho_c A_c (y_c^2 + z_c^2) \\
 b_7 &= (E_c A_c + T)(-z_c)
 \end{aligned} \tag{A.2}$$

where, y_c and z_c are the position coordinates of the cable. I_{zz} and I_{yy} are the area moment of inertias of the beam about z-axis and y-axis respectively, J is the torsion constant of the beam, $I_{xx} = I_{yy} + I_{zz}$ is the polar moment of inertia of the beam. Other parameters are defined in the nomenclature table. Eq. (A.1) represents the coefficients for Timoshenko theory and Eq. (A.2) represents the coefficients for Euler-Bernoulli theory.

Appendix B

Strain and Kinetic Energy Coefficients for Periodic Cable Wrapping Pattern

$$\begin{aligned}
 c_1 &= E_b A_b + E_c A_c \cos^3 \mu & c_{15} &= -(E_c A_c \sin \mu \cos^2 \mu + T \sin \mu) \\
 c_2 &= \kappa A_b G_b + E_c A_c \cos \mu \sin^2 \mu & c_{16} &= -(E_c A_c \sin \mu \cos^2 \mu + T \sin \mu)(z_c) \\
 c_3 &= \kappa A_b G_b & c_{22} &= -(E_c A_c \cos^2 \mu \sin \mu)(z_c^2) \\
 c_4 &= G_b J + E_c A_c z_c^2 \cos \mu \sin^2 \mu + T(y_c^2 + z_c^2) \cos \mu - \frac{TJ \cos \mu}{A_b} & c_{23} &= \kappa A_b G_b \\
 c_5 &= E_b I_{zz} + E_c A_c y_c^2 \cos^3 \mu + T \cos \mu y_c^2 - \frac{TI_{zz} \cos \mu}{A_b} & c_{24} &= \kappa A_b G_b \\
 c_6 &= E_b I_{yy} + E_c A_c z_c^2 \cos^3 \mu + T \cos \mu z_c^2 - \frac{TI_{yy} \cos \mu}{A_b} & k_1 &= \rho_b A_b + \frac{\rho_c A_c}{\cos \mu} + \frac{\rho_c A_c}{L} [4\bar{h} + 2\bar{b}] \\
 c_7 &= \kappa A_b G_b + E_c A_c \cos \mu \sin^2 \mu & k_2 &= \rho_b A_b + \frac{\rho_c A_c}{\cos \mu} + \frac{\rho_c A_c}{L} [4\bar{h} + 2\bar{b}] \\
 c_8 &= (E_c A_c \cos^3 \mu + T \cos \mu)(y_c) & k_2 &= \rho_b A_b + \frac{\rho_c A_c}{\cos \mu} + \frac{\rho_c A_c}{L} [4\bar{h} + 2\bar{b}] \quad (\text{B.1}) \\
 c_9 &= (E_c A_c \cos^3 \mu + T \cos \mu)(z_c) & k_4 &= \rho_b I_{xx} + \frac{\rho_c A_c}{\cos \mu} (y_c^2 + z_c^2) \\
 & & & \quad + \frac{\rho_c A_c}{L} \left(4\bar{b}^2 \bar{h} + \frac{4\bar{h}^3}{3} + \frac{2\bar{b}^3}{3} + 2\bar{b} \bar{h}^2 \right) \\
 c_{10} &= (E_c A_c \cos^3 \mu + T \cos \mu)(y_c z_c) & k_5 &= \rho_b I_{zz} + \frac{\rho_c A_c}{\cos \mu} (y_c^2) \\
 & & & \quad + \frac{\rho_c A_c}{L} \left(4\bar{b}^2 \bar{h} + \frac{2\bar{b}^3}{3} \right) \\
 c_{11} &= -\kappa A_b G_b - E_c A_c \cos \mu \sin^2 \mu & k_6 &= \rho_b I_{yy} + \frac{\rho_c A_c}{\cos \mu} (z_c^2) \\
 & & & \quad + \frac{\rho_c A_c}{L} \left(\frac{4\bar{h}^3}{3} + 2\bar{b} \bar{h}^2 \right) \\
 c_{12} &= E_c A_c z_c \cos \mu \sin^2 \mu & c_{14} &= T \cos \mu y_c \\
 c_{13} &= -(E_c A_c \cos \mu \sin^2 \mu + T \cos \mu)(z_c)
 \end{aligned}$$

$$\begin{aligned}
b_1 &= E_b A_b + E_c A_c \cos^3 \mu \\
b_2 &= E_b I_{zz} + E_c A_c y_c^2 \cos^3 \mu + T y_c^2 \cos \mu - \frac{T I_{zz} \cos \mu}{A_b} \\
b_3 &= E_b I_{yy} + E_c A_c z_c^2 \cos^3 \mu + T z_c^2 \cos \mu - \frac{T I_{yy} \cos \mu}{A_b} \\
b_4 &= G_b J + E_c A_c z_c^2 \cos \mu \sin^2 \mu + T (y_c^2 + z_c^2) \cos \mu - \frac{T J \cos \mu}{A_b} \\
b_5 &= (E_c A_c \cos^3 \mu + T \cos \mu) (y_c z_c) \\
b_6 &= -E_c A_c z_c \sin \mu \cos^2 \mu \\
b_7 &= E_c A_c z_c y_c \sin \mu \cos^2 \mu \\
b_8 &= E_c A_c z_c^2 \sin \mu \cos^2 \mu \\
b_9 &= -(E_c A_c \cos^3 \mu + T \cos \mu) (y_c) \\
b_{10} &= -(E_c A_c \cos^3 \mu + T \cos \mu) (z_c) \\
b_{11} &= T \cos \mu y_c \\
b_{12} &= -T \cos \mu z_c \\
b_{13} &= T \sin \mu z_c \\
k_1 &= \rho_b A_b + \frac{\rho_c A_c}{\cos \mu} + \frac{\rho_c A_c}{L} [4\bar{h} + 2\bar{b}] \\
k_2 &= \rho_b A_b + \frac{\rho_c A_c}{\cos \mu} + \frac{\rho_c A_c}{L} [4\bar{h} + 2\bar{b}] \\
k_3 &= \rho_b A_b + \frac{\rho_c A_c}{\cos \mu} + \frac{\rho_c A_c}{L} [4\bar{h} + 2\bar{b}] \\
k_4 &= \rho_b I_{xx} + \frac{\rho_c A_c}{\cos \mu} (y_c^2 + z_c^2) + \frac{\rho_c A_c}{L} \left(4\bar{b}^2 \bar{h} + \frac{4\bar{h}^3}{3} + \frac{2\bar{b}^3}{3} + 2\bar{b} \bar{h}^2 \right)
\end{aligned} \tag{B.2}$$

Eq. (B.1) represents the coefficients for Timoshenko theory and Eq. (B.2) represents the coefficients for Euler-Bernoulli theory. μ is the wrapping angle.

Appendix C

Additional mode shapes for bare beam and cabled beam using Timoshenko beam theory for both Spectra

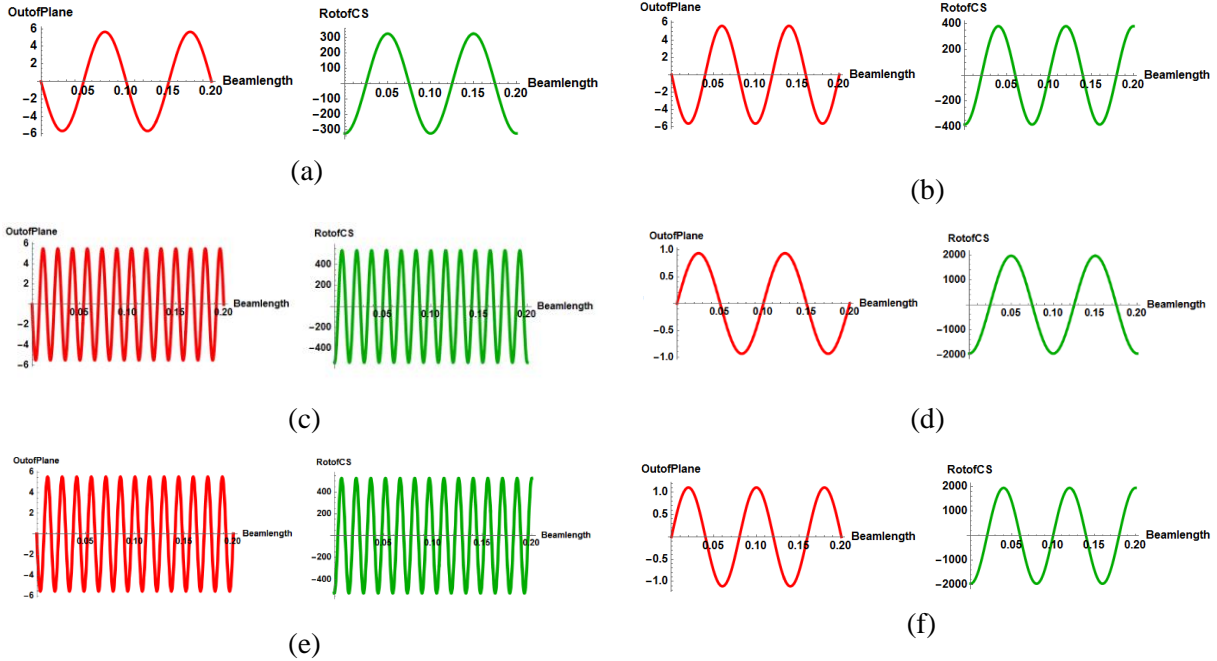


Fig. C. 1 Additional Mode shapes for (a)-(b) frequencies in first spectrum; (c)-(f) frequencies in the second spectrum for bare beam.

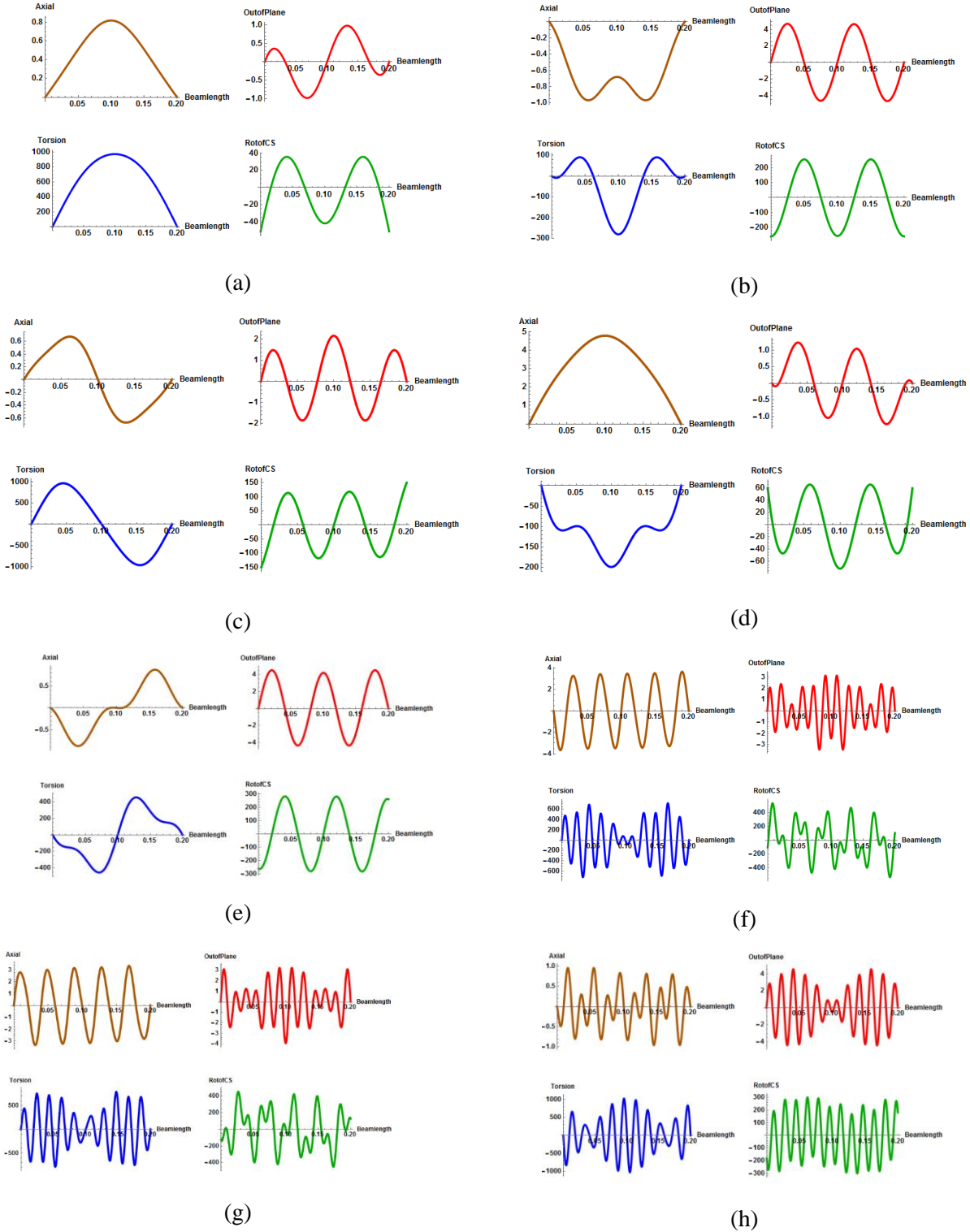
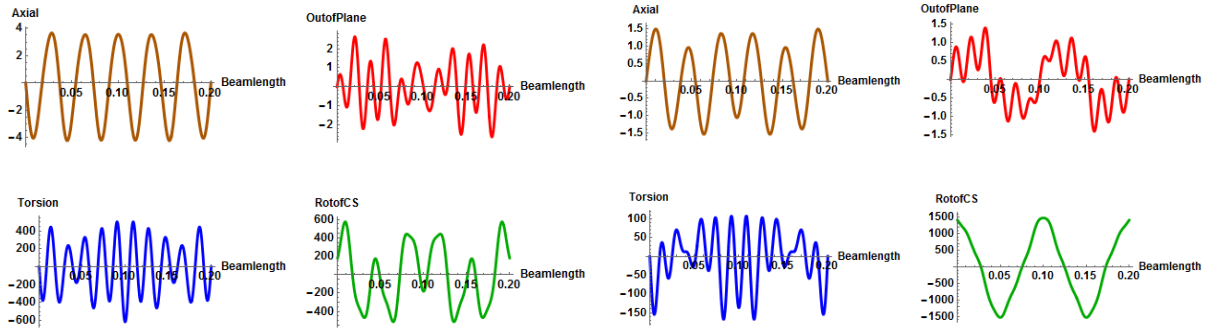
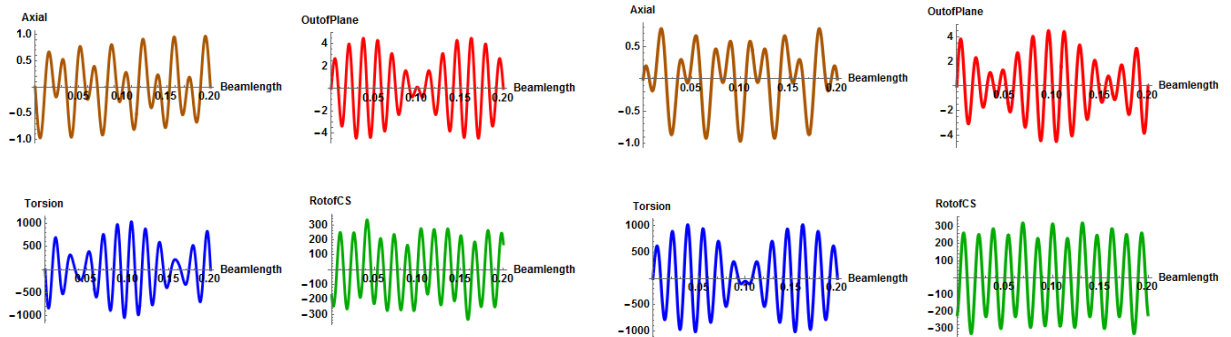


Fig. C. 2 Additional Mode shapes for (a)-(e) frequencies in first spectrum; (f)-(h) frequencies in the second spectrum for cabled beam with periodic wrapping pattern.



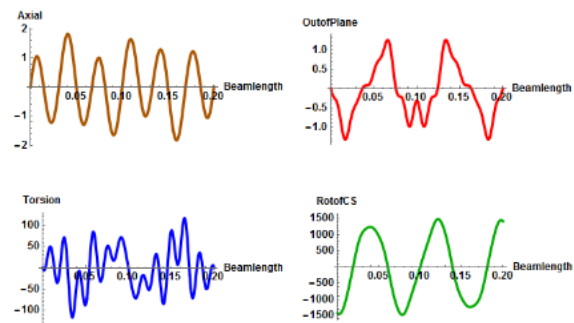
(i)

(j)



(k)

(l)



(m)

Fig. C. 3 Additional Mode shapes for (i)-(m) frequencies in the second spectrum for cabled beam with periodic wrapping pattern.

Appendix D

Strain and Kinetic Energy Coefficients for Non-Periodic Cable Wrapping Pattern

$$\begin{aligned}
\widehat{c}_{1i} &= E_b A_b + E_c A_c \cos^3 \psi_i \\
\widehat{c}_{2i} &= E_b I_{zz} + E_c A_c y_c^2 \cos^3 \psi_i + T y_c^2 \cos \psi_i - \frac{T I_{zz} \cos \psi_i}{A_b} \\
\widehat{c}_{3i} &= E_b I_{yy} + E_c A_c z_c^2 \cos^3 \psi_i + T z_c^2 \cos \psi_i - \frac{T I_{yy} \cos \psi_i}{A_b} \\
\widehat{c}_{4i} &= G_b J + E_c A_c z_c^2 \cos \psi_i \sin^2 \psi_i + T (y_c^2 + z_c^2) \cos \psi_i - \frac{T J \cos \psi_i}{A_b} \\
\widehat{c}_{5i} &= (E_c A_c \cos^3 \psi_i + T \cos \psi_i) (y_c z_c) \\
\widehat{c}_{6i} &= -E_c A_c z_c \sin \psi_i \cos^2 \psi_i \\
\widehat{c}_{7i} &= E_c A_c z_c y_c \sin \psi_i \cos^2 \psi_i \\
\widehat{c}_{8i} &= E_c A_c z_c^2 \sin \psi_i \cos^2 \psi_i \\
\widehat{c}_{9i} &= -(E_c A_c \cos^3 \psi_i + T \cos \psi_i) (y_c) \\
\widehat{c}_{10i} &= -(E_c A_c \cos^3 \psi_i + T \cos \psi_i) (z_c) \\
\widehat{c}_{11i} &= T \cos \psi_i y_c \\
\widehat{c}_{12i} &= -T \cos \psi_i z_c \\
\widehat{c}_{13i} &= T \sin \psi_i z_c \\
\widehat{k}_{1i} &= \rho_b A_b + \frac{\rho_c A_c}{\cos \psi_i} \\
\widehat{k}_{2i} &= \rho_b A_b + \frac{\rho_c A_c}{\cos \psi_i} \\
\widehat{k}_{3i} &= \rho_b A_b + \frac{\rho_c A_c}{\cos \psi_i} \\
\widehat{k}_{4i} &= \rho_b I_{xx} + \frac{\rho_c A_c}{\cos \psi_i} (y_c^2 + z_c^2)
\end{aligned} \tag{D.1}$$

i represents the index of the fundamental element. ψ_i is the wrapping angle of the i^{th} fundamental element.